Essays on the ACOPF Problem: Formulations, Approximations, and Applications in the Electricity Markets

by

Anya Castillo

A dissertation submitted to The Johns Hopkins University in conformity with the requirements for the degree of Doctor of Philosophy.

Baltimore, Maryland

February, 2016

Abstract

The alternating current optimal power flow (ACOPF) problem, also referred to as the optimal power flow (OPF) problem, is at the core of competitive wholesale electricity markets and vertically integrated utility operations. ACOPF simultaneously co-optimizes real and reactive power. First formulated over half a century ago in 1962 by Carpentier, the ACOPF is the most representative mathematical programming-based formulation of steady-state operations in AC networks. However the ACOPF is not solved in practice due to the nonconvex structure of the problem, which is known to be NP-hard. Instead, least-cost unit commitment and generation dispatch in the day-ahead, intra-day, and real-time markets is determined with numerous simplifications of the ACOPF constraint set.

This work presents a series of essays on the ACOPF problem, which include formulations, approximations, and applications in the electricity markets. The main themes center around ACOPF modeling fundamentals, followed by local and global solution methods for a variety of applications in the electricity markets. Original contributions of these essays include an alternative formulation of the ACOPF, a successive linear programming algorithm to solving the ACOPF for the real-time energy

market, an outer approximation method to solving integrated ACOPF-unit commitment as a mixed-integer linear program for the day-ahead market, and applications of convex relaxations to the ACOPF and its approximations for the purpose of globally optimal storage integration. These contributions are concluded with a discussion of potential future directions for work.

Academic Co-advisor and Reader:

Dennice F. Gayme, Assistant Professor

Department of Mechanical Engineering

The Johns Hopkins University

Academic Co-advisor and Reader:

Benjamin F. Hobbs, Schad Professor of Environmental Management

Department of Geography and Environmental Engineering

The Johns Hopkins University

Reader:

Sauleh Siddiqui, Assistant Professor

Department of Civil Engineering

The Johns Hopkins University

Dedication

For my husband Mashama, our son Kamali, and our baby girl: A dedication isn't enough, but it's a start.

Acknowledgements

The struggle has been real and my success is not mine alone.

I thank my family for their motivation and belief in me, because behind every worthwhile success are lifelong lessons and failures, many that have challenged me to work harder and stay persistent.

I have had the rare, enlightening, and fortunate opportunity to work with a powerhouse trifecta: my co-advisor Dennice Gayme, my other co-advisor Ben Hobbs and my supervisor Dick O'Neill. I thank you for giving profusely in your mentorship role, which has been principle to my success and has inspired me to pay it forward.

I thank Jean-Paul Watson for facilitating research development and strong synergies with other practitioners in the field.

I thank my coauthors Dennice Gayme, Xinyi Jiang, Carl Laird, Paula Lipka, César Silva-Monroy, Dick O'Neill, Shmuel Oren and Jean-Paul Watson for their excellence in the publications related to the enclosed works.

I thank my third dissertation committee member Sauleh Siddiqui who has provided encouraging and insightful feedback on my research presentations and proposals throughout the years.

I thank Brent Eldridge, Roderick Go, Robin Hytowitz, Saamrat Kasina, Francisco Muñoz, Venkat Prava and Andrea Staid for their companionship and collegiality in this grad school journey.

I am eternally grateful to my husband Mashama McFarlane, who says to me when life gets hard: "to those whom much is given, much is expected." And so, true to our undergrad alma mater, 'my heart is in the work' (Andrew Carnegie). I love my profession, I thank those individuals mentioned here along with those along the way who also gave me a chance, and I hope to have the opportunity to make meaningful contributions in the lives of others.

This work was made possible by the Heath fellowship, the NSF graduate research supplement to the U.S. NSF EFRI Grant 0835879, the U.S. NSF Grant IIA-1243482 (WINDINSPIRE), Sandia National Laboratories, and the Federal Energy Regulatory Commission.

Contents

CONTENTS

CONTENTS

List of Tables

List of Figures

List of Symbols

A	Ampere
AC	Alternating Current
ACPF	Alternating Current Power Flow
ACOPF	Alternating Current Optimal Power Flow (synonymous with OPF)
ACOPF+S	ACOPF with Storage Model
BD	Benders Decomposition
CAISO	California Independent System Operator
DC	Direct Current
DCPF	Direct Current Power Flow (not a PF for a DC network)
DCOPF	Direct Current Optimal Power Flow (not an OPF for a DC network)
DCOPF+S	DCOPF with Storage Model
DOE	Department of Energy
ED	Economic Dispatch
ERCOT	Electric Reliability Council of Texas
ESS	Energy Storage System
FACTS	Flexible AC Transmission System
FERC	Federal Energy Regulatory Commission
GBD	Generalized Benders Decomposition
GRG	Generalized Reduced Gradient
ISO	Independent System Operator
ISO-NE	Independent System Operator of New England
IV	Current-Voltage
KCL	Kirchhoff's Current Law (First Law)
KKT	Karush-Kuhn-Tucker
KVL	Kirchhoff's Voltage Law (Second Law)
ℓ-DCOPF+S	Lossy DCOPF with Storage Model
LMI	Linear Matrix Inequality
LMP	Locational Marginal Price
LP	Linear Programming
LR	Lagrange Relaxation
MILP	Mixed Integer Linear Programming
MINLP	Mixed Integer Nonlinear Programming
MIP	Mixed Integer Programming (synonymous with MILP)

LIST OF SYMBOLS

MISO	Midwest Independent System Operator
MW	Mega Watt
MVAr	Mega Volt-Ampere reactive
NERC	North American Electric Reliability Corporation
NP	Non-Deterministic Polynomial-Time
NLP	Nonlinear Programming
NYISO	New York Independent System Operator
O&M	Operation and Maintenance
OA	Outer Approximation
OATT	Open Access Transmission Tariff
OPF	Optimal Power Flow (synonymous with ACOPF)
PJM	PJM Interconnection LLC
PTDF	Power Transfer Distribution Factor
p.u.	Per Unit
pwl	Piecewise Linear
RMSE	Root Mean Squared Error
RTO	Regional Transmission Operator
RUC	Residual Unit Commitment
SCED	Security-Constrained Economic Dispatch
SCUC	Security-Constrained Unit Commitment
SDP	Semidefinite Programming
SDR	Semidefinite Relaxation
SLP	Successive (Sequential) Linear Programming
SQP	Sequential Quadratic Programming
SOCP	Second Order Conic Programming
SOCR	Second Order Conic Relaxation
QCQP	Quadratically Constrained Quadratic Program
UC	Unit Commitment
UC+ACOPF	Unit Commitment with ACOPF Constraint Set
UC+DCOPF	Unit Commitment with DCOPF Constraint Set
VAr	Volt-Ampere reactive; a unit measurement of reactive power
W	Watt; a unit measurement of real (active) power

List of Nomenclature

Sets

$\mathcal{A}$	Set of adjacent buses
$\mathcal{C}$	Subset of synchronous condensers, $\mathcal{C} \subseteq \mathcal{I}$
$\mathcal{F}$	Set of directional line flows $\{1, \ldots, 2K\}$
Γ	Set of outer loop iterations, $\{1, \ldots, \lvert\Gamma\rvert\}$
$\mathcal{G}$	Subset of thermal generating units, $\mathcal{G} \subseteq \mathcal{I}$
$\mathcal{H}$	Set of successive linear programming iterations $\{1, \ldots, H\}$
$\mathcal{I}$	Set of generating units, $\{1, \ldots, I\}$
$\mathcal{I}(n)$	Set of generating units at node n
$\mathcal{K}$	Set of transmission branches $\{1, \ldots, K\}$
$\mathcal{L}$	Set of piecewise linear segments $\{1, \ldots, L\}$
$\mathcal{N}$	Set of buses $\{1, \ldots, N\}$
$\mathcal{S}_i$	Set of start-up segments, $\{1, \ldots, S\}$, associated with the costs for start-up types (i.e., running from hottest to coldest start [1]) of unit $i \in \mathcal{G}$
$\mathcal{T}$	Set of time periods $\{1, \ldots, T\}$
$\mathcal{W}$	Set of wind farms, $\mathcal{W} \subseteq \mathcal{I}$

Indices

γ	Outer loop iteration; $\gamma \in \Gamma$
h	Successive linear programming iteration $h \in \mathcal{H}$
i	Generating unit index; $i \in \mathcal{I}$
k	Transmission branch $k \in \mathcal{K}$
k'	Monitored flowgate $k' \in \mathcal{K}'^{(h)} \subset \mathcal{K}$
$k\,(n,m)$	Flow $k\,(n,m) \in \mathcal{F}$ on branch k from bus n to m
$k\,(\cdot)$	Bidirectional flows $k\,(\cdot) \in \mathcal{F}$ on branch k
$k\,(n,\cdot)$	Withdrawals from bus n
$k\,(\cdot,n)$	Injections into bus n
l	Piecewise linear segment $l \in \mathcal{L}$
n, m	Bus (node) indices $n, m \in \mathcal{N}$
t	Time period $t \in \mathcal{T}$

Variables

$b_{i,t}$	Binary equal to 1 if unit i is online in time t
$b^u_{i,t}$	Binary equal to 1 if unit i is started up in time t
$b^d_{i,t}$	Binary equal to 1 if unit i is shut down in time t
$b^0_{i,s,t}$	Binary equal to 1 if unit i is in start-up timeframe s in time t
$c^d_{i,t}$	Shut-down cost for unit i in time t
$c^u_{i,t}$	Start-up cost for unit i in time t
c_n	Energy storage capacity at bus n
i	Nodal current phasor vector
$i^r_{n,t}$	Real part of current injection at bus n in time t
$i^j_{n,t}$	Imaginary part of current injection at bus n in time t
$i_{k(\cdot),t}$	Bidirectional current phasors on branch k in time t
$\lvert i_{k(\cdot),t}\rvert$	Bidirectional current magnitudes on branch k in time t
$i^{sq}_{k(\cdot),t}$	Linearization of $\left(\lvert i_{k(\cdot),t}\rvert\right)^2$
$i^r_{k(\cdot),t}$	Real part of bidirectional current flows on branch k in time t
$i^j_{k(\cdot),t}$	Imaginary part of bidirectional current flows on branch k in time t in time t
$i^{viol,+}_{k(\cdot),t}$	Violation slack variable on thermal line limit for flow $k(\cdot)$ in time t
p	Real power vector
$p^g_{i,t}$	Total real power generation from unit i in time t
$p^{g\Delta}_{i,t}$	Real power generation above P^{min}_i from unit i in time t
$p^g_{i,l,t}$	Linear segment l of real power generation from unit i in time t
$p^{viol,+}_{i,t}$	Violation slack variable on real power upperbound for unit i in time t
$p^{viol,-}_{i,t}$	Violation slack variable on real power lowerbound for unit i in time t
$p_{n,t}$	Total real power generation from units at bus n in time t
$p^\ell_{k,t}$	Real power losses on branch k in time t
$p_{k(\cdot),t}$	Bidirectional real power transfers on branch k in time t
$\hat{p}_{k(\cdot),t}$	Approximations of bidirectional real power transfers (including flows and losses) on branch k in time t
$\tilde{p}_{k(\cdot),t}$	Approximations of bidirectional real power flows on branch k in time t
$\tilde{p}^\ell_{k,t}$	Real power loss approximation for the bidirectional flow on branch k
q	Reactive power vector
$q^g_{i,t}$	Total reactive power from unit i in time t
$q^{viol,+}_{i,t}$	Violation slack variable on reactive power upperbound for unit i in time t
$q^{viol,-}_{i,t}$	Violation slack variable on reactive power lowerbound for unit i in time t
$q_{n,t}$	Total reactive power from units at bus n in time t
$q^{\epsilon,+}_{n,t}$	Positive reactive power load mismatch at bus n in time t
$q^{\epsilon,-}_{n,t}$	Negative reactive power load mismatch at bus n in time t
$q_{k(\cdot),t}$	Bidirectional reactive power flows on branch k from bus n to m in time t
$r^c_{n,t}$	Power charging rate for storage at bus n in time t
$r^d_{n,t}$	Power discharging rate for storage at bus n in time t
s	Apparent power vector

$s_{n,t}$	Energy storage level for technology j at bus n in time t
$\theta_{n,t}$	Voltage angle at bus n in time t
$\theta_{nm,t}$	Voltage angle difference between bus n and bus m in time t
$\Theta_{nm,t}$	Slack variable on the voltage angle difference between bus n and bus m in time t
$\tilde{\Theta}_{nm,t}$	Matrix on the voltage angle difference between bus n and bus m in time t
v	Nodal voltage phasor vector
$v_{n,t}$	Voltage phasor at bus n in time t
$\lvert v_{n,t}\rvert$	Voltage magnitude at bus n in time t
$v_{n,t}^{sq}$	Linearization of $(\lvert v_{n,t}\rvert)^2$
$v_{n,t}^{r}$	Real part of the voltage phasor at bus n in time t
$v_{n,t}^{j}$	Imaginary part of the voltage phasor at bus n in time t
$v_{n,t}^{viol,+}$	Violation slack variable on voltage magnitude upperbound for node n in time t
$v_{n,t}^{viol,-}$	Violation slack variable on voltage magnitude lowerbound for node n in time t
$v_{n,t}^{\epsilon,+}$	Positive voltage slack for node n in time t
$v_{n,t}^{\epsilon,-}$	Negative voltage slack for node n in time t
$z_{n,t}$	Reactive power compensation for storage at bus n in time t

Dual Variables

$\underline{\alpha}_{i,t}$	Lagrange multiplier on wind real power production lowerbound at unit i in time t
$\overline{\alpha}_{i,t}$	Lagrange multiplier on wind real power production upperbound at unit i in time t
$\underline{\beta}_{n,t}$	Lagrange multiplier on energy storage capacity lowerbound at bus n in time t
$\overline{\beta}_{n,t}$	Lagrange multiplier on energy storage capacity upperbound at bus n in time t
$\underline{\delta}_{i,t}$	Lagrange multiplier on thermal generator real power ramping lowerbound at unit i in time t
$\overline{\delta}_{i,t}$	Lagrange multiplier on thermal generator real power ramping upperbound at unit i in time t
$\gamma_{n,t}$	Lagrange multiplier on energy storage level balance at bus n in time t
$\overline{\kappa}_{k(\cdot),t}$	Matrix scalar of the Lagrange multiplier on the LMI for the bidirectional apparent power flow limits on branch k in time t
$\lambda_{n,t}$	Lagrange multiplier on nodal real power balance (i.e., the LMP) at bus n in time t
$\underline{\lambda}_{i,t}$	Lagrange multiplier on thermal generator real power production lowerbound at unit i in time t
$\overline{\lambda}_{i,t}$	Lagrange multiplier on thermal generator real power production upperbound at unit i in time t

$\mu^{g}_{i,t}$	Matrix scalar of the Lagrange multiplier on the LMI for the generator cost function at unit i in time t
$\mu^{w}_{i,t}$	Matrix scalar of the Lagrange multiplier on the LMI for the wind farm cost function at unit i in time t
$\mu^{s}_{n,t}$	Matrix scalar of the Lagrange multiplier on the LMI for the storage cost function at unit i in time t
ϕ	Lagrange multiplier on the overall energy storage capacity installed in the network
$\underline{\psi}_{n,t}$	Lagrange multiplier on storage reactive power dispatch lowerbound at bus n in time t
$\overline{\psi}_{n,t}$	Lagrange multiplier on storage reactive power dispatch upperbound at bus n in time t
$\underline{\rho}_{n,t}$	Lagrange multiplier on storage charging lowerbound at bus n in time t
$\overline{\rho}_{n,t}$	Lagrange multiplier on storage charging upperbound at bus n in time t
$\underline{\sigma}_{n,t}$	Lagrange multiplier on storage discharging lowerbound at bus n in time t
$\overline{\sigma}_{n,t}$	Lagrange multiplier on storage discharging upperbound at bus n in time t
$\varkappa_{n}$	Lagrange multiplier on the terminal storage level constraint for the energy storage at bus n
$\varphi_{n,t}$	Lagrange multiplier on nodal reactive power balance (i.e., the Q-LMP) at bus n in time t
$\underline{\varphi}_{i,t}$	Lagrange multiplier on thermal generator reactive power production lowerbound at unit i in time t
$\overline{\varphi}_{i,t}$	Lagrange multiplier on thermal generator reactive power production upperbound at unit i in time t
$\underline{\vartheta}_{n,t}$	Lagrange multiplier on nodal voltage lowerbound at bus n in time t
$\overline{\vartheta}_{n,t}$	Lagrange multiplier on nodal voltage upperbound at bus n in time t

Parameters

B	Nodal susceptance matrix
B^{MVA}	Power base in MVA
B^{0}_{i}	Binary equal to 1 if unit i is online at time 0
b_{k}	Series susceptance of branch k
b^{s}_{kn}	Shunt susceptance on the bus n-side of branch k
B^{s}_{n}	Shunt susceptance at bus n
$C^{g,0}_{i}$	Nonnegative fixed cost coefficient for generating unit i
$C^{g,1}_{i}$	Nonnegative linear cost coefficient for generating unit i
$C^{g,2}_{i}$	Nonnegative quadratic cost coefficient for generating unit i
$C^{s,1}_{s}$	Nonnegative linear cost coefficient for storage at bus n
$\overline{C}^{d}_{i}$	Nonnegative shut-down capability for unit i
$\overline{C}^{u}_{i}$	Nonnegative start-up capability for unit i

$\underline{C}_n$	Minimum energy storage capacity at bus n
$C^w_{i,t}$	Power output availability for wind farm i in time t
$C^g_{i,l}$	Nonnegative linear segment l of the quadratic cost for unit i
δ^ϵ_n	Mismatch penalty factor on branch k
η^c_j	Storage charging efficiency for technology j
η^d_j	Storage discharging efficiency for technology j
G	Nodal conductance matrix
g_k	Series conductance of branch k
g^s_{kn}	Shunt conductance on the bus n-side of branch k
G^s_n	Shunt conductance at bus n
$\overline{I}_k$	Maximum current magnitude (thermal capacity limit) on branch k
I^ϵ_k	Current penalty factor on branch k
K^d_i	Shut-down cost of unit i
$K^u_{i,s}$	Start-up cost of unit i in segment s
ϕ_{kn}	Phase-shifter on the bus n-side of branch k
P^0_i	Power generated by unit i at $t = 0$
$\overline{P}_i$	Maximum real power generation for unit i
$\underline{P}_i$	Minimum real power generation for unit i
$P^d_{n,t}$	Real power demand at bus n
P^r_t	Reserve requirements
P^ϵ_n	Real power penalty factor at bus n
$P^g_{i,l}$	Maximum length of piecewise segment l from unit i
$Q^d_{n,t}$	Reactive power demand at bus n
Q^ϵ_n	Reactive power penalty factor at bus n
$\overline{Q}_i$	Maximum reactive power generation for unit i
$\underline{Q}_i$	Minimum reactive power generation for unit i
$\overline{R}^c_n$	Maximum power charge rating for storage at bus n
R^d_n	Maximum power discharge rating for storage at bus n
r_k	Series resistance of branch k
RR^d_i	Ramp down limit for unit i
RR^u_i	Ramp up limit for unit i
$\overline{S}_k$	Apparent power flow limit on branch k
τ_{kn}	Ideal transformer on the bus n-side of branch k
$\lvert\tau_{kn}\rvert$	Transformer turns ratio on the bus n-side of branch k
$\underline{\Theta}_{nm}$	Lower bound on angle difference between interconnected buses n and m
$\overline{\Theta}_{nm}$	Upper bound on angle difference between interconnected buses n and m
$\overline{T0}^d_i$	Initial time periods the unit i has been offline before the scheduling horizon
$\overline{T0}^u_i$	Initial time periods the unit i has been online before the scheduling horizon
$T0^d_i$	Initial time periods the unit i must be offline
$T0^u_i$	Initial time periods the unit i must be online
T^d_i	Minimum downtime for unit i
$T^l_{i,s}$	Start-up lag to define the length of segment s

T_i^u	Minimum uptime for unit i
V_n^ϵ	Voltage penalty factor at bus n
$\underline{V}_n$	Minimum voltage magnitude at bus n
$\overline{V}_n$	Maximum voltage magnitude at bus n
$V_{n,t}^{(h)}$	Step-size bound on the voltage at bus n time t in iter h
x_k	Series reactance of branch k
Y^k	Unified branch admittance matrix for k
Y	Nodal admittance matrix
y_k	Series admittance of branch k
y_{kn}^s	Shunt admittance on the bus n-side of branch k
Y_n^s	Shunt admittance at bus n
z_k	Impedance of branch k

1 Introduction

1.1 Background and Motivation

Computational advancements are enabling independent system operators (ISOs) and regional transmission operators (RTOs) to adopt more efficient market designs. Unlike other commodities, electricity markets have strict physical constraints related to the network structure, Kirchhoff's laws, and electric power technologies. The alternating current optimal power flow (ACOPF) problem, also referred to as the optimal power flow (OPF)[1] problem, simultaneously co-optimizes real (MW)[2] and reactive (MVAr)[3] power dispatch to promote reliable system operation and market efficiency. The ACOPF formulation is a nonconvex, nonlinear optimization problem, which is known to be non-deterministic polynomial-time (NP) hard [2, 3]; discrete variables, e.g., to represent equipment state controls, generator unit commitments and network topology control, further complicate the ACOPF. The ACOPF originated from Carpentier's reformulation of the economic dispatch problem based on the Karush-

[1] ACOPF and OPF are used synonymously and interchangeably throughout this work to denote the full optimal power flow problem for AC networks, whereas approximations of the OPF problem are otherwise denoted.

[2] Mega Watt

[3] Mega Volt-Ampere reactive

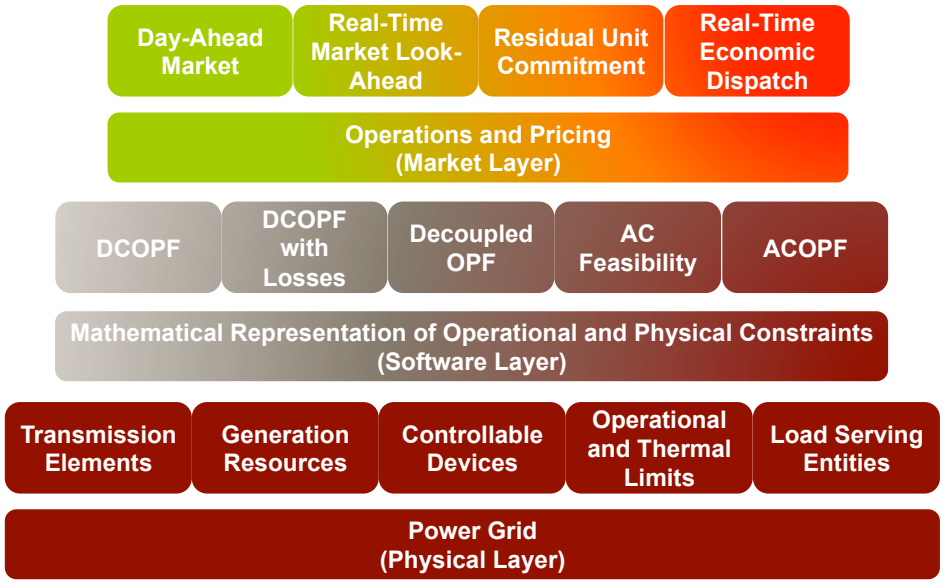

Figure 1.1: *Real-world OPF-based applications.* Green in the upper heat map denotes up to a 24-hour lead time for the decision making process, whereas red denotes an increase in the time-criticality. In the middle heat map, grey denotes highly approximated mathematical representations whereas dark red denotes the most representative mathematical programming-based formulation of steady-state operations in AC networks. The lower heat map is in solid dark red to indicate the actual AC network.

Kuhn-Tucker (KKT) conditions in 1962 [4]. Today, over 50 years after the problem was formulated, there is still no fast and robust solution technique for the full ACOPF. Instead ISOs and RTOs leverage approximations along with commercial mixed-integer linear programming (MILP) commercial solvers to ensure convergence and computation of prices within acceptable timeframes. For the purpose of this discussion, the ISO/RTO *market software* is defined as follows: *The modeling and solution techniques applied to implement the day-ahead, intra-day, and real-time markets.*

In practice, the application of approximations, decompositions and engineering judgment are applied to obtain solutions within reasonably acceptable runtimes [5,6],

as depicted in Figure 1.1. The locational marginal price (LMP), which is central to market settlements in the U.S. electricity markets, is a function of both time and location and can be disaggregated into the following three components for a given terminal bus [7]:

1. The price of the next incremental unit of energy at the reference bus;

2. The marginal congestion cost associated with delivering energy from the reference bus to the terminal bus;

3. The marginal losses cost associated with delivering energy from the reference bus to the terminal bus.

Fundamentally, the LMP reflects parallel flows by respecting Kirchhoff's current law[4] (KCL) and Kirchhoff's voltage law[5] (KVL). Mathematically, the LMP corresponds to the marginal value of the real power balancing constraint. The real power balancing is affected by resource constraints such as ramp rates and minimum operating levels as well as reliability requirements (e.g., nodal voltage limits and angle difference limits). Furthermore, start-up and no-load costs make the price of the next incremental unit of energy more complicated and therefore the market software becomes more complex.

ISOs/RTOs frequently use a linear approximation of the OPF called the DCOPF [6,8]. The DCOPF is computationally tractable but does not include all the physical constraints in the LMP; finding ways to account for these constraints is an ongoing

[4]The sum of all current flowing out of and into a given bus is zero.
[5]The total voltage change around a closed loop must be zero.

challenge. In DC-based algorithms, the power flow constraints linearly relate the MW controls to the real power flows on the network, and as a result optimal MVAr dispatch is neglected. Then alternating current (AC) feasibility, which is the physical feasibility of the injections and withdrawals on an AC network, is tested through an iterative process with metaheuristics in order to ensure that a realistic engineering solution is obtained [6]. Such approaches become ineffective when the system is stressed; for example, when there is a strong physical coupling between real and reactive power availability (e.g., when the system is operating along the boundary of a generator capability curve), when voltage drops restrict real power dispatch, or when reactive power compensation can increase the network throughput. In fact, the ACOPF is the only AC-based problem that simultaneously co-optimizes real and reactive power dispatch for steady-state operations.

Currently, security constrained economic dispatch (SCED) is the basic way that all ISOs and RTOs (or utilities) dispatch resources to meet electricity load, and is defined as: "the operation of generation facilities to produce energy at the lowest cost to reliably serve consumers, recognizing any operational limits of generation and transmission facilities" [9]. The "security" aspect of the SCED requires that flows are within reliability limits and the voltages within stability ranges. The SCED algorithm is implemented differently in each ISO but typically includes a DCOPF with a

AC feasibility check [6]. The SCED is used in the day-ahead,[6] intra-day,[7] and real-time[8] markets of ISOs in order to balance the trade-offs between economic value and reliability requirements. Adjustments occur as often as every five minutes in some markets and can result in corrective actions such as curtailing transmission service or energy schedules, adjusting operating equipment (e.g., generators, phase shifters, breakers), or shedding firm load in order to alleviate operating emergencies to meet North American Electric Reliability Corporation (NERC) standards [12]. Furthermore, some system operators plan for N-1-1 contingencies;[9] when N-1-1 resources are secured outside of the security constrained unit commitment (SCUC) and SCED, these additional units are unrepresented in the market software and can negatively impact market settlements.

The SCUC is applied in the day-ahead market prior to the SCED and determines committed resources based on load forecasting, intermittent energy resource forecasting, and transmission constraints. In selecting the most economic generation mix, the SCUC accounts for each generator's bid offer, including start-up, shut-down and production costs, as well as its physical operating characteristics, including ramp rates,

[6]The day-ahead energy market enables market participants to commit to buy or sell wholesale electricity one day before the operating day to mitigate price volatility that may occur at time of use [10].

[7]The intra-day market enables market participants to adjust their day-ahead schedules at predetermined times during delivery day [11].

[8]The real-time market enables market participants to buy and sell wholesale electricity during the course of the operating day by balancing the differences between the day-ahead commitments and the actual real-time demand for and production of electricity. The real-time locational marginal price (LMP) produces a separate financial settlement, which is either paid or charged to participants in the day-ahead market for demand or generation that deviates from the day-ahead commitments [10].

[9]a second contingency that occurs quickly after a primary contingency

power rating, minimum runtime, and environmental restrictions. The "security" aspect of the SCUC accounts for how forecasted conditions can affect system reliability, network line capacity, and facility outages. After the day-ahead market takes place, a residual unit commitment (RUC) is performed in the intra-day market[10] in order to address: (1) resource gaps; (2) reliability issues; and (3) other operational issues as a result of uncertainty (e.g., weather and load forecast uncertainty) [13]. The RUC normally maintains the commitment and dispatch determined in the day-ahead market and either increases the dispatch levels of units that are already committed or makes additional commitments; this intra-day market minimizes the additional costs associated with any incremental commitments beyond the day-ahead schedule [13].

Since the approximations in both the SCED and SCUC can oversimplify the physical problem, operators intervene to satisfy reliability requirements and other physical constraints that are unrepresented in the market software. The Federal Energy Regulatory Commission (FERC) recently reported that uplift, which represents out-of-market payments that result when a higher generation cost is incurred and possibly other lower cost units are reduced in order to relieve a constraint [14], can arise due to the inability of ISOs to fully model the physical constraints on an AC network [15]. As a result, certain resources are consistently committed outside of the market to address reliability issues; this results in concentrated uplift payments [15]. Such resources are often required for reactive power compensation in order to provide system

[10]Excluding New York ISO (NYISO), which integrates the RUC into the day-ahead market.

voltage control that enables more efficient delivery and utilization of real power [16]. However, there is currently no uniform approach across the U.S. electricity markets for remunerating resources for reactive power capability and dispatch. In some markets, the out-of-market commitments corresponding to reactive power compensation are included into the day-ahead schedule; for further details see [13]. Although these resources normally do not set the clearing price,[11] the clearing price can be affected because these out-of-market commitments displace resources that have lower costs for providing real power dispatch. As a result these out-of-market commitments are more likely to require uplift payments. In the real-time market, operators may also have to manually commit and dispatch a resource that is needed to resolve a constraint, while also manually re-dispatching or de-committing other resources.[12]

The Joint Board on Economic Dispatch for the Northeast Region stated in 2006 that some operational constraints are not fully represented within the current software, and the benefits of economic dispatch can be negatively impacted if all the available services and products are not accurately considered [9]. Inaccuracies in the market software and the subsequent operator intervention cause economic inefficiencies due to suboptimal dispatch in the short term and misplaced incentives for long term decision making.

By improving the DCOPF through the addition of an AC feasibility check that

[11] The out-of-market commitments are absent from the day-ahead schedule because such resources are not cost effective given that the reliability requirements are unmodeled.

[12] e.g., exceptional dispatches in California ISO (CAISO) [17], out-of-merit generation in New York ISO (NYISO) [18], and balancing operating reserves in PJM Interconnection LLC (PJM) [19]

is utilized in the SCED and SCUC, voltage and reactive power schedules that are physically feasible may be obtained. Ideally, incorporating the ACOPF directly into the SCED and SCUC would result in the optimal real and reactive power schedules. However given the nonconvex nature of the ACOPF, there may be formidable challenges with current computing power to solve the nonlinear program (NLP) directly on a large-scale (10,000+ nodes) power system within the operational time frames required for the day-ahead, intra-day, and real-time markets. Furthermore, the presence of stationary points in the solution space (i.e., local optima and saddlepoints) that are not a global optimum may result in prices that do not cover the system costs.[13] Until optimization techniques can be applied to obtain a global optimum of the ACOPF in practice, approaches to make current practices more accurate and tractable are also desirable. Along those lines, research in both local and global solution methods to solve the ACOPF, as well as alternative ways to formulate and approximate the ACOPF, are all paths to advancement.

A report to Congress prepared by the U.S. Department of Energy (DOE) states: "the technical quality of current economic dispatch tools–software, data, algorithms, and assumptions–deserves scrutiny. Any enhancements to these tools will improve the reliability and affordability of the nation's electricity supplies" [20]. Reports by the FERC concluded that since the cost of upgrading existing ISO market software is less than $10 million dollars [6] and small increases in the economic efficiency of

[13]Revenue adequacy is also an issue for generator start-up and shut-down costs, which are nonconvex and discrete.

dispatch can be measured in billions of dollars per year, the potential benefit-to-cost ratio of better market software is at least 100 fold [21].

As discussed above, ignoring or approximating the AC network can result in a divergence between the solution and actual operating conditions. As a result, the present market software may compute market settlements based on assumptions that do not reflect the true marginal value of the products and services being bought and sold in electricity markets. Historically, continual operator intervention has been necessary to correct problems arising because the market software can not physically dispatch and price resources in a manner that respects unrepresented physical constraints. To conclude, the essays in this work address a variety of aspects related to the core issues presented above.

1.2 Scope and Outline

This dissertation is a collection of essays on the ACOPF, which can be grouped as follows:

Part 1 *ACOPF Modeling Fundamentals.* The following essay reviews steady-state AC network modeling and then presents a novel ACOPF formulation that is proven to be equivalent to canonical ACOPF formulations.

- *Chapter 2.2. The ACOPF Problem and its Formulations*: This primer extends the numerous concepts discussed in the "Background and Motivation" section of Chapter 1 by discussing the history of ACOPF so-

lution techniques in more detail. It then establishes a modeling framework for the ACOPF formulation and its approximations, including a proposed IV-ACOPF formulation that has a different mathematical representation from canonical ACOPF formulations but is provably equivalent. In particular, the IV-ACOPF computes linear current flows based on the current injections method and then balances the nodal power injections and withdrawals through nonconvex constraints that relate the bilinear terms within each node, whereas the canonical ACOPF formulations compute the nonlinear and nonconvex apparent power flows. This work was originally published in [22].

Part 2 *Local Solution Methods.* These essays propose improved formulations of and solution techniques for the ACOPF problem for applications in economic dispatch (ED) and unit commitment (UC).[14]

- *Chapter 3. A Successive Linear Programming Approach to Solving the IV-ACOPF*: A successive linear programming (SLP) approach is proposed to solve the IV-ACOPF. The SLP IV-ACOPF leverages commercial linear programming (LP) solvers and can be readily extended and integrated into more complex decision processes, e.g., unit commitment and transmission switching. This work demonstrates an acceptable quality of convergence to a best-known solution and linear scaling

[14]Certain security constraints, e.g., forecast uncertainty, are omitted due to lack of data.

of computational time in proportion to network size. Moreover, the time complexity of the SLP algorithm outperforms that of the NLP commercial solvers for the full range of test networks. As a result, the SLP algorithm is expected to outperform the NLP solvers tested, i.e., IPOPT and KNITRO, on larger scale networks. Furthermore, the SLP algorithm could be applied in parallel with both Gurobi and CPLEX from various starting points, which may further improve the reported linear time complexity. I originally published this work in [22].

- *Chapter 4. The Unit Commitment Problem with AC Optimal Power Flow Constraints*: A mathematical programming-based approach to optimize the unit commitment problem with ACOPF constraints is proposed in this study. An outer approximation method is proposed to solve this nonconvex mixed-integer nonlinear program (MINLP). The solution technique simultaneously co-optimizes real and reactive power scheduling and dispatch subject to both unit commitment constraints and ACOPF constraints. The proposed approach is a local solution method that incorporates the SLP IV-ACOPF proposed in Chapter 3 in order to leverage powerful linear and mixed-integer commercial solvers. This work demonstrates the relative economic and operational impact of more accurate ACOPF constraint modeling on the unit commitment problem, when compared to copperplate and DCOPF approaches. Fur-

thermore, a DCOPF approach including real power losses and another DCOPF approach with a RUC-based routine are also modeled and included in the analysis. The results indicate considerable divergence between the market settlements and the stability and reliability requirements when overly approximated network models are assumed. The computational speeds for both the ACOPF and the ACOPF for RUC approaches are promising: the ACOPF approach is 5×–15× slower than the DCOPF approach and incorporating the RUC to the DCOPF approach is 1.5×–5× slower than the DCOPF alone. Since the proposed OA method spends most of the computational time in the single iteration of the master problem, further improvements to the MILP and leveraging decomposition techniques for distributed, parallel optimization could lead to significant gains. This work was initially published in [23].

Part 3 *Global Solution Methods.* These essays propose novel applications, new formulations, and theoretical properties to optimal storage integration in AC networks.

- *Chapter 5. Energy Storage for Transmission System VAr Support: Trade-offs Between Grid Benefits and Storage Operator Profit*: This work examines trade-offs that arise when energy storage systems provide reac-

tive power (VAr) support on the transmission system in addition to traditional power and energy services. The ACOPF with storage model is formulated and then the semidefinite relaxation (SDR) proposed in [24] is applied; the SDR is a convex problem for which theoretical properties can be derived under strong duality [25]. The main contribution uses a novel analytical approach to relate the energy storage system (ESS) services, including power, energy, and reactive power compensation, to its profits through nodal pricing theory. The analysis demonstrates that energy storage operators can make substantially higher profits by providing not only power and energy services but also reactive power compensation. This study also compares payments based on the nodal prices for reactive power to the remuneration approaches in current market practice. The results demonstrate that there may be a disincentive for storage operators to provide this service if it is not adequately paid for in the market. The results highlight the tight connections between market design and the financial viability of large-scale storage integration in the power system. The proposed framework can be extended to incorporate other valuable ESS services (e.g., regulation)[15] as well as further to investigate market design for reactive power compensation. This work is an extension of a conference proceeding [26].

[15]Regulation service is the continuous balancing of resources with load in order to control system frequency.

- *Chapter 6. The Role of Network Losses in Optimal Storage Allocation*: A DCOPF with losses formulation is proposed in order to analyze how real power losses improve the DCOPF approach for optimal storage integration in AC networks when storage is remunerated for power and energy services but for not reactive power compensation, as is the case for most ESS installations in current market design. This work incorporates quadratic loss approximations derived from the AC power flows (ACPF); the resulting formulation of the DCOPF with losses and storage model is a nonconvex quadratically constrained quadratic program (QCQP). Both a SDR and a second-order cone relaxation (SOCR) are proposed to reformulate the original QCQP as a convex problem. The main theoretical results prove that both of these relaxations provide an exact lower bound to the original QCQP. The work demonstrates that costs due to real power losses are a key component of the LMP and therefore are critical in determining optimal ESS dynamics and allocation. This work can be extended to provide an analytical model for losses for a variety of other applications. This work is an extension of a conference proceeding [27].

These essays are the central contributions of the dissertation. Then Chapter 7 completes the dissertation with concluding remarks including a summary of the main contributions, limitations of the current work, and future extensions.

I ACOPF Modeling Fundamentals

2 The ACOPF Problem and its Formulations

2.1 Introduction

The field of power engineering deals with the generation, transmission, distribution and utilization of electric power. Essentially the power grid is an electric system that transfers power from generators to demand (load). This system has been analyzed as an undirected network from a graph-theoretic perspective where the generators and loads map to buses (also referred to as nodes) that represent sources and sinks, respectively, and are connected by branches which are arcs that transmit power between the buses in the network.

To understand the notions of operation and efficiency, a circuit-based mathematical model of the network is applied to understand how power and current flow in a power grid. The U.S. electric grid is mostly an AC system,[16] meaning that voltage[17] (v) and current[18] (i) are assumed to be sinusoidal wave patterns that cycle at a constant of 60 times per second (or 60 Hertz). Technically the system can be represented

[16] e.g., DC power lines, also referred to as "asynchronous links," connect the Eastern Interconnect, Western Interconnect, and the Texas grid (ERCOT)

[17] Potential electrical energy, i.e., energy/charge, expressed in Volt (V).

[18] Rate of movement of charge, i.e., charge/time, expressed in Ampere (A).

with phasors when a constant frequency is assumed. Therefore apparent power[19] is the measure of power on an AC system and is the product of the phasor value of voltage and phasor value of the complex conjugate of current; apparent power (s) is a complex number representing both active[20] (p) and reactive[21] (q) power, i.e.,

$$s = p + \mathbf{j}q = \text{diag}(v)i^* \tag{2.1}$$

where the complex number form is denoted with $\mathbf{j} \coloneqq \sqrt{-1}$, * denotes the complex conjugate, $\text{diag}(\cdot)$ denotes the square diagonal matrix with the entries of the vector argument on its diagonals, and vectors are written as column vectors by default. The analysis of apparent power on AC networks is the basis of this dissertation work. The analysis of AC networks is grounded in the law of conservation of complex power, where the amount of energy going into the circuit must equal the amount of energy coming out of the circuit at any instant.

Following a brief history of the ACOPF problem, this chapter introduces some of the basic power engineering principles and mathematical programming approaches to analyzing steady-state operations on AC networks. This overview is foundational to the work presented in this dissertation; a more thorough treatment can be found in e.g., [8, 28–32]. The end of this chapter proposes the IV-ACOPF formulation; an

[19] The measure of AC power, i.e., energy per unit time, in Volt-Amperes (VA).

[20] Also referred to as real power, produced when the current waveform is in phase with the voltage waveform, expressed in Watt (W).

[21] Produced when the current waveform is out of phase with the voltage waveform, expressed in Volt-Amperes reactive (VAr).

original proof of mathematical equivalence to canonical ACOPF formulations is also presented.

2.2 History of the ACOPF Problem

There are three types of problems commonly referred to in the power systems literature: the power flow (or load flow), economic dispatch, and optimal power flow. These terms are defined below.

1. The *power flow* or *load flow* determines a solution to the set of power balance equations for an electric system for a given load. Power flow methods find a mathematically but not necessarily physically feasible or optimal solution. The power flow equations themselves do not take into account generator limits or transmission line limits, but these constraints can be incorporated into many power flow solution techniques.

2. *Economic dispatch* describes a variety of formulations to determine the least-cost generation dispatch to serve a given load with a reserve margin, but these formulations simplify or sometimes altogether ignore power flow constraints.

3. The *OPF* finds the optimal solution to an objective function subject to the power flow constraints and other operational constraints, such as generator, transmission, stability, and voltage constraints. Optimal power flow is sometimes referred to as SCED; however most implementations of SCED include

only thermal limits and proxies for voltage limits. For the purpose of this work, the OPF (or ACOPF) is the simultaneous co-optimization of real and reactive power dispatch subject to operational and physical network constraints in order to minimize system operating costs. The DCOPF is a linear simplification that only considers real power and ignores reactive power dispatch; details of the DCOPF are presented in Section 2.6.2.

In the 1930's, the economic dispatch problem was solved analytically using the principle of equal incremental loading; these early computations of economic dispatch were slow [33]. Kirchmayer estimated that it would take 10 minutes of computational time to produce the schedules for a 10 generator system at a given system price [34]. In contrast, ISOs and RTOs today solve economic dispatch for systems of hundreds of generators in a matter of seconds.

As early as 1929, the power flow problem was solved with analog network analyzers in order to simulate power systems prior to the digital era [35]. Ward and Hale published the first automated digital solution to the power flow problem in 1956 [36]. Sasson and Jaimes provide a survey and comparison of early load flow solution methods, which are various iterative methods based on the nodal admittance matrix (Y matrix) or its inverse, the nodal impedance matrix (Z matrix) [35]. Early researchers, including Carpentier, applied the Gauss-Siedel method to solve for the system of equations, whereas the Newton-Raphson method became the commonly applied solution method during the 1960's [37]. Tinney and others made the Newton-Raphson method

more practical to apply on the ACOPF by developing sparsity techniques to take advantage of the structure of the admittance matrix. As a result the ACOPF was solved with both reduced data storage requirements and increased computational speed [38].

Early research on OPF applied classical Lagrangian techniques for the optimality conditions,[22] but neglected bounds on variables [40]. In 1962, Carpentier published the optimality conditions for an OPF including variable bounds, based on the Kuhn-Tucker conditions; this is generally considered the first publication of a fully formulated OPF including the full AC power flow equations, generator apparent power bounds, voltage magnitude bounds, and voltage angle difference bounds for interconnected buses [4]. Carpentier assumed that the applicable functions displayed "suitable convexity" for the Kuhn-Tucker (now referred to as the Karush-Kuhn-Tucker or KKT) conditions[23] for first-order optimality when the linear independence constraint

[22]The variable vector $\tilde{x} \in \mathcal{F}^*$ is a *local minimum* of an arbitrary nonlinear problem $\inf\{f(x)\,|g(x) \leq 0, h(x) = 0, x \in \mathcal{X}\}$ if there exists $\varepsilon > 0$ such that $f(\tilde{x}) \leq f(x)$ for all $x \in \mathcal{B}(\tilde{x}, \varepsilon) \cap \mathcal{F}^*$ where $\mathcal{B}$ defines a ball with center $\tilde{x}$ and radius ε, and $\mathcal{F}^*$ defines the feasible region $\mathcal{F}^* = \{x|g(x) \leq 0, h(x) = 0, x \in \mathcal{X}\}$. If $f(\tilde{x}) \leq f(x)$ for all $x \in \mathcal{F}^*$ then $\tilde{x} \in \mathcal{F}^*$ is a *global minimum* [39].

[23]Consider the general constrained primal problem (P)

$$\begin{aligned} &\min_x f(x) \\ &\text{s.t.} \\ &c_i(x) = 0, i \in \mathcal{E}, \\ &c_i(x) \geq 0, i \in \mathcal{I}, \end{aligned}$$

where $x \in \mathbb{R}^n$, f and the functions c_i are all continuously differentiable, real-valued functions on a subset of $x \in \mathbb{R}^n$, and $\mathcal{I}$ and $\mathcal{E}$ are two finite sets of indices. The Lagrange function for P is defined as: $\mathcal{L}(x, \lambda) = f(x) - \sum_{i \in \mathcal{E} \cup \mathcal{I}} \lambda_i c_i(x)$. Suppose that x^* is a local solution of P and that the linear independence constraint qualification holds at x^*. Then there is a Lagrange multiplier vector λ^*, with components λ_i^*, $i \in \mathcal{E} \cup \mathcal{I}$, such that the following KKT conditions are satisfied at (x^*, λ^*) [41]:

1. $\nabla_x \mathcal{L}(x^*, \lambda^*) = 0$,
2. $c_i(x^*) = 0, \forall i \in \mathcal{E}$ and $c_i(x^*) \geq 0, \forall i \in \mathcal{I}$,
3. $\lambda_i^* \geq 0, \forall i \in \mathcal{I}$ and $\lambda_i^* c_i(x^*) = 0, \forall i \in \mathcal{E} \cup \mathcal{I}$.

qualification[24] (LICQ) holds. Given the structure of the power flow equations, this may be a detrimental assumption because the approach ignores the solution boundary and could result in less robust operations [42]. Then in 1969, Carpentier and Abadie published the generalized reduced gradient method (GRG) [25] for nonlinear constraints. The GRG method is a generalization of Carpentier's "differential injections" method that was originally conceived in 1964 to solve the OPF problem [43]. Since Carpentier's initial contributions, there has been a wealth of research done on algorithms to solve the ACOPF.

Huneault and Galiana provide an extensive survey of optimal power flow literature up to 1991, surveying over 300 articles and citing 163 of these [44]: "The history of optimal power flow (OPF) research can be characterized as the application of increasingly powerful optimization tools to a problem that basically has been well-defined since the early 1960's." Given the mathematical structure and real-world applications of the OPF, this statement still holds today, over half a century after the problem was initially formulated by Carpentier. Throughout the history of OPF research, trends in algorithmic approaches to solving the problem have shadowed the latest

[24]Define the active set $\mathcal{A}(x)$ at any feasible x as that consisting of the equality constraint indices from $\mathcal{E}$ together with the indices of the inequality constraints i for which $c_i(x) = 0$; that is, $\mathcal{A} = \mathcal{E} \cup \{i \in \mathcal{I} | c_i(x) = 0\}$. Given the point x and the active set $\mathcal{A}(x)$, the linear independence constraint qualification holds if the set of active constraint gradients $\{\nabla c_i(x), i \in \mathcal{A}(x)\}$ is linearly independent [41].

[25]Although there are several variations of the generalized reduced gradient method, the basis is a steepest descent method in reduced space where the condition for accepting a new point can be the simple reduction $f(x_{k+1}) < f(x_k)$. The advantage of this approach is that the dimension of the problem is reduced due to variable elimination (i.e., partitioning of variables into basic and nonbasic), and the method can also make use of special problem structures including nonlinear problems with many linear constraints or with sparse structures [41].

developments in nonlinear optimization techniques; surveys of recent developments are provided in [21, 44–51]. However most algorithms to date compute a KKT point that is potentially a local minimum and a handful of more recent algorithms compute a global minimum upon satisfying a sufficient condition, e.g., see [24, 52]; these most recent advancements are summarized in the beginning of Chapter 3. Still the practical extensions to the OPF including transmission contingency constraints (e.g., security constrained OPF) and modeling discrete variables (e.g., unit commitment) pose formidable challenges to computing such OPF solutions quickly and reliably.

2.3 Modeling Assumptions

Asssuming balanced three-phase, steady-state conditions, consider a power network with the set of buses $\mathcal{N} \coloneqq \{1, \ldots, N\}$ and the set of branches $\mathcal{K} \coloneqq \{1, \ldots, K\}$. Each branch k is associated with the ordered pair $(n, m) \in \mathcal{A}$ where $\mathcal{A}$ is the set of interconnected buses $n, m \in \mathcal{N}$. Furthermore, $k\,(n, m)$ is the directional flow on branch k from bus n to bus m for the same ordered bus pair $(n, m) \in \mathcal{A}$ and $k\,(m, n)$ is the directional flow on branch k from bus m to bus n for the ordered bus pair $(n, m) \in \mathcal{A}$, where $k\,(\cdot) = \{k\,(n, m)\,, k\,(m, n)\}$ and $k\,(\cdot) \in \mathcal{F} \coloneqq \{1, \ldots, 2K\}$ where $\mathcal{F}$ is the set of directional line flows. The directional notation of $k\,(\cdot) \in \mathcal{F}$ becomes important depending on the presence of network devices such as transformers and shunts; i.e., the current flows in both directions on a branch k are not symmetric.

2.4 Branch Admittance Matrix

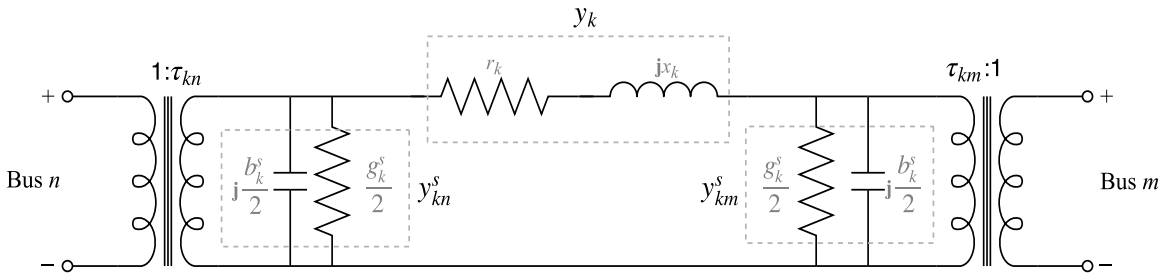

Figure 2.1: The generalized π-model diagram for branch k.

The generalized π-model is shown in Figure 2.1. The series admittance $y_k = g_k + \mathbf{j}b_k$ is equivalent to the inverse of the branch impedance z_k where the series conductance g_k and series susceptance b_k are determined as:

$$g_k = r_k \Big/ \left(r_k^2 + x_k^2\right), \tag{2.2}$$

$$b_k = -x_k \Big/ \left(r_k^2 + x_k^2\right) \tag{2.3}$$

for all transmission lines $k \in \mathcal{K}$.

Furthermore, actual transmission lines that are medium and long distance overhead lines or underground cables can have significant charging currents due to the separation of the conductive material by an insulating medium; as a result there is an effective capacitance between the conductors and potentially a conductance, which is the result of leakage over the surface of the insulating medium. These line characteristics are accounted for with a shunt component $y_k^s = g_k^s + \mathbf{j}b_k^s$ to represent the shunt

susceptance b_k^s (i.e., the reactive capacitance) and the shunt conductance g_k^s. This line shunt is incorporated into the generalized π-model as two equal shunt elements y_{km}^s and y_{kn}^s distributed at each end of line k, assuming homogeneous line parameters along the length of k. Typically the shunt conductance is negligible, which leads to the assumption that only the shunt susceptance is nonnegative, i.e., $g_{kn}^s = g_{km}^s = 0$ and $b_{kn}^s, b_{km}^s \geq 0$.

The π-model can be generalized to incorporate an in-phase or phase-shifting transformer at either the bus n-side or the m-side of branch k; therefore the generalized π-model is defined for each branch $k \in \mathcal{K}$ interconnecting buses n and m according to the ordered pair $(n, m) \in \mathcal{A}$. A practical transformer that is located on the bus n-side of k can be modeled as an ideal transformer with turns ratio $|\tau_{kn}|$ in series with admittance y_k, in order to characterize the resistive losses and leakage flux (i.e., self-resistance). Depending on if τ_{kn} is real or complex, the transformer is in-phase or phase-shifting. If in-phase on the bus n-side of k, then $\tau_{kn} = |\tau_{kn}|$; otherwise for a phase-shift of ϕ_{kn} radians, then $\tau_{kn} = |\tau_{kn}| e^{\mathbf{j}\phi_{kn}} = |\tau_{kn}| \cos\phi_{kn} + \mathbf{j} |\tau_{kn}| \sin\phi_{kn}$ (by Euler's formula). Therefore the generalized branch (primitive) admittance matrix [28] for a π-model for a line or transformer is defined as

$$\begin{bmatrix} Y_{1,1}^k & Y_{1,2}^k \\ Y_{2,1}^k & Y_{2,2}^k \end{bmatrix} := \begin{bmatrix} |\tau_{kn}|^2 (y_k + y_{kn}^s) & -\tau_{kn}^* \tau_{km} y_k \\ -\tau_{kn} \tau_{km}^* y_k & |\tau_{km}|^2 (y_k + y_{km}^s) \end{bmatrix} \tag{2.4}$$

for all $k \in \mathcal{K}$. Note that for modeling a transmission line, $|\tau_{kn}| = |\tau_{km}| = 1$ and

$\phi_{kn} = \phi_{km} = 0$; for an in-phase transformer on the n-side of k, then $y^s_{kn} = y^s_{km} = 0$, $|\tau_{km}| = 1$, and $\phi_{kn} = \phi_{km} = 0$; and for a phase-shifting transformer on the n-side of k, then $y^s_{kn} = y^s_{km} = 0$, $|\tau_{km}| = 1$, and $\phi_{km} = 0$. Furthermore, the above representation models a two-winding transformer; generally for a P-winding ($P > 1$) transformer at branch k, the Y^k matrix would be of size $P \times P$.

2.5 Nodal Admittance Matrix

To calculate the nodal admittance matrix, Thévenin's theorem[26] can be applied to represent a complicated circuit, i.e., a circuit with numerous network elements between connecting buses, with a simple equivalent circuit, i.e., a single equivalent element between connecting buses. For example, for transmission lines in series, the equivalent branch impedance is $\sum_k z_k$; furthermore, for transmission lines in parallel, the equivalent branch impedance is $\sum_k 1/z_k$. However, when transmission elements such as transformers (in-phase or phase-shifting) or flexible AC transmission system (FACTS) devices are present, then constructing the equivalent branch admittance matrix requires special treatment, as detailed in reference [53].

The nodal admittance matrix $Y = G + \mathbf{j}B$ for $Y \in \mathbb{C}^{|\mathcal{N}|\times|\mathcal{N}|}$ for the *equivalent*

[26] Any combination of sinusoidal AC sources and impedances with two terminals can be replaced by a single voltage source in series with a single impedance [32].

network can then be specified as [28]

$$Y \coloneqq \begin{cases} Y_{nn} = Y_n^s + \sum_{k(n,\cdot)} |\tau_{kn}|^2 (y_k + y_{kn}^s) \\ Y_{nm} = -\tau_{kn}^* \tau_{km} y_k \qquad\qquad n \neq m. \end{cases} \tag{2.5}$$

The nodal shunt is $Y_n^s = G_n^s + \mathbf{j}B_n^s$. Note that for $(n, m) \notin \mathcal{A}$, the off-diagonal entry $Y_{nm} = 0$; since actual power systems are not densely connected infrastructures, typically the nodal admittance matrix is a sparse matrix with numerous zero off-diagonal entries. The corresponding nodal conductance matrix G and nodal susceptance matrix B for the *equivalent network* are

$$G \coloneqq \begin{cases} G_{nn} = G_n^s + \sum_{k(n,\cdot)} |\tau_{kn}|^2 g_k \\ G_{nm} = -\tau_{kn}^* \tau_{km} g_k \qquad\qquad n \neq m, \end{cases} \tag{2.6}$$

and

$$B \coloneqq \begin{cases} B_{nn} = B_n^s + \sum_{k(n,\cdot)} |\tau_{kn}|^2 (b_k + b_{kn}^s) \\ B_{nm} = -\tau_{kn}^* \tau_{km} b_k \qquad\qquad n \neq m, \end{cases} \tag{2.7}$$

respectively. The construction of the nodal admittance matrix leads to the following lemma.

Lemma 2.1. *By the superposition theorem,*[27] *the nodal admittance matrix of the equivalent network is equal to the sum of linear algebraic expressions that are comprised of the branch admittance matrices for each element in the full network.*

Proof. Define the vectors $Y_{1,1}, Y_{1,2}, Y_{2,1}, Y_{2,2} \in \mathbb{C}^{|\mathcal{K}|}$ constructed from the branch admittance matrix Y^k (2.4) for all $k \in \mathcal{K}$. Further define connection matrices $C_f, C_t \in \mathcal{R}^{|\mathcal{K}|\times|\mathcal{N}|}$ where $C_f(k,n)$ and $C_t(k,m)$ are equal to 1 for each branch k connecting buses n and m; all other elements of C_f and C_t are zero. Given the nodal shunts $\tilde{Y}^s \coloneqq \operatorname{diag}(Y^s) \in \mathbb{C}^{|\mathcal{N}|\times|\mathcal{N}|}$, the following equivalence relation holds [55, 56]:

$$Y \sim C_f^T \left(Y_{1,1} C_f + Y_{1,2} C_t\right) + C_t^T \left(Y_{2,1} C_f + Y_{2,2} C_t\right) + \tilde{Y}^s, \tag{2.8}$$

where $Y \in \mathbb{C}^{|\mathcal{N}|\times|\mathcal{N}|}$ is the nodal admittance matrix defined in (2.7). □

2.6 Power Flows

This section presents the power flow equations for AC networks, which is a system of equations that is nonlinear and nonconvex. Therefore approximations are also presented.

[27] The current flow or voltage across any network element is equal to the algebraic sum of the currents or voltages produced independently by each source [54].

2.6.1 Alternating Current Power Flows (ACPF)

The physical constraints of the power system determine the operational characteristics and power flows for the AC network. The solution to Kirchhoff's Laws is equivalent to a solution of the ACPF [7]. This is a solution to the system of equations involving both real and reactive power dispatch with voltage magnitude and angles.

The nodal voltage phasor can be expressed in polar or rectangular (Cartesian) coordinates, i.e., $v_{n,t} = |v_{n,t}|e^{\mathbf{j}\theta_{n,t}} = |v_{n,t}|\cos\theta_{n,t} + \mathbf{j}|v_{n,t}|\sin\theta_{n,t}$ or $v_{n,t} = v^r_{n,t} + \mathbf{j}v^j_{n,t}$, for each bus $n \in \mathcal{N}$ given the time interval $t \in \mathcal{T}$. In matrix form, the net current injected at each bus into the power network is a linear function of the nodal voltage phasor vector $v = [v_1, \ldots, v_N]^T$ for the given nodal admittance matrix Y as shown below:

$$i = Yv, \tag{2.9}$$

where $i = [i_1, \ldots, i_N]^T$ is the nodal current phasor vector.

The complex power $s = p + \mathbf{j}q$ for $s \in \mathbb{C}^{|\mathcal{N}|\times 1}$ is expressed as

$$\begin{aligned} s &= \text{diag}(v)i^* \\ &= \text{diag}(v)\left[Yv\right]^*. \end{aligned} \tag{2.10}$$

Substituting in the conductance and susceptance components of the nodal admittance

matrix Y, the real (p) and reactive (q) parts of the apparent power are

$$p + \mathbf{j}q = \operatorname{diag}(v)\left[G - \mathbf{j}B\right] v^{*}. \tag{2.11}$$

This set of equalities guarantee that both KCL and KVL are satisfied for the system. Expanding (2.11) for each bus $n \in \mathcal{N}$ results in the respective real and reactive nodal power flow balance, shown in both polar and rectangular forms:

$$\begin{aligned} p_{n,t} &= |v_{n,t}| \sum_{m\in\mathcal{N}} |v_{m,t}| \Big(G_{nm}\cos\theta_{nm,t} + B_{nm}\sin\theta_{nm,t} \Big) \qquad (2.12)\\ &= v^{r}_{n,t} \sum_{m\in\mathcal{N}} \Big(G_{nm} v^{r}_{m,t} - B_{nm} v^{j}_{m,t} \Big) + v^{j}_{n,t} \sum_{m\in\mathcal{N}} \Big(G_{nm} v^{j}_{m,t} + B_{nm} v^{r}_{m,t} \Big), \\ q_{n,t} &= |v_{n,t}| \sum_{m\in\mathcal{N}} |v_{m,t}| \Big(G_{nm}\sin\theta_{nm,t} - B_{nm}\cos\theta_{nm,t} \Big) \qquad (2.13)\\ &= v^{j}_{n,t} \sum_{m\in\mathcal{N}} \Big(G_{nm} v^{r}_{m,t} - B_{nm} v^{j}_{m,t} \Big) - v^{r}_{n,t} \sum_{m\in\mathcal{N}} \Big(G_{nm} v^{j}_{m,t} + B_{nm} v^{r}_{m,t} \Big), \end{aligned}$$

where $\theta_{nm,t} \coloneqq \theta_{n,t} - \theta_{m,t}$.

Furthermore, the power flows $p_{k(n,m),t}$ and $q_{k(n,m),t}$ for the *equivalent network* can be computed with the nodal admittance matrix Y as

$$\begin{aligned} p_{k(n,m),t} &= -\Big(G_{nm}\Big)|v_{n,t}|^{2} + |v_{n,t}||v_{m,t}|\Big(G_{nm}\cos\theta_{nm,t} + B_{nm}\sin\theta_{nm,t} \Big) \qquad (2.14)\\ &= -G_{nm}\left(\left(v^{r}_{n,t}\right)^{2} + \left(v^{j}_{n,t}\right)^{2} \right) + v^{r}_{n,t}\Big(G_{nm} v^{r}_{m,t} - B_{nm} v^{j}_{m,t} \Big) \\ &\quad + v^{j}_{n,t}\Big(G_{nm} v^{j}_{m,t} + B_{nm} v^{r}_{m,t} \Big), \end{aligned}$$

$$
\begin{aligned}
q_{k(n,m),t} &= \Big(B_{nm} - b^s_{kn}\Big)|v_{n,t}|^2 + |v_{n,t}||v_{m,t}|\Big(G_{nm}\sin\theta_{nm,t} - B_{nm}\cos\theta_{nm,t}\Big) \qquad (2.15)\\
&= \Big(B_{nm} - b^s_{kn}\Big)\left(\left(v^r_{n,t}\right)^2 + \left(v^j_{n,t}\right)^2\right) + v^j_{n,t}\Big(G_{nm}v^r_{m,t} - B_{nm}v^j_{m,t}\Big)\\
&- v^r_{n,t}\Big(G_{nm}v^j_{m,t} + B_{nm}v^r_{m,t}\Big),
\end{aligned}
$$

where both polar and rectangular formulations appear above. Furthermore, the power flows in the other direction, i.e., $p_{k(m,n),t}$ and $q_{k(m,n),t}$, are similarly computed as follows:

$$
\begin{aligned}
p_{k(m,n),t} &= -\Big(G_{mn}\Big)|v_{m,t}|^2 + |v_{n,t}||v_{m,t}|\Big(G_{mn}\cos\theta_{nm,t} - B_{mn}\sin\theta_{nm,t}\Big) \qquad (2.16)\\
&= -G_{mn}\left(\left(v^r_{m,t}\right)^2 + \left(v^j_{m,t}\right)^2\right) + v^r_{n,t}\Big(G_{mn}v^r_{m,t} - B_{mn}v^j_{m,t}\Big)\\
&+ v^j_{n,t}\Big(G_{mn}v^j_{m,t} - B_{mn}v^r_{m,t}\Big),\\
q_{k(m,n),t} &= \Big(B_{mn} - b^s_{km}\Big)|v_{m,t}|^2 - |v_{n,t}||v_{m,t}|\Big(G_{mn}\sin\theta_{nm,t} + B_{mn}\cos\theta_{nm,t}\Big) \qquad (2.17)\\
&= \Big(B_{mn} - b^s_{km}\Big)\left(\left(v^r_{m,t}\right)^2 + \left(v^j_{m,t}\right)^2\right) - v^j_{n,t}\Big(G_{mn}v^r_{m,t} + B_{mn}v^j_{m,t}\Big)\\
&- v^r_{n,t}\Big(G_{mn}v^j_{m,t} + B_{mn}v^r_{m,t}\Big),
\end{aligned}
$$

Note that the above formulations of (2.16) and (2.17) apply the following respective even and odd function identities: $\cos(-x) = \cos(x), \sin(-x) = -\sin(x)$.

Also, the power flows on the *full network*[28] can be determined in both polar and

[28]If only one network element exists between connecting nodes, then the *equivalent network* power flow equations are identical for that branch.

rectangular forms as follows:

$$
\begin{aligned}
p_{k(n,m),t} &= g_k \left(|\tau_{kn}|\,|v_{n,t}|\right)^2 \\
&\quad - \left(|\tau_{kn}|\,|v_{n,t}|\right)\left(|\tau_{km}|\,|v_{m,t}|\right)\Big(g_k \cos\left(\theta_{nm,t}+\phi_{kn}-\phi_{km}\right) \\
&\quad + b_k \sin\left(\theta_{nm,t}+\phi_{kn}-\phi_{km}\right)\Big) \\
&\quad = g_k\,|\tau_{kn}|^2\left(\left(v^r_{n,t}\right)^2+\left(v^j_{n,t}\right)^2\right) - v^r_{n,t}\Big(g_k|\tau_{kn}||\tau_{km}|\cos\left(\phi_{kn}-\phi_{km}\right)v^r_{m,t} \\
&\quad - b_k|\tau_{kn}||\tau_{km}|\cos\left(\phi_{kn}-\phi_{km}\right)v^j_{m,t}\Big) - v^j_{n,t}\Big(g_k|\tau_{kn}||\tau_{km}|\cos\left(\phi_{kn}-\phi_{km}\right)v^j_{m,t} \\
&\quad + b_k|\tau_{kn}||\tau_{km}|\cos\left(\phi_{kn}-\phi_{km}\right)v^r_{m,t}\Big) + v^r_{n,t}\Big(b_k|\tau_{kn}||\tau_{km}|\sin\left(\phi_{kn}-\phi_{km}\right)v^r_{m,t} \\
&\quad - g_k|\tau_{kn}||\tau_{km}|\sin\left(\phi_{kn}-\phi_{km}\right)v^j_{m,t}\Big) + v^j_{n,t}\Big(b_k|\tau_{kn}||\tau_{km}|\sin\left(\phi_{kn}-\phi_{km}\right)v^j_{m,t} \\
&\quad + g_k|\tau_{kn}||\tau_{km}|\sin\left(\phi_{kn}-\phi_{km}\right)v^r_{m,t}\Big), \qquad (2.18)
\end{aligned}
$$

$$
\begin{aligned}
q_{k(n,m),t} &= -\left(b_k+b^s_{kn}\right)\left(|\tau_{kn}|\,|v_{n,t}|\right)^2 \\
&\quad - \left(|\tau_{kn}|\,|v_{n,t}|\right)\left(|\tau_{km}|\,|v_{m,t}|\right)\Big(g_k \sin\left(\theta_{nm,t}+\phi_{kn}-\phi_{km}\right) \\
&\quad - b_k \cos\left(\theta_{nm,t}+\phi_{kn}-\phi_{km}\right)\Big) \\
&\quad = -\left(b_k+b^s_{kn}\right)|\tau_{kn}|^2\left(\left(v^r_{n,t}\right)^2+\left(v^j_{n,t}\right)^2\right) - v^j_{n,t}\Big(g_k|\tau_{kn}||\tau_{km}|\cos\left(\phi_{kn}-\phi_{km}\right)v^r_{m,t} \\
&\quad - b_k|\tau_{kn}||\tau_{km}|\cos\left(\phi_{kn}-\phi_{km}\right)v^j_{m,t}\Big) + v^r_{n,t}\Big(g_k|\tau_{kn}||\tau_{km}|\cos\left(\phi_{kn}-\phi_{km}\right)v^j_{m,t} \\
&\quad + b_k|\tau_{kn}||\tau_{km}|\cos\left(\phi_{kn}-\phi_{km}\right)v^r_{m,t}\Big) + v^j_{n,t}\Big(g_k|\tau_{kn}||\tau_{km}|\sin\left(\phi_{kn}-\phi_{km}\right)v^r_{m,t} \\
&\quad - b_k|\tau_{kn}||\tau_{km}|\sin\left(\phi_{kn}-\phi_{km}\right)v^j_{m,t}\Big) - v^r_{n,t}\Big(g_k|\tau_{kn}||\tau_{km}|\sin\left(\phi_{kn}-\phi_{km}\right)v^j_{m,t} \\
&\quad + b_k|\tau_{kn}||\tau_{km}|\sin\left(\phi_{kn}-\phi_{km}\right)v^r_{m,t}\Big). \qquad (2.19)
\end{aligned}
$$

Furthermore the power flows in the other direction, i.e., $p_{k(m,n),t}$ and $q_{k(m,n),t}$, are similarly computed as follows:

$$
\begin{aligned}
p_{k(m,n),t} &= g_k \left(|\tau_{km}|\,|v_{m,t}|\right)^2 \\
&\quad - \left(|\tau_{kn}|\,|v_{n,t}|\right)\left(|\tau_{km}|\,|v_{m,t}|\right)\Big(g_k \cos\left(\theta_{nm,t}+\phi_{kn}-\phi_{km}\right) \\
&\quad - b_k \sin\left(\theta_{nm,t}+\phi_{kn}-\phi_{km}\right)\Big) \\
&= g_k\,|\tau_{km}|^2\left(\left(v^r_{m,t}\right)^2+\left(v^j_{m,t}\right)^2\right) - v^r_{n,t}\Big(g_k|\tau_{kn}||\tau_{km}|\cos\left(\phi_{kn}-\phi_{km}\right)v^r_{m,t} \\
&\quad - b_k|\tau_{kn}||\tau_{km}|\cos\left(\phi_{kn}-\phi_{km}\right)v^j_{m,t}\Big) - v^j_{n,t}\Big(g_k|\tau_{kn}||\tau_{km}|\cos\left(\phi_{kn}-\phi_{km}\right)v^j_{m,t} \\
&\quad + b_k|\tau_{kn}||\tau_{km}|\cos\left(\phi_{kn}-\phi_{km}\right)v^r_{m,t}\Big) - v^r_{n,t}\Big(b_k|\tau_{kn}||\tau_{km}|\sin\left(\phi_{kn}-\phi_{km}\right)v^r_{m,t} \\
&\quad - g_k|\tau_{kn}||\tau_{km}|\sin\left(\phi_{kn}-\phi_{km}\right)v^j_{m,t}\Big) - v^j_{n,t}\Big(b_k|\tau_{kn}||\tau_{km}|\sin\left(\phi_{kn}-\phi_{km}\right)v^j_{m,t} \\
&\quad + g_k|\tau_{kn}||\tau_{km}|\sin\left(\phi_{kn}-\phi_{km}\right)v^r_{m,t}\Big), \qquad (2.20) \\
q_{k(m,n),t} &= -\left(b_k+b^s_{km}\right)\left(|\tau_{km}|\,|v_{m,t}|\right)^2 \\
&\quad + \left(|\tau_{kn}|\,|v_{n,t}|\right)\left(|\tau_{km}|\,|v_{m,t}|\right)\Big(g_k \sin\left(\theta_{nm,t}+\phi_{kn}-\phi_{km}\right) \\
&\quad + b_k \cos\left(\theta_{nm,t}+\phi_{kn}-\phi_{km}\right)\Big) \\
&= -\left(b_k+b^s_{km}\right)|\tau_{km}|^2\left(\left(v^r_{m,t}\right)^2+\left(v^j_{m,t}\right)^2\right) - v^j_{n,t}\Big(g_k|\tau_{kn}||\tau_{km}|\cos\left(\phi_{kn}-\phi_{km}\right)v^r_{m,t} \\
&\quad - b_k|\tau_{kn}||\tau_{km}|\cos\left(\phi_{kn}-\phi_{km}\right)v^j_{m,t}\Big) + v^r_{n,t}\Big(g_k|\tau_{kn}||\tau_{km}|\cos\left(\phi_{kn}-\phi_{km}\right)v^j_{m,t} \\
&\quad + b_k|\tau_{kn}||\tau_{km}|\cos\left(\phi_{kn}-\phi_{km}\right)v^r_{m,t}\Big) - v^j_{n,t}\Big(g_k|\tau_{kn}||\tau_{km}|\sin\left(\phi_{kn}-\phi_{km}\right)v^r_{m,t}
\end{aligned}
$$

$$- b_k|\tau_{kn}||\tau_{km}|\sin\left(\phi_{kn}-\phi_{km}\right)v^j_{m,t}\Big) + v^r_{n,t}\Big(g_k|\tau_{kn}||\tau_{km}|\sin\left(\phi_{kn}-\phi_{km}\right)v^j_{m,t}$$

$$+ b_k|\tau_{kn}||\tau_{km}|\sin\left(\phi_{kn}-\phi_{km}\right)v^r_{m,t}\Big). \tag{2.21}$$

These equations are nonlinear and nonconvex in nature due to the bilinear terms comprised of the variables: $|v_{n,t}|, |v_{m,t}|$, and $\theta_{nm,t}$ in the polar form and $v^r_{n,t}, v^r_{m,t}, v^j_{n,t}$, and $v^j_{m,t}$ in the rectangular form. If network devices are treated as variables, then these equations are multilinear in nature, with possible discontinuities if discrete variables are present.

2.6.2 Linearized Real Power Flows and Quadratic Loss Approximations

Given the nonlinear and nonconvex nature of the above power flow equations (2.14) – (2.21), many research and practical applications resort to a linearized OPF approach. The most common approximation is referred to as the DC power flow (DCPF) [8, 29] which is applied to the polar form of the ACPF. In particular, this approach assumes:

1. Small angle differences $\theta_{nm,t}$ such that $\sin\theta_{nm,t} \approx \theta_{nm,t}$ for all $(n,m) \in \mathcal{A}$ in time $t \in \mathcal{T}$.

2. Unitary voltage, i.e., $|v_{n,t}| = 1$ for all $n \in \mathcal{N}$ in time $t \in \mathcal{T}$.

3. Low resistance-to-reactance ratios, i.e., $r_k \ll x_k$ for all $k \in \mathcal{K}$.

As a result, the DCPF approach works better on transmission networks in a normal operating state since large angle differences and increased line loading correspond

to higher stress (i.e., an operating condition that leads to pre- or post-contingency stability violations) [57]. Furthermore, these load flow assumptions become more inaccurate for lower voltage, sub-transmission and distribution systems due to higher resistance-to-reactance ratios.

For a transmission branch $k \in \mathcal{K}$ in time $t \in \mathcal{T}$, the above assumptions lead to approximations of (2.19) and (2.21) that give negligible reactive power flow and the following real power flow approximation of (2.18) in polar form

$$\tilde{p}_{k(n,m),t} = -b_k \theta_{nm,t}, \tag{2.22}$$

where $\tilde{p}_{k(m,n),t} = -\tilde{p}_{k(n,m),t}$. Note that in the presence of an in-phase transformer, the approximation in (2.22) remains unchanged since assuming $|\tau_{kn}| = |\tau_{km}| = 1$ is analogous to the unitary voltage approach; but for a phase-shifter the DCPF power flows are

$$\tilde{p}_{k(n,m),t} = -b_k \left(\theta_{nm,t} + \phi_{kn} - \phi_{km}\right), \tag{2.23}$$

where $\phi_{km} = 0$ for a phase-shifter on the n-side of k and $\phi_{kn} = 0$ for a phase-shifter on the m-side of k.

The linear angle-to-power relationship in (2.22) and (2.23) is the basis of the DCPF approach, which can be further extended to account for the real power losses that occur through Joule heating. Based on (2.18) and (2.20) the total real power losses on each transmission line $k \in \mathcal{K}$ in time $t \in \mathcal{T}$ in polar form can be calculated

as

$$\begin{aligned} p_{k,t}^{\ell} &= p_{k(n,m),t} + p_{k(m,n),t} \\ &= g_k \left(|\upsilon_{n,t}|^2 + |\upsilon_{m,t}|^2 - 2 |\upsilon_{n,t}| |\upsilon_{m,t}| \cos \theta_{nm,t} \right). \end{aligned} \tag{2.24}$$

In the presence of a phase-shifter, then the total real power losses are

$$p_{k,t}^{\ell} = g_k \left(|\upsilon_{n,t}|^2 + |\upsilon_{m,t}|^2 - 2 |\upsilon_{n,t}| |\upsilon_{m,t}| \cos \left(\theta_{nm,t} + \phi_{kn} - \phi_{km} \right) \right). \tag{2.25}$$

Applying the voltage related DCPF assumptions to (2.24), the real power losses can be approximated as

$$p_{k,t}^{\ell} \approx g_k \left(\theta_{nm,t} \right)^2, \tag{2.26}$$

where for all $(n,m) \in \mathcal{A}, t \in \mathcal{T}$ the approximation $\cos \theta_{nm,t} \approx 1 - \left(\theta_{nm,t} \right)^2 / 2$ is based on the first two terms in its Taylor series. Assuming that the real power losses are equally distributed between the bidirectional flow components for a given line leads to the following real power loss approximation

$$\tilde{p}_{k,t}^{\ell} = \frac{1}{2} g_k \left(\theta_{nm,t} \right)^2 \tag{2.27}$$

for all lines $k \in \mathcal{K}$ where $\tilde{p}^{\ell}_{k,t} = \tilde{p}^{\ell}_{k(n,m),t} = \tilde{p}^{\ell}_{k(m,n),t}$ and $\tilde{p}^{\ell}_{k,t}$ is treated as a withdrawal at both buses n and m, i.e., $2\tilde{p}^{\ell}_{k,t}$ approximates the total loss on the line. The DCPF loss approximation of (2.25) in the presence of a phase-shifter yields

$$\tilde{p}^{\ell}_{k,t} = \frac{1}{2} g_k \left(\theta_{nm,t} + \phi_{kn} - \phi_{km}\right)^2, \tag{2.28}$$

where $|\tau_{kn}| = |\tau_{km}| = 1$ and $\phi_{km} = 0$ for a phase-shifter on the n-side of k; otherwise $|\tau_{kn}| = |\tau_{km}| = 1$ and $\phi_{kn} = 0$ for a phase-shifter on the m-side of k.

As a result, the real power flows for the DCPF with losses are

$$\hat{p}_{k(n,m),t} = \tilde{p}_{k(n,m),t} + \tilde{p}^{\ell}_{k,t} \tag{2.29}$$

for all $k \in \mathcal{K}, t \in \mathcal{T}$.

The above DCPF assumptions can be directly applied to the following ACOPF polar formulation (in Section 2.7.1) in order to formulate the DCOPF or DCOPF with losses optimization problem. However unlike the DCOPF, the DCOPF with losses is not a linear optimization problem but rather a nonconvex QCQP due to the quadratic equality in (2.27). Chapter 6 proposes a global solution method to make this problem tractable and the solution exact.

In practice system operators use similar assumptions in their market software to those presented in this section when building the power transfer distribution factor (PTDF) linear model of the power system [6]; instead of calculating an angle-to-power

relationship, the PTDF model expresses the percentage of a power transfer that flows on a particular network branch. This approach can be extended to include marginal loss modeling, as demonstrated by the ISO New England (ISO-NE) in [58]. However, such approximations still consider only real power dispatch. Reactive power dispatch can be increasingly important since it affects both real power losses and voltage magnitudes.

2.6.3 Decoupled Power Flows

Initially proposed by Stott and Alsaç in 1974, the decoupled power flow solves for the real and reactive power injections sequentially instead of simultaneously [38]. This approach is based on the principle that when the Jacobian of the power flow equations

$$\begin{bmatrix} \partial p/\partial \theta & \partial p/\partial v \\ \partial q/\partial \theta & \partial q/\partial v \end{bmatrix}$$

is evaluated numerically, the off-diagonal submatrices are much smaller in magnitude than the diagonal submatrices, i.e., $\partial p/\partial \theta >> \partial q/\partial \theta$ and $\partial q/\partial v >> \partial p/\partial v$. By setting the off-diagonal entries of the Jacobian to zero, the ACPF problem can be decomposed into a pair of subproblems where a $p-\theta$ model solves for the real power dispatch and voltage angles, and a $q-v$ model solves for the reactive power dispatch and voltage magnitudes. This approach may assume small angle differences and low resistance-to-reactance ratios in order to construct a pair of linear subproblems.

Typically this method iterates between the pair of subproblems with updates to the $p-\theta$ parameterization in the $q-v$ model, and vice-versa, until a convergence criteria is met.

However when the system has high losses, is highly loaded, or either subproblem is infeasible, the decoupled approach becomes ineffective; Chapters 3 and 4 propose an approach that instead solves a coupled model where the real and reactive power injections are simultaneously co-optimized.

2.7 The Canonical Alternating Current Optimal Power Flow (ACOPF) Formulation

The ACOPF formulation minimizes or maximizes some objective function, subject to the apparent power flows in (2.11) and other operational constraints. The objective generally minimizes system cost or maximizes surplus. Since the ACOPF is an optimization problem where the number of variables does not have to equal the number of constraints, specifying a slack or reference bus is unnecessary [4].

The optimal set of real and reactive generation profiles and phasor voltages for each bus that satisfies KCL and KVL is the OPF solution. Although the problem presented in this work minimizes system costs in terms of real power dispatch alone, it could be desirable to include a price on reactive power compensation; this concept is explored further in Chapter 5.

2.7.1 Polar Form

Most of the ACOPF literature uses the polar form based on the early work of Carpentier during the 1960's [4]. The polar form of the ACOPF problem for time t where the objective minimizes the system costs for linear or convex quadratic generator bid curves f_i is:

$$\min_{\theta,v,p^g,q^g} \sum_{i\in\mathcal{I}} f_i\left(p^g_{i,t}\right) \tag{2.30}$$

subject to the respective real and reactive nodal power flow balances in

$$|v_{n,t}| \sum_{m\in\mathcal{N}} |v_{m,t}| \left(G_{nm}\cos\theta_{nm,t} + B_{nm}\sin\theta_{nm,t}\right) - p^+_{n,t} + p^-_{n,t} = 0, \qquad \forall n \in \mathcal{N}, \tag{2.31}$$

$$|v_{n,t}| \sum_{m\in\mathcal{N}} |v_{m,t}| \left(G_{nm}\sin\theta_{nm,t} - B_{nm}\cos\theta_{nm,t}\right) - q^+_{n,t} + q^-_{n,t} = 0, \qquad \forall n \in \mathcal{N}, \tag{2.32}$$

the limits on real and reactive power outputs on generating units in

$$\underline{P}_i \le p^g_{i,t} \le \overline{P}_i, \qquad \forall i \in \mathcal{I}, \tag{2.33}$$

$$\underline{Q}_i \le q^g_{i,t} \le \overline{Q}_i, \qquad \forall i \in \mathcal{I}, \tag{2.34}$$

the nodal voltage limits in

$$\underline{V}_n \le |v_{n,t}| \le \overline{V}_n, \qquad \forall n \in \mathcal{N}, \tag{2.35}$$

the apparent power capacity limit on transmission elements in

$$\left(p_{k(\cdot),t}\right)^2 + \left(q_{k(\cdot),t}\right)^2 \leq \left(\overline{S}_k\right)^2, \qquad \forall k\,(\cdot) \in \mathcal{F}, \ (2.36)$$

and the limit on the voltage angle difference for interconnected buses in

$$\underline{\Theta}_{nm} \leq \theta_{nm,t} \leq \overline{\Theta}_{nm}, \qquad \forall\,(n,m) \in \mathcal{A}, \ (2.37)$$

where for a given node $n \in \mathcal{N}$ the real and reactive power injections equal the generation, e.g., $p^+_{n,t} = \sum_{i\in\mathcal{I}(n)} p^g_{i,t}$ and $q^+_{n,t} = \sum_{i\in\mathcal{I}(n)} q^g_{i,t}$, and the real and reactive power withdrawals equal the demand, e.g., $p^-_{n,t} = P^d_{n,t}$ and $q^-_{n,t} = Q^d_{n,t}$. These nodal power balance equations can be extended to incorporate other sources of power injections and withdrawals in the power system. By Lemma 2.1, note that (2.31) and (2.32) can be formulated analogously with the power flow equations for the *equivalent network*, i.e., (2.18) and (2.19), or with the power flow equations for the *full network*, i.e., (2.20) and (2.21), as follows:

$$\sum_{k(n,\cdot)\in\mathcal{K}} p_{k(n,m),t} + |v_{n,t}|^2 G^s_n - p^+_{n,t} + p^-_{n,t} = 0, \qquad \forall n \in \mathcal{N}, \ (2.38)$$

$$\sum_{k(n,\cdot)\in\mathcal{K}} q_{k(n,m),t} - |v_{n,t}|^2 B^s_n - q^+_{n,t} + q^-_{n,t} = 0, \qquad \forall n \in \mathcal{N}. \ (2.39)$$

For the OPF optimization problem in (2.30) – (2.37), the variables are as follows: $\theta = [\theta_{1,t}, \ldots, \theta_{N,t}]^T$ is the vector of nodal voltage angles, $v = [v_{1,t}, \ldots, v_{N,t}]^T$ is the

vector of nodal voltage magnitudes, $p^g = \left[p^g_{1,t}, \ldots, p^g_{I,t}\right]^T$ is the vector of real power generation, and $q^g = \left[q^g_{1,t}, \ldots, q^g_{I,t}\right]^T$ is the vector of reactive power compensation.

2.7.2 Rectangular Form

To derive the ACOPF formulation in rectangular coordinates, the voltage phasor is converted to rectangular form, which results in $v^r_{n,t} = |v_{n,t}| \cos\theta_{n,t}$ and $v^j_{n,t} = |v_{n,t}| \sin\theta_{n,t}$ for all $n \in \mathcal{N}, t \in \mathcal{T}$. Then the equivalent ACOPF problem in rectangular form for time t is

$$\min_{v^r, v^j, p^g, q^g} \sum_{i \in \mathcal{I}} f_i\left(p^g_{i,t}\right) \tag{2.40}$$

subject to the respective real and reactive nodal power flow balance in

$$v^r_{n,t} \sum_{m \in \mathcal{N}} \left(G_{nm} v^r_{m,t} - B_{nm} v^j_{m,t}\right) + v^j_{n,t} \sum_{m \in \mathcal{N}} \left(G_{nm} v^j_{m,t} + B_{nm} v^r_{m,t}\right) - p^+_{n,t} + p^-_{n,t} = 0, \qquad \forall n \in \mathcal{N}, \tag{2.41}$$

$$v^j_{n,t} \sum_{m \in \mathcal{N}} \left(G_{nm} v^r_{m,t} - B_{nm} v^j_{m,t}\right) - v^r_{n,t} \sum_{m \in \mathcal{N}} \left(G_{nm} v^j_{m,t} + B_{nm} v^r_{m,t}\right) - q^+_{n,t} + q^-_{n,t} = 0, \qquad \forall n \in \mathcal{N}, \tag{2.42}$$

the limits on real and reactive power outputs on generating units in

$$\underline{P}_i \leq p^g_{i,t} \leq \overline{P}_i, \qquad \forall i \in \mathcal{I}, \tag{2.43}$$

$$\underline{Q}_i \leq q^g_{i,t} \leq \overline{Q}_i, \qquad \forall i \in \mathcal{I}, \ (2.44)$$

the nodal voltage limits in

$$\left(\underline{V}_n\right)^2 \leq \left(v^r_{n,t}\right)^2 + \left(v^j_{n,t}\right)^2 \leq \left(\overline{V}_n\right)^2, \qquad \forall n \in \mathcal{N}, \ (2.45)$$

the apparent power capacity limit on transmission elements in

$$\left(p_{k(\cdot),t}\right)^2 + \left(q_{k(\cdot),t}\right)^2 \leq \left(\overline{S}_k\right)^2, \qquad \forall k\,(\cdot) \in \mathcal{F}, \ (2.46)$$

and the limit on the voltage angle difference for interconnected buses in

$$\underline{\Theta}_{nm} \leq \arctan\left(v^j_{n,t}/v^r_{n,t}\right) - \arctan\left(v^j_{m,t}/v^r_{m,t}\right) \leq \overline{\Theta}_{nm}, \qquad \forall\,(n,m) \in \mathcal{A}, \ (2.47)$$

where for a given node $n \in \mathcal{N}$ the real and reactive power injections equal the generation, e.g., $p^+_{n,t} = \sum_{i \in \mathcal{I}(n)} p^g_{i,t}$ and $q^+_{n,t} = \sum_{i \in \mathcal{I}(n)} q^g_{i,t}$, and the real and reactive power withdrawals equal the demand, e.g., $p^-_{n,t} = P^d_{n,t}$ and $q^-_{n,t} = Q^d_{n,t}$. Similar to the polar approach, again by Lemma 2.1 the nodal power flow balance in (2.41) and (2.42) can be formulated analogously with the power flow equations for the *equivalent network*, i.e., (2.18) and (2.19), or with the power flow equations for the *full network*,

i.e., (2.20) and (2.21), as follows:

$$\sum_{k(n,\cdot)\in\mathcal{F}} p_{k(n,m),t} + \left(\left(v_{n,t}^{r}\right)^2 + \left(v_{n,t}^{j}\right)^2\right) G_n^s - p_{n,t}^{+} + p_{n,t}^{-} = 0, \qquad \forall n \in \mathcal{N}, \ (2.48)$$

$$\sum_{k(n,\cdot)\in\mathcal{F}} q_{k(n,m),t} - \left(\left(v_{n,t}^{r}\right)^2 + \left(v_{n,t}^{j}\right)^2\right) B_n^s - q_{n,t}^{+} + q_{n,t}^{-} = 0, \qquad \forall n \in \mathcal{N}. \ (2.49)$$

For the optimization problem in $(2.40) - (2.47)$, the variables are as follows: $v^r = \left[v_{1,t}^r, \ldots, v_{N,t}^r\right]^T$ is the vector of real part of the voltage phasors, $v^j = \left[v_{1,t}^j, \ldots, v_{N,t}^j\right]^T$ is the vector of imaginary part of the voltage phasors, $p^g = \left[p_{1,t}^g, \ldots, p_{I,t}^g\right]^T$ is the vector of real power generation, and $q^g = \left[q_{1,t}^g, \ldots, q_{I,t}^g\right]^T$ is the vector of reactive power compensation.

2.8 Spot Pricing Theory

The LMP is derived from the Lagrange multiplier[29] on the nodal real power balance of the OPF optimization model, i.e., equation (2.31) in polar form or equation (2.41) in rectangular form, and reflects parallel flow effects through obeying Kirchhoff's laws. The LMP is the marginal cost of suppling the next MW of load at a particular location and time, and accounts for the next incremental unit of energy, network congestion, and transmission losses. Therefore, the value of the Lagrange multiplier is the rate at which the optimal value of the objective function changes when augmenting the corresponding constraint.[30] The LMP is therefore both spatially and temporally

[29] also referred to as the dual variable or the "shadow price" of the resource

[30] assuming no degeneracy

dependent, i.e., this spot price of electricity depends on where the customer is located in the network, and when the customer is consuming since the system is more heavily loaded during peak time periods. Furthermore, there is an analogous shadow price on nodal reactive power balances, which is referred to as the Q-LMP and later explored in Chapter 5.

2.9 The Proposed IV-ACOPF Formulation

The proposed IV-ACOPF problem is expressed in terms of the current-voltage (IV) equations in (2.9) and extends the initial concepts for an alternative OPF formulation presented in [59]; this work was originally published in [22]. Unlike the canonical ACOPF formulations which represent the network balancing through a nonlinear coupling of the apparent power flows through each branch k, the IV-ACOPF leverages the current injections method where the network flows are linear and the nonconvexities appear in the constraints relating bilinear terms (i.e., $v^r_{n,t}i^r_{n,t}, v^j_{n,t}i^r_{n,t}, v^r_{n,t}i^j_{n,t}$, and $v^j_{n,t}i^j_{n,t}$) within each node. The current injections method for the power flow equations was originally expressed by Dommel et al. in 1970 as a mix of state variables in both polar and rectangular form [60]. The IV-ACOPF formulation is in rectangular coordinates and applies the branch admittance matrix to determine the current flows,

instead of the apparent power flows, as

$$\begin{bmatrix} i_{k(n,m),t} \\ \\ i_{k(m,n),t} \end{bmatrix} = \begin{bmatrix} Y^k_{1,1} & Y^k_{1,2} \\ \\ Y^k_{2,1} & Y^k_{2,2} \end{bmatrix} \times \begin{bmatrix} v_{n,t} \\ \\ v_{m,t} \end{bmatrix} \tag{2.50}$$

for all $k \in \mathcal{K}$ where

$$\begin{aligned} i^r_{k(n,m),t} &= \text{Re}\left(Y^k_{1,1} v_{n,t} + Y^k_{1,2} v_{m,t}\right) \qquad (2.51) \\ &= \Big[g_k \left|\tau_{kn}\right|^2 v^r_{n,t} - \Big(g_k|\tau_{kn}||\tau_{km}|\cos\left(\phi_{kn} - \phi_{km}\right) + b_k|\tau_{kn}||\tau_{km}|\sin\left(\phi_{kn} \\ &\quad -\phi_{km}\right)\Big) v^r_{m,t}\Big] - \Big[\left(b_k + b^s_{kn}\right)\left|\tau_{kn}\right|^2 v^j_{n,t} - \Big(b_k|\tau_{kn}||\tau_{km}|\cos\left(\phi_{kn} - \phi_{km}\right) \\ &\quad - g_k|\tau_{kn}||\tau_{km}|\sin\left(\phi_{kn} - \phi_{km}\right)\Big) v^j_{m,t}\Big], \\ i^j_{k(n,m),t} &= \text{Im}\left(Y^k_{1,1} v_{n,t} + Y^k_{1,2} v_{m,t}\right) \qquad (2.52) \\ &= \Big[g_k \left|\tau_{kn}\right|^2 v^j_{n,t} - \Big(g_k|\tau_{kn}||\tau_{km}|\cos\left(\phi_{kn} - \phi_{km}\right) + b_k|\tau_{kn}||\tau_{km}|\sin\left(\phi_{kn} \\ &\quad -\phi_{km}\right)\Big) v^j_{m,t}\Big] + \Big[\left(b_k + b^s_{kn}\right)\left|\tau_{kn}\right|^2 v^r_{n,t} - \Big(b_k|\tau_{kn}||\tau_{km}|\cos\left(\phi_{kn} - \phi_{km}\right) \\ &\quad - g_k|\tau_{kn}||\tau_{km}|\sin\left(\phi_{kn} - \phi_{km}\right)\Big) v^r_{m,t}\Big], \\ i^r_{k(m,n),t} &= \text{Re}\left(Y^k_{2,1} v_{n,t} + Y^k_{2,2} v_{m,t}\right) \qquad (2.53) \\ &= -\Big[\Big(g_k|\tau_{kn}||\tau_{km}|\cos\left(\phi_{kn} - \phi_{km}\right) + b_k|\tau_{kn}||\tau_{km}|\sin\left(\phi_{kn} - \phi_{km}\right)\Big) v^r_{n,t} \\ &\quad - g_k \left|\tau_{km}\right|^2 v^r_{m,t}\Big] + \Big[\Big(b_k|\tau_{kn}||\tau_{km}|\cos\left(\phi_{kn} - \phi_{km}\right) - g_k|\tau_{kn}||\tau_{km}|\sin\left(\phi_{kn} \\ &\quad -\phi_{km}\right)\Big) v^j_{n,t} - \left(b_k + b^s_{kn}\right)\left|\tau_{km}\right|^2 v^j_{m,t}\Big], \\ i^j_{k(m,n),t} &= \text{Im}\left(Y^k_{2,1} v_{n,t} + Y^k_{2,2} v_{m,t}\right) \qquad (2.54) \\ &= -\Big[\Big(g_k|\tau_{kn}||\tau_{km}|\cos\left(\phi_{kn} - \phi_{km}\right) + b_k|\tau_{kn}||\tau_{km}|\sin\left(\phi_{kn} - \phi_{km}\right)\Big) v^j_{n,t} \end{aligned}$$

$$- g_k \left|\tau_{km}\right|^2 v_{m,t}^j \Big] - \Big[\Big(b_k |\tau_{kn}||\tau_{km}| \cos\left(\phi_{kn} - \phi_{km}\right) - g_k |\tau_{kn}||\tau_{km}| \sin\left(\phi_{kn} - \phi_{km}\right) \Big) v_{n,t}^r - \left(b_k + b_{kn}^s\right) \left|\tau_{km}\right|^2 v_{m,t}^r \Big].$$

Then the IV-ACOPF formulation minimizes the system costs as follows:

$$\min_{v^r, v^j, p^g, q^g} \sum_{i \in \mathcal{I}} f_i \left(p_{i,t}^g\right) \tag{2.55}$$

subject to the linear constraints on the respective real and imaginary parts of the current flows, which are fully derived above, in

$$i_{k(n,m),t}^r = \mathrm{Re}\left(Y_{1,1}^k v_{n,t} + Y_{1,2}^k v_{m,t}\right), \qquad \forall k\,(n,m) \in \mathcal{F}, \tag{2.56}$$

$$i_{k(n,m),t}^j = \mathrm{Im}\left(Y_{1,1}^k v_{n,t} + Y_{1,2}^k v_{m,t}\right), \qquad \forall k\,(n,m) \in \mathcal{F}, \tag{2.57}$$

$$i_{k(m,n),t}^r = \mathrm{Re}\left(Y_{2,1}^k v_{n,t} + Y_{2,2}^k v_{m,t}\right), \qquad \forall k\,(m,n) \in \mathcal{F}, \tag{2.58}$$

$$i_{k(m,n),t}^j = \mathrm{Im}\left(Y_{2,1}^k v_{n,t} + Y_{2,2}^k v_{m,t}\right), \qquad \forall k\,(m,n) \in \mathcal{F}, \tag{2.59}$$

the following linear constraints on the nodal current balances in

$$i_{n,t}^r - \Big(\sum_{k(n,\cdot) \in \mathcal{F}} i_{k(n,m),t}^r + G_n^s v_{n,t}^r - B_n^s v_{n,t}^j \Big) = 0, \qquad \forall n \in \mathcal{N}, \tag{2.60}$$

$$i_{n,t}^j - \Big(\sum_{k(n,\cdot) \in \mathcal{F}} i_{k(n,m),t}^j + G_n^s v_{n,t}^j + B_n^s v_{n,t}^r \Big) = 0, \qquad \forall n \in \mathcal{N}, \tag{2.61}$$

the real and reactive nodal power injections balance in

$$\left(v_{n,t}^{r} i_{n,t}^{r} + v_{n,t}^{j} i_{n,t}^{j}\right) - p_{n,t}^{+} + p_{n,t}^{-} = 0, \qquad \forall n \in \mathcal{N}, \ (2.62)$$

$$\left(v_{n,t}^{j} i_{n,t}^{r} - v_{n,t}^{r} i_{n,t}^{j}\right) - q_{n,t}^{+} + q_{n,t}^{-} = 0, \qquad \forall n \in \mathcal{N}, \ (2.63)$$

the limits on real and reactive power outputs on generating units in

$$\underline{P}_{i} \leq p_{i,t}^{g} \leq \overline{P}_{i}, \qquad \forall i \in \mathcal{I}, \ (2.64)$$

$$\underline{Q}_{i} \leq q_{i,t}^{g} \leq \overline{Q}_{i}, \qquad \forall i \in \mathcal{I}, \ (2.65)$$

the nodal voltage limits in

$$\left(\underline{V}_{n}\right)^{2} \leq \left(v_{n,t}^{r}\right)^{2} + \left(v_{n,t}^{j}\right)^{2} \leq \left(\overline{V}_{n}\right)^{2}, \qquad \forall n \in \mathcal{N}, \ (2.66)$$

the thermal capacity limit on transmission elements in

$$\left(i_{k(\cdot),t}^{r}\right)^{2} + \left(i_{k(\cdot),t}^{j}\right)^{2} \leq \left(\overline{I}_{k}\right)^{2}, \qquad \forall k\left(\cdot\right) \in \mathcal{F}, \ (2.67)$$

and the limit on the voltage angle difference for interconnected buses in

$$\underline{\Theta}_{nm} \leq \arctan\left(v_{n,t}^{j} / v_{n,t}^{r}\right) - \arctan\left(v_{m,t}^{j} / v_{m,t}^{r}\right) \leq \overline{\Theta}_{nm}, \qquad \forall \left(n, m\right) \in \mathcal{A}, \ (2.68)$$

where for a given node $n \in \mathcal{N}$ the real and reactive power injections equal the generation, i.e., $p^+_{n,t} = \sum_{i \in \mathcal{I}(n)} p^g_{i,t}$ and $q^+_{n,t} = \sum_{i \in \mathcal{I}(n)} q^g_{i,t}$, and the real and reactive power withdrawals equal the demand, i.e., $p^-_{n,t} = P^d_{n,t}$ and $q^-_{n,t} = Q^d_{n,t}$. For the optimization problem in (2.55)−(2.68), the variables are the same as in the rectangular formulation in Section 2.7.2.

2.10 Mathematically Equivalent ACOPF Formulations

The following proves that the polar ACOPF, rectangular ACOPF, and the IV-ACOPF excluding line capacity limits are mathematically equivalent formulations.

Theorem 2.2. *The polar ACOPF (mP) in* (2.30)−(2.35) *and* (2.37)*, the rectangular ACOPF (mR) in* (2.40) − (2.45) *and* (2.47)*, and the IV-ACOPF (mC) in* (2.55) − (2.66) *and* (2.68) *are isomorphic.*

Proof. In order to prove this theorem, Euler's Law, Thévenin's theorem and the superposition theorem as applied in Lemma 2.1, and trigonometric identities are invoked. First the equivalence between the polar ACOPF and rectangular ACOPF is proven. Second, the equivalence between the rectangular ACOPF and IV-ACOPF is proven. Third, by transitivity the equivalence of the polar ACOPF and IV-ACOPF holds. In other words,

$$mP, mR, mC \Longrightarrow (mP = mR \wedge mR = mC)\,, \tag{2.69}$$

$$(mP = mR \wedge mR = mC) \Longrightarrow mP = mC. \tag{2.70}$$

Step 1. *Show $mP = mR$.*

(a). First, by Euler's Law:

$$v^r_{n,t} = |v_{n,t}| \cos\theta_{n,t}, \tag{2.71}$$

$$v^j_{n,t} = |v_{n,t}| \sin\theta_{n,t}. \tag{2.72}$$

Given the following nodal power flow balances of mP as:

$$|v_{n,t}| \sum_{m\in\mathcal{N}} |v_{m,t}| \left(G_{nm}\cos\theta_{nm,t} + B_{nm}\sin\theta_{nm,t}\right) - p^+_{n,t} + p^-_{n,t} = 0,$$

$$|v_{n,t}| \sum_{m\in\mathcal{N}} |v_{m,t}| \left(G_{nm}\sin\theta_{nm,t} - B_{nm}\cos\theta_{nm,t}\right) - q^+_{n,t} + q^-_{n,t} = 0,$$

and then applying sine and cosine angle sum and difference identities leads to:

$$\begin{aligned}
&|v_{n,t}| \sum_{m\in\mathcal{N}} |v_{m,t}| \left(G_{nm}\cos\theta_{n,t}\cos\theta_{m,t} + G_{nm}\sin\theta_{n,t}\sin\theta_{m,t}\right)\\
&+ |v_{n,t}| \sum_{m\in\mathcal{N}} |v_{m,t}| \left(B_{nm}\sin\theta_{n,t}\cos\theta_{m,t} - B_{nm}\cos\theta_{n,t}\sin\theta_{m,t}\right) - p^+_{n,t} + p^-_{n,t} = 0,\\
&|v_{n,t}| \sum_{m\in\mathcal{N}} |v_{m,t}| \left(G_{nm}\sin\theta_{n,t}\cos\theta_{m,t} - G_{nm}\cos\theta_{n,t}\sin\theta_{m,t}\right)\\
&- |v_{n,t}| \sum_{m\in\mathcal{N}} |v_{m,t}| \left(B_{nm}\cos\theta_{n,t}\cos\theta_{m,t} + B_{nm}\sin\theta_{n,t}\sin\theta_{m,t}\right) - q^+_{n,t} + q^-_{n,t} = 0.
\end{aligned}$$

Next, using the substitutions in (2.71) *and* (2.72) *results in the nodal power flow*

balances of mQ as follows:

$$v_{n,t}^r \sum_{m\in\mathcal{N}} \left(G_{nm}v_{m,t}^r - B_{nm}v_{m,t}^j\right) + v_{n,t}^j \sum_{m\in\mathcal{N}} \left(G_{nm}v_{m,t}^j + B_{nm}v_{m,t}^r\right) - p_{n,t}^+ + p_{n,t}^- = 0,$$

$$v_{n,t}^j \sum_{m\in\mathcal{N}} \left(G_{nm}v_{m,t}^r - B_{nm}v_{m,t}^j\right) - v_{n,t}^r \sum_{m\in\mathcal{N}} \left(G_{nm}v_{m,t}^j + B_{nm}v_{m,t}^r\right) - q_{n,t}^+ + q_{n,t}^- = 0,$$

for all $n \in \mathcal{N}$.

(b). Second, by Euler's Law,

$$|v_{n,t}| = \sqrt{\left(v_{n,t}^r\right)^2 + \left(v_{n,t}^j\right)^2},$$

and applying it to the nodal voltage constraint of mP:

$$\underline{V}_n \le |v_{n,t}| \le \overline{V}_n, \qquad \forall n \in \mathcal{N},$$

results in the nodal voltage constraint of mQ:

$$(\underline{V}_n)^2 \le \left(v_{n,t}^r\right)^2 + \left(v_{n,t}^j\right)^2 \le \left(\overline{V}_n\right)^2, \qquad \forall n \in \mathcal{N}.$$

(c). Last, by Euler's Law:

$$|v_{n,t}| = \sqrt{\left(v_{n,t}^r\right)^2 + \left(v_{n,t}^j\right)^2},$$

and applying it to the angle difference constraint of mP:

$$\underline{\Theta}_{nm} \leq \theta_{nm,t} \leq \overline{\Theta}_{nm}, \qquad \forall\,(n,m) \in \mathcal{A},$$

results in the angle difference constraint of mQ:

$$\underline{\Theta}_{nm} \leq arctan\left(v^j_{n,t}/v^r_{n,t}\right) - arctan\left(v^j_{m,t}/v^r_{m,t}\right) \leq \overline{\Theta}_{nm}, \qquad \forall\,(n,m) \in \mathcal{A}.$$

Therefore, $mP = mQ$ holds.

Step 2. *Show $mR = mC$. Substituting for the $i^r_{n,t}$ and $i^j_{n,t}$ terms in the real and reactive nodal power injections balance of mC, i.e.,*

$$\left(v^r_{n,t} i^r_{n,t} + v^j_{n,t} i^j_{n,t}\right) - p^+_{n,t} + p^-_{n,t} = 0, \qquad \forall n \in \mathcal{N},$$

$$\left(v^j_{n,t} i^r_{n,t} - v^r_{n,t} i^j_{n,t}\right) - q^+_{n,t} + q^-_{n,t} = 0, \qquad \forall n \in \mathcal{N},$$

with the linear constraints on the nodal current balances in

$$i^r_{n,t} - \Big(\sum_{k(n,\cdot)\in\mathcal{F}} i^r_{k(n,m),t} + G^s_n v^r_{n,t} - B^s_n v^j_{n,t} \Big) = 0, \qquad \forall n \in \mathcal{N},$$

$$i^j_{n,t} - \Big(\sum_{k(n,\cdot)\in\mathcal{F}} i^j_{k(n,m),t} + G^s_n v^j_{n,t} + B^s_n v^r_{n,t} \Big) = 0, \qquad \forall n \in \mathcal{N},$$

results in the following expressions for mC:

$$v^r_{n,t}\Big(\sum_{k(n,\cdot)\in\mathcal{F}} i^r_{k(n,m),t} + G^s_n v^r_{n,t} - B^s_n v^j_{n,t}\Big) + v^j_{n,t}\Big(\sum_{k(n,\cdot)\in\mathcal{F}} i^j_{k(n,m),t} + G^s_n v^j_{n,t} + B^s_n v^r_{n,t}\Big)$$

$$- p^+_{n,t} + p^-_{n,t} = 0, \tag{2.73}$$

$$v^j_{n,t}\Big(\sum_{k(n,\cdot)\in\mathcal{F}} i^r_{k(n,m),t} + G^s_n v^r_{n,t} - B^s_n v^j_{n,t}\Big) - v^r_{n,t}\Big(\sum_{k(n,\cdot)\in\mathcal{F}} i^j_{k(n,m),t} + G^s_n v^j_{n,t} + B^s_n v^r_{n,t}\Big)$$

$$- q^+_{n,t} + q^-_{n,t} = 0. \tag{2.74}$$

Then by incorporating the linear current flow constraints of mC, i.e.,

$$i^r_{k(n,m),t} = \mathrm{Re}\left(Y^k_{1,1} v_{n,t} + Y^k_{1,2} v_{m,t}\right), \qquad \forall k\,(n,m) \in \mathcal{F},$$

$$i^j_{k(n,m),t} = \mathrm{Im}\left(Y^k_{1,1} v_{n,t} + Y^k_{1,2} v_{m,t}\right), \qquad \forall k\,(n,m) \in \mathcal{F},$$

$$i^r_{k(m,n),t} = \mathrm{Re}\left(Y^k_{2,1} v_{n,t} + Y^k_{2,2} v_{m,t}\right), \qquad \forall k\,(m,n) \in \mathcal{F},$$

$$i^j_{k(m,n),t} = \mathrm{Im}\left(Y^k_{2,1} v_{n,t} + Y^k_{2,2} v_{m,t}\right), \qquad \forall k\,(m,n) \in \mathcal{F},$$

into expressions (2.73) *and* (2.74)*, the real and reactive power flows, i.e.,* (2.20) *and* (2.21)*, for the full network can be aggregated as follows:*

$$\sum_{k(n,\cdot)\in\mathcal{F}} p_{k(n,m),t} + \left(\left(v^r_{n,t}\right)^2 + \left(v^j_{n,t}\right)^2\right) G^s_n - p^+_{n,t} + p^-_{n,t} = 0, \tag{2.75}$$

$$\sum_{k(n,\cdot)\in\mathcal{F}} q_{k(n,m),t} - \left(\left(v^r_{n,t}\right)^2 + \left(v^j_{n,t}\right)^2\right) B^s_n - q^+_{n,t} + q^-_{n,t} = 0. \tag{2.76}$$

Consequently, the expressions (2.75) *and* (2.76) *are equivalent to constraints* (2.48) *and* (2.49) *of mQ. Therefore by Lemma 2.1, the expressions* (2.75) *and* (2.76) *are equivalent to the nodal power balance of mQ:*

$$v_{n,t}^r \sum_{m\in\mathcal{N}} \left(G_{nm}v_{m,t}^r - B_{nm}v_{m,t}^j\right) + v_{n,t}^j \sum_{m\in\mathcal{N}} \left(G_{nm}v_{m,t}^j + B_{nm}v_{m,t}^r\right) - p_{n,t}^+ + p_{n,t}^- = 0,$$

$$v_{n,t}^j \sum_{m\in\mathcal{N}} \left(G_{nm}v_{m,t}^r - B_{nm}v_{m,t}^j\right) - v_{n,t}^r \sum_{m\in\mathcal{N}} \left(G_{nm}v_{m,t}^j + B_{nm}v_{m,t}^r\right) - q_{n,t}^+ + q_{n,t}^- = 0,$$

for all $n \in \mathcal{N}$.

As a result, $mQ = mC$ *holds.*

Step 3. *Since* $mP = mR$ *and* $mR = mC$ *holds, by transitivity* $mP = mC$ *holds.* □

2.11 Discussion and Extensions

The key distinction between the canonical ACOPF formulations and the IV-ACOPF are the way that the network flows are modeled. The canonical ACOPF formulations compute the nonlinear and nonconvex apparent power flows, whereas the IV-ACOPF computes linear current flows and then balances the nodal power injections and withdrawals through constraints that relate the bilinear terms within each node. As proven above, the polar and rectangular forms of the canonical ACOPF problem as well as the IV-ACOPF are mathematically equivalent approaches, excluding the line capacity limits on the apparent power in (2.36) and (2.46) compared to the line ther-

mal limits on the current magnitude in (2.67). The line flow constraints[31] in terms of thermal limits on the current magnitude is a more direct function of the actual physical limits due to the temperature sensitivity of the conductor and supporting material in the transmission line and elements, where the heating of the material is a function of the current; in fact, current is the only crucial quantity to be measured with respect to thermal capacity limits [54].

There are some similarities in the three presented OPF formulations: the upper bound on the voltage magnitude in (2.35), (2.45) and (2.66), as well as the upper bound on the line capacity in (2.36), (2.46) and (2.67), are nonlinear and convex. The lower bound on the voltage magnitude in (2.35), (2.45) and (2.66), as well as the arctan functions in (2.47) and (2.68) are nonlinear and concave. Often the angle difference constraint in (2.37), (2.47) and (2.68) is omitted since there are capacity limits on the lines between interconnected nodes.

The following chapters extend the network modeling principles presented here. More specifically, Chapters 3 and 4 of Part II introduce novel local solution methods in order to solve the proposed IV-ACOPF formulation for day-ahead, intra-day, and

[31] Typically the only available line parameters are the impedance, line charge, and the nominal voltage limits of the interconnecting buses. Therefore it is common to estimate the thermal limit with the Surge Impedance Loading (SIL) defined as

$$SIL = V_{LL}^2 \Big/ Z_0 \tag{2.77}$$

where V_{LL} is the line-to-line voltage in volts, $Z_0 = \sqrt{L/C}$, L is the inductance per unit length, and C is the capacitance per unit length. A significant shortcoming of this approach is that all lines within a given voltage level have the same thermal limit which is not reflective of actual physical conditions [61, 62].

real-time market applications. Then Chapters 5 and 6 of Part III focus on global solution techniques to solve OPF models for the particular application of optimal storage integration.

II Local Solution Methods

3 A Successive Linear Programming Approach to Solving the IV-ACOPF

3.1 Prologue and Motivation

Chapter 2 presented the steady-state modeling framework underlying the ACOPF, which is defined as:

The simultaneous co-optimization of real and reactive power dispatch subject to operational and physical network constraints in order to minimize system operating costs.

However as discussed in Chapters 1 and 2, the ACOPF formulation is a nonlinear and nonconvex problem that is currently impractical to solve directly in electricity markets. Improved formulations of and solution techniques for the ACOPF problem are critical to improving current practices in the day-ahead, intra-day, and real-time markets. Chapter 3 extends the proposed IV-ACOPF formulation introduced in Section 2.9 and presents a SLP approach, which is a local solution method to solve the problem; global solution methods are later explored in Part II of this dissertation

work.

A sequential linear program solves a sequence of linear approximations, converging to a stationary point, i.e., a KKT point [63]. The sequence of linear approximations are based on a first order Taylor series approximation of nonlinear terms in the objective functions and constraints. For an arbitrary multivariate function $f : \mathbb{R}^N \to \mathbb{R}$ and variable vector $\boldsymbol{x} \in \mathbb{R}^N$,

$$f(\boldsymbol{x}) \coloneqq f\left(\hat{\boldsymbol{x}}^{(\boldsymbol{h})}\right) + J_f\left(\hat{\boldsymbol{x}}^{(\boldsymbol{h})}\right)\left(\boldsymbol{x} - \hat{\boldsymbol{x}}^{(\boldsymbol{h})}\right) + o\left(\|\boldsymbol{x} - \hat{\boldsymbol{x}}^{(\boldsymbol{h})}\|\right)$$

where $\hat{\boldsymbol{x}}^{(\boldsymbol{h})}$ is a fixed point in $\mathbb{R}^N$, $J_f\left(\hat{\boldsymbol{x}}^{(\boldsymbol{h})}\right) = \bigtriangledown_{\hat{\boldsymbol{x}}^{(\boldsymbol{h})}} f^T$, and o is the little o-notation, which is used to denote the asymptotic behavior of the approximation error. For functions with bilinear terms only, the first two terms analytically derive a linear approximation of the nonlinear function and can be solved as a SLP for $\boldsymbol{x} \to \hat{\boldsymbol{x}}^{(\boldsymbol{h})}$ in iterations $h \in \mathcal{H}$; therefore the last (remainder) term is an indication of the approximation error. As such, this method may be used in conjunction with a penalty term. As discussed in Chapter 2, the necessary conditions are not sufficient to prove optimality of the KKT point to the original nonlinear program if it is nonconvex; in this case, the KKT point can be a local optimum, a saddlepoint, or a global optimum.

For large-scale problems, SLP approaches are more computationally efficient than sequential quadratic programming (SQP) approaches; however SQP approaches are

robust in inducing global convergence.[32] Furthermore, both approaches have the potential difficulty of finding a global optimum of the nonconvex subproblems in the iterates [64]. A significant disadvantage of SLP approaches includes the violating of nonlinear constraints during the iterative process to achieve optimality [65]. This work presents novel infeasibility handling that utilizes the mathematical structure of the OPF to address this drawback.

The approach proposed in this chapter leverages commercial LP solvers Gurobi [66] and CPLEX [67], which are the current industry standard. As a result, the SLP approach can be readily extended and integrated into more complex decision processes, e.g., unit commitment as presented next in Chapter 4. This chapter demonstrates that the proposed SLP approach achieves an acceptable quality of convergence to a best-known solution and linear scaling of computational time in proportion to network size. Moreover, the time complexity of the SLP algorithm outperforms that of the NLP commercial solvers for the full range of test networks. As a result, the SLP algorithm is expected to outperform the NLP solvers tested, i.e., IPOPT and KNITRO, on larger scale networks. Furthermore, the SLP algorithm could be applied in parallel with both Gurobi and CPLEX from various starting points, which may further improve the reported linear time complexity. These results were originally published in [22].

[32]For an arbitrary initialization, the sequence of solutions generated by the iterative algorithm converges to a stationary point [41].

3.2 Introduction

The ACOPF problem co-optimizes real and reactive power dispatch in order to promote reliable operation and efficient markets. The ACOPF originated from Carpentier's reformulation of the economic dispatch problem based on the KKT conditions [4]. Identifying a globally optimal solution to the ACOPF is known to be NP hard [2, 3]. Consequently, this key dispatch problem is not presently solved exactly, although doing so would address many of the operational challenges in markets today. According to Stott and Alsaç [5], there are basic requirements other than absolute optimality for practical and non-trivial applications, and the appropriate amount of detail is a balance among several objectives which are situationally dependent.

As such, ISOs and other grid operators use approximations in order to leverage the performance of commercial LP/MILP solvers such as Gurobi [66] and CPLEX [67]. System operators frequently solve the DCOPF problem adjusted with loss factors. As detailed in Chapter 2, the DCOPF approach holds voltage constant, ignores reactive power flows, assumes small voltage angle differences, and models resistances as much less than reactances on network components. Subsequently, AC feasibility is achieved through an iterative process in which metaheuristics are applied in order to ensure that a realistic engineering solution is obtained by the DCOPF model and to identify constraint violations that may require preventive actions including re-dispatch, reactive power compensation, and voltage support. Some system operators solve a

decoupled OPF model, which iterates between $p - \theta$ and $q - v$ subproblems in order to check for AC feasibility [6]. As a result, dispatch and prices are usually obtained within the required time limits, but these approximations can lead to suboptimal solutions, e.g., when the system is stressed or when there is a strong physical coupling between real and reactive power.

The DCOPF and decoupled OPF approaches oversimplify the physical problem and require operator intervention in the day-ahead, intra-day, and real-time markets. Purchala et al. [68] demonstrate that the DCOPF approach is acceptable if the voltage profile is sufficiently flat, the resistance-to-reactance ratio of transmission lines is less than 0.25, and the network is not heavily loaded. In many cases these conditions do not hold in actual networks, therefore the DCOPF approach may not be able to physically dispatch the resources that are required to satisfy constraints, such as voltage limits, that are not accurately reflected in the market software. For example, system operators intervene in order to commit units for voltage and local reliability requirements within load pockets; producing voltage and reactive power schedules without compromising MW line capacity limits and efficiency would require ACOPF constraint modeling [69].

The computational tractability and convexity of any solution approach is critical to support market clearing strategies based on the LMP. In the DCOPF and decoupled OPF models, the LMP is highly dependent on the modeling assumptions.[33] Without

[33]see Sections 2.6.2 and 2.6.3

transparency into the exact form of the problem solved in the markets, it is difficult to assess to what extent price signals are ensuring efficient and reliable operations. In 2009, Liu et al. [70] reported that full derivations of the LMP are not available in ISO tariffs and other publicly available manuals. Furthermore, the clearing prices in current markets do not reflect the true marginal cost of production, which accounts for all physical and operational system constraints and also fully compensates all resources for the variable cost of providing service [13]. Subsequently, certain resources may be committed outside of the market to address reliability issues, which results in uplift payments [15]. A central challenge in accounting for better physical and operational constraints is to apply better representations of the underlying AC power system in the market software [13].

Efforts to incorporate all physical and operational constraints have been an important part of the last half century's work on load flow and ACOPF formulations, decomposition methods, and algorithms; please see [21, 44–51] for comprehensive surveys. Kirchhoff's laws impose nonconvex constraints through the products of unknown bus voltages, which are represented in either polar or rectangular coordinates, or a combination of both [60]. Both power injection [71] and current injection [60] formulations have been developed to solve the load flow problems. When rectangular coordinates with current injections are applied to determine the load flow, the network balancing becomes a linear system of equations. This load flow approach is

applied in the proposed IV-ACOPF problem,[34] which is mathematically equivalent to the canonical ACOPF.[35]

In this work the SLP algorithm is presented to solve the proposed IV-ACOPF problem. This algorithm uses first-order Taylor series expansions to construct local subproblems, along with a combination of outer approximation and constraint reduction techniques. Each subproblem solves a coupled model and the solution technique iteratively co-optimizes real and reactive power dispatch simultaneously. This approach can be extended to include discrete controls and also can be embedded within branch-and-bound algorithms to support more complex decision processes, including unit commitment and transmission switching. Since ISO market software depends on commercial LP/MILP solvers, this proposed approach is suitable for such applications; furthermore the solution is tractable and the LMPs and Q-LMPs are recoverable. This approach demonstrates an acceptable quality of convergence to the best-known solution and linear scaling of computational time in proportion to network size as compared to that of the reported nonlinear programming (NLP) approaches. These performance characteristics may be achieved in real-world applications.

The remainder of this chapter is organized as follows. Section 3.3 provides a literature review of seminal and recent linearization and convexification techniques for the ACOPF. Section 3.4 introduces the framework and convergence quality for general SLP algorithms. Then Section 3.5 summarizes the proposed SLP algorithm

[34] see Section 2.9
[35] see Section 2.10

and Section 3.6 formulates the local subproblem of the SLP. Section 3.7 demonstrates the computational performance and convergence quality of the SLP IV-ACOPF algorithm. Section 3.8 concludes this chapter with a brief discussion of the results.

3.3 Related Work

Most LP approaches take advantage of the loose coupling between voltage angle and magnitude, as initially proposed by Alsaç and Stott [72]. Such decoupled approaches can be difficult to resolve if the system has high losses, is highly loaded, or either subproblem is infeasible. Kirschen and Meeteren [73] propose an improved method which reschedules real power controls in order to correct voltage magnitude violations that arise in the decoupled subproblem. However, when there is a strong physical coupling between $p - q$, even such reschedules can be ineffective.

Coupled models, such as the one proposed in this work, respect bus voltage limits and reactive power requirements during real power scheduling. Although the decoupled model has smaller subproblems in each iteration, the coupled version can take fewer iterations and be faster overall depending upon the linearization technique and underlying network [74]. Other coupled models include the recent works described in [75–77]. Franco et al. [75] apply a least-squares regression to obtain a non-iterative linear approximation of the ACOPF in terms of the real and imaginary voltage components. However, the study omits numerous physical constraints (e.g., voltage magnitudes, reactive power, and line limits) that are important to power sys-

tems operations. Mohapatra et al. [76] formulate the ACOPF in terms of incremental variables and then solve the nonlinear formulation by applying Newton's method and the primal-dual interior point methods; however this approach neglects thermal line limits. Coffrin et al. [77] apply piecewise linear approximations of the cosine term and Taylor series expansions of the remaining nonlinear terms. The piecewise linear approximations result in discontinuous derivatives and moreover the accuracy of this approach depends on the number of segments used, which can result in a heavy computational burden for large-scale or more densely connected networks. All three studies report applications on limited sized networks and apply local solution methods, which are not guaranteed to converge to a global optimum since the ACOPF is nonconvex.

Therefore there is growing interest in applying convexification techniques to the ACOPF in order to find a global optimum. Like linear and quadratic programs,

semidefinite programming[36] (SDP) and second-order conic programming[37] (SOCP) approaches can be solved in polynomial time by interior point methods. Such convex reformulations can be valuable in determining bounds on nonconvex problems and also to initialize local solution methods. Bai et al. [52] propose a SDR for which Lavaei and Low [24] derive a rank-one sufficient condition under which the SDR is exact, i.e., a global optimum is guaranteed. It has been proven that if the network is radial, then this sufficient condition always holds [24, 79] and the SOCR is equivalent to solving the ACOPF for these cases [80]; this can be attributed to the fact that

[36]For example, for the standard form LP expressed as:

$$\begin{aligned} &\min_{x} c^T x \\ &\text{s.t.} \\ &Ax = b \\ &x \geq 0, \end{aligned}$$

where $A \in \mathbb{R}^{p \times n}$, $c \in \mathbb{R}^{n \times 1}$, and $b \in \mathbb{R}^{p \times 1}$, a standard form SDP has linear equality constraints and a matrix nonnegativity constraint on the variable $X \in \mathcal{S}^n$:

$$\begin{aligned} &\min_{X} \operatorname{tr}(CX) \\ &\text{s.t.} \\ &\operatorname{tr}(A_i X) = b_i, \quad i = 1, ..., p \\ &X \succeq 0, \end{aligned}$$

where $\operatorname{tr}\{\cdot\}$ is the trace operator, and $C, A_i, ..., A_p \in \mathcal{S}^n$. Recall that $\operatorname{tr}(CX) = \sum_{i,j=1}^{n} C_{ij} X_{ij}$. The notation $\mathcal{S}^k$ denotes the set of symmetric $k \times k$ matrices [78].

[37]For example, a SOCP can be expressed as:

$$\begin{aligned} &\min_{x} f^T x \\ &\text{s.t.} \\ &\|A_i x + b_i\|_2 \leq c_i^T x + d_i, \quad i = 1, ..., m \\ &Fx = g, \end{aligned}$$

where $x \in \mathbb{R}^n$ is the optimization variable, $A_i \in \mathbb{R}^{n_i \times n}$, and $F \in \mathbb{R}^{p \times n}$. The second-order cone constraint requires the affine function $\left(A_i x + b_i, c_i^T x + d_i\right)$ to lie in the second-order cone in $\mathbb{R}^{n_i \times 1}$. If $A_i = 0, i = 1, ..., m$, then the SOCP reduces to a general LP [78].

the power flow solution of a radial network is unique [81]. A shortcoming of these convexifications is that there is no mechanism to recover an ACOPF feasible solution when the sufficient condition is not satisfied. Therefore Molzahn and Hiskens [82] and Josz et al. [83] propose moment relaxations in order to obtain tighter lower bounds. Furthermore, there are still practical difficulties in efficiently implementing a SDR in a mixed integer problem (MIP) including the lack of an initialization method and limitations in scalability due to the number of linear algebraic iterations required during the solution process. Moreover, Lesieutre et al. [84] illustrate practical scenarios where the SDR fails to produce physically meaningful solutions.

There has been a number of SOCR applied to the ACOPF, e.g., please see [85–89], which is a weaker relaxation than the SDR in general. The computational effort per iteration to solve SOCP problems is greater than that required to solve linear and quadratic programs, but less than that required to solve a SDP problem of similar size and structure [78]. Kocuk et al. propose strong SOCR formulations, which are an order of magnitude faster than standard SDR formulations but not as tight, and are also an order of magnitude slower yet more accurate than Jabr's original SOCR formulation [85]. The SOCR solutions are often inexact but with a finite optimality gap; closing the gap may require stronger bounds (which could guarantee a global optimum when exact) or a local solution method in order to achieve ACOPF feasibility. Although these approaches may be more suitable than SDR in a mixed integer approach, current drawbacks include the need to initialize from a strictly

feasible primal-dual pair of solutions, and determining feasibility with respect to the integer variables on inexact solutions. Incorporating convex relaxations into more complex decision processes that also include mixed integer variables is a growing research area that is still in early stages of development.

In conclusion, current state-of-the-art advancements continue to demonstrate trade-offs between convergence quality and computational performance.

3.4 Fundamentals of General SLP Algorithms

The earliest known application of SLP is the 1961 publication by Griffith and Stewart where the authors apply this approach to optimize a large-scale nonlinear chemical process model [90]. In general, the SLP algorithm seeks to solve a penalty problem P^{ε} in order to solve the original nonlinear problem P of the form

$$
\begin{aligned}
P : & \min_{x} f(x) \\
& \text{s.t.} \\
& g_i(x) \leq 0, \quad i = 1, ..., m \\
& h_i(x) = 0, \quad i = 1, ..., p \\
& x \in \mathcal{X} \coloneqq \{x : Ax \leq b\},
\end{aligned}
$$

where all the functions are continuously differentiable, $x \in \mathbb{R}^n$, and the linear constraints defining the problem are included into the set $\mathcal{X}$; the penalty problem P^{ε} is

as follows:

$$P^{\varepsilon} : \min_{x} \left\{ f^{\varepsilon}(x) : x \in \mathcal{X} \right\},$$

where

$$f^{\varepsilon}(x) = f(x) + \mu \left[\sum_{i=1}^{m} \max \left\{ 0, g_i(x) \right\} + \sum_{i=1}^{p} |h_i(x)| \right]$$

for penalty parameter $\mu > 0$. Bazaraa et al. prove that solving P^{ε} is equivalent to solving P, i.e., a KKT point is a solution in P^{ε} if and only if the KKT point is a solution in P [65]. Furthermore, by Theorem 10.3.1 [65], the authors prove the following convergence behavior for a SLP:

1. If x_k in iteration k of the SLP is a KKT point for P^{ε} and it is feasible to P, then it is a KKT point for P.

2. The solution to the SLP with direction $d_k = 0$ is optimal[38] for the LP(x_k, δ_k)[39] for step size δ_k if and only if x_k is a KKT point for P^{ε}.

[38]The stopping criterion $d_k = 0$ is typically replaced by several practical termination criteria. For example, given a specified tolerance ε if the iterate is ε-feasible and either the KKT conditions are satisfied within an ε-tolerance or the fractional change in the objective function value for P is less than ε for c consecutive iterations, the procedure can be terminated [65].

[39]The linear program LP(x_k, δ_k) represents the direction finding subproblem for iterate k, which yields an optimal direction d_k [65]. In other words, given a feasibly point x_k, a direction d_k is determined such that for step size $\delta_k > 0$, the following properties hold true:

(a) $x_k + \delta_k d_k$ is feasible, and

(b) the objective value at $x_k + \delta_k d_k$ is better than the objective value at x_k.

3. Either the SLP terminates finitely or else an infinite sequence $\{x_k\}$ is generated such that if the problem is bounded, then $\{x_k\}$ has an accumulation point, and every such accumulation point is a KKT point for P^{ε}.

Only if x_k satisfies the second-order sufficiency conditions for P is it then a global optimum. However, convergence to a global optimum is not guaranteed.

Not to be mistaken with convergence to a global optimum, Fletcher, Leyffer and Toint [91] prove global convergence to a KKT point by incorporating second-order information used in conjunction with a trust region, merit function,[40] and filter method.[41] Even so, the sufficient conditions for optimality can not be guaranteed a priori since the SLP is a local solution method and not a global solution method. Given the above convergence qualities of SLP, this work proceeds to formulate the SLP IV-ACOPF algorithm. Then the scalability and performance of the proposed approach is demonstrated on a full range of test networks.

3.5 Algorithm Outline

The overall solution strategy in the SLP IV-ACOPF is depicted in the process diagram of Figure 3.1. In the initial iteration ($h = 0$), the algorithm initializes the variables and the evaluation point for the first order Taylor series approximations using a flat

[40] A merit function in constrained optimization allows iterates to violate the constraints and requires some means to assess the quality of the steps [41].

[41] Filter techniques are a step acceptance mechanism based on ideas from multiobjective optimization where the filter method accepts a trial step x^+ as a new iterate if the pair $(f_k(x^+), h_k(x^+))$ for the objective function f_k and the measure of infeasibility in function h_k for iteration k is not dominated by a previous pair $(f_{k-n}(x^+), h_{k-n}(x^+))$ for $0 \leq k - n < k$ [41].

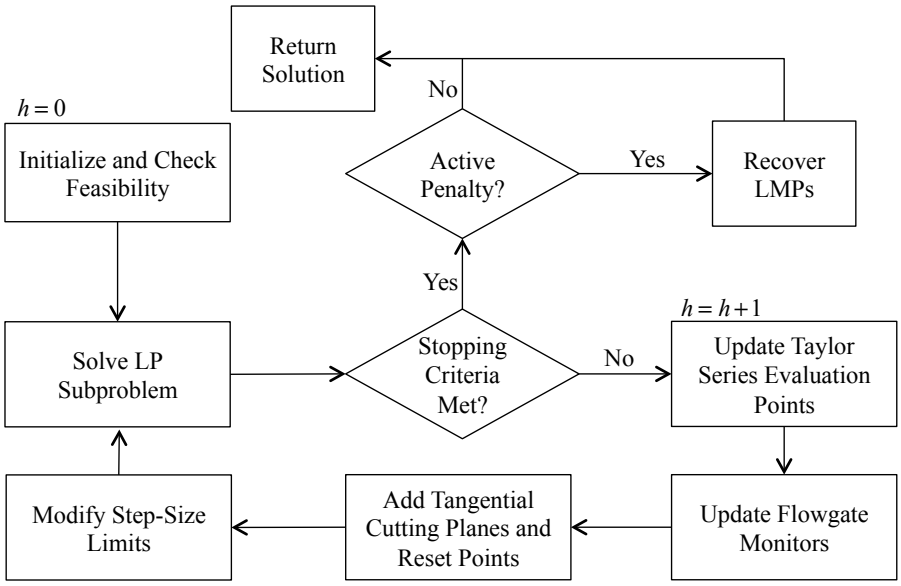

Figure 3.1: The SLP IV-ACOPF algorithm

start, warm start, or cold start. If the calculated power flows from this initialization are not feasible, the algorithm updates the initializations to reside within constraint bounds. The algorithm then iteratively solves the resulting LP subproblem by first updating the Taylor series evaluation points, which are denoted by placing a caret or "hat" over the corresponding parameter; for an arbitrary evaluation point $\hat{x}^{(h)}$, $\hat{x}^{(h)} = x^*$, which is the optimal solution from iteration $h - 1$.

After updating the evaluation points, the algorithm updates all flowgate monitors[42] in order to identify lines that are near or at capacities. For any evaluation point that is ACOPF infeasible according to the nodal voltage magnitude limits or the flowgate monitors, the algorithm projects the evaluation point to be within the original bounds and incorporates cutting planes to enforce feasibility in the following

[42]line capacity constraints that are observed

iteration; further details provided in Section 3.6.1.3. The step size bounds are also modified before re-solving the LP subproblem; these bounds limit the approximation error and control oscillations in the first order Taylor series. The algorithm imposes constraint satisfaction of the inequality constraints by introducing slack variables that are penalized in the cost function.

Following each iteration h, the stopping criteria assesses three possible scenarios: (1) the mismatch error on real and reactive power injections for all buses $n \in \mathcal{N}$ and time periods $t \in \mathcal{T}$ is less than a specified tolerance, (2) the net of these mismatches is less than a specified tolerance, or (3) the maximum iteration limit has been reached.

1: $P^*_{n,t} = P^d_{n,t} + v^{r*}_{n,t} i^{r*}_{n,t} + v^{j*}_{n,t} i^{j*}_{n,t}$

2: $Q^*_{n,t} = Q^d_{n,t} + v^{j*}_{n,t} i^{r*}_{n,t} - v^{r*}_{n,t} i^{j*}_{n,t}$

3: **for all** $n \in \mathcal{N}, t \in \mathcal{T}$ **do**

4: $\quad \delta^p_{n,t} \leftarrow \left|P^*_{n,t} - p^g_{n,t}\right| \Big/ \min\left(\left|P^*_{n,t}\right|, \left|p^g_{n,t}\right|\right)$

5: $\quad \delta^q_{n,t} \leftarrow \left|Q^*_{n,t} - q^g_{n,t}\right| \Big/ \min\left(\left|Q^*_{n,t}\right|, \left|q^g_{n,t}\right|\right)$

6: **end for**

7: **if** $\left(\begin{array}{c} \max\limits_{n\in\mathcal{N},t\in\mathcal{T}} \delta^p_{n,t} \le \Delta^P_n \textbf{ and } \max\limits_{n\in\mathcal{N},t\in\mathcal{T}} \delta^q_{n,t} \le \Delta^Q_n \\ \textbf{or } \sum_{n\in\mathcal{N},t\in\mathcal{T}} \delta^p_{n,t} \le \Delta^P \textbf{ and } \sum_{n\in\mathcal{N},t\in\mathcal{T}} \delta^q_{n,t} \le \Delta^Q \\ \textbf{or } h \ge \text{LIM} \end{array}\right)$ **then**

8: $\quad$ **return solution;**

9: **end if**

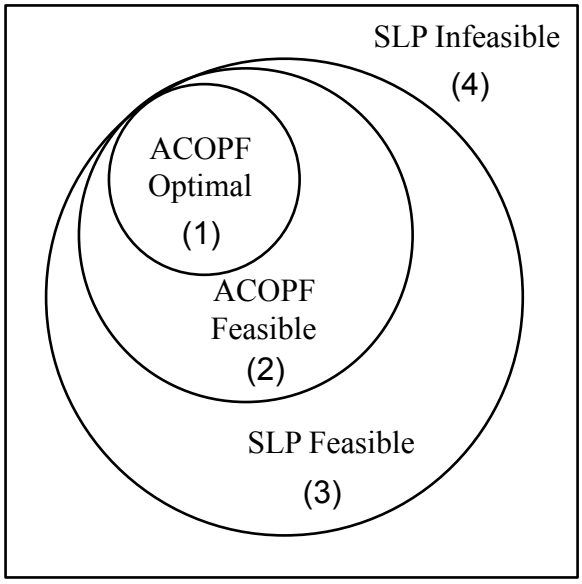

Figure 3.2: The SLP IV-ACOPF algorithm solution outcome

Upon termination, the algorithm can yield one of the four following outcomes[43] as illustrated in Figure 3.2: (1) a KKT point to the ACOPF is identified, (2) the SLP solution is ACOPF feasible but not optimal, (3) the SLP solution is ACOPF infeasible (i.e., there are active penalties present), or (4) the SLP solution is infeasible. Results meeting criteria (1) through (3) may be meaningful in practice. An additional step to recover the non-penalized LMPs is required if the criterion (3) is met; to recover the LMPs, the algorithm resets all the penalty factors to equal zero and re-solves the LP subproblem where the step-size limit is set to an infinitesimal quantity. However the solution to (3) would require operator judgment in order to assess whether the infeasibilities present in the model would cause undue operational stress.

A converged solution is defined as one meeting the mismatch tolerances as set in

[43]These outcomes are equivalent to the proven properties presented for general SLP algorithms in Section 3.4.

the stopping criteria. Since the necessary optimality conditions are related to the Taylor series approximations through first order derivatives, and first order Taylor series approximations are applied to all the nonlinear terms in the formulation, the algorithm is guaranteed a KKT point[44] to the ACOPF when the SLP algorithm converges with no active penalties, i.e., outcome (1). For a converged solution with active penalties, the algorithm has outcome (3). Outcome (2) is a result of early termination[45] and outcome (4) is due to poor parameterization, e.g., the SLP IV-ACOPF requires a better initialization or the step size was not appropriately computed from the prior iteration [65], of the SLP, or infeasibility or unboundedness in the ACOPF.

3.6 Algorithm Details

This section details a successive linearization of the proposed IV-ACOPF formulation presented in (2.55) − (2.67). Without loss of generality, this approach assumes all generating units to be thermal generation, i.e., $\mathcal{G} = \mathcal{I}$, where $p^g_{n,t} = \sum_{i \in \mathcal{G}(n)} p^g_{i,t}$ and $q^g_{n,t} = \sum_{i \in \mathcal{G}(n)} q^g_{i,t}$ for all $n \in \mathcal{N}, t \in \mathcal{T}$. However this approach can be readily extended to include other energy resources.

3.6.1 Linearization and Reduction Methods

This work applies approximations, relaxations, penalty variables, and constraint set reduction in order to reformulate the nonlinearities in (2.55) − (2.67) where the gen-

[44] within the specified tolerances

[45] When the ACOPF is bounded, otherwise outcome (4) occurs as $k \to \infty$.

erator cost function with nonnegative cost coefficients $C_i^{g,2}$ and $C_i^{g,1}$ is defined as

$$f_i(\cdot) = \sum_{t \in \mathcal{T}} \left[C_i^{g,2} \left(p_{i,t}^g \right)^2 + C_i^{g,1} p_{i,t}^g \right] \tag{3.1}$$

and is continuous in $p_{i,t}^g \in \left[\underline{P}_i, \overline{P}_i \right]$ for all $i \in \mathcal{G}$.

3.6.1.1 Piecewise Linear Interpolations

A piecewise linear interpolation can be applied to approximate the quadratic generator offer curve in (3.1) where the generators offer real power at marginal cost. Typically, generator offer curves are monotonically increasing, and by partitioning the interval into more linear segments, the approach detailed below results in a tighter upper bound[46] on the quadratic cost function. In practice, generators typically offer into the market where its supply offer is a step function; thus a piecewise linearization is an appropriate approach.

To construct the piecewise linear function, the real power production interval $\left[\underline{P}_i, \overline{P}_i \right]$ is partitioned into $|\mathcal{L}|$ into linear segments with length $P_i^g = \left(\overline{P}_i - \underline{P}_i \right) / |\mathcal{L}|$. There are $|\mathcal{L}|+1$ points where the l-th segment is associated with points

$$[x_{i,l}, x_{i,l+1}] := [\underline{P}_i + l P_i^g, \underline{P}_i + (l+1) P_i^g]. \tag{3.2}$$

For $l = 0, \ldots, |\mathcal{L}|$, $x_{i,0} < x_{i,1} < \ldots < x_{i,|\mathcal{L}|+1}$.

[46] See Theorem 3.1 for proof.

By calculating the midpoint and applying the slope of the offer curve for each segment $l \in \mathcal{L}$ and thermal generating unit $i \in \mathcal{G}$, the resulting cost coefficient is

$$C_{i,l}^{g} = C_{i}^{g,1} + \left(B^{\mathrm{MVA}}\right)^{2} C_{i}^{g,2} \left(x_{i,l} + x_{i,l+1}\right). \tag{3.3}$$

Note that the $\left(B^{\mathrm{MVA}}\right)^{2}$ is a constant accounting for any per-unit scaling of the power variables. The aggregate offer curve in (2.55) is approximated as

$$\text{offers}\left(\cdot\right)^{(h)} = \sum_{i \in \mathcal{G}, l \in \mathcal{L}, t \in \mathcal{T}} \left[C_{i,l}^{g} p_{i,l,t}^{g} + C_{i}^{g,0}\right] \tag{3.4}$$

for iteration h, where $C_{i}^{g,0} = \left(B^{\mathrm{MVA}}\right)^{2} C_{i}^{g,2} \left(\underline{P}_{i}\right)^{2} + C_{i}^{g,1} \underline{P}_{i}$ when $\underline{P}_{i} > 0$.

Furthermore, each segment $p_{i,l,t}^{g}$ of the piecewise linear function is limited by P_{i}^{g}, that is

$$p_{i,l,t}^{g} \leq P_{i}^{g} \tag{3.5}$$

for all $i \in \mathcal{G}$, $l \in \mathcal{L}, t \in \mathcal{T}$. The aggregate of the segments for thermal generator i in time t must equal the real power generation

$$p_{i,t}^{g} = \sum_{l \in \mathcal{L}} p_{i,l,t}^{g} + \underline{P}_{i} \tag{3.6}$$

for all $i \in \mathcal{G}, t \in \mathcal{T}$.

Theorem 3.1. *The piecewise linear function*

$$\text{offers}_i\left(\cdot\right)^{(h)} = \sum_{l\in\mathcal{L},t\in\mathcal{T}}\left[C_{i,l}^{g}p_{i,l,t}^{g} + C_i^{g,0}\right]$$

is an upper bound of the form

$$f_i\left(\cdot\right) \leq \text{offers}_i\left(\cdot\right)^{(h)}$$

on the quadratic objective function $f_i\left(\cdot\right)$ *in* (3.1) *for all thermal generating units* $i \in \mathcal{G}$.

Proof. Without loss of generality, set the minimum real power output parameter to zero (i.e., $\underline{P}_i = 0$), the linear cost coefficient to zero (i.e., $C_i^{g,1} = 0$), and represent the real power generation (i.e., $p_{i,t}^{g}$ for all time periods $t \in \mathcal{T}$) in nominal scaling (i.e., $\left(B^{\text{MVA}}\right)^2 = 1$) for each generator $i \in \mathcal{G}$.

Since $\partial^2 f_i\left(\cdot\right) \Big/ \partial\left(p_{i,t}^{g}\right)^2 \geq 0$ for the nonnegative cost coefficient $C_i^{g,2}$, the function $f_i\left(\cdot\right)$ is convex for all real power production outputs $p_{i,t}^{g} \in \left[\underline{P}_i, \overline{P}_i\right]$. Therefore, $f_i\left(\cdot\right)$ is also midpoint convex, i.e.,

$$\begin{aligned}
&f_i\left(\frac{x_{i,l} + x_{i,l+1}}{2}\right) \leq \frac{f_i\left(x_{i,l}\right) + f_i\left(x_{i,l+1}\right)}{2},\\
&f_i\left(\frac{\left(2l+1\right)P_i^{g}}{2}\right) \leq \frac{f_i\left(lP_i^{g}\right) + f_i\left(\left(l+1\right)P_i^{g}\right)}{2},\\
&\sum_{t\in\mathcal{T}}\left[C_i^{g,2}\left(\frac{\left(2l+1\right)P_i^{g}}{2}\right)^2\right] \leq \frac{\sum_{t\in\mathcal{T}}\left[C_i^{g,2}\left(lP_i^{g}\right)^2\right] + \sum_{t\in\mathcal{T}}\left[C_i^{g,2}\left(\left(l+1\right)P_i^{g}\right)^2\right]}{2},
\end{aligned}$$

$$\sum_{t\in\mathcal{T}}\left[C_i^{g,2}\left(P_i^g\right)^2\left(l^2+l+0.25\right)\right]\leq\sum_{t\in\mathcal{T}}\left[C_i^{g,2}\left(P_i^g\right)^2\left(l^2+l+0.5\right)\right]$$

for all points $\underline{P}_i \leq x_{i,0} < x_{i,1} < \ldots < x_{i,|\mathcal{L}|+1} \leq \overline{P}_i$. Furthermore, for any l-th segment $[x_{i,l}, x_{i,l+1}]$,

$$\frac{f_i\left(x_{i,l}\right)+f_i\left(x_{i,l+1}\right)}{2}=\frac{\text{offers}_i\left(x_{i,l}\right)^{(h)}+\text{offers}_i\left(x_{i,l+1}\right)^{(h)}}{2}$$

holds, i.e.,

$$\begin{aligned}
&\frac{\text{offers}_i\left(x_{i,l}\right)^{(h)}+\text{offers}_i\left(x_{i,l+1}\right)^{(h)}}{2}\\
&=\sum_{t\in\mathcal{T}}\left[\frac{C_i^{g,2}\left(P_i^g\right)^2\left(\sum_{\tilde{l}=0}^{l-1}(2\tilde{l}+1)\right)+C_i^{g,2}\left(P_i^g\right)^2\left(\sum_{\tilde{l}=0}^{l}(2\tilde{l}+1)\right)}{2}\right],\\
&=\sum_{t\in\mathcal{T}}\left[\frac{C_i^{g,2}\left(P_i^g\right)^2\left[\left(l+2\sum_{\tilde{l}=1}^{l-1}\tilde{l}\right)+\left((l+1)+2\sum_{\tilde{l}=1}^{l}\tilde{l}\right)\right]}{2}\right],\\
&=\sum_{t\in\mathcal{T}}\left[\frac{C_i^{g,2}\left(P_i^g\right)^2\left[\left(l+(l-1)\,l\right)+\left((l+1)+l\,(l+1)\right)\right]}{2}\right], \qquad (\star)\\
&=\sum_{t\in\mathcal{T}}\left[C_i^{g,2}\left(P_i^g\right)^2\left(l^2+l+0.5\right)\right].
\end{aligned}$$

Note that in step $(\star)$ above, the arithmetic series is finite and $\sum_{\tilde{l}=0}^{l}(2\tilde{l}+1)=(l+1)+2\frac{l(l+1)}{2}$ because

$$\sum_{\tilde{l}=1}^{l}\tilde{l}=1+2+3+\ldots+(l-2)+(l-1)+l=\frac{l}{2}\left(l+1\right).$$

Similarly, $\sum_{\tilde{l}=0}^{l-1}(2\tilde{l}+1) = l + 2\frac{(l-1)l}{2}$.

Moreover, since $\text{offers}_i\left(\cdot\right)^{(h)}$ is an affine function, the equality

$$\text{offers}_i\left(\frac{x_{i,l}+x_{i,l+1}}{2}\right)^{(h)} = \frac{\text{offers}_i\left(x_{i,l}\right)^{(h)} + \text{offers}_i\left(x_{i,l+1}\right)^{(h)}}{2}$$

holds. Therefore the piecewise linear function $\text{offers}_i\left(\cdot\right)^{(h)}$ is an upperbound to the quadratic function $f_i\left(\cdot\right)$, i.e.,

$$f_i\left(\cdot\right) \leq \text{offers}_i\left(\cdot\right)^{(h)}.$$

□

3.6.1.2 Taylor Series Approximations

The SLP algorithm applies first order Taylor series approximations to address the nonlinear terms in constraints (2.60), (2.61), (2.64) and (2.65), respectively. For iteration h, a multivariate Taylor series expansion about an evaluation point (denoted with a caret or "hat") is as follows:

$$v_n^{sq} = 2\hat{v}_{n,t}^{r(h)} v_{n,t}^r + 2\hat{v}_{n,t}^{j(h)} v_{n,t}^j - \left(\hat{v}_{n,t}^{r(h)}\right)^2 - \left(\hat{v}_{n,t}^{j(h)}\right)^2, \tag{3.7}$$

$$p_{n,t}^g = \hat{v}_{n,t}^{r(h)} i_{n,t}^r + \hat{v}_{n,t}^{j(h)} i_{n,t}^j + v_{n,t}^r \hat{i}_{n,t}^{r(h)} + v_{n,t}^j \hat{i}_{n,t}^{j(h)} - \hat{v}_{n,t}^{r(h)} \hat{i}_{n,t}^{r(h)} - \hat{v}_{n,t}^{j(h)} \hat{i}_{n,t}^{j(h)} + P_{n,t}^d, \tag{3.8}$$

$$q_{n,t}^g = \hat{v}_{n,t}^{j(h)} i_{n,t}^r - \hat{v}_{n,t}^{r(h)} i_{n,t}^j + v_{n,t}^j \hat{i}_{n,t}^{r(h)} - v_{n,t}^r \hat{i}_{n,t}^{j(h)} - \hat{v}_{n,t}^{j(h)} \hat{i}_{n,t}^{r(h)} + \hat{v}_{n,t}^{r(h)} \hat{i}_{n,t}^{j(h)} + Q_{n,t}^d \tag{3.9}$$

for all buses $n \in \mathcal{N}$ in time periods $t \in \mathcal{T}$, and

$$i^{sq}_{k(\cdot),t} = 2\hat{i}^{r(h)}_{k(\cdot),t} i^{r}_{k(\cdot),t} + 2\hat{i}^{j(h)}_{k(\cdot),t} i^{j}_{k(\cdot),t} - \left(\hat{i}^{r(h)}_{k(\cdot),t}\right)^2 - \left(\hat{i}^{j(h)}_{k(\cdot),t}\right)^2 \tag{3.10}$$

for all flows $k(\cdot) \in \mathcal{F}$ in time periods $t \in \mathcal{T}$. Since a first order method is used, larger step sizes result in larger approximation error. Therefore, this algorithm requires step sizes that are small enough to gain reasonable accuracy (i.e., low truncation error) but large enough to result in a reasonably small number of iterations. Depending on the penalty and real power mismatch costs, the step size $V^{(h)}_{n,t}$ is restricted at an accelerated or decelerated rate.

At the end of each iteration $h > 0$, the tunable parameter $V^{(h)}_{n,t}$ is modified to control the approximation error. As the approximation nears ACOPF feasibility, the convergence rate accelerates; if the approximation worsens, this rate decelerates as a function of the ratio

$$\gamma^{(h)} = \frac{\text{penalty}\,(\cdot)^{(h)} + f\,(\cdot)^{(h)}}{\text{cost}\,(\cdot)^{(h)} + f\,(\cdot)^{(h)}}, \tag{3.11}$$

where $0 \leq \gamma^{(h)} \leq 1$,

$$f\,(\cdot)^{(h)} = \sum_{n \in \mathcal{N}, t \in \mathcal{T}} \delta^{\epsilon}_{n} \left| P^{*}_{n,t} - p^{g}_{n,t} \right|, \tag{3.12}$$

and

$$P^*_{n,t} = P^d_{n,t} + v^{r*}_{n,t} i^{r*}_{n,t} + v^{j*}_{n,t} i^{j*}_{n,t}. \tag{3.13}$$

As $\gamma^{(h)} \to 0$, the solution becomes ACOPF feasible, i.e., $f(\cdot)^{(h)} = 0$ and penalty $(\cdot)^{(h)} = 0$. The tunable parameters are $\beta = -a \log \gamma^{(h)} + b$ and $\alpha = \delta/\beta$ for $\delta = 1 - \lfloor 10\gamma^{(h)} \rfloor / 10$ where the allowable step-size is

$$V^{(h)}_{n,t} \leftarrow \alpha \left| \overline{V}_n \right| \Big/ h^{\beta}. \tag{3.14}$$

For faster decay, the user can increase a. When $\gamma^{(h)} = 1$, then $\beta = b$.

The algorithm applies the above approach to update the tunable parameter $V^{(h)}_n$ and then introduces the step size limits

$$\left| v^r_{n,t} - \hat{v}^{r(h)}_{n,t} \right| \leq V^{(h)}_{n,t} \tag{3.15}$$

$$\left| v^j_{n,t} - \hat{v}^{j(h)}_{n,t} \right| \leq V^{(h)}_{n,t} \tag{3.16}$$

on the real and imaginary parts of the nodal voltage, $v^r_{n,t}$ and $v^j_{n,t}$, for all buses $n \in \mathcal{N}$ in time periods $t \in \mathcal{T}$. Controlling the step size for the real and imaginary parts of the nodal voltages in turn limits the approximation error in the real and reactive power, and the corresponding error in LMP as derived from the dual variable to the nodal real power balance in (3.8).

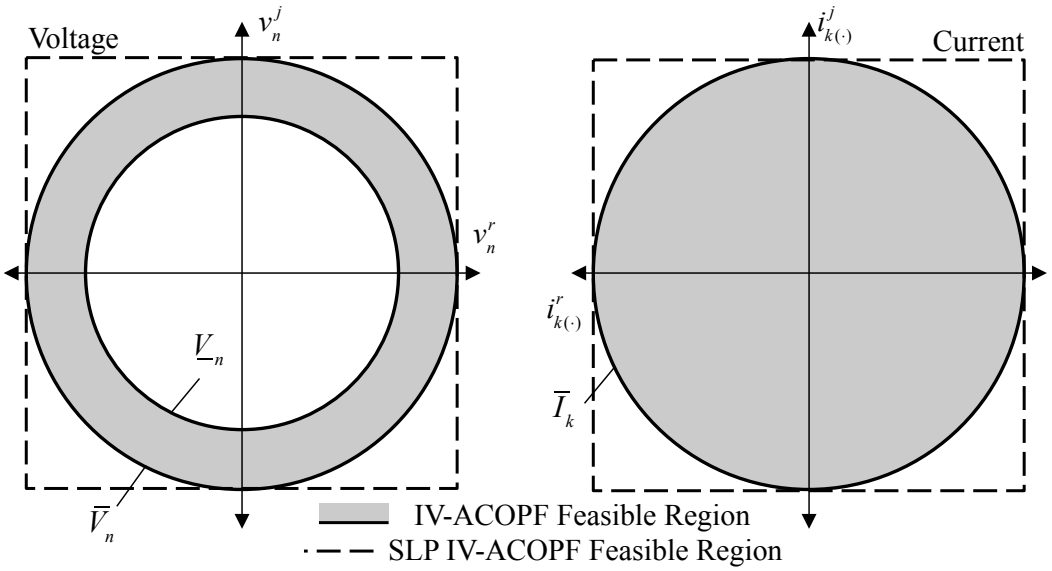

Figure 3.3: Outer approximation of the voltage and current phasor bounds with box constraints

3.6.1.3 Outer Approximations with Infeasibility Handling and Penalty Factors

In conjunction with the voltage magnitude linearization in (3.7), the algorithm introduces box constraints on the real and imaginary parts of the nodal voltage as

$$-\overline{V}_n \leq v_{n,t}^r \leq \overline{V}_n, \tag{3.17}$$

$$-\overline{V}_n \leq v_{n,t}^j \leq \overline{V}_n \tag{3.18}$$

for all buses $n \in \mathcal{N}$ in time periods $t \in \mathcal{T}$, and in conjunction with the current magnitude linearization in (3.10), the algorithm also introduces

$$-\overline{I}_k \leq i^r_{k(\cdot),t} \leq \overline{I}_k, \tag{3.19}$$

$$-\overline{I}_k \leq i^j_{k(\cdot),t} \leq \overline{I}_k \tag{3.20}$$

on the real and imaginary parts for all current flows $k(\cdot) \in \mathcal{F}$ in time periods $t \in \mathcal{T}$. These box constraints are outer approximations, as illustrated in Figure 3.3.

Given that these outer approximations are not tight, ACOPF infeasible solutions may result. The following routine determines the updated evaluation point and resulting tangential cutting plane

$$\hat{x}^{r(h)} x^r + \hat{x}^{j(h)} x^j \leq \left(\overline{X}\right)^2 + x^{viol,+} \tag{3.21}$$

when either the voltage magnitude upper bound in (2.64) or the thermal line limit in (2.65) is violated by the optimal solution of the LP subproblem in iteration h. Without loss of generality, the real part is denoted as x^r, the imaginary part as x^j, and the upper bound as $\overline{X}$. The cutting plane is calculated as follows:

1: **if** $\left(\hat{x}^{r(h)}\right)^2 + \left(\hat{x}^{j(h)}\right)^2 > \overline{X}^2$ **then**

2: $\quad \mu \leftarrow \hat{x}^{j(h)} / \hat{x}^{r(h)}$

3: $\quad \hat{x}^{r(h)} \leftarrow \text{sign}\left(\hat{x}^{r(h)}\right) \sqrt{\overline{X}^2 \Big/ (1+\mu^2)}$

4: $\quad \hat{x}^{j(h)} \leftarrow \text{sign}\left(\hat{x}^{j(h)}\right) \left|\mu \hat{x}^{r(h)}\right|$

5: $\quad$ **add constraint:** $\hat{x}^{r(h)} x^r + \hat{x}^{j(h)} x^j \leq \overline{X}^2 + x^{viol,+}$

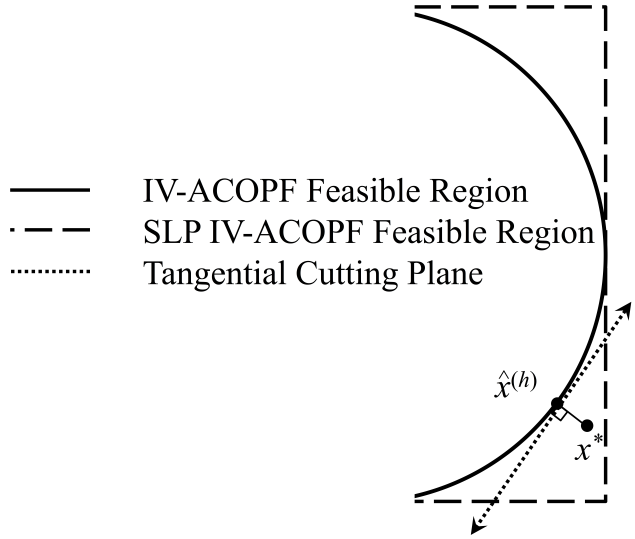

Figure 3.4: The infeasible solution x^* from iteration $h-1$, the updated evaluation point $\hat{x}^{(h)}$, and the tangential cutting plane included to the constraint set for iteration h.

6: **end if**

In other words, when an ACOPF infeasibility occurs due to violations of the voltage (2.64) or current (2.65) upperbound, the algorithm resets the violating evaluation points of the Taylor series approximation to be within these bounds. The algorithm then includes a tangential cutting plane to the constraint set for the subsequent iteration, as illustrated in Figure 3.4. The algorithm imposes constraint satisfaction of the tangential cutting plane by introducing a slack variable, which is penalized in the cost function. This approach only applies for the outer approximation on the upper bounds.

When the lower bound constraint in (2.64) is violated, the algorithm does not introduce a tangential cutting plane, which would eliminate parts of the ACOPF

feasible region. Instead, the algorithm only imposes constraint satisfaction by introducing slack variables that are penalized in the cost function. The algorithm treats the bounds on the first order Taylor approximations similarly. As a result $(2.62) - (2.65)$ are reformulated as

$$\underline{P}_i - p_{i,t}^{viol,-} \leq p_{i,t}^{g} \leq \overline{P}_i + p_{i,t}^{viol,+} \tag{3.22}$$

$$\underline{Q}_i - q_{i,t}^{viol,-} \leq q_{i,t}^{g} \leq \overline{Q}_i + q_{i,t}^{viol,+} \tag{3.23}$$

$$\underline{V}_n^2 - v_{n,t}^{viol,-} \leq v_{n,t}^{sq} \leq \overline{V}_n^2 + v_{n,t}^{viol,+} \tag{3.24}$$

$$i_{k(\cdot),t}^{sq} \leq \overline{I}_k^2 + i_{k(\cdot),t}^{viol,+} \tag{3.25}$$

where the slack variables $p_{i,t}^{viol,-}, q_{i,t}^{viol,-}, p_{i,t}^{viol,+}, q_{i,t}^{viol,+}, v_{n,t}^{viol,-}, v_{n,t}^{viol,+}$, and $i_{k(\cdot),t}^{viol,+}$ are penalized in the objective function.

3.6.1.4 Constraint Reduction

The algorithm incorporates the concept of flowgate monitors to solve the linearized formulation with a reduced constraint set. The algorithm computes and monitors the flows for a subset of lines $k' \in \mathcal{K}'^{(h)} \subset \mathcal{K}$ where $k'(\cdot) \in \mathcal{F}$ are near or at $r^2\overline{I}_{k'}^2$ for the flowgate monitor rate $0 \leq r \leq 1$ and the thermal capacity limit $\overline{I}_{k'}$. The subset of lines $\mathcal{K}'^{(h)} \subset \mathcal{K}$ is updated at each iteration $h > 0$. The constraint set is therefore reduced to only include (3.10), (3.19), (3.20), and (3.25) for all $k(\cdot) = k(\cdot)' \in \mathcal{F}$.

3.6.2 LP Subproblem Formulation

For each iteration h, the SLP IV-ACOPF solves the following LP subproblem:

$$\text{cost}\,(\cdot)^{(h)} = \min\Big(\text{offers}\,(\cdot)^{(h)} + \text{penalty}\,(\cdot)^{(h)}\Big) \tag{3.26}$$

subject to

$$(2.56) - (2.61), (3.5) - (3.25), \tag{3.27}$$

where $\text{offers}\,(\cdot)^{(h)}$ is defined in (3.4) and $\text{penalty}(\cdot)^{(h)}$ is defined as

$$\begin{aligned}\text{penalty}\,(\cdot)^{(h)} = &\sum_{n\in\mathcal{N},t\in\mathcal{T}}\Bigg[\sum_{i\in\mathcal{I}(n)}\Big[P_n^{\epsilon}\left(p_{i,t}^{viol,-}+p_{i,t}^{viol,+}\right)\\ &+Q_n^{\epsilon}\left(q_{i,t}^{viol,-}+q_{i,t}^{viol,+}\right)\Big]+V_n^{\epsilon}\left(v_{n,t}^{viol,-}+v_{n,t}^{viol,+}\right)\Bigg]\\ &+\sum_{k'(\cdot)\in\mathcal{K}'^{(h)},t\in\mathcal{T}} I_{k'}^{\epsilon} i_{k'(\cdot),t}^{viol,+}\end{aligned} \tag{3.28}$$

where $P_n^{\epsilon}, Q_n^{\epsilon}, V_n^{\epsilon}$, and $I_{k'}^{\epsilon}$ are user-specified penalty factors.

3.7 Results

This work now reports on the computational performance and convergence quality of the SLP IV-ACOPF and compares the results to solving the nonlinear IV-ACOPF as

defined by the constraint set in $(2.56) - (2.61)$, and the piecewise linear cost function in $(3.4) - (3.6)$. In [92], Castillo et al. demonstrate that the mathematical formulation, solver algorithm, and initialization all contribute to the performance of ACOPF solution techniques. Therefore this work focuses on the mathematical formulations proposed here, and compares performance of the SLP versus NLP approaches for various solvers and initializations.

A globally optimal solution to the nonlinear IV-ACOPF is not readily attainable via SDR for each and every problem in the entire test suite; often the SDR is augmented, e.g., to include penalties on constraint violations, and in many cases these penalties are non-uniform and thus make it difficult to determine a global optimum. Instead, this study reports an upper bound on the solution cost by solving the IV-ACOPF with KNITRO MS (multi-start) using the default settings [93], which is referred to as NLP/KNITRO MS. Although a global optimum is not guaranteed, the probability of finding a better local solution is higher using a multi-start approach on the globally convergent KNITRO algorithms (Interior/CG, Interior/Direct, Active-Set). Since the KNITRO multi-start runtime is much longer than that of the SLP IV-ACOPF algorithm, the CPU time reported is for KNITRO without multi-start. The nonlinear IV-ACOPF is also solved with IPOPT, which uses a filter line search to ensure global convergence under mild assumptions [94].

Both the IV-ACOPF model and SLP IV-ACOPF algorithm are implemented in Python 2.7 with Pyomo 3.5 [95] and executed on a workstation with four quad-

core Intel Xeon 2.7 GHz processors with hyper-threading and 512GB RAM. The LP subproblems of the SLP IV-ACOPF are solved with either Gurobi 5.6.2 [66] or CPLEX 12.5.1 [67] barrier method limited to two threads, and the IV-ACOPF with either IPOPT 3.11.4 configured using the MA27 linear sub-solver (no multi-threading support) [94] or KNITRO 9.1, where KNITRO chooses the algorithm to apply [93]; each set of simulations is referred to as SLP/Gurobi, SLP/CPLEX, NLP/IPOPT, and NLP/KNITRO, respectively. Since MATPOWER 5.1 [56] specifically formulates the ACOPF in polar coordinates and augments user-specified initializations by selecting an interior point, the MATPOWER 5.1 solvers could not be readily included into the testing. A feasibility and optimality tolerance of 1.0×10^{-6} is applied to each solver in this study.

The algorithm is executed from multiple starting points on a publicly available test suite consisting of: (1) IEEE networks with 14, 30, 57, 118, and 300 buses, and (2) Polish networks 2383wp, 2737sop, 2746wop, 3012wp, 3120sp, 3375wp, where the number represents the number of buses in the respective network model, and the acronyms are "sp" for summer peak, "sop" for summer off-peak, "wp" for winter peak, and "wop" for winter off-peak [56]; for ease of reference in the subsequent analysis, the acronyms are omitted. These data sets include demand for a single time period, i.e., $|\mathcal{T}| = 1$. For buses with multiple generators, these units are aggregated with an average cost function; therefore $\mathcal{I} \subseteq \mathcal{N}$. In the baseline case these networks are solved without line limits and in the thermally constrained case with line limits

(not including limits on transformers). The line ratings in terms of current are systematically computed from the approach by Lipka et al. [96] and presented in Table 3.2.

The performance of any SLP-based algorithm is highly dependent on strategies used, the computer implementation, and parameter settings [97]. In the proposed SLP algorithm, there are parameters to control penalty factors, constraint reduction, iterative step-size, and power mismatch tolerances. It is impossible to fine-tune these parameters to have optimal settings for all possible problems without positively biasing the results, so this study demonstrates the performance for the default values as reported in Table 4.2. The magnitude of the penalties, on average, are loosely correlated to the types of constraint most likely require slacks to be incorporated. For example, the penalty on the real power is the lowest since dispatching it is already priced into the market. The iteration limit was arbitrarily set to 20 for the reported test suite, but it could be set higher for larger scale or more constrained networks that might require more iterations. The step-size parameters a and b tune the parameters α and β as described in Section 3.6.1.2. Most importantly, a controls the rate of decay in the allowable step-size, where the default step-size region varies in proportion to the power of the iteration count, as determined by b when there are excessive penalties present. Finally, power mismatch tolerances well below the threshold of known

state estimator precision[47] are applied; in practice and as demonstrated below, high accuracy in convergence is not required to obtain a meaningful result.

This analysis considers four types of initialization methods: (1) flat start, (2) DC warm start, (3) AC warm start, and (4) uniform cold start. The flat start assumes unit voltage and real power output of $\left(\overline{P}_i - \underline{P}_i\right)/2$ for all generation. The DC and AC warm starts are constructed from DCOPF and ACOPF locally optimal solutions, respectively, where the demand is parameterized as $P^d_{n,t} \sim \mathcal{U}\left(0.9P^d_{n,t}, 1.1P^d_{n,t}\right)$ for all $n \in \mathcal{N}, t \in \mathcal{T}$. The uniform starts assume that $v^r_{n,t} \sim \mathcal{U}\left(\underline{V}_n, \overline{V}_n\right)$ and $v^j_{n,t} = 0$ for all $n \in \mathcal{N}, t \in \mathcal{T}$; given that the uniform start does not incorporate any knowledge of a prior operating state, it is by definition a cold start. The sample size for the various initialization types is one sample for the flat start and 10 samples for the remaining start types. To reduce variance in the comparison, this analysis uses identical starting points to test SLP/Gurobi, SLP/CPLEX, NLP/Ipopt, and NLP/KNITRO.

The overall frequency of convergence is as follows. For the nonlinear IV-ACOPF, NLP/KNITRO and NLP/Ipopt converged 99.7% and 96.9% of the time, respectively. For the SLP algorithms a converged solution is defined as meeting the mismatch tolerances specified in Table 4.2 of the algorithm's stopping criteria. For LP subproblem iterations that are locally infeasible or if the iteration count reaches the user defined limit, then the simulation is labeled as unconverged. SLP/CPLEX converged in 98.4%

[47]The primary state estimator measurement in PJM is on the MW flows where metering accuracy ranges between 1.0×10^{-2} and 5.0×10^{-2}, as compared to the P-mismatch tolerance Δ^P_n in Table 4.2. This range results in a moderate impact on the state estimator solution accuracy and furthermore there are unobservable measurements due to lack of telemetry [98].

Parameter	Description	Value
LIM	Iteration Limit	20
$\|\mathcal{L}\|$	Piecewise Segments	10
a	Step-Size Parameter	0.25
b	Step-Size Parameter	1.5
$r^2\overline{I}_k^2$	Flowgate Monitor Rate	$r = 0.9$
$I_{k'}^{\epsilon}$	Line Current Penalty	$25 \max_i C_i^{g,1}$
V_n^{ϵ}	Voltage Penalty	$15 \max_n C_n^{g,1}$
Q_n^{ϵ}	Reactive Power Penalty	$12.5 \max_i C_i^{g,1}$
P_n^{ϵ}	Real Power Penalty	$2.5 \max_i C_i^{g,1}$
Δ_n^P	P-Mismatch Tolerance	1.0×10^{-3}
Δ_n^Q	Q-Mismatch Tolerance	5.0×10^{-3}
Δ^P	Total P-Mismatch Tolerance	$5\Delta_n^P$
Δ^Q	Total Q-Mismatch Tolerance	$10\Delta_n^Q$

Table 3.1: The SLP IV-ACOPF parameter defaults.

Network	Line Limits (MVA)
IEEE-14	26.75
IEEE-30	31.25
IEEE-57	142.75
IEEE-118	114
IEEE-300	682
Polish Networks	$\overline{S}_{k(\cdot)} / \min_{i=n,m\in k(\cdot)} \overline{V}_i \quad \forall k \in \mathcal{K}$

Table 3.2: Thermal line limits in terms of current (MVA) at 1 p.u. voltage.

of the runs and the SLP/Gurobi in 99.1% of the runs. Of the converged runs, 10.3% of the SLP/CPLEX and 10.3% of the SLP/Gurobi runs resulted in active penalties; these only occurred in the IEEE-118 and Polish-2,383 thermally constrained cases. The active penalty in the thermally constrained IEEE-118 is due to reactive power compensation requirements at a single bus located in a congested area of the network. The active penalty in the Polish-2,383 system is on a real power injection at a single generator bus; by increasing the real power penalty by a factor of three so

that $P_n^{\epsilon} = 7.5 \max_i C_i^{g,1}$ for all $n \in \mathcal{N}$, SLP/CPLEX and SLP/Gurobi converge to the unpenalized optimum. As is evident, the SLP parameterization should ideally be determined on a case-by-case basis, but for the purpose of demonstrating general application and performance, default parameters are applied here.

	Best-Case Simulations			All Converged Simulations		
Baseline	p	R^2	RMSE (s)	p	R^2	RMSE (s)
NLP/KNITRO	1.42	0.83	1.46	1.47	0.82	1.40
NLP/Ipopt	1.13	0.95	0.60	1.34	0.97	0.50
SLP/CPLEX	0.97	0.99	0.20	1.01	0.98	0.33
SLP/Gurobi	1.01	0.99	0.21	1.03	0.98	0.33
Thermally Constrained						
NLP/KNITRO	1.39	0.88	1.13	1.39	0.89	1.08
NLP/Ipopt	1.11	0.98	0.36	1.22	0.97	0.50
SLP/CPLEX	0.99	0.99	0.17	1.00	0.98	0.31
SLP/Gurobi	1.06	0.99	0.23	1.05	0.97	0.36

Table 3.3: The scaling factor p for the experimental time complexity, $\Theta\left(n^p\right)$, with corresponding R-squared (R^2) and root mean squared error (RMSE) values, of NLP/KNITRO, NLP/Ipopt, SLP/CPLEX, and SLP/Gurobi. The exponent $p = 1$ corresponds to linear algorithmic scaling. The high R^2 values indicate that the time complexity model n^p explains nearly all the variability in computational time as a function of the network size. RMSE is reported in seconds (s); a value closer to zero indicates a fit that is more useful for prediction.

To analyze algorithm scaling properties, the experimental time complexity $\Theta\left(T\left(n\right)\right)$ is classified by the nature of the function $T\left(n\right) = n^p$ for network size n and unknown exponent $p > 0$. Instead of reporting numerous run time samples, Big-Theta ("Θ") notation describes the asymptotic behavior for large problem sizes by reporting the exact dependence of the run time on network size for the subset of converged simulations in this study. A regression model with logarithmic transformations is applied to

Solver CPU Time (s)	NLP/Knitro	NLP/Ipopt	SLP/CPLEX	SLP/Gurobi
	Baseline Case			
IEEE-14	0.12	0.16	0.24 (4)	0.25 (4)
IEEE-30	0.19	0.2	0.84 (9)	0.89 (9)
IEEE-57	0.32	0.38	0.76 (5)	0.95 (5)
IEEE-118	0.84	1.18	2.53 (7)	3.49 (7)
IEEE-300	2.27	2.63	4.88 (6)	9.23 (6)
Polish-2,383	38.65	88.47	37.05 (6)	68.62 (6)
Polish-2,737	29.57	25.29	42.69 (6)	58.63 (6)
Polish-2,746	42.43	20.67	51.71 (7)	70.62 (7)
Polish-3,012	96.51	33.15	49.73 (6)	68.22 (6)
Polish-3,120	84.34	30.47	57.17 (6)	70.55 (6)
Polish-3,375	6,473.40	145.05	59.39 (6)	83.97 (6)
	Thermally Constrained Case			
IEEE-14	0.12	0.19	0.19 (3)	0.17 (3)
IEEE-30	0.19	0.19	0.58 (6)	0.67 (6)
IEEE-57	0.32	0.35	0.79 (5)	1.03 (5)
IEEE-118	1.23	1.18	2.86 (7)	3.49 (7)
IEEE-300	1.96	2.22	5.23 (6)	8.86 (6)
Polish-2,383	43.63	26.32	36.42 (6)	64.27 (6)
Polish-2,737	31.29	46.37	41.79 (6)	54.69 (6)
Polish-2,746	82.02	39.66	43.78 (6)	68.34 (6)
Polish-3,012	99.53	35.56	46.34 (6)	68.69 (6)
Polish-3,120	66.46	31.22	49.54 (6)	75.73 (6)
Polish-3,375	2,348.57	80.51	61.95 (6)	89.28 (6)

Table 3.4: The fastest recorded solver CPU time s across all simulations for both baseline and thermally constrained networks. The number of SLP subproblem iterations is denoted in parentheses.

determine whether a linear or nonlinear relationship exists, and the characteristic of that relationship, between the network size and the computational time. Therefore a linear regression is applied on $\log(s) = p\log(n) + \log(b)$ to determine the power function $s = bn^p$, where s is the simulation run time and the coefficient b (relating to the y-intercept of $\log(b)$) is irrelevant when determining the order of $T(n)$. The

Offer Production Cost ($)	Baseline Case NLP/Knitro MS	Thermally Constrained Case NLP/Knitro MS
IEEE-14	8,091	9,294
IEEE-30	575	582
IEEE-57	41,817	41,978
IEEE-118	129,903	135,189
IEEE-300	720,149	726,794
Polish-2,383	1,858,447	1,863,627
Polish-2,737	742,679	742,688
Polish-2,746	1,185,115	1,185,507
Polish-3,012	2,581,020	2,597,386
Polish-3,120	2,137,309	2,140,727
Polish-3,375	7,402,883	7,415,108

Table 3.5: Offer production costs for the best-known multi-start solutions found by NLP/KNITRO MS.

MATLAB function `polyfit` is applied to minimize the sum of the squares of the data deviations that yield the least-squares fit [99]. Table 3.3 reports the experimental best-case and overall (i.e., for all the converged runs) time complexity exponent, along with the corresponding R-squared for the log-log regression and root mean squared error (RMSE) values. The high R-squared values and low RMSE values (for NLP/Ipopt, SLP/CPLEX, and SLP/Gurobi) indicate the potential for IV-ACOPF and the SLP IV-ACOPF algorithm in practical applications. When p is near 1 (linear), this indicates that the running time of the SLP algorithm grows almost directly proportional to the network size n. Furthermore, the time complexity of the SLP algorithm outperforms that of the NLP commercial solvers for the full range of test networks.

The time complexity across all the simulations, as reported in the right column of

Relative Change to Table 3.5 Solution	NLP/Knitro	NLP/Ipopt	SLP/CPLEX	SLP/Gurobi
	Baseline Case			
IEEE-14	0	0	1.2×10^{-4}	1.2×10^{-4}
IEEE-30	0	0	0	0
IEEE-57	0	0	5.3×10^{-4}	1.7×10^{-4}
IEEE-118	0	0	1.2×10^{-3}	1.2×10^{-3}
IEEE-300	0	0	3.6×10^{-5}	1.9×10^{-5}
Polish-2,383	0	0	2.6×10^{-4}	4.8×10^{-4}
Polish-2,737	0	0	1.1×10^{-4}	1.1×10^{-4}
Polish-2,746	0	0	1.8×10^{-4}	1.8×10^{-4}
Polish-3,012	0	0	1.4×10^{-4}	3.7×10^{-4}
Polish-3,120	0	0	2.0×10^{-4}	1.4×10^{-4}
Polish-3,375	5.4×10^{-7}	2.7×10^{-7}	1.2×10^{-3}	1.4×10^{-3}
	Thermally Constrained Case			
IEEE-14	0	0	-3.2×10^{-4}	-3.2×10^{-4}
IEEE-30	0	0	1.7×10^{-2}	2.4×10^{-2}
IEEE-57	0	0	2.4×10^{-4}	-4.8×10^{-5}
IEEE-118	0	0	3.0×10^{-3}	5.1×10^{-3}
IEEE-300	0	0	2.3×10^{-5}	2.2×10^{-5}
Polish-2,383	0	0	-1.4×10^{-3}	-1.8×10^{-3}
Polish-2,737	0	0	7.3×10^{-5}	5.1×10^{-5}
Polish-2,746	0	0	2.4×10^{-4}	2.3×10^{-4}
Polish-3,012	0	0	4.7×10^{-4}	4.1×10^{-4}
Polish-3,120	0	0	3.2×10^{-4}	3.0×10^{-4}
Polish-3,375	2.1×10^{-7}	1.5×10^{-7}	1.3×10^{-3}	1.3×10^{-3}

Table 3.6: The relative convergence quality in the optimal solution, as compared to the best-known multi-start solution in Table 3.5, for the fastest recorded run as presented in Table 3.4; a positive (negative) metric indicates the relative increase (decrease) amount in solution value. Decreasing the mismatch tolerance in the SLP algorithm, as defined in Table 4.2, also effectively decreases the relative change in exchange for more computational time.

Table 3.3, is comparable to that of the best-case, as reported in the left column. The best-case corresponds to the fastest recorded solver CPU time for each test configuration; the run times for these simulations are reported in Table 3.4, and the number of SLP subproblem iterations (where applicable) are reported in parentheses. Moreover

the time complexity results reported for the best-case indicate that the proposed SLP algorithm is expected to outperform the NLP/IPOPT and NLP/KNITRO approaches on larger scale networks. Furthermore, the SLP algorithm could be applied in parallel with both Gurobi and CPLEX from various starting points, which may further improve the reported trends.

Table 3.5 reports the offer production costs associated with the best-known multi-start solutions, i.e., offers $(\cdot)^{(h)}$ in Equation (3.26), as determined by NLP/KNITRO MS (multi-start). Table 3.6 reports how the best-case solutions from the various algorithmic approaches compare to the multi-start solution.[48] The results indicate that the SLP algorithm solutions are close in convergence quality to the multi-start solutions, with the deviation representing a fractional cost of the overall real power dispatched. By decreasing the mismatch tolerance and any active penalties if present, the SLP algorithm can effectively decrease the relative change in exchange for more computational time. Since NLP/KNITRO and NLP/Ipopt do no worse than the NLP/KNITRO MS, the best-known optimum is most likely the only optimum found.

Figures 3.5 and 3.6 report the fastest recorded solve times across the four initialization types for SLP/CPLEX and SLP/Gurobi, aggregating on both the baseline and thermally constrained cases. The flat start does not perform competitively for the IV-ACOPF formulation. With the flat start ($v^r_{n,t} = 1$ and $v^j_{n,t} = 0$ for all $n \in \mathcal{N}, t \in \mathcal{T}$),

[48] Although the same parameter default values are applied for all simulations on the full range of test networks in this study, the convergence quality on the thermally constrained IEEE-30, for example, can be improved (i.e., obtain lower relative deviations) by increasing the line current penalty factors $I^{\epsilon}_{k'}$. Ideally the SLP algorithm parameters are fine-tuned for the power system under consideration.

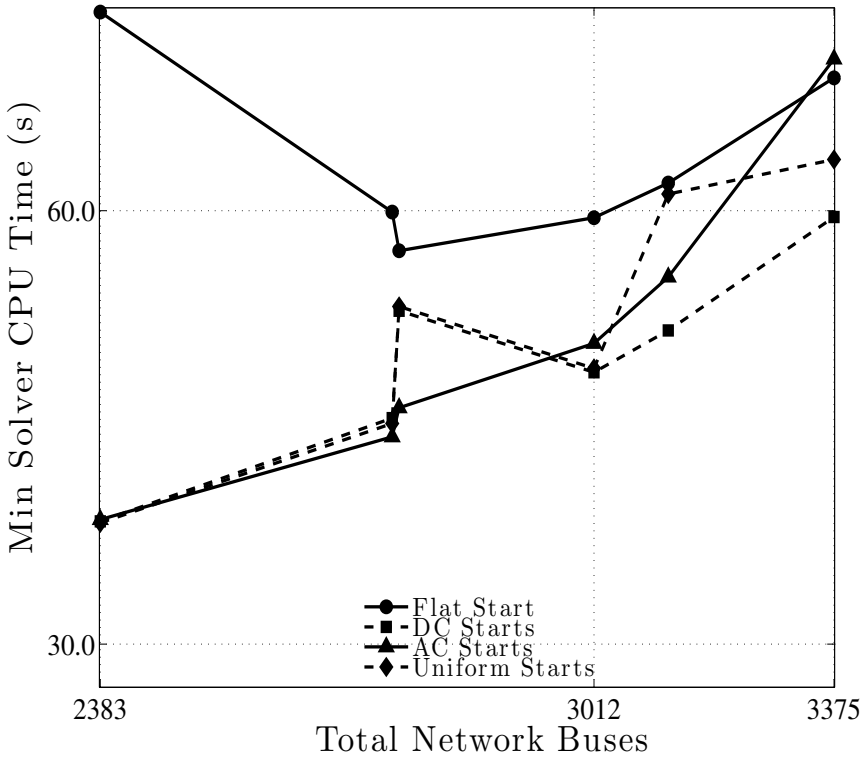

Figure 3.5: The fastest recorded CPU time for SLP/CPLEX on each initialization type in both the baseline and thermally constrained Polish networks.

the current flows are initialized to zero across symmetric transmission elements, and the Taylor series approximations in Equations (3.7) − (3.9) are such that the entire first order expansion is not assessed for the initial iteration $h = 0$. However, the uniform starts perform competitively compared to the DCOPF and ACOPF starts. The uniform starts do not require any knowledge of the prior operating state; by initializing $v^r_{n,t}$ with some variation, the voltage magnitudes become nonzero while the voltage angles remain zero. In the initial iteration, the current flows are nonzero; as a result, the nodal real power injections are calculated in terms of the network conductance and the nodal reactive power injections in terms of the network susceptance.

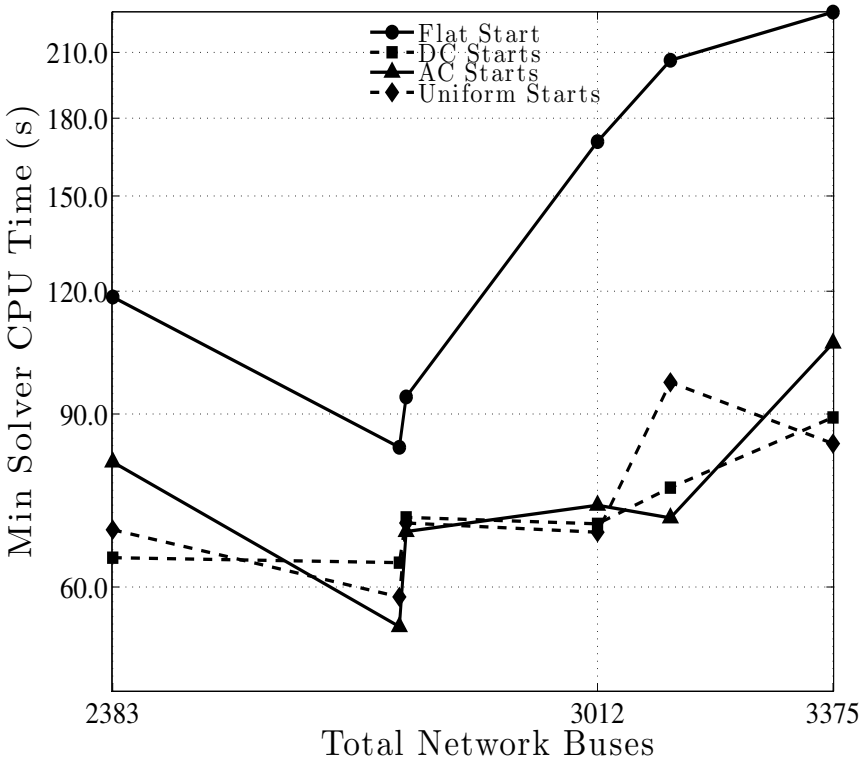

Figure 3.6: The fastest recorded CPU time for SLP/Gurobi on each initialization type in both the baseline and thermally constrained Polish networks.

3.8 Discussion

This work proposes a SLP algorithm to solve the proposed IV-ACOPF formulation which leverages the current injections method, where the network flows are linear and the nonconvexities appear in the constraints relating bilinear terms within each node. This study demonstrates acceptable quality of convergence to best-known solutions and linear scaling of computational time in proportion to network size using commercial LP solvers. Moreover, the time complexity of the SLP algorithm outperforms that of the NLP commercial solvers for the full range of test networks. As a re-

sult, the SLP algorithm is expected to outperform the NLP on larger scale networks. Furthermore, the SLP algorithm could be solved in parallel with both Gurobi and CPLEX from various starting points, which may further improve the reported linear time complexity.

The proposed approach has flexibility in balancing the trade-offs between optimality and computational tractability and can be integrated into more complex models (e.g., including integer variables) that include discrete controls or system states in order to represent decision-making processes in both the operational and planning levels, while still leveraging commercial LP/MILP solver performance. Unlike well-established methods of approximation, such as the DCOPF with AC feasibility, the SLP IV-ACOPF simultaneously co-optimizes real and reactive power dispatch and enables the system operator more optimal control over system resources.

A current limitation of the proposed work is that for nonconvex problems, there is no known theoretical convergence results to a global optimum for local solution methods such as the SLP algorithm. Despite the fact that the proposed SLP algorithm is not a global solution method, guaranteeing convergence to a local optimum is useful in practice. Global convergence to a stationary point has been proven for general SLP algorithms [91], which is a robust convergence quality of any solution technique. Extending the SLP IV-ACOPF to include such global convergence properties could make the computational performance slower but improve the convergence quality (i.e., accuracy of the solution).

4 The Unit Commitment Problem with AC Optimal Power Flow Constraints

4.1 Prologue

Chapter 3 proposed an SLP algorithm to solve the proposed IV-ACOPF formulation.[49] In this chapter a mathematical-programming based approach that extends the SLP algorithm is presented in order to optimize the UC problem subject to ACOPF network constraints. This problem is a MINLP that is nonconvex in the continuous variables and is solved here through a solution technique based on the outer approximation (OA) method; based on principles of decomposition, outer-approximation and relaxation, the OA algorithm as originally proposed by Duran and Grossman [100] solves an alternating finite sequence of NLP subproblems and a mixed-integer linear master program. The proposed approach is a local solution method that leverages powerful linear and mixed-integer commercial solvers; global solution methods are explored later in Chapters 5 and 6 for the particular application of optimal storage integration. This chapter demonstrates the relative economic and operational impact of more accurate ACOPF constraint modeling on the unit commitment problem when

[49] see Section 2.9

compared to copperplate and DCOPF constraint modeling approaches. An intermediate model is also proposed, which is a hybrid of DCOPF and ACOPF approaches, where the initial UC schedule is determined with the DCOPF, which is then made AC feasible through a RUC-based process. The results indicate considerable divergence between the market settlements and the stability and reliability requirements for the full model versus the commonly applied approximations. The computational speeds for both the ACOPF and the ACOPF for RUC approaches are promising: the ACOPF approach is 5–15 times slower than the DCOPF approach and incorporating an ACOPF-based RUC to the DCOPF approach is 1.5–5 times slower than the DCOPF alone. Since the proposed OA method spends most of the computational time in the master problem, further improvements to the MILP and leveraging decomposition techniques for distributed, parallel optimization could lead to significant gains. This work was originally published in [23].

4.2 Introduction and Background

Operational constraints on thermal generation units such as ramping limits and minimum up/down times require those units to be committed in advance of when they are needed, typically via day-ahead unit commitment (UC). UC is a decision-making process executed by utilities, ISOs, and other system operators to minimize cost production schedules for thermal generating fleets. Although variants of UC have been used in practice since the 1970s, algorithmic techniques for computing UC schedules

have changed drastically over the years. This large-scale combinatorial optimization problem is the focus of significant, active research due to the potential savings in operational costs.

What has varied most significantly in practice as well as in the state-of-the-art research on deterministic UC modeling are the assumptions in security (i.e., contingency [5]), network and operational constraints for AC power systems. Improving on the seminal UC formulation by Garver [101], many notable approaches to-date have focused on MILP with tighter convex hull representations of the thermal unit operations without network constraints [1, 102–106]; such UC formulations have been extended to include a linear (DC) representation of the network either with (e.g., [107, 108]) or without (e.g., [109]) real power losses. The resulting commitment schedules ignore reactive power dispatch and AC power flow constraints, which must subsequently be accounted for via corrective and typically ad-hoc processes. For extensive literature surveys, see [110, 111].

Because the subclass of the UC problem formulated as a MILP is NP-hard [112] and the subclass of the ACOPF problem as a nonconvex NLP is also NP-hard [2,3], the MINLP problem of UC and ACOPF combines the difficulties of both subclasses and is (not surprisingly) very challenging to solve [113]. A limited number of previous works have applied solution techniques such as Lagrangian relaxation (LR) and Benders decomposition (BD) in order to solve some form of this problem [114–120]. MILP is preferred to LR [114] since LR usually yields an infeasible primal solution due to

a nonzero duality gap. Ma and Shahidehpour [115] apply BD to iteratively perform unit commitment rescheduling in order to satisfy real power flow (capacity) limits and to make reactive power adjustments to control bus voltage magnitudes. Fu et al. [116] apply BD to maintain an AC feasible UC schedule, which is later extended in [117] to include contingencies. Similar to [116], Nasri et al. [120] also apply BD to solve the unit commitment for AC feasibility, but further decompose the problem by scenario and time period in order to model the stochasticity of wind power production.

Although the above approaches aim to provide least cost UC schedules that are also physically feasible on AC power systems, none of these studies focus on co-optimization of real and reactive power scheduling and dispatch, which is referred to as the UC problem subject to ACOPF constraints (UC+ACOPF). Sifuentes et al. [118] use an ACOPF subproblem to generate Benders cuts for optimal short-term hydrothermal scheduling. Then more recently Murillo-Sánchez et al. [119] presented a formulation framework for the stochastic UC+ACOPF problem but left computational results for future work.

Another technique for solving MINLP is the OA algorithm [100], which has been applied to variants of both the UC [121] and UC with DC network constraints [122]. For MINLPs with a convex relaxation of the mixed-integer variables (e.g., the aforementioned studies [121] and [122]), the OA as presented by Duran and Grossmann [100] is an exact algorithm provided assumptions hold on convexity, differentiability, and constraint qualifications [123]. Moreover, Generalized Benders decomposition

(GBD) [124], which is the framework for many of the studies discussed above, is a particular case of OA where the lower bounds are generally weaker (i.e., the lower bound predicted by the relaxed master problem of the OA is provably greater than or equal to that predicted by the master problem of the GBD [100]); although GBD commonly requires a large number of cycles or major iterations as the number of binary variables increases, the computational cost of solving the master problem in OA is greater due to the number of constraints added per iteration [125, 126]. Therefore both approaches have advantages and disadvantages.

Regardless, for a MINLP with nonconvex continuous variables such as the UC with AC network constraints, OA and GBD methods are heuristics. Determining a tight lower bound for nonconvex MINLP and more specifically solving the UC+ACOPF or even the UC+AC feasibility (with/without security constraints) to global optimality are complementary areas of active research [127, 128]. Bai and Wei [127] perform the only other study to date to solve the UC subject to ACOPF constraints; however in order to reformulate the problem as a SDP, the 0-1 variables are relaxed and therefore are likely to be infeasible. As a result, a heuristic rounding strategy is applied [127]. Therefore, the approach in [127] is comparable to other local solution methods instead of a being classified as a global optimization method, yet does not have the scalability of MILP. However other local solution methods, such as the approach presented here, can leverage the powerful linear and mixed-integer commercial solvers that are applied in the ISO market software.

The novel contributions in this work are in the formulation, the solution technique, as well as an extensive comparative analysis. Based on the OA algorithm, this work proposes to solve the UC+ACOPF problem through an iterative, finite sequence of MILP master problems and NLP subproblems. To solve the NLP subproblems, the algorithm leverages the linearization technique in [22],[50] which enables the construction and inclusion of a localized ACOPF constraint set into the commitment scheduling of the MILP master problem. This approach extends the power production constraints in [1], which is the tightest known convex hull representation for the unit operation without ramping constraints; this selection is confirmed through an independent assessment comparing the UC formulations presented in [1, 103–105] using copperplate, DCOPF, and ACOPF constraint sets for the network modeling.

This proposed approach co-optimizes real and reactive power scheduling and dispatch with respect to all unit operational constraints, bus voltage limits, and thermal line limits. The subsequent analysis demonstrates the monetary value of real and reactive power co-optimization for the UC+ACOPF problem by comparing costs savings relative to feasible schedules obtained by more simplified network modeling assumptions. This is the first study known to analyze the economic and operational impact of more accurate ACOPF constraint modeling on the UC problem when compared to copperplate and DCOPF constraint modeling approaches. The study also includes estimates of the cost of network losses for the UC+DCOPF, an AC feasibility check

[50] see Section 2.9

of the UC+DCOPF commitment schedule, and a RUC-based approach to adjusting AC infeasible UC+DCOPF commitment schedules. This analysis is performed on a six-bus, the IEEE RTS-79, and the IEEE-118 test systems over a day with hourly time periods.

The remainder of this chapter is organized as follows. Sections 4.3 and 4.4 detail the UC+ACOPF nonconvex MINLP formulation and solution technique, with supporting material provided in Section 4.7. Section 4.5 compares the proposed UC+ACOPF problem with the UC problem and the UC+DCOPF problem. Section 4.6 concludes by discussing limitations and future extensions for this area of research.

4.3 Problem Formulation

This work formulates the unit commitment model with ACOPF constraints, also referred to as UC+ACOPF, in which the objective is to minimize the total generation cost required to meet the load (and reserve) requirements as follows:

$$\min \sum_{i \in \mathcal{G}} \left(f_i^p + f_i^u + f_i^d \right) + \delta \tag{4.1}$$

subject to ACOPF network and power production constraints. In (4.1) f_i^p represents the production cost function (including no-load costs, i.e., fixed costs incurred every time interval a unit is running), f_i^u represents the start-up cost function, and f_i^d

represents the shut-down cost function; these quantities are defined for each thermal generator $i \in \mathcal{G}$. The quantity δ abstractly denotes a penalty function associated with constraint violations.

This section details the constraint set of the UC+ACOPF as follows. The ACOPF constraints in Section 4.3.1 is equivalent to the IV-ACOPF constraint set presented in equations $(2.56) - (2.67)$. The power production constraints in Section 4.3.2, are a function of the thermal unit characteristics. Finally Section 4.3.3 includes details on the objective function.

4.3.1 ACOPF Constraint Set

This work assumes balanced three-phase, steady-state conditions and extends the proposed IV-ACOPF network constraints presented in $(2.56) - (2.63), (2.66)$ and (2.67) which includes the following respective real and imaginary parts of the linear current flows

$$i^r_{k(n,m),t} = \text{Re}\left(Y^k_{1,1} v_{n,t} + Y^k_{1,2} v_{m,t}\right), \tag{4.2}$$

$$i^j_{k(n,m),t} = \text{Im}\left(Y^k_{1,1} v_{n,t} + Y^k_{1,2} v_{m,t}\right), \tag{4.3}$$

$$i^r_{k(m,n),t} = \text{Re}\left(Y^k_{2,1} v_{n,t} + Y^k_{2,2} v_{m,t}\right), \tag{4.4}$$

$$i^j_{k(m,n),t} = \text{Im}\left(Y^k_{2,1} v_{n,t} + Y^k_{2,2} v_{m,t}\right), \tag{4.5}$$

for all $k \in \mathcal{K}$ and the following linear constraints on the nodal current balances

$$i^r_{n,t} - \Big(\sum_{k(n,\cdot)\in\mathcal{F}} i^r_{k(n,m),t} + G^s_n v^r_{n,t} - B^s_n v^j_{n,t} \Big) = 0, \tag{4.6}$$

$$i^j_{n,t} - \Big(\sum_{k(n,\cdot)\in\mathcal{F}} i^j_{k(n,m),t} + G^s_n v^j_{n,t} + B^s_n v^r_{n,t} \Big) = 0 \tag{4.7}$$

for all $n \in \mathcal{N}$. The respective real and reactive nodal power injections balance are

$$p^g_{n,t} - \left(v^r_{n,t} i^r_{n,t} + v^j_{n,t} i^j_{n,t}\right) = P^d_{n,t} + \left(p^{\epsilon,+}_{n,t} - p^{\epsilon,-}_{n,t}\right), \tag{4.8}$$

$$q^g_{n,t} - \left(v^j_{n,t} i^r_{n,t} - v^r_{n,t} i^j_{n,t}\right) = Q^d_{n,t} + \left(q^{\epsilon,+}_{n,t} - q^{\epsilon,-}_{n,t}\right) \tag{4.9}$$

for all $n \in \mathcal{N}$, where $p^g_{n,t} = \sum_{i\in\mathcal{I}(n)} p^g_{i,t}$ and $q^g_{n,t} = \sum_{i\in\mathcal{I}(n)} q^g_{i,t}$. The nodal voltage limits are

$$\underline{V}^2_n - v^{\epsilon,-}_{n,t} \leq (v^r_{n,t})^2 + (v^j_{n,t})^2 \leq \overline{V}^2_n + v^{\epsilon,+}_{n,t} \tag{4.10}$$

for all $n \in \mathcal{N}$, and the thermal line limits are

$$\left(i^r_{k(\cdot),t}\right)^2 + \left(i^j_{k(\cdot),t}\right)^2 \leq \overline{I}^2_k + i^{\epsilon,+}_{k(\cdot),t} \tag{4.11}$$

for all $k(\cdot) \in \mathcal{F}$. Then the spinning reserve requirements are defined as

$$\sum_{i\in\mathcal{I}} r^g_{i,t} \geq P^r_t - r^{\epsilon,-}_t. \tag{4.12}$$

The slack variables $i^{\epsilon,+}_{k(\cdot),t}, v^{\epsilon,-}_{n,t}, v^{\epsilon,+}_{n,t}, p^{\epsilon,+}_{n,t}, p^{\epsilon,-}_{n,t}, q^{\epsilon,+}_{n,t}, q^{\epsilon,-}_{n,t}$, and $r^{\epsilon,-}_t$ are nonnegative penalties in the penalty function (4.32) below.

The ACOPF network constraint set is nonconvex in the lowerbound of (4.10) and the equalities of (4.8) and (4.9). Furthermore, the upperbounds of (4.10) and (4.11) are nonlinear but convex. In order to seamlessly co-optimize the real and reactive power needs during the commitment scheduling within a MILP framework,

the linearizations $(3.5) - (3.25)$ introduced in Section 3.6.1 are applied directly to the above network constraint set in the UC+ACOPF formulation.

4.3.2 Power Production Constraint Set

Extending the model by Morales-España et al. [1] to include reactive power dispatch, this section details the generating unit constraints below. The following set of constraints $(4.13) - (4.16)$ and $(4.18) - (4.20)$, as originally proposed in Morales-España et al., the tightest known convex hull for the unit operation without ramping constraints [1]. Although the presented ramp constraints (4.21) and (4.22) can be tightened (e.g., see equations $(21) - (24)$ of [104]), this extension is omitted due to data limitations.[51]

Furthermore, this work details models specifically for thermal units only, i.e., $\mathcal{G} = \mathcal{I}$, also due to data limitations; however, modeling other types of generating units[52] could be a linear or mixed-integer extension to the presented formulation.

4.3.2.1 Binary Constraint

For the three-binary approach, constraint

$$b_{i,t} - b_{i,t-1} = b^u_{i,t} - b^d_{i,t} \tag{4.13}$$

for all $i \in \mathcal{G}, t \in \mathcal{T}$ enforces that $b^u_{i,t}$ and $b^d_{i,t}$ take on the appropriate values when a unit starts up or shuts down (i.e., $b^u_{i,t} = 1$ if unit i is started up in time t or $b^d_{i,t} = 1$

[51] The publicly available data sets to perform a UC+ACOPF study characterize thermal units that are capable of ramping to full capacity within the modeled hourly time frame.

[52] e.g., must-run generators, energy storage systems, and renewable energy resources

if unit i is shut down in time t, 0 otherwise), respectively; note that $b_{i,t-1} = B_i^0$ for $t = 1$.

4.3.2.2 Minimum Uptime and Downtime Constraints

The minimum uptime and downtime constraints respectively refer to the minimum time the unit has to be on once it starts up (i.e., $b_{i,t}^u = 1$) and the minimum time it has to be off once a shutdown occurs (i.e., $b_{i,t}^d = 1$). The minimum uptime and downtime constraints from [1] extending [102] are formulated as

$$\sum_{t'=t-T_i^u+1}^{t} b_{i,t'}^u \leq b_{i,t} \tag{4.14}$$

for all $i \in \mathcal{G}, t \in \{T_i^u, \ldots, T\}$ and

$$\sum_{t'=t-T_i^d+1}^{t} b_{i,t'}^d \leq 1 - b_{i,t} \tag{4.15}$$

for all $i \in \mathcal{G}, t \in \left\{T_i^d, \ldots, T\right\}$, respectively. The initial up/down time constraints are enforced in

$$b_{i,t} = B_i^0 \tag{4.16}$$

for all $i \in \mathcal{G}, t \in \left\{1, \ldots, T0_i^d + T0_i^u\right\}$ where $T0_i^d = \max\left\{0, \left(T_i^d - \overline{T0}_i^d\right)\left(1 - B_i^0\right)\right\}$ and $T0_i^u = \max\left\{0, \left(T_i^u - \overline{T0}_i^u\right)B_i^0\right\}$.

4.3.2.3 Real Power Dispatch Constraints

For thermal units $i \in \mathcal{G}$, the total unit production is the aggregate of the minimum power output $\underline{P}_i$, otherwise known as the minimum operating level (MOL), and the

generation over that minimum, $p_{i,t}^{g\Delta}$, where

$$p_{i,t}^{g} = \underline{P}_i b_{i,t} + p_{i,t}^{g\Delta}, \tag{4.17}$$

for all $i \in \mathcal{G}, t \in \mathcal{T}$. The generation over the MOL and the spinning reserves are limited by

$$p_{i,t}^{g\Delta} + r_{i,t}^{g} \leq \left(\overline{P}_i - \underline{P}_i\right) b_{i,t} - \left(\overline{P}_i - \overline{C}_i^{u}\right) b_{i,t}^{u} - \left(\overline{P}_i - \overline{C}_i^{d}\right) b_{i,t+1}^{d} \tag{4.18}$$

when $T_i^u \geq 2$ for all $i \in \mathcal{G}, t \in \mathcal{T}$. The constraint (4.18) is invalid when $T_i^u = 1$ (e.g., the case when $b_{i,t} = 1, b_{i,t}^u = 1$ and $b_{i,t+1}^d = 1$) and therefore the constraints

$$p_{i,t}^{g\Delta} + r_{i,t}^{g} \leq \left(\overline{P}_i - \underline{P}_i\right) b_{i,t} - \left(\overline{P}_i - \overline{C}_i^{u}\right) b_{i,t}^{u}, \tag{4.19}$$

$$p_{i,t}^{g\Delta} + r_{i,t}^{g} \leq \left(\overline{P}_i - \underline{P}_i\right) b_{i,t} - \left(\overline{P}_i - \overline{C}_i^{d}\right) b_{i,t+1}^{d}, \tag{4.20}$$

are applied instead; note that $\overline{C}_i^u$ and $\overline{C}_i^d$ are the start-up and shut-down MW capability, which can be assumed to equal the unit minimum output (i.e., $\underline{P}_i$) unless otherwise specified [1]. The ramp-up constraint for all $i \in \mathcal{G}, t \in \mathcal{T}$ is

$$p_{i,t}^{g\Delta} + r_{i,t}^{g} - p_{i,t-1}^{g\Delta} \leq RR_i^u \tag{4.21}$$

which ensures that the unit can provide spinning reserve without violating the upwards ramp limit. The ramp-down constraint for all $i \in \mathcal{G}, t \in \mathcal{T}$ is

$$-p_{i,t}^{g\Delta} + p_{i,t-1}^{g\Delta} \leq RR_i^d. \tag{4.22}$$

4.3.2.4 Reactive Power Dispatch Constraints

Synchronous condensers $i \in \mathcal{C}$ have reactive power dispatch limited by

$$\underline{Q}_i \leq q_{i,t}^{g} \leq \overline{Q}_i \tag{4.23}$$

for all $t \in \mathcal{T}$; note that these units are modeled with no variable costs[53] nor are these units required to schedule commitment into the market (and therefore have no associated binary variables) since synchronous condensers do not produce energy. Then the reactive power dispatch for the thermal generation fleet is limited by

$$\underline{Q}_i b_{i,t} \leq q^g_{i,t} \leq \overline{Q}_i b_{i,t} \tag{4.24}$$

for all $i \in \mathcal{G}, t \in \mathcal{T}$.

4.3.3 Objective Function

This section details the computation of the objective function in (4.1). The production cost f^p_i depends on generator i's offer curve, which in turn is a function of the real power dispatch $p^g_{i,t}$ across all time periods $t \in \mathcal{T}$. Generator offer curves for thermal units $i \in \mathcal{G}$ can be expressed as the convex quadratic cost function

$$f^p_i = \sum_{t \in \mathcal{T}} C^2_i \left(p^g_{i,t}\right)^2 + C^1_i p^g_{i,t} + C^0_i b_{i,t}, \tag{4.25}$$

but are modeled in the ISO markets as piecewise linear offer curves.[54]

Furthermore for all thermal units $i \in \mathcal{G}$, the start-up and shut-down costs are calculated as

$$f^u_i = \sum_{t \in \mathcal{T}} c^u_{i,t}, \tag{4.26}$$

$$f^d_i = \sum_{t \in \mathcal{T}} c^d_{i,t}, \tag{4.27}$$

[53] Although a synchronous condenser does consume a small amount of station power, these motors do not burn fuel to provide reactive power [129]. Furthermore synchronous condensers have much higher capital costs as compared to its operational costs, with minor maintenance costs typically priced on the capacity at around \$0.4 to \$0.8/kVAr per year [130].

[54] see Section 3.6.1.1

where the nonnegative variables $c^u_{i,t}$ and $c^d_{i,t}$ are defined as

$$c^u_{i,t} \geq \sum_{s \in \mathcal{S}_i} K^u_{i,s} b^0_{i,s,t}, \tag{4.28}$$

$$c^d_{i,t} \geq K^d_i b^d_{i,t}, \tag{4.29}$$

respectively, for all $t \in \mathcal{T}$. Extending Morales-España et al. [1], the binary variable $b^0_{i,s,t}$ in the above constraint (4.28) associates the corresponding start-up cost $K^u_{i,s}$ based on the start-up type (i.e., cold, warm, or hot start) to the amount of time elapsed since the last time period that thermal unit i was online

$$b^0_{i,s,t} \leq \sum_{t'=T^l_{i,s}}^{T^l_{i,s+1}-1} b^d_{i,t-t'} \tag{4.30}$$

for all $i \in \mathcal{G}, s \in \mathcal{S}_i, t \in \left\{T^l_{i,s+1}, \ldots, T\right\}$, and

$$\sum_{s \in \mathcal{S}_i} b^0_{i,s,t} = b^u_{i,t} \tag{4.31}$$

for all $i \in \mathcal{G}, t \in \mathcal{T}$, where $b^u_{i,t}$ is equal to 1 if unit i is started up in time t, and 0 otherwise. The timeframes $\left[T^l_{i,s}, T^l_{i,s+1}\right)$ are defined by the length of the start-up lag segment s.

Finally, the penalty function is

$$\begin{aligned}\delta = \sum_{t \in \mathcal{T}} \Big[\sum_{n \in \mathcal{N}} \Big(& P^\epsilon_n \left(p^{\epsilon,+}_{n,t} + p^{\epsilon,-}_{n,t}\right) + Q^\epsilon_n \left(q^{\epsilon,+}_{n,t} + q^{\epsilon,-}_{n,t}\right) \\ & + V^\epsilon_n \left(v^{\epsilon,+}_{n,t} + v^{\epsilon,-}_{n,t}\right) \Big) + R^\epsilon r^{\epsilon,-}_t + \sum_{k \in \mathcal{K}} I^\epsilon_k i^{\epsilon,+}_{k(\cdot),t} \Big].\end{aligned} \tag{4.32}$$

In conclusion, the offer curve in (4.25), start-up and shut-down costs in (4.26) and (4.27), and penalty in (4.32) define the objective function initially presented in equation (4.1).

4.4 The Solution Technique

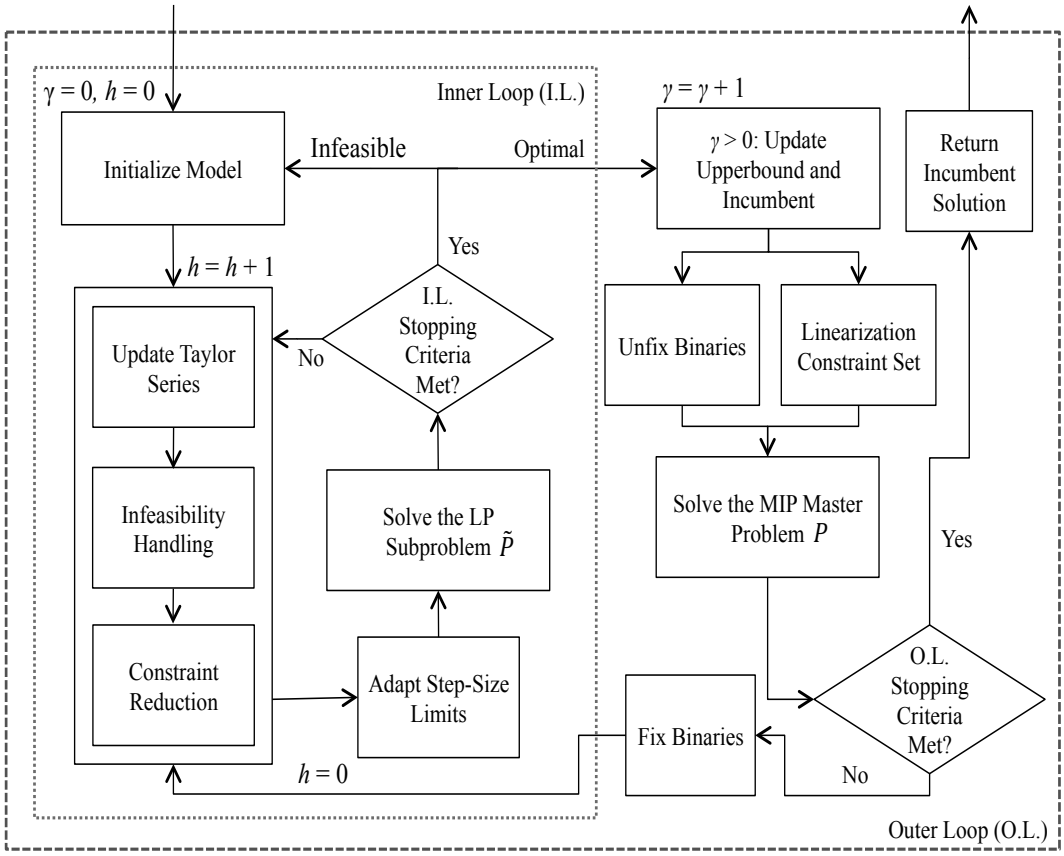

Figure 4.1: The UC+ACOPF algorithm flow diagram

The MINLP UC+ACOPF formulation includes (4.1) − (4.32) and is nonconvex due to the network constraints detailed in Section 4.3.1, the mixed-integer power production constraints detailed in Section 4.3.2, and the start-up constraints in Section 4.3.3. The proposed approach solves an alternating finite sequence of NLP subproblems (with binary variables fixed) and a mixed-integer linear master program. The NLP subproblem is equivalent to solving the ACOPF, which is approximated as a

Algorithm 1 The UC+ACOPF algorithm description

$f^U := +\infty$ (cost upperbound)
$\delta^U := +\infty$ (penalty upperbound)
incumbent $:= \varnothing$
$\gamma^* := 0$ (iteration of most recent incumbent solution)
$\gamma = 0$
$\Omega := \left\{x^{\text{init}}, y^{\text{init}} | x^{\text{init}} \text{ continuous}; 0 \leq y^{\text{init}} \leq 1\right\}$
$(x^*, y^*) :=$ optimal solution of $\tilde{P}(\Omega)$
$\Omega := \{x^*, y^* | x^* \text{ continuous}; y^* \in \{0, 1\}\}$
$(x^\gamma, y^\gamma) :=$ optimal solution of $P(\Omega)$
while *true* **do**
    $\Omega := \{x^\gamma, y^\gamma | x^\gamma \text{ continuous}; y^\gamma \text{ fixed}\}$
    $(x^*, y^*) :=$ optimal solution of $\tilde{P}(\Omega)$
    if $\tilde{P}(\Omega)$ infeasible **then**
        break;
    end if
    $\gamma := \gamma + 1$
    if $f(x^*, y^*) < f^U$ or $\delta(x^*, y^*) < \delta^U$ **then**
        $f^U := f(x^*, y^*)$
        $\delta^U := \delta(x^*, y^*)$
        incumbent $:= (x^*, y^*)$
        $\gamma^* := \gamma$
        add constraint: $f(\cdot) < f^U - \epsilon$ to $P(\cdot)$
    end if
    $\Omega := \{x^*, y^* | x^* \text{ continuous}; y^* \in \{0, 1\}\}$
    $V^\gamma \leftarrow$ see Section 4.7.2 (linearized constraint set)
    $(x^\gamma, y^\gamma) :=$ optimal solution of $P(\Omega; V^\gamma)$
    if $P(\Omega)$ infeasible or $\gamma > |\Gamma|$ or $\gamma > \gamma^* + \text{LIM}$ **then**
        break;
    end if
end while

SLP. The MILP master problem is equivalent to solving the unit commitment schedule subject to ACOPF network constraints that are constructed from a linearization around the optimal solution to the SLP. See the UC+ACOPF algorithm flow diagram and description above for more details.

The NLP subproblem is solved as a SLP subproblem $\tilde{P}$ using a user-specified commercial LP solver. Then the MILP master problem P is solved directly with a user-specified commercial MIP solver. The resulting formulation that is applied in the inner and outer loops of this algorithm includes: the objective function (4.1), constraints $(4.2) - (4.7)$, the linearization[55] of $(4.8) - (4.11)$, constraints $(4.12) - (4.24)$, the linearization[56] of (4.25), and constraints $(4.26) - (4.32)$. The linearized constraint set is a reduced set of constraints within an evaluation region that defines the neighborhood around the KKT point to the SLP; therefore active constraints that are outside this evaluation region would never bind and are excluded. This is valid because the master problem only solves a single iteration of the Taylor series evaluation points through solving for both the binary and continuous variables simultaneously.

Upon termination within specified tolerances, the SLP algorithm yields: (1) a KKT point to the ACOPF, (2) a SLP solution that is ACOPF feasible but not optimal, (3) a SLP solution that is ACOPF infeasible (i.e., there are active penalties present), or (4) a SLP solution that is infeasible.[57] Because the algorithm balances improving the upper bound with decreasing active penalties when searching for an incumbent

[55] see Section 3.6.1.2 and Section 4.7
[56] see Section 3.6.1.1
[57] see Section 3.5

solution, results that are a KKT point to the SLP[58] are acceptable outcomes to then construct the linearized constraint set that is applied in the outer loop. A solution that is infeasible in the SLP indicates that the inner loop routine requires better SLP parameterization or that the underlying problem is unbounded or has no solution. If the SLP solution is ACOPF feasible but not optimal (early termination), further parameter tuning can be employed to drive the system closer to optimality (e.g., increasing the inner loop iteration limit or improving the initialization).

The lowest cost incumbent solution is a locally optimal solution (within the specified tolerances) to the original MINLP UC+ACOPF formulation when $\delta = 0$; when active penalties are present ($\delta > 0$), the solution may still be physically practical depending on whether soft or hard constraints are violated. In the event that no incumbent solution is determined, the algorithm parameters must be adjusted. However a problem that is unbounded or has no solution will have no incumbent solution and this cannot be known *a priori*. Otherwise the proposed algorithm terminates in a finite number of iterations by solving a sequence of increasingly tighter outer approximations through iterative upperbound cuts (i.e., if $f(x^*, y^*) < f^U$ or $\delta(x^*, y^*) < \delta^U$ then update f^U, δ^U, and the incumbent solution) on more restricted evaluation regions. In essence, since bounding properties cannot be guaranteed, the search is terminated when there is no further improvement in the incumbent solution; according to Grossmann [125], OA heuristics work well for many problems.

[58] with the potential of also being a KKT point to the ACOPF

4.5 Case Studies

The proposed UC+ACOPF algorithm is applied to a six-bus test system [117], the IEEE RTS-79 24-bus test system [131], and a modified IEEE 118-bus test system [117] as summarized in Table 4.1; the six-bus data set is provided in Section 4.7.3 and the larger data sets are available online [132]. Note that the 6-Bus and RTS-79 have nodal voltage limits specified in general for all buses, and the IEEE-118 has nodal voltage limits that are bus dependent with the most restrictive bounds being $0.95 - 1.00$ p.u. A comparative analysis of the relative impacts of copperplate (no network), DC, and AC transmission network models on UC solutions is conducted for each test system. These variants are referred to as UC, UC+DCOPF ($B\Theta$ formulation), and UC+ACOPF. The UC and UC+DCOPF are MILP problems. The UC+ACOPF is solved with the OA algorithm in Section 4.4 that is composed of LP subproblems and a MILP master problem.

Then this study extends the UC+DCOPF model to perform a more in depth comparison. Incorporated into this analysis is a UC+DCOPF with losses in which the demand buses are uniformly scaled by the computed loss factor from the UC+ACOPF results. Ideally, a loss factor formulation is endogenous to the solution, but this study applies a straightforward loss estimation into the analysis. Additionally, this study checks the UC+DCOPF solutions for AC feasibility by fixing the resulting commitment schedule (but not the dispatch) and solving for this resource availability problem

with the ACOPF constraint set specified in Section 4.3.1 with generator dispatch limits. If the result is AC infeasible, then the incremental unit commitments are solved for with the proposed UC+ACOPF approach in order to determine additional commitments in the current schedule that attains AC feasibility. The UC+DCOPF+RUC does not result in de-commitments of any units but rather determines the residual commitments and updated dispatch; this is referred to as the UC+DCOPF+RUC for its similarities to RUC in practice. Furthermore, in this RUC-based implementation, there is no recourse to exclude thermal units cleared in the day-ahead from dispatch in the real-time market.

All UC+ACOPF trials are executed using the parameter values specified in Table 4.2. These parameters as well as the solver parameters can be fine-tuned to further improve computational performance. The UC+ACOPF approximation is initialized with $v^r_{n,t} = 1$ and $v^j_{n,t} = 0$ for all buses $n \in \mathcal{N}$, and then feasible power flows are determined subject to generator and network constraints. This initialization requires no prior knowledge of the operating state, but a better initialization strategy could further improve computational performance.

In the UC+DCOPF runs, line capacity limits specified in apparent power (MVA) for the above systems are translated into MW limits at an ideal power factor. Because in actual practice the capacity line ratings can be specified as thermal line ratings, apparent power limits can be transformed to limits on the current magnitude (assuming a nominal voltage, i.e., 1 p.u.) for use in the UC+ACOPF. Because the DCOPF

model approximates these current limits using real power flow limits while assuming nominal voltage and lossless transfers, the DCOPF results can be either too relaxed or restrictive depending upon whether the actual system voltages are lower or higher than 1 p.u., respectively, at terminal buses.

	6-Bus	RTS-79	IEEE-118
Buses	6	24	118
Generators	3	33	54
Synchronous Condensers	0	1	14
Loads	3	17	90
Lines	7	38	186
Tap Transformers (static)	2	5	8
Phase Shifters (static)	0	0	1
Voltage Limits (p.u.)	$[0.85, 1.15]$	$[0.94, 1.06]$	bus dependent within $[0.94, 1.06]$

Table 4.1: Overview of case study characteristics

Parameter	Description	Value
$\|\mathcal{H}\|$	Inner Loop Iteration Limit	50
$\|\Gamma\|$	Outer Loop Iteration Limit	10
LIM	No Improvement Iteration Limit	2
ϵ	Upperbound Relative Decrease	1.0×10^{-4}
$\|\mathcal{L}\|$	Piecewise Segments	10
$r^2 \left(\overline{I}_k\right)^2$	Flowgate Monitor Rate	$r = 0.9$
$I^{\epsilon}_{k'}$	Line Current Penalty ($<$ 100 buses, 100+ buses)	$1.0 \times 10^5, 1.0 \times 10^7$
V^{ϵ}_{n}	Voltage Penalty ($<$ 100 buses, 100+ buses)	$1.0 \times 10^5, 1.0 \times 10^7$
$P^{\epsilon}_{n}, Q^{\epsilon}_{n}$	Power Mismatch Penalties	1.0×10^5
Δ^P_n, Δ^Q_n	Mismatch Tolerances	1.0×10^{-4}
Δ^P, Δ^Q	Total Mismatch Tolerances	$5\Delta^P_n$,$5\Delta^Q_n$

Table 4.2: UC+ACOPF algorithm parameter defaults

The models are implemented in Python 2.7 with Pyomo 3.5 [95] and solved on

a 2.2 GHz Intel Core i7 with 16GB RAM. The LP and MILP problems are solved with CPLEX 12.6.2 [133] using a 1.0×10^{-4} relative MIP gap tolerance, except for the initial iteration of the UC+ACOPF algorithm outer loop in which a 1% gap is used in order to quickly warm-start the algorithm with an integer feasible, empirically near optimal solution. The UC+ACOPF optimal solutions reported here are without active penalties ($\delta = 0$). This approach also further validates the UC+ACOPF optimal solution by solving the original MINLP formulation (2.56)−(2.61) and (4.1)−(4.32) as a nonlinear ACOPF with binary variables fixed at the solution reported by the OA algorithm. The resulting model is solved with IPOPT [94], which uses a line search filter method to ensure global convergence under mild assumptions [134]; the OA results reported here are within a 1.0×10^{-4} relative tolerance of the nonlinear ACOPF with binary variables fixed. This study does not directly solve the MINLP due to lack of accessibility to scalable MINLP solvers.

4.5.1 Six-Bus Test System

		UC	UC+DCOPF	UC+ACOPF	UC+DCOPF+RUC
Costs ($)		$101,269$	$106,887$	$101,763$	$102,523$
		Commitment (h)			
Bus 1	G1	$1-24$	$1-24$	$1-24$	$1-24$
Bus 2	G2	$1, 12-21$	$1, 11-22$	$1, 12-21$	$1, 11-22$
Bus 6	G3	$10-22$	$10-22$	$10-22$	$10-22$

Table 4.3: System costs and commitments for the six-bus test system

The six-bus test system [117], shown in Figure 4.2, consists of three generators,

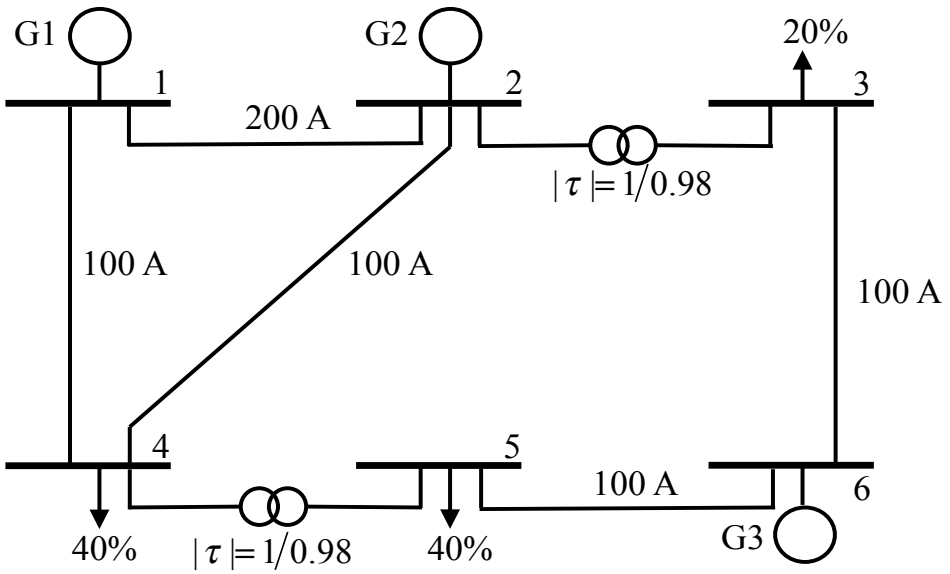

Figure 4.2: The six-bus test system, annotated with line limits, transformer tap ratios, and demand distribution factors

three loads, and two tap transformers; the data set is fully specified in the supporting material provided in Section 4.7.3. System costs and commitment schedules are shown in Table 4.3, while dispatch levels are shown in Figures 4.3 – 4.5.

The UC+DCOPF model increases system costs relative to the base UC model due to a congested transmission line between buses 1 and 4 in time periods 10 through 22. Hence, more energy must be supplied by the more expensive unit G2 at bus 2 to meet the demand at bus 4; this increase of generation from G2 in the UC+DCOPF model is illustrated in Figures 4.3 and 4.4. System costs under the UC+ACOPF model are 4.8% lower than those under the UC+DCOPF model, as reported in Table 4.3. This difference is due to the more realistic thermal line ratings in the UC+ACOPF, which are expressed in terms of MVA whereas the UC+DCOPF approximates these limits

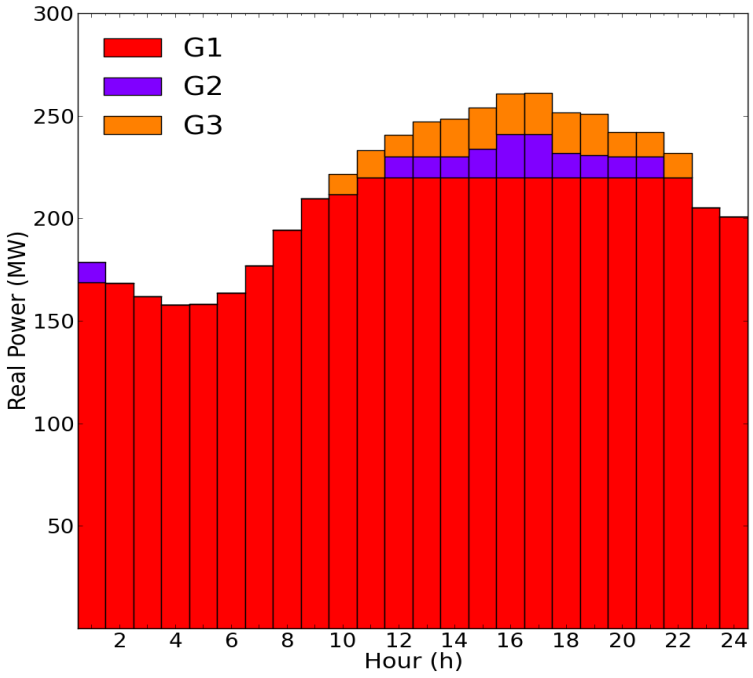

Figure 4.3: Generator dispatch stack for the copperplate unit commitment problem with no network constraints (UC)

in terms of MW while assuming a nominal voltage. In the UC+ACOPF solution, high system voltages (i.e., greater than the nominal voltage 1 p.u.) enable higher power transfers as compared to the binding limits imposed in the UC+DCOPF model; as a result there is no line congestion in the UC+ACOPF.[59] For the six-bus case, the power transfer limits used in the UC+DCOPF model are more restrictive than the UC+ACOPF thermal limits due to the nominal voltage assumption. For example, the UC+DCOPF+RUC with AC feasibility enforced results in a system cost of

[59]In instances where the actual system voltages are lower than the nominal voltage assumed in the UC+DCOPF, then the UC+DCOPF could imply higher power transfers than what may be AC feasible.

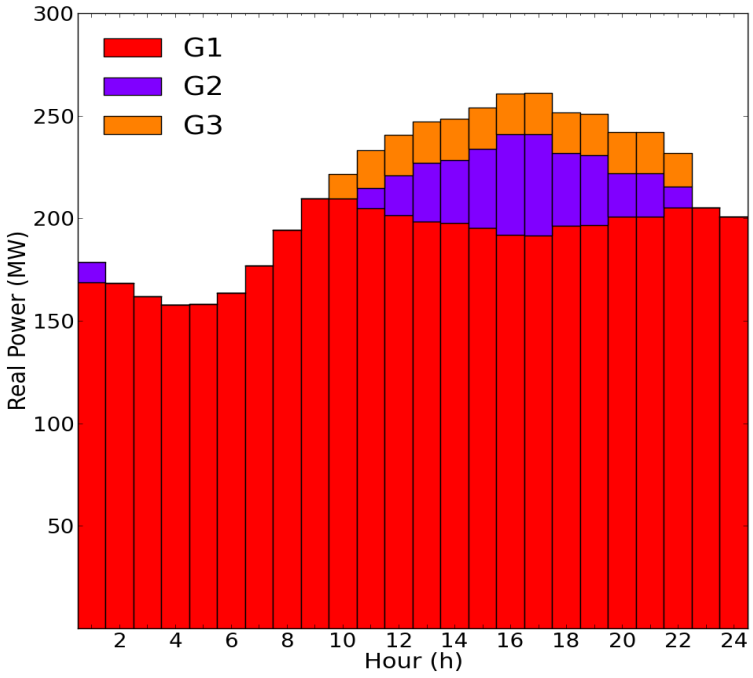

Figure 4.4: Generator dispatch stack for the unit commitment problem with DCOPF network constraints (UC+DCOPF)

$\$102,523$, which is lower compared to the initial solution of the UC+DCOPF that is AC infeasible. This is due to the former approach achieving higher power transfers from the least expensive generator at bus 1 and no network congestion; however, the UC+DCOPF+RUC at a system cost of $\$102,523$ is still more expensive than the UC+ACOPF at a system cost of $\$101,763$ due to the over commitment in the DCOPF approach of G2 in time periods 11 and 22.

System costs under the UC+ACOPF model are slightly more expensive than in the copperplate UC solution due to costs associated with real power losses (total losses of 20.15 MW, 0.4% of dispatch), which is evident in the dispatch stacks as

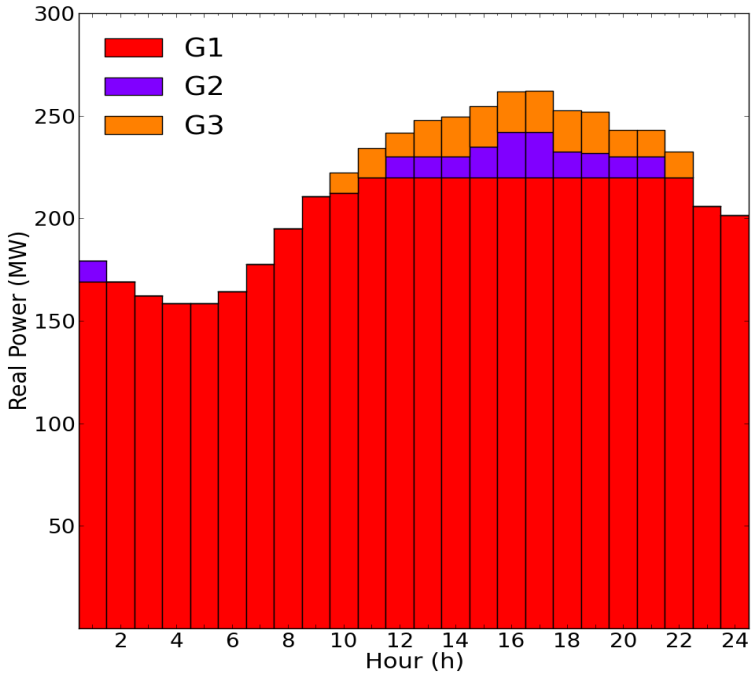

Figure 4.5: Generator dispatch stack for the unit commitment problem with ACOPF network constraints (UC+ACOPF)

shown in Figures 4.3 and 4.5. Solving the UC+DCOPF with uniform losses through scaling the demand by 0.4%, the estimated system cost increases to $\$107,689$.

4.5.2 IEEE RTS-79 Test System

The RTS-79 [131] includes 24 buses, 32 generators, 17 loads, and 1 synchronous condenser (SC) with a reactive power compensation between -50 MVAr to 200 MVAr. The 24-hour time period load is representative of a summer weekday. Generator type and cost characteristics are reported in Table 4.4.

System costs and commitment schedules are reported in Table 4.5. In the commit-

Generator type (U$\bar{P}$) and size ($\bar{P}$ MW)	Start-up Cost ($)		Production Cost ($/h)		
	Hot	Cold	No Load	Linear	Quadratic
U12 (Oil\Steam)	209	374	86.39	56.56	0.33
U20 (Oil\CT)	50	50	400.68	130	0
U50 (Hydro)	0	0	0	0	0
U76 (Coal\Steam)	894	894	212.31	16.08	0.01
U100 (Oil\Steam)	1,375	3,113	781.52	43.66	0.05
U155 (Coal\Steam)	390	1,429.5	382.24	12.39	0.01
U197 (Oil\Steam)	2,436.5	4,262.5	832.76	48.58	0.01
U350 (Coal\Steam)	2,872.5	6,702	665.11	11.85	0
U400 (Nuclear)	0	0	395.37	4.42	0
SC (Sync Cond)	0	0	0	0	0

Table 4.4: Generator characteristics for RTS-79 test system

ment schedules, multiple solutions for similar fuel generating unit types are observed, for instance, at buses 7 and 13, respectively. The UC+ACOPF system cost accounts for an additional $1,382$ MW in losses, which is 2.4% of the overall dispatch; the UC+DCOPF with uniform losses using a 2.4% demand scaling results in a system cost of $\$891,453$ which is an increase 8.2% cost increase of the UC+DCOPF results.

Then the 0.1% cost increase from UC to UC+DCOPF is due to a binding power flow limit on the line between buses 7 and 8 in time period 10. Bus 7 is radially connected to bus 8 (as shown in Figures 4.6 and 4.7), and connects 3 oil generators to the grid. Because of the congestion, energy from these generators cannot be supplied to the rest of the system and generator 16 (located at bus 15) is brought online for compensation.

The 8.7% cost increase from UC+DCOPF to UC+ACOPF is mainly due to commitments of the more expensive oil generators with larger reactive power capability

		UC	UC+DCOPF	UC+ACOPF	UC+DCOPF+RUC
Costs ($)		$823,145$	$823,894$	$895,281$	$896,169$
		Commitment (h)			
Bus 1	G1.U20	$\varnothing$	$\varnothing$	$\varnothing$	$\varnothing$
Bus 1	G2.U20	$\varnothing$	$\varnothing$	$\varnothing$	$\varnothing$
Bus 1	G3.U76	$8-23$	$8-23$	$8-23$	$8-23$
Bus 1	G4.U76	$8-23$	$8-23$	$8-23$	$8-23$
Bus 2	G5.U20	$\varnothing$	$\varnothing$	10	10
Bus 2	G6.U20	$\varnothing$	$\varnothing$	10	10
Bus 2	G7.U76	$8-23$	$8-23$	$8-23$	$8-24$
Bus 2	G8.U76	$8-23$	$8-23$	$8-23$	$8-23$
Bus 7	G9.U100	$10-22$	$9-16$	$10-23$	$1-24$
Bus 7	G10.U100	$9-16$	$10-22$	$1-18$	$10-22$
Bus 7	G11.U100	$10-18$	$10-18$	$9-24$	$9-18$
Bus 13	G12.U197	$\varnothing$	$11-23$	$\varnothing$	$11-23$
Bus 13	G13.U197	$\varnothing$	$\varnothing$	$\varnothing$	$\varnothing$
Bus 13	G14.U197	$11-23$	$\varnothing$	$11-22$	$\varnothing$
Bus 14	G15.SC	$\varnothing$	$\varnothing$	$1-24$	$1-24$
Bus 15	G16.U12	$\varnothing$	$9-12$	$10-13$	$9-12$
Bus 15	G17.U12	$10-13$	$9-12$	$10-15$	$9-15$
Bus 15	G18.U12	$10-13$	$9-12$	$10-15$	$10-15$
Bus 15	G19.U12	$\varnothing$	$\varnothing$	$10-15$	$9-12$
Bus 15	G20.U12	$9-12$	$9-12$	$10-13$	$9-15$
Bus 15	G21.U155	$1-24$	$1-24$	$9-24$	$1-24$
Bus 16	G22.U155	$9-24$	$1-24$	$1-24$	$1-24$
Bus 18	G23.U400	$1-24$	$1-24$	$1-24$	$1-24$
Bus 21	G24.U400	$1-24$	$1-24$	$1-24$	$1-24$
Bus 22	G25.U50	$1-24$	$1-24$	$1-24$	$1-24$
Bus 22	G26.U50	$1-24$	$1-24$	$1-24$	$1-24$
Bus 22	G27.U50	$1-24$	$1-24$	$1-24$	$1-24$
Bus 22	G28.U50	$1-24$	$1-24$	$1-24$	$1-24$
Bus 22	G29.U50	$1-24$	$1-24$	$1-24$	$1-24$
Bus 22	G30.U50	$1-24$	$1-24$	$1-24$	$1-24$
Bus 23	G31.U155	$1-24$	$9-24$	$1-24$	$9-24$
Bus 23	G32.U155	$1-24$	$1-24$	$1-24$	$1-24$
Bus 23	G33.U350	$1-24$	$1-24$	$1-24$	$1-24$

Table 4.5: System costs and commitments for each {generator ID}.{generator type} in the RTS-79 test system

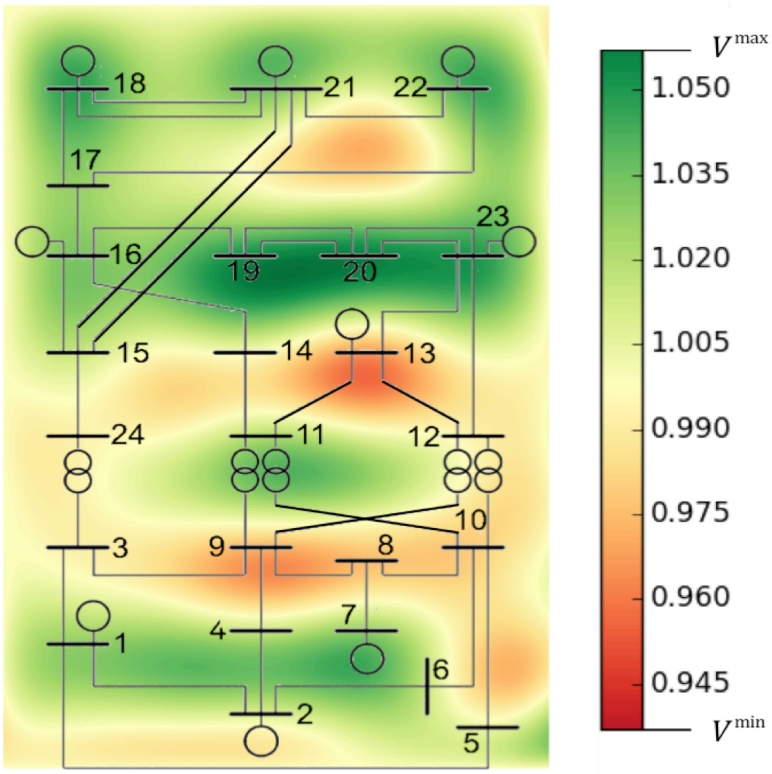

Figure 4.6: UC+ACOPF: The voltage heat map for a normal operating state for voltage limits $0.94 - 1.06$p.u. in time period 20.

used to meet reactive power demand and manage under-voltage conditions. For instance, commitment of the larger oil\steam unit G10.U100 is expanded to replace the smaller oil\steam unit G12.U197 because of the larger reactive power capability it provides; more specifically unlike any other commitment schedule, thermal unit G10.U100 is operated at its MOL for an extended time frame in the early day, i.e., from time periods 1 through 8. In actual practice, where such reliability commitments aren't included in the day-ahead market settlement, this additional \$15.2K in costs to the system would be incorporated into the side payments for reliability commitments [13].

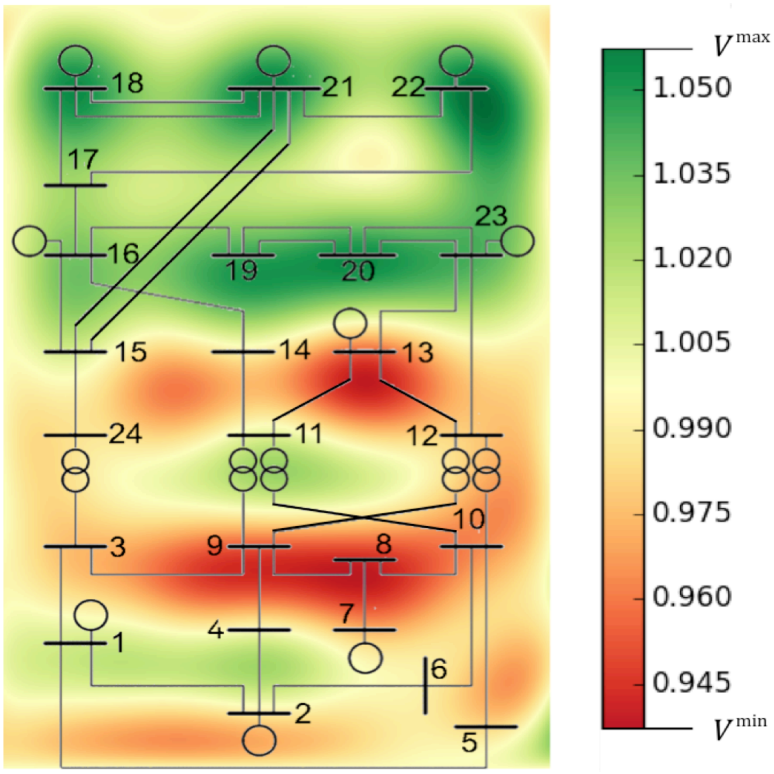

Figure 4.7: UC+DCOPF: The voltage heat map for an alert operating state, as a result of an AC feasibility check of the UC+DCOPF commitment schedule (i.e., production levels allowed to vary), in time period 20. For voltage limits 0.94−1.06p.u., there are voltage violations and load mismatches for the UC+DCOPF commitment schedule, which is AC infeasible.

Meeting reactive power demand is imperative to ensure normal operations. If implemented directly, the UC+DCOPF commitment schedule results in real and reactive load shedding. The voltage heat maps in Figures 4.6 and 4.7 compare the UC+ACOPF solution to an AC feasibility check of the UC+DCOPF commitment schedule (i.e., production levels allowed to vary), specifically when the system is at 92% of peak demand at time period 20. Without the additional commitments to increase reactive power dispatch, there are voltage violations as well as unmet load.

These conditions are unacceptable and drive the system out of its normal operating state into an emergency state [135]. One way to attain AC feasibility in the UC+DCOPF model is to determine the additional commitments required in order to satisfy the AC network constraints; therefore the commitments resulting from the UC+DCOPF model are fixed and then the above proposed solution technique is applied to solve for the residual commitments, referred to as the UC+DCOPF+RUC. This local solution method determines a cost effective solution that resolves the load mismatch and other violations in the problematic time periods. In such a case, the UC+DCOPF system cost increases to $\$896,169$ in the UC+DCOPF+RUC, which is slightly more expensive than the UC+ACOPF solution.

The IEEE RTS-79 exhibits solutions to the UC+ACOPF in which system voltages are lower than nominal (i.e., 1 p.u.). The lower voltages cause thermal line limits to be more restrictive in the UC+ACOPF results as compared to the UC+DCOPF results. This also indicates that power transfers in the UC+DCOPF might violate actual power transfer limits. In such a case, transmission limits could be tightened in the UC+DCOPF model as a way to proxy AC feasibility; this approach is frequently applied in actual operations (i.e., using nomograms)[60] which in turn drive the solution cost up and can result in a dramatically different commitment schedule than a more efficient UC+ACOPF approach.

[60] a constraint set that approximates actual nodal voltage limits and reactive power needs through restricting real power imports

	UC	UC+DCOPF	UC+ACOPF	UC+DCOPF+RUC
Costs ($)	$811,658$	$814,715$	$843,591$	$844,922$
	Commitment (h)			
G1	∅	∅	∅	∅
G2	∅	∅	∅	∅
G3	∅	∅	∅	∅
G4	$1-24$	$1-24$	$1-24$	$1-24$
G5	$1-24$	$1-24$	$1-24$	$1-24$
G6	∅	∅	∅	∅
G7	∅	∅	$10-23$	$10-22$
G8	∅	∅	∅	∅
G9	∅	∅	∅	∅
G10	$1-24$	$1-24$	$1-24$	$1-24$
G11	$1-24$	$1-24$	$1-24$	$1-24$
G12	∅	∅	∅	∅
G13	∅	∅	∅	∅
G14	∅	∅	$9-22$	$11-18$
G15	∅	∅	∅	∅
G16	∅	$10-18$	$10-23$	$9-22$
G17	∅	∅	∅	∅
G18	∅	∅	∅	∅
G19	∅	∅	∅	∅
G20	$1-23$	$1-24$	$1-24$	$1-24$
G21	∅	∅	$8-24$	$8-23$
G22	∅	∅	∅	∅
G23	∅	∅	∅	∅
G24	∅	∅	$9-23$	$9-23$
G25	∅	$10-22$	∅	∅
G26	∅	∅	∅	∅
G27	$1-24$	$1-24$	$1-24$	$1-24$

Table 4.6: System costs and commitments for each generator in the IEEE-118 test system (Table 1 of 2)

4.5.3 IEEE-118 Test System

The modified IEEE-118 test system from [117] has 118 buses, 54 generators, 14 synchronous condensers, and 90 loads; for this test system there are no buses with

	UC	UC+DCOPF	UC+ACOPF	UC+DCOPF+RUC
Costs ($)	$811,658$	$814,715$	$843,591$	$844,922$
	Commitment (h)			
G28	$1-23$	$1-24$	$1-24$	$1-24$
G29	$1-24$	$1-24$	$1-24$	$1-24$
G30	$9-23$	$8-23$	$7-24$	$7-24$
G31	$\varnothing$	$\varnothing$	$\varnothing$	$\varnothing$
G32	$\varnothing$	$\varnothing$	$\varnothing$	$\varnothing$
G33	$\varnothing$	$\varnothing$	$\varnothing$	$\varnothing$
G34	$8-24$	$7-24$	$7-24$	$7-24$
G35	$1-24$	$1-24$	$1-24$	$1-24$
G36	$1-24$	$1-24$	$1-24$	$1-24$
G37	$8-24$	$1-24$	$11-17$	$1-24$
G38	$\varnothing$	$\varnothing$	$\varnothing$	$\varnothing$
G39	$1-24$	$1-24$	$1-24$	$1-24$
G40	$1-24$	$1-24$	$1-24$	$1-24$
G41	$\varnothing$	$\varnothing$	$\varnothing$	$\varnothing$
G42	$\varnothing$	$\varnothing$	$\varnothing$	$\varnothing$
G43	$1-24$	$9-24$	$10-23$	$1-24$
G44	$\varnothing$	$\varnothing$	$\varnothing$	$\varnothing$
G45	$1-24$	$1-24$	$1-24$	$1-24$
G46	$\varnothing$	$\varnothing$	$\varnothing$	$\varnothing$
G47	$\varnothing$	$\varnothing$	$\varnothing$	$\varnothing$
G48	$\varnothing$	$\varnothing$	$\varnothing$	$\varnothing$
G49	$\varnothing$	$\varnothing$	$\varnothing$	$\varnothing$
G50	$\varnothing$	$\varnothing$	$\varnothing$	$16-17$
G51	$10-22$	$\varnothing$	$9-24$	$1-24$
G52	$\varnothing$	$\varnothing$	$\varnothing$	$\varnothing$
G53	$8-24$	$8-24$	$1-24$	$1-24$
G54	$9-23$	$9-23$	$9-20$	$9-23$

Table 4.7: (Table 4.6 Continued) System costs and commitments for each generator in the IEEE-118 test system (Table 2 of 2)

multiple thermal units, but a thermal unit may be co-located with a synchronous condenser.

The system costs and commitment schedules are reported in Tables 4.6 and 4.7. The UC+ACOPF system cost accounts for an additional 2.6% in network losses;

the UC+DCOPF with uniform losses using a 2.6% demand scaling results in a 3.1% cost increase. Network congestion on three transmission lines for bus pairs (77,82), (82,83), and (30,38) results in a 0.4% cost increase from the UC to the UC+DCOPF solution. However the UC+DCOPF is AC infeasible, primarily due to over-voltages at bus 111 which is radially connected to bus 110; the voltage limits of $1 - 1.06$p.u. at bus 111 are tighter nodal voltage bounds than for most of the network. The UC+DCOPF+RUC results in additional commitments of G50 at bus 110 and G51 at bus 111 in order to address the over-voltages at bus 111. Also the UC+DCOPF+RUC solution includes additional commitments that appear in the UC+ACOPF schedule but not in the UC+DCOPF schedule. The resulting UC+DCOPF+RUC system cost of $\$844,922$ is a 3.7% increase in the UC+DCOPF system cost in order to make its commitment schedule AC feasible. Although the UC+ACOPF solution has a 3.5% cost increase over the UC+DCOPF, applying the UC+ACOPF is more cost effective than determining residual commitments to make the UC+DCOPF an AC feasible solution.

4.5.4 Computational Results

Table 4.8 reports the computational results for the three case studies when assuming 10 piecewise linear segments for the production cost function. The performance metrics include solution time as reported by CPLEX 12.6.2, as well as outer loop (UC+ACOPF MILP) and inner loop (UC+ACOPF SLP) iterations in

10 piecewise linear segments, relative MIP gap tolerance 0.1%						
	UC	UC+DCOPF	UC+ACOPF		UC+DCOPF+RUC	
	MILP	MILP	MILP	SLP	MILP	SLP
Solution Time (s)						
6-Bus	0.13	0.21	0.88(3)	0.07(50)	1.02(1, 1)	0.06(33)
RTS-79	1.86	6.76	88.71(3)	0.75(36)	10.37(1, 2)	0.45(26)
IEEE-118	5.04	21.42	110.17(2)	5.06(46)	57.2(1, 1)	3.71(33)
Cost ($)						
6-Bus	101, 270	106, 987	101, 763		102, 523	
RTS-79	823, 145	823, 894	895, 281		896, 169	
IEEE-118	811, 658	814, 715	843, 591		844, 922	

Table 4.8: Summary computational results

parentheses. Note that these metrics are parameter and implementation dependent, as specified in Table 4.2. The UC+ACOPF is around 5–15 times slower than the UC+DCOPF problem for the simulations reported. More notably, however, is the computational performance and system costs for the UC+DCOPF+RUC problem; the UC+DCOPF+RUC is around 1.5–5 times slower than the UC+DCOPF problem but obtains AC feasibility through ACOPF optimal residual commitments for the simulations reported. Therefore, the UC+DCOPF+RUC results in system costs that are akin to the UC+ACOPF system costs, with a slight upwards deviation no greater than 0.74%. Since the OA method spends most of the computational time in the master problem, further improvements to the MILP could lead to significant computational gains.

4.6 Discussion

This work proposes a formulation and algorithm to solve the UC with ACOPF constraints, which is a nonconvex MINLP. Then an extensive, comparative analysis is performed to assess the economic and operational impact of more accurate ACOPF constraint modeling on the UC problem when compared to copperplate and DCOPF approaches. This analysis is extended to consider losses in the DCOPF approach, and also to check that the commitment schedule determined by the UC with DCOPF constraints is AC feasible. When the commitment schedule is AC infeasible, then residual commitments are determined with the proposed UC+ACOPF method in order to achieve AC feasibility.

Overall the results indicate a significant disparity in the unit commitment schedules due to the differences in the physical and operational constraints for the copperplate, DCOPF, and ACOPF approaches. The differences in the overly approximated copperplate and DCOPF approaches as compared to the ACOPF approach indicate a divergence between the market settlements and the stability and reliability requirements for normal grid operations. However the computational cost of the more accurate ACOPF approach could be considerable, its computation times are 5–15 times slower than the UC with DCOPF constraints for the systems tested. More promising is the computational speeds for updating the DCOPF approach to include residual commitments for AC feasibility; this approach is only 1.5–5 times slower

than the UC+DCOPF problem but has system costs that are similar to the ACOPF approach. The relative computational speeds for more realistic size examples can be different than this outcome. More generally, since the OA method spends most of the computational time in the single iteration of the master problem, further improvements to the MILP could lead to significant computational gains. For example, tighter convex hull representations in the master problem of the OA method and potentially decomposing the algorithm for distributed, parallel optimization could improve the solution times for both the ACOPF and the ACOPF for RUC approaches.

4.7 Supporting Material

4.7.1 Adaptive Step-size Region

At each inner loop iteration h, the adaptive step-size regions $V_{n,t}^{r(h)}$ and $V_{n,t}^{j(h)}$ are updated to constrain the difference between the real and imaginary parts of the nodal voltage with their corresponding Taylor series evaluation points in the following manner

$$-V_{n,t}^{r(h)} \leq v_{n,t}^{r} - \hat{v}_{n,t}^{r(h)} \leq V_{n,t}^{r(h)} \tag{4.33}$$

$$-V_{n,t}^{j(h)} \leq v_{n,t}^{j} - \hat{v}_{n,t}^{j(h)} \leq V_{n,t}^{j(h)} \tag{4.34}$$

for all $n \in \mathcal{N}, t \in \mathcal{T}$. At the end of each iteration $h > 0$, this tunable parameter $V_{n,t}^{(h)}$ is modified in order to control the approximation error in the first-order Taylor

series linearization. This parameter is adapted based on the relative real and reactive power mismatch error:

$$\varphi_{n,t}^{P(h)} = \max\left(0.001, \left|P_{n,t}^{(h)} - P_{n,t}\right| / \min\left(P_{n,t}^{(h)}, P_{n,t}\right)\right)$$
$$\varphi_{n,t}^{Q(h)} = \max\left(0.001, \left|Q_{n,t}^{(h)} - Q_{n,t}\right| / \min\left(Q_{n,t}^{(h)}, Q_{n,t}\right)\right)$$

where $P_{n,t}^{(h)}$ and $Q_{n,t}^{(h)}$ are respectively calculated from the Taylor series approximations of (3.8) and (3.9) applied directly to (4.8) and (4.9), and then $P_{n,t}$ and $Q_{n,t}$ are respectively calculated from the bilinear terms in (4.8) and (4.9) for the solution to iteration $h-1$. Note that if one of the values within the absolute difference term is within some epsilon of zero, then the denominator should be computed as $1 + \min(\cdot)$.

Calculating parameters $\beta_{n,t}^{r(h)} = -a \log \varphi_{n,t}^{Q(h)} + b$, $\beta_{n,t}^{j(h)} = -a \log \varphi_{n,t}^{P(h)} + b$, $\alpha_{n,t}^{r(h)} = 1/\beta_{n,t}^{r(h)}$, and $\alpha_{n,t}^{j(h)} = 1/\beta_{n,t}^{j(h)}$, the adaptive step-size regions are specified as:

$$V_{n,t}^{r(h)} \leftarrow \alpha_{n,t}^{r(h)} \left|\overline{V}_n\right| \Big/ h^{\beta_{n,t}^{r(h)}}$$
$$V_{n,t}^{j(h)} \leftarrow \alpha_{n,t}^{j(h)} \left|\overline{V}_n\right| \Big/ h^{\beta_{n,t}^{j(h)}}.$$

For some intuition on the above approach, the relative reactive power mismatch error is associated to the approximation of $v_{n,t}^{r}$ because the coupling between Q–Θ is relatively weak [136] and as $v_{n,t}^{j} \to 0$, then $v_{n,t}^{r}$ converges to the voltage magnitude (V); the weak coupling similarly applies to P–V.

This study assumes $a = 0.15$ and then tunes $b = 1$ for the six-bus, $b = 1.485$ for

the RTS-79, and $b = 1.5$ for the IEEE-118; for faster decay, the user can increase a, and as $\varphi_{n,t}^{Q(h)} \to 1$, then $\beta_{n,t}^{r(h)} \to b$; similarly for $\varphi_{n,t}^{P(h)}$.

4.7.2 Linearized Constraint Set

At each outer loop iteration $\gamma > 0$, this approach first updates the evaluation point to the optimal solution from the inner loop, i.e., $\hat{x}^\gamma = x^*$ where x^* is the optimal solution from the last iteration h in the inner loop. Then the evaluation region V^γ is set as

$$V^\gamma \leftarrow c/\mathrm{e}^{\gamma/d}$$

where $c = 0.1$ and $d = 1$ is tuned for the smaller networks (six-bus and RTS-79) and $c = 1/3$ and $d = 10$ for the larger network (IEEE-118). Then γ is incorporated into the outer loop

$$-V^\gamma \leq v_{n,t}^r - \hat{v}_{n,t}^{r(\gamma)} \leq V^\gamma \tag{4.35}$$

$$-V^\gamma \leq v_{n,t}^j - \hat{v}_{n,t}^{j(\gamma)} \leq V^\gamma \tag{4.36}$$

for all $n \in \mathcal{N}, t \in \mathcal{T}$. Finally, the linearized constraint set is constructed as the reduced set of constraints within the region V^γ, i.e., excluding constraints that would never bind. For the initial outer loop iteration, an evaluation region is not defined for the first order approximation, which enables an unconstrained search for the best

integer feasible solution in the ACOPF constraint set for the given Taylor series evaluation points; however, the trade-off results in higher error terms in the first order approximations, which then must be corrected in subsequent inner and outer loop iterations.

4.7.3 Six-Bus Data Set

Cost Data	Thermal Unit G1	G2	G3
Fuel Price ($/Mbtu)	1.2469	1.2461	1.2462
Quadratic Cost (Mbtu/MW^{2}h)	0.0004	0.001	0.005
Linear Cost (Mbtu/MWh)	13.5	32.6	17.6
Fixed Cost (Mbtu)	176.9	129.9	137.4

Table 4.9: Thermal unit production cost data

Branch Flow $k\,(n,m)$	Resistance r_k	Reactance x_k	Tap Transformer $\lvert\tau_{kn}\rvert$	Thermal Limit $\overline{I}_k$
$1\,(1,2)$	0.005	0.17	1	200
$2\,(1,4)$	0.003	0.258	1	100
$3\,(2,4)$	0.007	0.197	1	100
$4\,(5,6)$	0.002	0.140	1	100
$5\,(3,6)$	0	0.018	1	100
$6\,(2,3)$	0	0.037	1/0.98	10,000
$7\,(4,5)$	0	0.037	1/0.98	10,000

Table 4.10: Relevant network data; voltage in [0.85,1.15]

Parameter	Description	Thermal Unit G1	G2	G3
$\overline{C}_i^d$	Shutdown capacity (MW)	55	50	20
$\overline{C}_i^u$	Startup capacity (MW)	55	50	20
$K_{i,s}^u$	Single segment startup cost ($)	124.69	249.22	0
$\overline{T0}_i^d$	Initial time periods offline (hr)	0	0	1
$\overline{T0}_i^u$	Initial time periods online (hr)	4	1	0
T_i^d	Min downtime (hr)	4	3	1
T_i^u	Min uptime (hr)	4	2	1
P_i^0	Power generated $t = 0$ (MW)	160	55	0
$\overline{P}_i$	Max real dispatch (MW)	220	100	20
$\underline{P}_i$	Min real dispatch (MW)	100	10	10
$\overline{Q}_i$	Max reactive dispatch (MVAr)	200	70	50
$\underline{Q}_i$	Min reactive dispatch (MVAr)	-80	-40	-40
RR_i^d	Ramp down limit (MW/h)	55	50	20
RR_i^u	Ramp up limit (MW/h)	55	50	20
s'	Single segment startup lag (hr)	4	3	1

Table 4.11: Thermal unit parameterization

	Real Power Demand $P^d_{n,t}$ (MW)			Reactive Power Demand $Q^d_{n,t}$ (MVAr)		
Hour	Bus 3	Bus 4	Bus 5	Bus 3	Bus 4	Bus 5
1	35.738	71.476	71.476	10.074	20.148	20.148
2	33.690	67.380	67.380	9.496	18.992	18.992
3	32.368	64.736	64.736	9.124	18.248	18.248
4	31.566	63.132	63.132	8.898	17.796	17.796
5	31.632	63.264	63.264	8.916	17.832	17.832
6	32.738	65.476	65.476	9.228	18.456	18.456
7	35.372	70.744	70.744	9.970	19.940	19.940
8	38.842	77.684	77.684	10.212	20.424	20.424
9	41.934	83.868	83.868	10.742	21.484	21.484
10	44.308	88.616	88.616	11.900	23.800	23.800
11	46.636	93.272	93.272	13.146	26.292	26.292
12	48.164	96.328	96.328	13.576	27.152	27.152
13	49.406	98.812	98.812	13.926	27.852	27.852
14	49.694	99.388	99.388	14.006	28.012	28.012
15	50.766	101.532	101.532	14.310	28.620	28.620
16	52.180	104.360	104.360	14.708	29.416	29.416
17	52.224	104.448	104.448	14.720	29.440	29.440
18	50.336	100.672	100.672	14.188	28.376	28.376
19	50.178	100.356	100.356	14.144	28.288	28.288
20	48.420	96.840	96.840	13.648	27.296	27.296
21	48.410	96.820	96.820	13.646	27.292	27.292
22	46.336	92.672	92.672	13.378	26.756	26.756
23	41.014	82.028	82.028	11.266	22.532	22.532
24	40.138	80.276	80.276	11.246	22.492	22.492

Table 4.12: Demand profile per bus

III Global Solution Methods

5 Energy Storage for Transmission System VAr Support: Trade-offs Between Grid Benefits and Storage Operator Profit

5.1 Prologue and Motivation

The prior work presented in Chapters 3 and 4 focused on proposing local solution methods for practical applications of the ACOPF in real-time and day-ahead operations. The remaining chapters, which constitute Part III of this dissertation, focus on global solution techniques for solving OPF models and OPF approximations for optimal storage integration. Although local optima of the OPF have not been reported in practice [137], global solution techniques can guarantee no duality gap, which allows more vigorous analysis of the OPF problem as it relates to spot pricing theory. Chapter 5 investigates optimal storage integration in markets with payments for both real and reactive power. Then Chapter 6 proposes a global solution technique to solve DCOPF with losses approximation of the OPF and compares this approach to the DCOPF and ACOPF for optimal storage integration.

The global solution techniques applied in these studies reformulate nonconvex

problems as convex relaxations of the original problems. These relaxations are exact under certain conditions. These properties are discussed later in more detail but first, in order to motivate the necessity of a global solution method for optimal storage integration, this prologue presents a simple example where applying a local solution method results in a non-global local optima. The example demonstrates that solving the ACOPF with optimal storage integration using a commercial NLP solver may result in a sub-optimal local solution, whereas applying the semidefinite relaxation approach originally proposed in [24] guarantees a global optimum.[61]

A Motivating Example: Non-Global Local Optima

Consider the three-bus AC network shown in Figure 5.1 [84] where energy storage can be optimally integrated and operated at any bus, and the aggregate system storage capacity limit is 20 MWh. The storage technology under consideration has the following technical characteristics:

1. Unlimited power ratings on the charge and discharge dynamics,
2. A roundtrip efficiency of 81%, and
3. Reactive power compensation (dispatch availability up to 1/5 the energy capacity).

The optimization problem chooses where in the network to site the 20 MW of

[61] Given the rank one condition holds, i.e., $xx^T = X$, which is covered in more detail later in this chapter.

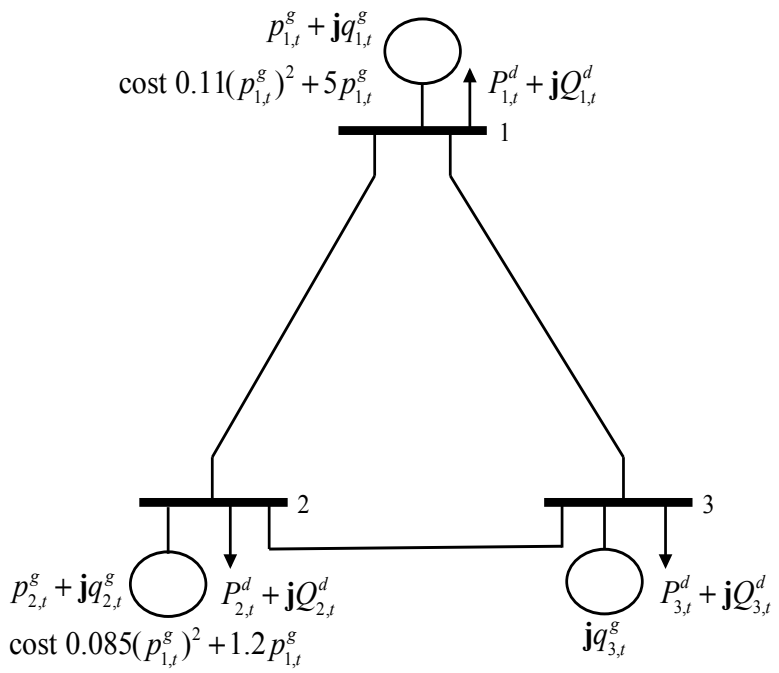

Figure 5.1: Three-bus network with conventional generators at buses 1 and 2, a synchronous condenser at bus 3, and load at all buses.

storage, which can be divided up continuously among more than one bus. The conventional generators at buses 1 and 2 have unconstrained power generation and the synchronous condenser at bus 3 is unconstrained in reactive power capacity. The real and reactive power demands at buses 1 and 2 for hours $t = [1, 5]$ where $p = 110$ MW and $q = 40$ MVAr are $P^d_{1,t} = P^d_{2,t} = [0.6p, 0.75p, p, 0.85p, 0.5p]$ and $Q^d_{1,t} = Q^d_{2,t} = [0.6q, 0.75q, q, 0.85q, 0.5q]$; the real and reactive power demands at bus 3 where $p = 95$ MW and $q = 50$ MVAr are $P^d_{3,t} = [0.6p, 0.75p, p, 0.85p, 0.5p]$ and $Q^d_{3,t} = [0.6q, 0.75q, q, 0.85q, 0.5q]$.

Table 5.1 presents results for solving the ACOPF with optimal storage integration

Time-Period		t = 1	t = 2	t = 3	t = 4	t = 5
	Bus	Storage Level in MWh				
opt^*	1	0.4	0.4	0	0	0
(global)	2	0	0	0	0	0
	3	19.6	19.6	0	0	0
	Bus	Storage Level in MWh				
$opt^{\mathcal{L}}$	1	20	20	0	0	0
(local)	2	0	0	0	0	0
	3	0	0	0	0	0
	Bus	Charging (+) & Discharging (-) in MW				
opt^*	1	0.5	0	-0.4	0	0
(global)	2	0	0	0	0	0
	3	21.7	0	-17.6	0	0
	Bus	Charging (+) & Discharging (-) in MW				
$opt^{\mathcal{L}}$	1	22.2	0	-18	0	0
(local)	2	0	0	0	0	0
	3	0	0	0	0	0

Table 5.1: Comparing a non-global local optima to a global optimum.

problem[62] (ACOPF+S or OPF+S). A local solution was recovered by solving the ACOPF+S directly as a NLP using Knitro 8.1.1 with the active-set algorithm and a relative error tolerance of 1.0×10^{-6} for first order optimality satisfaction [138]. The global solution was recovered by applying a semidefinite relaxation and solving this reformulation using Sedumi 1.21 with a desired accuracy of 1.0×10^{-9} [139]; the solution satisfies the rank-one sufficient condition and is feasible for the original ACOPF+S (i.e., the solution is exact). The global solution, denoted by opt^*, has

[62] more formally defined in Section 5.3

an objective function value of $\$17,047$ whereas the locally optimal solution, $opt^{\mathcal{L}}$, has a value of $\$31,157$; both solutions satisfy first order optimality conditions within Knitro 8.1.1, yet a global optimum has nearly half the cost function value of the local optima. Furthermore, the local optima is a low voltage solution that has higher current flows which result in higher losses compared to a global optimum; although such solutions are common outcomes of the optimization routine, the local optima may or may not be acceptable operating points in practice [137]. For the local optima, there is a higher MW dispatch from the more expensive generator at bus 1 than from the generator at bus 2 due to low voltage limits; therefore, in order to decrease the generation requirements during the peak period at bus 1, all 20 MW of storage is placed at that location and then charged to full capacity in the first period. In a global optimum, most of the storage is optimally integrated at bus 3; since bus 3 has no native generation to meet its demand, placing storage at this location decreases the required MW imports from elsewhere on the network. To summarize, the energy storage integration across the network is different in both solutions.

Although global techniques are much slower than local ones, the application of global solution techniques eliminates such suboptimal outcomes. Chapter 5 seeks globally optimal solutions by applying the semidefinite relaxation approach and uses the resulting problem to examine the trade-offs that arise when distributed energy storage is used to provide VAr support in addition to traditional grid-scale storage services. In particular, this work focuses on how the provision of reactive power

dispatch impacts the storage operator's marginal profits[63] using a novel analytical approach that relates real and reactive nodal price signals to energy storage dynamics. Such a study could not be completed with the DCPF-based assumptions that system operators use in their market software [6]. This work extends the preliminary results reported in [26].

5.2 Introduction and Background

The benefits of grid-scale storage are often discussed in the contexts of energy arbitrage, reserve power, frequency regulation and other power quality services for renewable energy integration; e.g., see [140–144]. One less discussed storage application is the provision of reactive power support through the power electronics connecting storage technologies such as batteries to the grid or the generator-motor excitation of a pumped hydro storage system [145].

Reactive power is critical to the efficient and reliable operation of the electric power grid. For example, reactive power is used to control voltage levels and ensure grid stability and power quality [142]. An energy storage system (ESS) refers to an energy storage technology with power electronics such as a converter or flexible AC transmission system (FACTS) device [146]. Such ESS installations can supply dynamic reactive power which has distinct advantages over the use of transmission equipment

[63]The marginal profits are equal to the marginal revenues minus marginal costs and does not include the entire cost structure (e.g., capital costs, fixed costs, and variable costs that are not related to incremental unit production are not included) of the market participant.

such as capacitors and inductors that supply and consumer static reactive power. This capability enables ESS to quickly change the amount of VAr support independent of the voltage level, which can provide faster response to sudden large voltage surges or drops [147–150]. Furthermore, renewables are displacing synchronous generators that have historically provided reactive power compensation; there is concern that this may lead to a reactive power deficiencies. Therefore system operators are currently assessing whether asynchronous resources should be required to provide reactive power compensation, similar to synchronous resources.

This study extends the preliminary work in [92] by augmenting the previously proposed ACOPF+S model to include VAr injection and absorption from ESS units. A number of other studies have employed ACOPF+S based analysis, see e.g., [25, 92, 151–156], and either neglected reactive power support in the formulation [92, 151–156] or excluded its effect in the analysis [25, 92]. However this study extends the OPF-based approach to investigate the economics of using ESS to provide VAr support in addition to the more traditional energy and power services. The proposed ACOPF+S problem is solved using the SDR technique originally presented in [25], which extends the work in [24]; this convex problem is referred to as the SDR-OPF+S. The solution of SDR-OPF+S is equivalent to the original ACOPF+S problem when the relaxation is exact.

The theoretical results of this study leverage the fact that the KKT point for the SDR-OPF+S problem is a global optimum of the ACOPF+S when the relaxation

is exact. First this work proves a sufficient condition for preventing simultaneous charging and discharging of individual ESS units governed by linear storage dynamics without having to incorporate mixed integer or nonlinear constraints as in [157–159]. Then the Lagrangian dual of the SDR is used to form a storage operator subproblem, which isolates the primal and dual variables related to storage. This problem defines the value of storage as a function of its cost and revenue streams from charging, discharging and VAr support. The second theoretical result exploits the properties of strong duality to prove that maximizing the marginal profits to the storage operator is equivalent to minimizing system costs in a purely competitive market.

The study further investigates the storage subproblem by examining the role of the Lagrange multipliers (dual variables) for the real and reactive power balance equations in the SDR-OPF+S problem; when the relaxation is exact, this provides insight to a global optimum of the ACOPF+S. In particular, this study examines the role of the Lagrange multiplier on the reactive power balance constraint, which indicates the economic value of leading/lagging VAr dispatch. This nodal (or shadow) price of VAr support is referred to as the Q-LMP due to its mathematical similarity to the LMP, which is the Lagrange multiplier on the real power balance constraint and determines the marginal clearing price of energy. Reactive power prices have also been investigated within a market design context in [160–164].

Case studies using an augmented IEEE-14 transmission system with wind power illustrate the effect of VAr support from ESS units. Since the SDR is exact in all

reported cases, the solutions obtained provide insight regarding a global optimum of the ACOPF+S problem. The case study results first demonstrate that the inclusion of VAr support can greatly change the optimal allocation of resources in the network and that the power system operations are more efficient, resulting in market settlements that clear at a lower operating cost. Storage is also more profitable due to revenues from providing VAr support.

A second case study examines how the compensation mechanism for VAr support affects the economic value proposition for a storage installation. The results demonstrate that a market design which does not compensate reactive power dispatch can actually disincentivize the willingness to provide it as a service. Then the Q-LMP, which reflects the marginal value of VAr support, is compared to current reactive power capability rates in NYISO and ISO-NE. The results demonstrate that the disconnect between these rates and nodal prices can lead to significant over-supply of VAr in some areas and scarcity in others. Problems also arise due to the differences in capability rates between system operators. The shortcomings of the current schemes mean that storage which dispatches reactive power more frequently than other storage with higher reactive power capability, for example, may not be compensated accordingly.

The combination of theoretical results and case studies provide insight that can be used to develop better models of ESS integration and dispatch, improve market design, and determine optimal scheduling policies for ESS units. This approach

provides insight to potential outcomes in purely competitive markets and does not consider strategic interactions or market power manipulation amongst market participants. This purely competitive market situation is also researched as a Bertrand game where the firm takes the nodal prices as fixed, and intense competition can result due to locational and temporal price variation caused by operational and other physical network constraints [165].

The remainder of the chapter is organized as follows. The ACOPF+S formulation is presented in Section 5.3 followed by a discussion of the SDR-OPF+S in Section 5.4. The main theoretical results are presented in Sections 5.5 and 5.6 with an illustrative example in Section 5.7. A case study on compensation mechanisms is presented in Section 5.8 and final remarks in Section 5.9.

5.3 Problem Formulation

This study extends the ACOPF formulation in rectangular coordinates, as presented in (2.40) − (2.46) of Chapter 2 by incorporating a linear storage model, renewable energy availability, and ramp rates on conventional generation as follows.

5.3.1 Storage Model

Here a generic storage model is proposed that can be adapted to specify a particular storage technology through parameterization. An ESS installation of energy capacity c_n is modeled as a single unit that can be located at each bus $n \in \mathcal{N}$. The energy

storage level $s_{n,t}$ is specified through a linear relationship between the charge $r^c_{n,t}$ and discharge $r^d_{n,t}$ dynamics; reactive power rates $z_{n,t}$ are also incorporated by determining the power converter size as a linear function of the energy capacity of the unit.

The storage level $s_{n,t}$ at each bus n during time interval $t \in \mathcal{T}$ is specified through the following linear storage dynamics

$$s_{n,t} = s_{n,t-1} + \eta^c_n r^c_{n,t} - \left(\eta^d_n\right)^{-1} r^d_{n,t}, \tag{5.1}$$

where $s_{n,0}$ is the initial storage level parameterized by the terminal storage level in the prior operating cycle. Here, $r^c_{n,t}$ and $r^d_{n,t}$ are the respective real power charge and discharge rates at each bus $n \in \mathcal{N}$ for time interval $t \in \mathcal{T}$. The parameters η^c_n and η^d_n denote the corresponding charge and discharge efficiencies. The real power charge and discharge rates are respectively bounded as

$$0 \leq r^c_{n,t} \leq R^c_n \tag{5.2}$$

$$0 \leq r^d_{n,t} \leq R^d_n. \tag{5.3}$$

The energy storage level $s_{n,t}$ at each bus n during time interval $t \in \mathcal{T}$ is bounded as

$$\underline{C}_n \leq s_{n,t} \leq c_n, \tag{5.4}$$

where $\underline{C}_n$ represents a technology dependent depth of discharge in the storage dispatch

problem.

Depending upon the controls, the active and reactive output of an ESS can be independent [146]. An ESS unit can also operate in all four quadrants in terms of delivering/absorbing controllable real and reactive power. VAr injection and absorption rates are bounded as

$$\underline{Z}_n \leq z_{n,t} \leq \overline{Z}_n \tag{5.5}$$

for all $n \in \mathcal{N}, t \in \mathcal{T}$, where $z_{n,t} > 0$ indicates VAr injection and $z_{n,t} < 0$ indicates absorption. The VAr rate bounds are determined by the power converter size as a linear function of the energy capacity c_n, i.e., $\underline{Z}_n = \alpha c_n$ and $\overline{Z}_n = \beta c_n$.

A single operating cycle is assumed in which the terminal storage level in the current cycle equals the terminal storage level in the prior operating cycle, that is

$$\tilde{s}_{n,T} - s_{n,T} = 0 \tag{5.6}$$

for all buses $n \in \mathcal{N}$, i.e., for a given optimization problem the initial and final storage levels are the same. This assumption is based on the notion of using a finite length time interval to approximate naturally occurring cyclic variations in demand and generation profiles, e.g., diurnal or seasonal cycles.

The Storage Allocation Problem

The formulation in (5.1)−(5.6) can be modified to solve the storage allocation problem by setting $\underline{C}_n := 0$ in (5.4) and adding the following constraint on the total overall energy storage allocated throughout the network

$$\sum_{n \in \mathcal{N}} c_n \leq h. \tag{5.7}$$

Here h is the total storage budget to be allocated.

Remark 5.1. *The generic storage model described by* (5.1) − (5.7) *can be adapted to specific storage technologies through parameterization of the model variables, e.g.,* R_n^d, R_n^c, $\overline{Z}_n$, $\underline{Z}_n$, η_n^d, η_n^c, α, β, $\underline{C}_n$, *and* c_n. *The model can also be easily extended to installations of more than one type of storage technology at a single bus, e.g., using the approach in [166].*

The apparent power rating of an ESS unit can be incorporated through the following constraint

$$(r_{n,t})^2 + (z_{n,t})^2 \leq (\overline{S}_{n,t})^2,$$

where $r_{n,t} \coloneqq r_{n,t}^c - r_{n,t}^d$ *and* $\overline{S}_{n,t}$ *denotes the apparent power rating of the technology. However given the the reactive power capability of an ESS unit is largely dependent on the power electronic technologies, sizing of the power converter, and overload capacity (i.e., capabilities higher than the specified power rating), a simplified box constraint,*

which is a typical construct when the resource capability curve is unknown, is assumed in this study.

5.3.2 Power Flow Constraints

The power balance constraint set includes $(2.43) - (2.46)$, along with modifications to the respective real and reactive nodal power flow balance in (2.41) and (2.42). This study also incorporates renewable energy availability where the real power injected to the grid in time $t \in \mathcal{T}$ from the wind farm $i \in \mathcal{W}$ is limited by

$$0 \leq p^w_{i,t} \leq C^w_{i,t} \tag{5.8}$$

where $C^w_{i,t}$ is the resource availability.

The real and reactive power injections from conventional generators $i \in \mathcal{G}$ are respectively bounded as

$$\underline{P}_i \leq p^g_{i,t} \leq \overline{P}_i \tag{5.9}$$

and

$$\underline{Q}_i \leq q^g_{i,t} \leq \overline{Q}_i \tag{5.10}$$

for all $t \in \mathcal{T}$; note that similar to the storage model, the conventional generators are

modeled with box constraints. The real power injection for each generator $i \in \mathcal{G}$ is also constrained through the following ramp rates

$$-RR_i^d \leq p_{i,t}^g - p_{i,t-1}^g \leq RR_i^u \tag{5.11}$$

in time $t \in \{2, \ldots, T\}$.

The respective real and reactive power flow balance for all buses $n \in \mathcal{N}$ and time periods $t \in \mathcal{T}$ is

$$v_{n,t}^r \sum_{m \in \mathcal{N}} \left(G_{nm} v_{m,t}^r - B_{nm} v_{m,t}^j\right) + v_{n,t}^j \sum_{n \in \mathcal{N}} \left(G_{nm} v_{m,t}^j + B_{nm} v_{m,t}^r\right) - p_{n,t}^+ + p_{n,t}^- = 0, \tag{5.12}$$

$$v_{n,t}^j \sum_{m \in \mathcal{N}} \left(G_{nm} v_{m,t}^r - B_{nm} v_{m,t}^j\right) - v_{n,t}^r \sum_{m \in \mathcal{N}} \left(G_{nm} v_{m,t}^j + B_{nm} v_{m,t}^r\right) - q_{n,t}^+ + q_{n,t}^- = 0, \tag{5.13}$$

where the injections equal the generation, i.e., $p_{n,t}^+ = r_{n,t}^d + \sum_{i \in \mathcal{I}(n)} \left(p_{i,t}^g + p_{i,t}^w\right)$ and $q_{n,t}^+ = z_{n,t} + \sum_{i \in \mathcal{I}(n)} \left(q_{i,t}^g + q_{i,t}^w\right)$, and the withdrawals equal the demand, i.e., $p_{n,t}^- = r_{n,t}^c + P_{n,t}^d$ and $q_{n,t}^- = Q_{n,t}^d$. The nodal voltage limits are

$$\left(\underline{V}_n\right)^2 \leq \left(v_{n,t}^r\right)^2 + \left(v_{n,t}^j\right)^2 \leq \left(\overline{V}_n\right)^2 \tag{5.14}$$

for all $n \in \mathcal{N}$ and on the apparent power transfers are

$$\left(p_{k(\cdot),t}\right)^2 + \left(q_{k(\cdot),t}\right)^2 \leq \left(\overline{S}_k\right)^2 \tag{5.15}$$

for all $k(\cdot) \in \mathcal{F}$ where $p_{k(\cdot),t}$ and $q_{k(\cdot),t}$ are derived in Section 2.6 of Chapter 2.

5.3.3 Optimal Power Flow with Storage

The multi-period ACOPF with storage dynamics, referred to as the ACOPF+S formulation, is defined as:

$$\mathbf{p} \coloneqq \min_{\mathbf{v},\mathbf{r^c},\mathbf{r^d},\mathbf{z},\mathbf{s},\mathbf{p^g},\mathbf{q^g},\mathbf{p^w},\mathbf{c}} f^g(\cdot) + f^w(\cdot) + f^s(\cdot) \tag{5.16}$$

subject to

$$(5.1) - (5.15), \tag{5.17}$$

where

$$f^g(\cdot) := \sum_{t\in\mathcal{T}} \sum_{i\in\mathcal{G}} C_i^{g,2} \left(p_{i,t}^g\right)^2 + C_i^{g,1} p_{i,t}^g \tag{5.18}$$

is a strictly convex cost function of real power generation,

$$f^w(\cdot) := \sum_{t\in\mathcal{T}} \sum_{i\in\mathcal{W}} C_i^{w,1} p_{i,t}^w \tag{5.19}$$

is a linear cost function of wind power production, and

$$f^s(\cdot) := \sum_{t\in\mathcal{T}} \sum_{n\in\mathcal{N}} C_n^{s,1} r_{n,t}^d \tag{5.20}$$

is a linear cost function of the storage discharge, which represents variable operation and maintenance (O&M) costs.

Instead of incorporating a marginal cost for charging dynamics, the storage operator implicitly pays the LMP when charging. This LMP is the sign indefinite Lagrange multiplier $\lambda_{n,t}$ corresponding to the real power balance in (5.12) and accounts for the marginal unit cost, congestion cost, and cost due to real power losses for each location $n \in \mathcal{N}$ and time period $t \in \mathcal{T}$. The value of the LMP indicates the rate at which the optimal value of the objective function changes when increasing or decreasing the corresponding constraint bound.[64]

Remark 5.2. *Alternatively, a capital cost for storage could be assumed, which would be levelized appropriately given the time horizon of the dispatch, e.g., see [166]. As a result the total capital and operating cost could be minimized.*

5.4 Solution Technique

The ACOPF+S in (5.16) and (5.17) is solved by first applying a SDR in order to obtain the SDR-OPF+S which is a convex problem. In this section, the SDR-OPF+S and its corresponding Lagrangian dual are formulated in the manner proposed in [24, 25]. The convex relaxation can then be solved as a SDP. For the opti-

[64] assuming no degeneracy

mal solution to the SDR-OPF+S, Slater's condition[65] is satisfied and strong duality holds [25]. Therefore the optimal solution of the Lagrangian dual of the SDR-OPF+S is always equivalent to the optimal solution of the SDR-OPF+S problem at the KKT point. When the rank one condition holds, then the SDR-OPF+S, the SDR-OPF+S dual, and the ACOPF+S are all equivalent. Therefore the SDR formulation can be exploited to derive properties that hold for a global optimum of the ACOPF+S.

5.4.1 Semidefinite Relaxation

The ACOPF+S formulation in (5.16) and (5.17) is solved by first applying a SDR to obtain a convex problem. In particular, the proposed approach defines $W_t \coloneqq \omega_t \omega_t^T \in \mathbb{R}^{2|\mathcal{N}|\times 2|\mathcal{N}|}$ for all $t \in \mathcal{T}$ where $\omega_t = \left[v_{1,t}^r, ..., v_{N,t}^r, v_{1,t}^j, ..., v_{N,t}^j\right]^T$.

[65] If the optimization problem is convex, i.e., of the form

$$\begin{aligned} &\min f_0(x) \\ &s.t. \quad f_i(x) \leq 0, i = 1, ..., m \\ &\qquad Ax = b, \end{aligned}$$

with variable $x \in \mathbb{R}^n$ and $f_0, ..., f_m$ convex, then under certain constraint qualifications (such as Slater's condition) beyond convexity, strong duality holds. Slater's condition states that there exists a $x \in$ **relint** $\mathcal{D}$, i.e., $\mathcal{D}$ has a nonempty interior, such that

$$\begin{aligned} &f_i(x) < 0, i = 1, ..., m, \\ &Ax = b. \end{aligned}$$

For this problem, **relint** $\mathcal{D} = \mathbb{R}^n$ and such a point $x \in$ **relint** $\mathcal{D}$ is called strictly feasible, since the inequality constraints hold with strict inequalities. The above condition can be weakened if some of the inequality constraint functions f_i are affine. Given the first k constraint functions are affine, strong duality holds if there exists a $x \in$ **relint** $\mathcal{D}$ with

$$\begin{aligned} &f_i(x) \leq 0, i = 1, ..., k, \\ &f_i(x) < 0, i = k+1, ..., m, \\ &Ax = b. \end{aligned}$$

Therefore, affine inequalities do not need to hold with strict inequality. Slater's condition in short states that if the optimization problem is strictly feasible (and convex), then strong duality holds [78].

Here the semidefinite convex relaxation for the ACOPF+S is formulated as the following primal optimization problem. Define $\overline{Y}_n := e_n e_n^T Y$ for each bus $n \in \mathcal{N}$ and $\overline{Y}^{\ell}_{k(n,m)} := |\tau_{kn}|^2 (y_k + y^s_{kn}) e_n e_n^T - \tau^*_{kn}\tau_{km}(y_k) e_n e_m^T$ for each line flow $k(\cdot) \in \mathcal{F}$, given the standard basis vector $e_n \in \mathbb{R}^N$, and the coefficient matrix $M_n := e_n e_n^T \bigoplus e_n e_n^T$.

Then $\Phi_n := h\left(\overline{Y}_n\right)$ is defined for $h : \mathbb{C}^{|\mathcal{N}|\times|\mathcal{N}|} \to \mathbb{R}^{2|\mathcal{N}|\times 2|\mathcal{N}|}$ and $\Phi^{\ell}_{k(\cdot)} := h\left(\overline{Y}^{\ell}_{k(\cdot)}\right)$ is defined for $h : \mathbb{C}^{|\mathcal{K}|\times|\mathcal{N}|} \to \mathbb{R}^{2|\mathcal{N}|\times 2|\mathcal{N}|}$ where

$$h(\Omega) := \frac{1}{2}\begin{bmatrix} \mathrm{Re}\left\{\Omega + \Omega^T\right\} & \mathrm{Im}\left\{\Omega - \Omega^T\right\} \\ \mathrm{Im}\left\{\Omega - \Omega^T\right\} & \mathrm{Re}\left\{\Omega + \Omega^T\right\} \end{bmatrix}$$

and $\mathrm{Re}\{\cdot\}$ and $\mathrm{Im}\{\cdot\}$ denote the real and imaginary parts, respectively. Similarly this study defines $\Psi_n := \tilde{h}\left(\overline{Y}_n\right)$ for $\tilde{h} : \mathbb{C}^{|\mathcal{N}|\times|\mathcal{N}|} \to \mathbb{R}^{2|\mathcal{N}|\times 2|\mathcal{N}|}$ and $\Psi^{\ell}_{k(\cdot)} := \tilde{h}\left(\overline{Y}^{\ell}_{k(\cdot)}\right)$ for $\tilde{h} : \mathbb{C}^{|\mathcal{K}|\times|\mathcal{N}|} \to \mathbb{R}^{2|\mathcal{N}|\times 2|\mathcal{N}|}$ where

$$\tilde{h}(\Omega) := -\frac{1}{2}\begin{bmatrix} \mathrm{Im}\left\{\Omega + \Omega^T\right\} & \mathrm{Re}\left\{\Omega^T - \Omega\right\} \\ \mathrm{Re}\left\{\Omega^T - \Omega\right\} & \mathrm{Im}\left\{\Omega + \Omega^T\right\} \end{bmatrix}.$$

The real and reactive power injections for each bus $n \in \mathcal{N}$ can be expressed as $\mathrm{tr}\{\Phi_n W_t\}$ and $\mathrm{tr}\{\Psi_n W_t\}$ where $\mathrm{tr}\{\cdot\}$ is the trace operator;[66] similarly, the real and reactive power flows $k(\cdot) \in \mathcal{F}$ can be expressed as $\mathrm{tr}\left\{\Phi^{\ell}_{k(\cdot)} W_t\right\}$ and $\mathrm{tr}\left\{\Psi^{\ell}_{k(\cdot)} W_t\right\}$, respectively.

[66] The trace of a square $n \times n$ matrix X, denoted by $\mathrm{tr}X$, is the sum of its diagonal elements, i.e., $\mathrm{tr}X = \sum_{i=1}^{n} X_{ii}$ [167].

The SDR-OPF+S is formulated as follows:

$$\mathbf{p}^* \coloneqq \min_{\mathbf{W},\boldsymbol{\alpha}^{\boldsymbol{g}},\boldsymbol{\alpha}^{\boldsymbol{w}},\boldsymbol{\alpha}^{\boldsymbol{s}},\mathbf{r}^{\mathbf{c}},\mathbf{r}^{\mathbf{d}},\mathbf{z},\mathbf{s},\mathbf{p}^{\mathbf{g}},\mathbf{q}^{\mathbf{g}},\mathbf{p}^{\mathbf{w}},\mathbf{c}} \sum_{t\in\mathcal{T}} \left(\sum_{i\in\mathcal{G}} \alpha_{i,t}^{g} + \sum_{i\in\mathcal{W}} C_i^{w,1} p_{i,t}^{w} + \sum_{n\in\mathcal{N}} C_n^{s,1} r_{n,t}^{d} \right) \quad (5.21)$$

subject to

$$\operatorname{tr}\{\Phi_n W_t\} = r_{n,t}^{d} - r_{n,t}^{c} + \sum_{i\in\mathcal{I}(n)} \left(p_{i,t}^{g} + p_{i,t}^{w}\right) - P_{n,t}^{d} \qquad \forall n\in\mathcal{N}, t\in\mathcal{T} \quad (5.22a)$$

$$\operatorname{tr}\{\Psi_n W_t\} = z_{n,t} + \sum_{i\in\mathcal{I}(n)} \left(q_{i,t}^{g} + q_{i,t}^{w}\right) - Q_{n,t}^{d} \qquad \forall n\in\mathcal{N}, t\in\mathcal{T} \quad (5.22b)$$

$$\underline{P}_i \le p_{i,t}^{g} \le \overline{P}_i \qquad \forall i\in\mathcal{G}, t\in\mathcal{T} \quad (5.22c)$$

$$-RR_i^{d} \le p_{i,t}^{g} - p_{i,t-1}^{g} \le RR_i^{u} \qquad \forall i\in\mathcal{G}, t\in\mathcal{T} \quad (5.22d)$$

$$\underline{Q}_i \le q_{i,t}^{g} \le \overline{Q}_i \qquad \forall i\in\mathcal{G}, t\in\mathcal{T} \quad (5.22e)$$

$$0 \le p_{i,t}^{w} \le C_{i,t}^{w} \qquad \forall i\in\mathcal{W}, t\in\mathcal{T} \quad (5.22f)$$

$$s_{n,t} = s_{n,t-1} + \eta_n^{c} r_{n,t}^{c} - \left(\eta_n^{d}\right)^{-1} r_{n,t}^{d} \qquad \forall n\in\mathcal{N}, t\in\mathcal{T} \quad (5.22g)$$

$$\tilde{s}_{n,T} - s_{n,T} = 0 \qquad \forall n\in\mathcal{N}, t\in\mathcal{T} \quad (5.22h)$$

$$0 \le r_{n,t}^{c} \le R_n^{c} \qquad \forall n\in\mathcal{N}, t\in\mathcal{T} \quad (5.22i)$$

$$0 \le r_{n,t}^{d} \le R_n^{d} \qquad \forall n\in\mathcal{N}, t\in\mathcal{T} \quad (5.22j)$$

$$\underline{C}_n \le s_{n,t} \le c_n \qquad \forall n\in\mathcal{N}, t\in\mathcal{T} \quad (5.22k)$$

$$\sum_{n\in\mathcal{N}} c_n \le h \qquad \forall n\in\mathcal{N}, t\in\mathcal{T} \quad (5.22l)$$

$$\underline{Z}_n \le z_{n,t} \le \overline{Z}_n \qquad \forall n\in\mathcal{N}, t\in\mathcal{T} \quad (5.22m)$$

$$\left(\underline{V}_n\right)^2 \leq \operatorname{tr}\left\{M_n W_t\right\} \leq \left(\overline{V}_n\right)^2 \qquad \forall n \in \mathcal{N}, t \in \mathcal{T} \qquad (5.22n)$$

$$\begin{bmatrix} C_i^{g,1} p_{i,t}^g - \alpha_{i,t}^g & \sqrt{C_i^{g,2}} p_{i,t}^g \\ \sqrt{C_i^{g,2}} p_{i,t}^g & -1 \end{bmatrix} \preceq 0 \qquad \forall i \in \mathcal{G}, t \in \mathcal{T} \qquad (5.22o)$$

$$\begin{bmatrix} -\left(\overline{S}_k\right)^2 & \operatorname{tr}\left\{\Phi_{k(\cdot)}^{\ell} W_t\right\} & \operatorname{tr}\left\{\Psi_{k(\cdot)}^{\ell} W_t\right\} \\ \operatorname{tr}\left\{\Phi_{k(\cdot)}^{\ell} W_t\right\} & -1 & 0 \\ \operatorname{tr}\left\{\Psi_{k(\cdot)}^{\ell} W_t\right\} & 0 & -1 \end{bmatrix} \preceq 0 \quad \forall k(\cdot) \in \mathcal{F}, t \in \mathcal{T} \qquad (5.22p)$$

$$W_t \succeq 0 \qquad \forall t \in \mathcal{T}, \qquad (5.22q)$$

where the nonconvex rank one constraint (i.e., $\operatorname{rank}(W_t) = 1, \forall t \in \mathcal{T}$) is omitted. Note that the above relaxation has a linear cost (5.21), linear equality and inequality constraints in equations (5.22a) – (5.22n), and linear matrix inequality[67] (LMI) constraints in (5.22o) – (5.22q) where the LMIs are obtained from the Schur complements[68] of (5.22o) and (5.22p). The matrices in (5.22o) and (5.22p) are negative

[67] A linear matrix inequality has the form

$$F(x) \coloneqq F_0 + \sum_{i=1}^{m} x_i F_i \succ 0,$$

where $x \in \mathbb{R}^m$ is the variable and the symmetric matrices $F_i = F_i^T \in \mathbb{R}^{n \times n}, i = 0, ..., m$ are given. The inequality symbol "$\succ$" means that $F(x)$ is positive definite (i.e., $u^T F(x) u > 0$ for all nonzero $u \in \mathbb{R}^n$). Furthermore, a *nonstrict* LMI has the form $F(x) \succeq 0$ (i.e., $u^T F(x) u \geq 0$ for all nonzero $u \in \mathbb{R}^n$) [168].

[68] Let X be a symmetric matrix partitioned into blocks

$$X = \begin{bmatrix} A & B \\ B^T & C \end{bmatrix},$$

where both A, C are symmetric and square. Assume that C is positive definite. Then the following properties are equivalent:

1. X is positive semidefinite (PSD).

semidefinite[69] (NSD) whereas the matrix in (5.22q) is positive semidefinite[70] (PSD). Furthermore, note that a limit on the apparent power rating for an ESS unit of the form

$$(r_{n,t})^2 + (z_{n,t})^2 \leq (\overline{S}_{n,t})^2,$$

is equivalently modeled as the following LMI:

$$\begin{bmatrix} -\left(\overline{S}_{n,t}\right)^2 & r_{n,t} & z_{n,t} \\ r_{n,t} & -1 & 0 \\ z_{n,t} & 0 & -1 \end{bmatrix} \preceq 0, \tag{5.23}$$

for all $n \in \mathcal{N}, t \in \mathcal{T}$, where $r_{n,t} \coloneqq r^c_{n,t} - r^d_{n,t}$ and $\overline{S}_{n,t}$.

Note that the SDR-OPF+S is equivalent to the ACOPF+S in (5.16) and (5.17) when the rank of W_t equals one for all $t \in \mathcal{T}$, i.e., the rank one solution is equivalent to a global optimum of the ACOPF+S problem. There is ongoing work describing conditions under which this rank condition is guaranteed to be satisfied, e.g., [79,169, 170]. It is verified that the rank one condition is satisfied for the examples presented in this work.

2. The Schur complement of C in X, defined as the matrix $A - BC^{-1}B^T$ (which is equivalent to $AC - B^TB$), is PSD [167].

[69]The inequality symbol denotes a componentwise 'less than or equal to' inequality and the notation $X \preceq 0$ for $X \in \mathbb{R}^{n\times n}$ means that X is a negative semidefinite (i.e., $u^TXu \leq 0$ for all nonzero $u \in \mathbb{R}^n$) [78,167].

[70]The inequality symbol denotes a componentwise 'greater than or equal to' inequality and the notation $X \succeq 0$ for $X \in \mathbb{R}^{n\times n}$ means that X is positive semidefinite (i.e., $u^TXu \geq 0$ for all nonzero $u \in \mathbb{R}^n$) [78,167].

5.4.2 Lagrangian Dual Function

The Lagrangian dual function $\Lambda(\cdot)$ for the SDR-OPF+S is

$$
\begin{aligned}
\Lambda(\cdot) = & \sum_{t\in\mathcal{T}}\Big[\sum_{i\in\mathcal{G}}\Big(C_{i,t}^{g,1}p_{i,t}^{g}+2\sqrt{C_{i}^{g,2}}p_{i,t}^{g}\left[\mu_{i,t}^{g}\right]_{1}-\left[\mu_{i,t}^{g}\right]_{2}\Big)+\sum_{i\in\mathcal{W}}\Big(C_{i,t}^{w,1}p_{i,t}^{w}\Big)\\
& +\sum_{n\in\mathcal{N}}\Big(C_{n,t}^{s,1}r_{n,t}^{d}\Big)\Big]+\sum_{t\in\mathcal{T}}\sum_{n\in\mathcal{N}}\Big(\underline{\vartheta}_{n,t}\left[\left(\underline{V}_{n}\right)^{2}-\mathrm{tr}\left\{M_{n}W_{t}\right\}\right]+\overline{\vartheta}_{n,t}\left[\mathrm{tr}\left\{M_{n}W_{t}\right\}-\left(\overline{V}_{n}\right)^{2}\right]\\
& +\gamma_{n,t}\left[s_{n,t}-s_{n,t-1}-\eta_{n}^{c}r_{n,t}^{c}+\left(\eta_{n}^{d}\right)^{-1}r_{n,t}^{d}\right]-\underline{\rho}_{n,t}r_{n,t}^{c}+\overline{\rho}_{n,t}\left[r_{n,t}^{c}-R_{n}^{c}\right]-\underline{\sigma}_{n,t}r_{n,t}^{d}\\
& +\overline{\sigma}_{n,t}\left[r_{n,t}^{d}-R_{n}^{d}\right]+\underline{\beta}_{n,t}\left[\underline{C}_{n}-s_{n,t}\right]+\overline{\beta}_{n,t}\left[s_{n,t}-c_{n}\right]+\underline{\psi}_{n,t}\left[\underline{Z}_{n}-z_{n,t}\right]\\
& +\overline{\psi}_{n,t}\left[z_{n,t}-\overline{Z}_{n}\right]+\lambda_{n,t}\Big[\sum_{i\in\mathcal{I}(n)}\left(p_{i,t}^{g}+p_{i,t}^{w}\right)+r_{n,t}^{d}-r_{n,t}^{c}-\mathrm{tr}\left\{\Phi_{n}W_{t}\right\}-P_{n,t}^{d}\Big] \qquad (5.24)\\
& +\varphi_{n,t}\Big[\sum_{i\in\mathcal{I}(n)}\left(q_{i,t}^{g}+q_{i,t}^{w}\right)+z_{n,t}-\mathrm{tr}\left\{\Psi_{n}W_{t}\right\}-Q_{n,t}^{d}\Big]\Big)+\sum_{t\in\mathcal{T}}\sum_{i\in\mathcal{W}}\Big(\overline{\alpha}_{i,t}\left[p_{i,t}^{w}-C_{i,t}^{w}\right]-\underline{\alpha}_{i,t}p_{i,t}^{w}\Big)\\
& +\sum_{t\in\mathcal{T}}\sum_{i\in\mathcal{G}}\Big(\underline{\lambda}_{i,t}\left[\underline{P}_{i}-p_{i,t}^{g}\right]+\overline{\lambda}_{i,t}\left[p_{i,t}^{g}-\overline{P}_{i}\right]+\underline{\varphi}_{i,t}\left[\underline{Q}_{i}-q_{i,t}^{g}\right]+\overline{\varphi}_{i,t}\left[q_{i,t}^{g}-\overline{Q}_{i}\right]\Big)\\
& +\sum_{t\in\mathcal{T}\cap\{t>1\}}\sum_{i\in\mathcal{G}}\Big(\underline{\delta}_{i,t}\left[-RR_{i}^{d}-p_{i,t}^{g}+p_{i,t-1}^{g}\right]+\overline{\delta}_{i,t}\left[p_{i,t}^{g}-p_{i,t-1}^{g}-RR_{i}^{u}\right]\Big)\\
& +\sum_{t\in\mathcal{T}}\sum_{k(\cdot)\in\mathcal{F}}\Big(2\left[\overline{\kappa}_{k(\cdot),t}\right]_{2}\mathrm{tr}\left\{\Phi_{k(\cdot)}^{\ell}W_{t}\right\}+2\left[\overline{\kappa}_{k(\cdot),t}\right]_{3}\mathrm{tr}\left\{\Psi_{k(\cdot)}^{\ell}W_{t}\right\}\\
& -\left[\overline{\kappa}_{k(\cdot),t}\right]_{1}\overline{S}_{k}^{2}-\left[\overline{\kappa}_{k(\cdot),t}\right]_{4}-\left[\overline{\kappa}_{k(\cdot),t}\right]_{6}\Big)+\phi\left[\sum_{n\in\mathcal{N}}c_{n}-h\right]+\sum_{n\in\mathcal{N}}\varkappa_{n}\left[s_{n,T}-\tilde{s}_{n,T}\right],
\end{aligned}
$$

where $\mathrm{tr}\{\cdot\}$ is the trace operator and the matrices

$$\mu_{i,t}^{g} \coloneqq \begin{bmatrix} 1 & \left[\mu_{i,t}^{g}\right]_1 \\ \left[\mu_{i,t}^{g}\right]_1 & \left[\mu_{i,t}^{g}\right]_2 \end{bmatrix} \succeq 0, \qquad i \in \mathcal{G}, t \in \mathcal{T}, \tag{5.25a}$$

$$\overline{\kappa}_{k(\cdot),t} \coloneqq \begin{bmatrix} \left[\overline{\kappa}_{k(\cdot),t}\right]_1 & \left[\overline{\kappa}_{k(\cdot),t}\right]_2 & \left[\overline{\kappa}_{k(\cdot),t}\right]_3 \\ \left[\overline{\kappa}_{k(\cdot),t}\right]_2 & \left[\overline{\kappa}_{k(\cdot),t}\right]_4 & \left[\overline{\kappa}_{k(\cdot),t}\right]_5 \\ \left[\overline{\kappa}_{k(\cdot),t}\right]_3 & \left[\overline{\kappa}_{k(\cdot),t}\right]_5 & \left[\overline{\kappa}_{k(\cdot),t}\right]_6 \end{bmatrix} \succeq 0, \qquad k(\cdot) \in \mathcal{F}, t \in \mathcal{T}, \tag{5.25b}$$

are the Lagrange multiplier associated with the LMIs in (5.22o) and (5.22p), respectively. The Lagrange multipliers $\gamma_{n,t}, \lambda_{n,t}, \varphi_{n,t}$ and $\varkappa_n$ are sign indefinite, and the remaining Lagrange multipliers $\underline{\vartheta}_{n,t}, \overline{\vartheta}_{n,t}, \underline{\rho}_{n,t}, \overline{\rho}_{n,t}, \underline{\sigma}_{n,t}, \overline{\sigma}_{n,t}, \underline{\beta}_{n,t}, \overline{\beta}_{n,t}, \underline{\psi}_{n,t}, \overline{\psi}_{n,t}, \underline{\alpha}_{i,t}, \overline{\alpha}_{i,t}$, $\underline{\lambda}_{i,t}, \overline{\lambda}_{i,t}, \underline{\varphi}_{i,t}, \overline{\varphi}_{i,t}, \underline{\delta}_{i,t}, \overline{\delta}_{i,t}$ and ϕ are nonnegative.

The corresponding Lagrange dual problem to the SDR-OPF+S is

$$\mathbf{d}^{*} \coloneqq \max_{\overline{\boldsymbol{\Omega}}} \min_{\underline{\boldsymbol{\Omega}}} \Lambda(\cdot), \tag{5.26}$$

which is referred to as the SDR-OPF+S dual for the dual variable set $\boldsymbol{\mu}^{\boldsymbol{g}}$, $\overline{\boldsymbol{\kappa}}$, $\boldsymbol{\gamma}$, $\boldsymbol{\lambda}$, $\boldsymbol{\varphi}$, $\boldsymbol{\varkappa}$, $\underline{\boldsymbol{\vartheta}}$, $\overline{\boldsymbol{\vartheta}}$, $\underline{\boldsymbol{\rho}}$, $\overline{\boldsymbol{\rho}}$, $\underline{\boldsymbol{\sigma}}$, $\overline{\boldsymbol{\sigma}}$, $\underline{\boldsymbol{\beta}}$, $\overline{\boldsymbol{\beta}}$, $\underline{\boldsymbol{\psi}}$, $\overline{\boldsymbol{\psi}}$, $\underline{\boldsymbol{\alpha}}$, $\overline{\boldsymbol{\alpha}}$, $\underline{\boldsymbol{\lambda}}$, $\overline{\boldsymbol{\lambda}}$, $\underline{\boldsymbol{\varphi}}$, $\overline{\boldsymbol{\varphi}}$, $\underline{\boldsymbol{\delta}}$, $\overline{\boldsymbol{\delta}}$, $\boldsymbol{\phi} \in \overline{\boldsymbol{\Omega}}$ and the primal variable set $\mathbf{W}$, $\boldsymbol{\alpha}^{\boldsymbol{g}}$, $\boldsymbol{\alpha}^{\boldsymbol{w}}$, $\boldsymbol{\alpha}^{\boldsymbol{s}}$, $\mathbf{r}^{\mathbf{c}}$, $\mathbf{r}^{\mathbf{d}}$, $\mathbf{z}$, $\mathbf{s}$, $\mathbf{p}^{\mathbf{g}}$, $\mathbf{q}^{\mathbf{g}}$, $\mathbf{p}^{\mathbf{w}}$, $\mathbf{c} \in \underline{\boldsymbol{\Omega}}$.

5.4.3 Strong Duality

The SDR approach results in a convex reformulation of the ACOPF+S. Therefore, both the SDR-OPF+S and its dual are convex problems that represent the same optimization problem; whereas the SDR-OPF+S is a cost minimization problem, its dual is a resource maximization problem. At the optimum of either the SDR-OPF+S or its dual, the equality

$$\mathbf{d}^* = \mathbf{p}^* \tag{5.27}$$

holds, i.e., the optimal duality gap is zero. In conclusion, the marginal values (i.e., dual variables) support the hyperplane (i.e., primal variables) of the SDR-OPF+S optimal solution; furthermore, when the relaxation is exact then a global optimum to the ACOPF+S has been recovered and strong duality holds.

5.5 Unimodal Storage Dynamics

The properties of the Lagrangian dual of the SDR-OPF+S problem are used to provide the first theoretical result, which proves a sufficient condition for unimodal storage dynamics. Unimodal storage dynamics is defined as the ESS in one of three modes:

1. Charging,

2. Discharging, or

3. Neither charging nor discharging.

In current market design, ESS technologies that can simultaneously charge and discharge (or cycle instantaneously within the given time period) would be paid to dissipate excess energy when LMPs are negative. Negative LMPs can occur in the real-time markets due to an over-supply on the network,[71] binding line limits, or more typically because of negative bid-in costs [171].

However the ability to simultaneously charge and discharge (i.e., multimodal operations) is largely dependent on the ESS configuration and storage technology; for example, a single battery unit is not capable of multimodal operations but certain configurations (e.g., pumped hydro systems with a separate pump and compressor) or storage technologies (e.g., vanadium redox and redox flow batteries) would be able to provide this service. Furthermore, multimodal operations is not as valuable as unimodal operations to the system operator nor the storage operator when LMPs are positive; in fact, such multimodal behavior is optimal for storage with roundtrip inefficiencies when LMPs are negative. A negative LMP suggests that an ESS unit would be paid to charge and then pay to discharge, where the payment to discharge is less due to the dissipated energy from the storage unit's roundtrip inefficiencies, as the following example demonstrates.

[71] This is for an equality constraint on the real power balancing, which is different than enforcing the ability to over-satisfy via an inequality on the real power balancing, as is discussed in further detail later in this section.

	Unimodal Operations			
Time-Period (h)	t = 1	t = 2	t = 3	Total Profit ($)
Storage Level (MWh)	1	1.5	0	
Charge (MW withdrawal)	$-1.\overline{11}$	$-0.\overline{55}$	0	
Discharge (MW injection)	0	0	1.35	
Positive LMP Scenario				
LMP ($/MWh)	$\lambda > 0$	$\lambda > 0$	$2\lambda > 0$	
Profit ($)	$-1.\overline{11}\lambda$	$-0.\overline{55}\lambda$	2.70λ	$= 1.04\lambda$
Negative LMP Scenario				
LMP ($/MWh)	$\lambda > 0$	$\lambda < 0$	$2\lambda > 0$	
Profit ($)	$-1.\overline{11}\lambda$	$0.\overline{55}\lambda$	2.70λ	$= 2.14\lambda$
	Multimodal Operations			
Time-Period (h)	t = 1	t = 2	t = 3	Total Profit ($)
Storage Level (MWh)	1	1.5	0	
Charge (MW withdrawal)	$-1.\overline{11}$	$-1.\overline{66}$	0	
Discharge (MW injection)	0	0.9	1.35	
Positive LMP Scenario				
LMP ($/MWh)	$\lambda > 0$	$\lambda > 0$	$2\lambda > 0$	
Profit ($)	$-1.\overline{11}\lambda$	$-0.7\overline{6}\lambda$	2.70λ	$= 0.83\lambda$
Negative LMP Scenario				
LMP ($/MWh)	$\lambda > 0$	$\lambda < 0$	$2\lambda > 0$	
Profit ($)	$-1.\overline{11}\lambda$	$0.7\overline{6}\lambda$	2.70λ	$= 2.35\lambda$

Table 5.2: The storage level, charging, and discharging operations along with the accrued marginal profits during unimodal operations and multimodal operations when negative or positive LMPs are present.

Example 5.1. *Assume an operating horizon of* $\mathcal{T} = \{1, 2, 3\}$ *with off-peak periods 1 and 2 denoted by a lower LMP (i.e.,* λ*) and peak period 3 denoted by a higher LMP (i.e.,* 2λ*). Consider an ESS unit with 1.5MWh capacity, roundtrip efficiency of* 81% *(i.e.,* $\eta^c = \eta^d = 0.9$*), and no discharge costs where the storage level is specified to be*

1 MWh in period 1 (i.e., partially charged), 1.5 MWh in period 2 (i.e., completely charged), and 0 MWh in period 3 (i.e., completely discharged). Table 5.2 reports the results for unimodal and multimodal operations when positive or negative LMPs are present. Unimodal behavior is more profitable than multimodal behavior when positive LMPs occur since the storage operator must pay to charge and is paid to discharge; however, multimodal behavior is more profitable to the storage operator than unimodal behavior when negative LMPs occur.

The linear storage dynamics in (5.1) and constraints in (5.2) − (5.7) do not explicitly prevent multimodal operations of the storage unit at bus $n \in \mathcal{N}$ in time interval $t \in \mathcal{T}$. In particular, there is no constraint preventing both $r^c_{n,t}$ and $r^d_{n,t}$ from being positive for the same n and t. In a number of formulations, this behavior is prevented through the use of a mixed integer or nonlinear approach, e.g., see [157–159]. Other studies assume a perfect roundtrip efficiency (i.e., $\eta^c_n = \eta^d_n = 1$) where multimodal operations result in a zero net injection to the network, i.e. no effect [25,154,172,173]. Yet a number of OPF-based storage integration studies allow unimodal storage dynamics but do not address whether or not this is a desirable behavior [151, 152, 166, 174].

The following theorem provides a condition that ensures $r^c_{n,t} r^d_{n,t} = 0$ for the storage model in (5.1) − (5.7), i.e., satisfying this condition obviates the need for integer variables or nonlinear constraints in ensuring unimodal storage dynamics at each bus. Therefore the following theorem addresses a shortcoming in the current storage

modeling literature.

Theorem 5.1. *Consider an ESS unit at bus $n \in \mathcal{N}$ with capacity $c_n > 0$ and positive cost coefficient $C_n^{s,1} > 0$ at the KKT point of the SDR-OPF+S. If the Lagrangian multiplier $\lambda_{n,t}$ associated with the real power balance* (5.12) *at bus $n \in \mathcal{N}$ is nonnegative, i.e., $\lambda_{n,t} \geq 0$ for all time intervals $t \in \mathcal{T}$, then $r_{n,t}^c r_{n,t}^d = 0$ for all $t \in \mathcal{T}$.*

Proof. At the KKT point for the SDR-OPF+S dual in (5.27), the storage variables c_n, $s_{n,t}$, $r_{n,t}^c$, $r_{n,t}^d$ and $z_{n,t}$ provide a feasible solution for every bus $n \in \mathcal{N}$. By construction, a rank one solution to the SDR-OPF+S problem satisfies the constraints $(5.1) - (5.7)$ and (5.12), as well as the associated complementary slackness conditions:

$$\gamma_{n,t}\left[s_{n,t} - s_{n,t-1} - \eta_n^c r_{n,t}^c + \left(\eta_n^d\right)^{-1} r_{n,t}^d\right] = 0, \tag{5.28}$$

$$\underline{\rho}_{n,t} r_{n,t}^c = 0, \tag{5.29}$$

$$\overline{\rho}_{n,t}\left[r_{n,t}^c - R_n^c\right] = 0, \tag{5.30}$$

$$\underline{\sigma}_{n,t} r_{n,t}^d = 0, \tag{5.31}$$

$$\overline{\sigma}_n\left[r_{n,t}^d - R_n^d\right] = 0, \tag{5.32}$$

$$\underline{\beta}_{n,t}\left[\underline{C}_n - s_{n,t}\right] = 0, \tag{5.33}$$

$$\overline{\beta}_{n,t}\left[s_{n,t} - c_n\right] = 0, \tag{5.34}$$

$$\varkappa_n\left[\tilde{s}_{n,T} - s_{n,T}\right] = 0, \tag{5.35}$$

$$\lambda_{n,t}\Big[\sum_{i \in \mathcal{I}(n)}\left(p_{i,t}^g + p_{i,t}^w\right) + r_{n,t}^d - r_{n,t}^c - p_{n,t} - P_{n,t}^d\Big] = 0, \tag{5.36}$$

$$\varphi_{n,t}\Big[\sum_{i\in\mathcal{I}(n)}\left(q^{g}_{i,t}+q^{w}_{i,t}\right)+z_{n,t}-q_{n,t}-Q^{d}_{n,t}\Big]=0, \tag{5.37}$$

$$\phi\left[\sum_{n\in\mathcal{N}}c_n-h\right]=0, \tag{5.38}$$

for all $t\in\mathcal{T}$ in (5.28) – (5.37), where $p_{n,t}$ and $q_{n,t}$ are determined by the affine functions

$$p_{n,t}=\operatorname{tr}\left\{\Phi_n W_t\right\}, \tag{5.39}$$

and

$$q_{n,t}=\operatorname{tr}\left\{\Psi_n W_t\right\} \tag{5.40}$$

respectively, of the SDR-OPF+S. Additionally, a rank one solution to the SDR-OPF+S problem satisfies the zero gradient conditions as follows:

$$\partial\Lambda\left(\cdot\right)/\partial c_n \coloneqq \phi-\overline{\beta}_{n,t}=0, \tag{5.41}$$

$$\partial\Lambda\left(\cdot\right)/\partial s_{n,t} \coloneqq \gamma_{n,t}-\gamma_{n,t-1}+\overline{\beta}_{n,t}-\underline{\beta}_{n,t}+\langle\varkappa_n|t=T\rangle=0, \tag{5.42}$$

$$\partial\Lambda\left(\cdot\right)/\partial r^{c}_{n,t} \coloneqq \overline{\rho}_{n,t}-\underline{\rho}_{n,t}-\lambda_{n,t}-\eta^{c}_{n}\gamma_{n,t}=0, \tag{5.43}$$

$$\partial\Lambda\left(\cdot\right)/\partial r^{d}_{n,t} \coloneqq \overline{\sigma}_{n,t}-\underline{\sigma}_{n,t}+\lambda_{n,t}+\left(\eta^{d}_{n}\right)^{-1}\gamma_{n,t}+C^{s,1}_{n}=0, \tag{5.44}$$

$$\partial\Lambda\left(\cdot\right)/\partial z_{n,t} \coloneqq \overline{\psi}_{n,t}-\underline{\psi}_{n,t}+\varphi_{n,t}=0, \tag{5.45}$$

for all $t \in \mathcal{T}$. The dual variables $\phi, \lambda_{n,t}, \varkappa_n$, and $\gamma_{n,t}$ are sign indefinite. Also by dual feasibility $\underline{\beta}_{n,t}, \overline{\beta}_{n,t}, \underline{\rho}_{n,t}, \overline{\rho}_{n,t}, \underline{\sigma}_{n,t}$, and $\overline{\sigma}_{n,t}$ are nonnegative.

From the zero gradient conditions, when $\lambda_{n,t} \geq 0$ the ESS dynamics at bus n are given by

$$-C_n^{s,1} + \underline{\rho}_{n,t} - \overline{\rho}_{n,t} + \underline{\sigma}_{n,t} - \overline{\sigma}_{n,t} + \left(\left[\eta_n^c \eta_n^d - 1 \right] \Big/ \eta_n^d \right) \gamma_{n,t} \geq 0, \tag{5.46}$$

where $C_n^{s,1}$ is a positive coefficient. Finally note that for any storage technology with efficiencies $\eta_n^c, \eta_n^d \in (0, 1]$, then $\left(\left[\eta_n^c \eta_n^d - 1 \right] \Big/ \eta_n^d \right) \leq 0$. Regardless of the values for $\underline{\rho}_{n,t}, \overline{\rho}_{n,t}, \underline{\sigma}_{n,t}$, and $\overline{\sigma}_{n,t}$,

$$-C_n^{s,1} + \left(\left[\eta_n^c \eta_n^d - 1 \right] \Big/ \eta_n^d \right) \gamma_{n,t} \leq 0 \tag{5.47}$$

when $\gamma_{n,t} \leq 0$ or $C_n^{s,1} \geq \left(\left[\eta_n^c \eta_n^d - 1 \right] \Big/ \eta_n^d \right) \gamma_{n,t}$.

However the following properties for any value of $\gamma_{n,t}$ at the KKT point ensure that if $\lambda_{n,t} \geq 0$, then $\overline{\rho}_{n,t}$ and $\overline{\sigma}_{n,t}$ are never simultaneously positive, which implies that $r_{n,t}^c r_{n,t}^d = 0$ implicitly holds for every time interval $t \in \mathcal{T}$:

1. If $\gamma_{n,t} \leq \max \left\{ 0, \eta_n^d C_n^{s,1} \Big/ \left[\eta_n^c \eta_n^d - 1 \right] \right\}$ from the inequality in (5.47), then one of the following outcomes must hold by condition (5.46):

   (a) For $-C_n^{s,1} + \underline{\rho}_{n,t} + \left(\left[\eta_n^c \eta_n^d - 1 \right] \Big/ \eta_n^d \right) \gamma_{n,t} \geq 0$, the following conditions hold: $\underline{\rho}_{n,t} > 0$, $\overline{\rho}_{n,t} = 0$, $\underline{\sigma}_{n,t} = 0$, and $\overline{\sigma}_{n,t} = 0$. Therefore, $r_{n,t}^c = 0$ and

$0 < r^d_{n,t} < R^d_n$ (i.e., the storage is partially discharging).

(b) For $-C^{s,1}_n + \underline{\rho}_{n,t} - \overline{\sigma}_{n,t} + \left(\left[\eta^c_n \eta^d_n - 1 \right] \Big/ \eta^d_n \right) \gamma_{n,t} \geq 0$, the following conditions hold: $\underline{\rho}_{n,t} > 0$, $\overline{\rho}_{n,t} = 0$, $\underline{\sigma}_{n,t} = 0$, and $\overline{\sigma}_{n,t} > 0$. Therefore, $r^c_{n,t} = 0$ and $r^d_{n,t} = R^d_n$ (i.e., the storage is fully discharging).

(c) For $-C^{s,1}_n + \underline{\sigma}_{n,t} + \left(\left[\eta^c_n \eta^d_n - 1 \right] \Big/ \eta^d_n \right) \gamma_{n,t} \geq 0$, the following conditions hold: $\underline{\rho}_{n,t} = 0$, $\overline{\rho}_{n,t} = 0$, $\underline{\sigma}_{n,t} > 0$, and $\overline{\sigma}_{n,t} = 0$. Therefore $0 < r^c_{n,t} < R^C_n$ and $r^d_{n,t} = 0$ (i.e., the storage is partially charging).

(d) For $-C^{s,1}_n - \overline{\rho}_{n,t} + \underline{\sigma}_{n,t} + \left(\left[\eta^c_n \eta^d_n - 1 \right] \Big/ \eta^d_n \right) \gamma_{n,t} \geq 0$, the following conditions hold: $\underline{\rho}_{n,t} = 0$, $\overline{\rho}_{n,t} > 0$, $\underline{\sigma}_{n,t} > 0$, and $\overline{\sigma}_{n,t} = 0$. Therefore, $r^c_{n,t} = R^c_n$ and $r^d_{n,t} = 0$ (i.e., the storage is fully charging).

(e) For $-C^{s,1}_n + \underline{\rho}_{n,t} + \underline{\sigma}_{n,t} + \left(\left[\eta^c_n \eta^d_n - 1 \right] \Big/ \eta^d_n \right) \gamma_{n,t} \geq 0$, the following conditions hold: $\underline{\rho}_{n,t} > 0$, $\overline{\rho}_{n,t} = 0$, $\underline{\sigma}_{n,t} > 0$ and $\overline{\sigma}_{n,t} = 0$. Therefore $r^c_{n,t} = 0$ and $r^d_{n,t} = 0$ (i.e., the storage is idle).

Note that for $\gamma_{n,t} \leq \max \left\{ 0, \eta^d_n C^{s,1}_n \Big/ \left[\eta^c_n \eta^d_n - 1 \right] \right\}$ the following cases, which enable multimodal operations, violate condition (5.46) and are mathematically invalid outcomes:

(a) For $-C^{s,1}_n - \overline{\rho}_{n,t} - \overline{\sigma}_{n,t} + \left(\left[\eta^c_n \eta^d_n - 1 \right] \Big/ \eta^d_n \right) \gamma_{n,t} \geq 0$, the following conditions hold: $\underline{\rho}_{n,t} = 0$, $\overline{\rho}_{n,t} > 0$, $\underline{\sigma}_{n,t} = 0$, and $\overline{\sigma}_{n,t} > 0$. Therefore $r^c_{n,t} = R^c_n$ and $r^d_{n,t} = R^d_n$ (i.e., the storage is fully charging and fully discharging).

(b) For $-C^{s,1}_n + \left(\left[\eta^c_n \eta^d_n - 1 \right] \Big/ \eta^d_n \right) \gamma_{n,t} \geq 0$, the following conditions hold:

$\underline{\rho}_{n,t} = 0$, $\overline{\rho}_{n,t} = 0$, $\underline{\sigma}_{n,t} = 0$, and $\overline{\sigma}_{n,t} = 0$. Therefore $0 < r^c_{n,t} < R^c_n$ and $0 < r^d_{n,t} < R^d_n$ (i.e., the storage is partially charging and partially discharging).

2. If $\gamma_{n,t} > \max\left\{0, \eta^d_n C^{s,1}_n \Big/ \left[\eta^c_n \eta^d_n - 1\right]\right\}$, then $\gamma_{n,t} > 0$ and the following conditions hold from (5.43) and (5.44):

$$-\lambda_{n,t} + \overline{\rho}_{n,t} - \underline{\rho}_{n,t} > 0, \tag{5.48}$$

$$-\lambda_{n,t} - C^{s,1}_n + \overline{\sigma}_{n,t} - \underline{\sigma}_{n,t} > 0, \tag{5.49}$$

where

$$(\lambda_{n,t} \geq 0) \wedge \left(-\lambda_{n,t} + \overline{\rho}_{n,t} - \underline{\rho}_{n,t} > 0\right) \implies \overline{\rho}_{n,t} - \underline{\rho}_{n,t} > \lambda_{n,t} \geq 0$$

and

$$\begin{aligned} &\left(C^{s,1}_n > 0\right) \wedge (\lambda_{n,t} \geq 0) \wedge \left(-\lambda_{n,t} - C^{s,1}_n + \overline{\sigma}_{n,t} - \underline{\sigma}_{n,t} > 0\right) \\ &\implies \overline{\sigma}_{n,t} - \underline{\sigma}_{n,t} > \lambda_{n,t} + C^{s,1}_n > 0. \end{aligned}$$

As a result, if $\gamma_{n,t} > 0$, then $\underline{\rho}_{n,t} = 0$, $\underline{\sigma}_{n,t} > 0$, and $\overline{\sigma}_{n,t} = 0$. Therefore $r^d_{n,t} = 0$ (i.e., the storage is not discharging) implies that the storage is in unimodal operations (i.e., the storage is charging only) or idle.

□

Theorem 5.1 provides a sufficient condition for unimodal storage dynamics when $\lambda_{n,t} \geq 0$ given $C_n^{s,1} > 0$. The following Corollary is an equivalent sufficient condition which does not require $\lambda_{n,t} \geq 0$ a priori to solving, nor does it require that $C_n^{s,1} > 0$, even though the operational costs for storage are typically positive in practice. Instead the real power balance equality (5.22a) is relaxed to an inequality which enables an over-satisfaction of loads;[72] this technique is commonly employed to enforce desirable solution properties in OPF problems (see e.g., [24,175,176]) such as enforcing nonnegative LMPs, which is proven in the following corollary.

Corollary 5.2. *The nonnegative LMP condition, i.e.,* $\lambda_{n,t} \geq 0$*, holds for all* $n \in \mathcal{N}, t \in \mathcal{T}$ *if and only if there can be an over-satisfaction of load, i.e.,* $p_{n,t} + P_{n,t}^d + r_{n,t}^c \leq \sum_{i \in \mathcal{I}(n)} \left(p_{i,t}^g + p_{i,t}^w\right) + r_{n,t}^d$.

Proof. The proof ($\Longleftarrow$) The real power balance equality (5.22a) can be equivalently formulated as the following two inequalities

$$p_{n,t} + P_{n,t}^d + r_{n,t}^c \leq \sum_{i \in \mathcal{I}(n)} \left(p_{i,t}^g + p_{i,t}^w\right) + r_{n,t}^d, \quad \lambda_{n,t}^+, \tag{5.50a}$$

$$p_{n,t} + P_{n,t}^d + r_{n,t}^c \geq \sum_{i \in \mathcal{I}(n)} \left(p_{i,t}^g + p_{i,t}^w\right) + r_{n,t}^d, \quad \lambda_{n,t}^-, \tag{5.50b}$$

[72] Over-satisfaction is where the nodal generation is allowed to be equal to or greater than the nodal demand for a given bus.

for all $t \in \mathcal{T}$, $n \in \mathcal{N}$ where for the corresponding duals $\lambda^+_{n,t}, \lambda^-_{n,t} \geq 0$, the condition

$$\lambda_{n,t} \coloneqq \lambda^+_{n,t} - \lambda^-_{n,t} \geq 0 \tag{5.51}$$

holds. This implies that if $\lambda^+_{n,t} \geq \lambda^-_{n,t}$, then $p_{n,t} + P^d_{n,t} + r^c_{n,t} \leq \sum_{i \in \mathcal{I}(n)} \left(p^g_{i,t} + p^w_{i,t}\right) + r^d_{n,t}$.

($\Longrightarrow$) Assume the real power balance equality (5.22a) is replaced by

$$p_{n,t} + P^d_{n,t} + r^c_{n,t} \leq \sum_{i \in \mathcal{I}(n)} \left(p^g_{i,t} + p^w_{i,t}\right) + r^d_{n,t}, \tag{5.52}$$

and suppose $p_{n,t}$, $r^c_{n,t}$, $p^g_{i,t}$, $p^w_{i,t}$, and $r^d_{n,t}$ for all $t \in \mathcal{T}$, $n \in \mathcal{N}$ is a feasible solution to this modified SDR-OPF+S. By dual feasibility, the modified SDR-OPF+S dual gives a nontrivial lower bound (i.e., strong duality is obtained) on the modified SDR-OPF+S only when (5.52) is binding, which implies $\lambda_{n,t} \geq 0$. □

The intuition for these results on unimodal storage dynamics is that for a rank one solution to the SDR-OPF+S, the above condition holds at a global optimum of the ACOPF+S.

5.6 Storage Operator Subproblem

This section formulates a storage operator subproblem that is derived from the SDR-OPF+S and its corresponding dual. It is then shown that the marginal profit maximization of the storage operator subproblem corresponds to optimizing storage allo-

cation and dispatch in a global optimum to the ACOPF+S. In a perfectly competitive market as modeled in this study, the profit maximizing behavior of the storage operator is dual to the cost minimization of the system operator.

5.6.1 Subproblem Formulation

An ESS unit differs from a conventional generator in that its available capacity depends on the energy storage level, which is determined by charging and discharging operations in previous time intervals. Therefore its marginal cost is dynamic and includes the discharge cost plus a payment originating from the nodal price signal, i.e., the LMP, for that location and time period.

The dependence of the ESS units on the nodal prices can be exploited to form a storage subproblem that isolates the interactions among the storage variables and the dual variables for the real and reactive power balance constraints in (5.22a) and (5.22b), respectively $\lambda_{n,t}$ and $\varphi_{n,t}$. Analogous to referring to $\lambda_{n,t}$ as the LMP, the $\varphi_{n,t}$ is referred to as the Q-LMP for each $n \in \mathcal{N}, t \in \mathcal{T}$ as it mathematically accounts for the nodal price of VAr support.

The corresponding storage subproblem is given by

$$g^s\left(\boldsymbol{\lambda}, \boldsymbol{\varphi}\right) := \min_{\mathbf{r^c}, \mathbf{r^d}, \mathbf{z}, \mathbf{s}, \mathbf{c}} \Lambda^s\left(\cdot\right) \tag{5.53}$$

subject to

$$(5.1) - (5.5), \tag{5.54}$$

where

$$\Lambda^s(\cdot) = f^s(\cdot) + \sum_{t\in\mathcal{T}}\sum_{n\in\mathcal{N}}\Big\{\lambda_{n,t}\big[r^c_{n,t} - r^d_{n,t}\big] - \varphi_{n,t}z_{n,t}\Big\}.$$

The storage operator subproblem is optimal for a rank one solution to the SDR-OPF+S for either a single storage operator or multiple storage operator subproblems (e.g., a storage operator per technology or per bus) due to strong duality. The KKT conditions ensure that the optimal solution to the subproblem is also optimal to the SDR-OPF+S and a global optimum of the ACOPF+S when the SDR-OPF+S fulfills the rank one condition.

5.6.2 Profit Maximizing Storage Allocation

Now the storage subproblem is applied to connect the storage operator's marginal profit maximization to the optimal allocation and dispatch of ESS units.

Theorem 5.3. *For an arbitrary operating cycle $\mathcal{T} := \{1,\ldots,T\}$, the energy storage capacity c_n receives the most incremental value at the bus n where the marginal profits of the storage operator are maximized, i.e.,*

$$\max_{n\in\mathcal{N}}\left(\max_{\boldsymbol{\lambda},\boldsymbol{\varphi}}\ \pi_n^{s,*}\right) \tag{5.55}$$

$$\text{for}\quad \pi_n^{s,*} = \pi_n^{s^P,*} + \pi_n^{s^Q,*}, \tag{5.56}$$

$$\pi_n^{s^P,*} = -f_n^{s,*}(\cdot) + \sum_{t\in\mathcal{T}} \lambda_{n,t}^* \left[r_{n,t}^{d,*} - r_{n,t}^{c,*} \right], \tag{5.57}$$

$$\text{and} \quad \pi_n^{s^Q,*} = \sum_{t\in\mathcal{T}} \varphi_{n,t}^* \left[z_{n,t}^* \right]. \tag{5.58}$$

Proof. Given the KKT point of the SDR-OPF+S dual in (5.27), the corresponding optimal solution to the storage subproblem in (5.53) and (5.54) is

$$\max_{\boldsymbol{\lambda},\boldsymbol{\varphi}} \; g^s(\boldsymbol{\lambda},\boldsymbol{\varphi}), \tag{5.59}$$

where $g^s(\boldsymbol{\lambda},\boldsymbol{\varphi})$ is equivalent to $g^{s,*}(\boldsymbol{\lambda},\boldsymbol{\varphi})$ and

$$g^{s,*}(\boldsymbol{\lambda},\boldsymbol{\varphi}) := \max_{\mathbf{r^c},\mathbf{r^d},\mathbf{z},\mathbf{s},\mathbf{c}} \; \sum_{n\in\mathcal{N}} \pi_n^s. \tag{5.60}$$

□

Therefore the greatest marginal profits are attained at the bus where $\pi_n^{s,*}$ is maximized. This theorem leads to an important observation about the relationship between maximizing storage operator profits and minimal operational costs (as defined by a global optimal solution of the ACOPF+S problem); these problems have a natural duality in a purely competitive market as summarized below.

Corollary 5.4. *Given the KKT point of the SDR-OPF+S, the marginal profit to the storage at bus n must be nonnegative, i.e.,* $\pi_n^s \geq 0$*, whenever the storage capacity is*

positive at that location, i.e., $c_n > 0$. *Therefore,*

$$g^{s,*}(\boldsymbol{\lambda}, \boldsymbol{\varphi}) \geq 0. \tag{5.61}$$

The condition in (5.61) *holds true for the optimal solution to the SDR-OPF+S dual, and as a result this optimal solution also minimizes costs in the SDR-OPF+S problem for a purely competitive market.*

5.6.3 Energy Storage for VAr Support

The results in Theorem 5.3 and Corollary 5.4 also point to the role of VAr support in maximizing the storage operator's marginal profits. In particular, if an ESS unit does not provide VAr support then $\underline{Z}_n = \overline{Z}_n = 0$ (i.e., $z_{n,t} = 0$) for all $n \in \mathcal{N}, t \in \mathcal{T}$ and in this case the total marginal profits to the storage operator can be computed solely based on (5.57). When an ESS unit provides VAr support, then the total marginal profits require the addition of the term in equation (5.58).

The role of the VAr support can be better understood by dividing the revenues and costs into those associated with real and reactive power. The total energy service revenues and costs associated with real power are respectively given by

$$\sum_{t\in\mathcal{T}} \sum_{n\in\mathcal{N}} \lambda^*_{n,t} r^{d,*}_{n,t}, \tag{5.62}$$

$$\sum_{t\in\mathcal{T}} \sum_{n\in\mathcal{N}} \left\{ \lambda^*_{n,t} r^{c,*}_{n,t} + C^{s,1}_n r^{d,*}_{n,t} \right\}. \tag{5.63}$$

The total VAr support revenues and costs are respectively given by

$$\sum_{t\in\mathcal{T}}\sum_{n\in\mathcal{N}}\left\{\varphi^*_{n,t}z^*_{n,t}\middle|\left(z^*_{n,t}\geq 0\ \wedge\ \varphi^*_{n,t}\geq 0\right)\ \vee\ \left(z^*_{n,t}\leq 0\ \wedge\ \varphi^*_{n,t}\leq 0\right)\right\}, \tag{5.64}$$

$$\sum_{t\in\mathcal{T}}\sum_{n\in\mathcal{N}}\left\{\varphi^*_{n,t}z^*_{n,t}\middle|\left(z^*_{n,t}\leq 0\ \wedge\ \varphi^*_{n,t}\geq 0\right)\ \vee\ \left(z^*_{n,t}\geq 0\ \wedge\ \varphi^*_{n,t}\leq 0\right)\right\}. \tag{5.65}$$

Note that the VAr support revenues depend on whether the ESS is consuming $(-)$ or supplying $(+)$, as well as the $-/+$ Q-LMP value. The next section illustrates the results in Theorem 5.3 and Corollary 5.4, paying particular attention to the role of VAr support.

5.7 Case Study: The role of VAr support

The case study is carried out over a single day on the IEEE-14 bus test system network [177]. The real power demand profile for each bus, shown in Fig. 5.3, is based on half-hour increments of demand data obtained from Southern California Edison for July 2010 [154]. A power factor of 0.98 is used to calculate the corresponding reactive power demand. The line ratings are specified as 80 MVA between buses $(1,2)$, 40 MVA between buses $(1,5)$ and $(2,5)$, and 30 MVA between buses $(2,3)$ and $(2,4)$.

The generator characteristics are provided in Table 5.3 and the ramp rates are set to 15% of the generating unit capacity; for more details refer [56]. The wind power availability for the wind farms at buses 1 and 2, shown in Fig. 5.4, is based on data

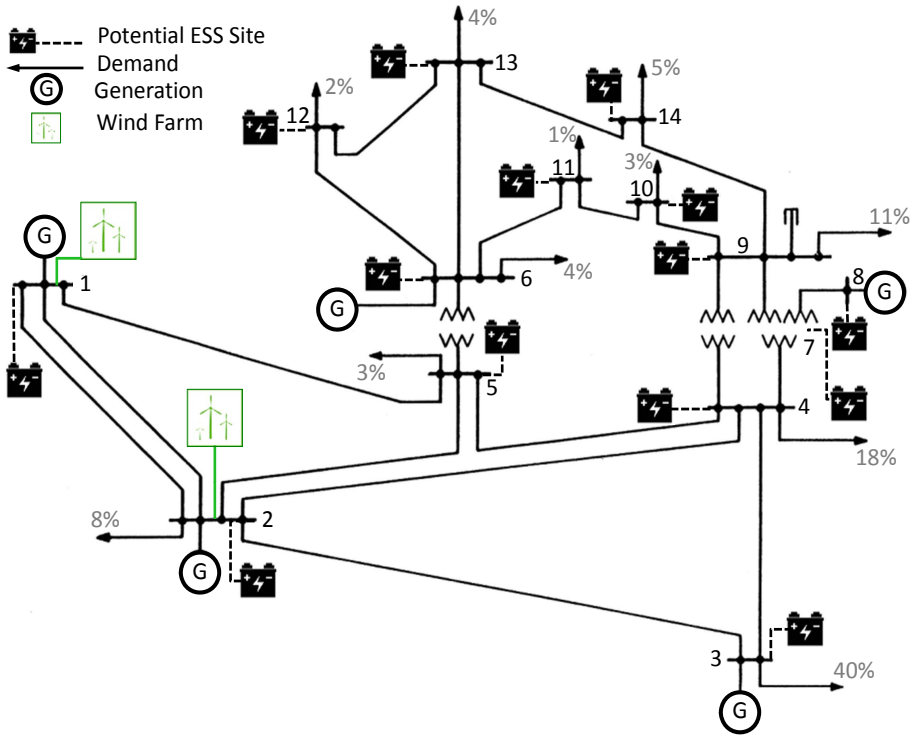

Figure 5.2: The IEEE 14-bus benchmark system topology with wind farms and potential ESS sitings as denoted with the battery storage icons. The percentages next to each bus represent the portion of aggregated demand at that bus.

Bus	$\underline{P}$ (MW)	$\overline{P}$ (MW)	$\underline{Q}$ (MVAr)	$\overline{Q}$ (MVAr)	$C^{g,2}$ (quadratic) ($/MW^{2}h)	$C^{g,1}$ (linear) ($/MW)
1	0	332.4	0	10	0.043	20
2	0	140	-40	50	0.25	20
3	0	100	0	40	0.01	40
6	0	100	-6	24	0.01	40
8	0	100	-6	24	0.01	40

Table 5.3: Generator characteristics for the IEEE14-bus system; a single generator corresponds to each bus shown.

from the NREL Western Wind Resources Dataset for 2006 [178]; the overall wind power capacity (MW) is determined as $\omega \Big/ (1-\omega) \sum_{i \in \mathcal{G}} \overline{P}_i$ where $\omega \in (0, 1]$ denotes the wind penetration as a portion of the overall generation capacity. The wind farms

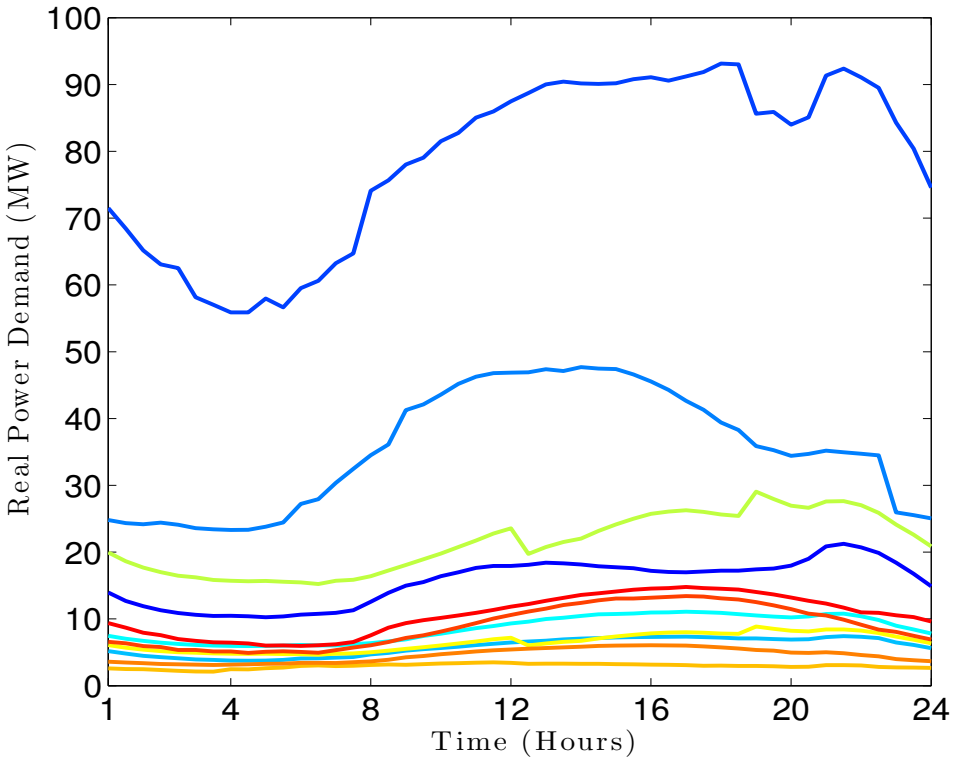

Figure 5.3: The total real power demand based on actual feeder data for an average day in Southern California, July 2010.

do not provide reactive power compensation.

A single storage technology is modeled with a network aggregate storage capacity of h =100 MWΔt where Δt= 30-minutes, i.e., 50 MWh. The storage technology has charging and discharging power rates of 8 MW per time interval and full discharge capability (i.e., $\underline{C}_n = 0$). A roundtrip efficiency of 81% (i.e., $\eta_n^c \times \eta_n^d = 0.81$) is assumed, which is consistent with a technology such as compressed air energy storage (CAES) [142]. When VAr support is employed, the reactive power range is half the energy storage capacity, i.e., $\underline{Z}_n = -0.5c_n$ and $\overline{Z}_n = 0.5c_n$. For ESS installations that do not provide VAr support, $\underline{Z}_n = \overline{Z}_n = 0$. Finally, the operational cost of

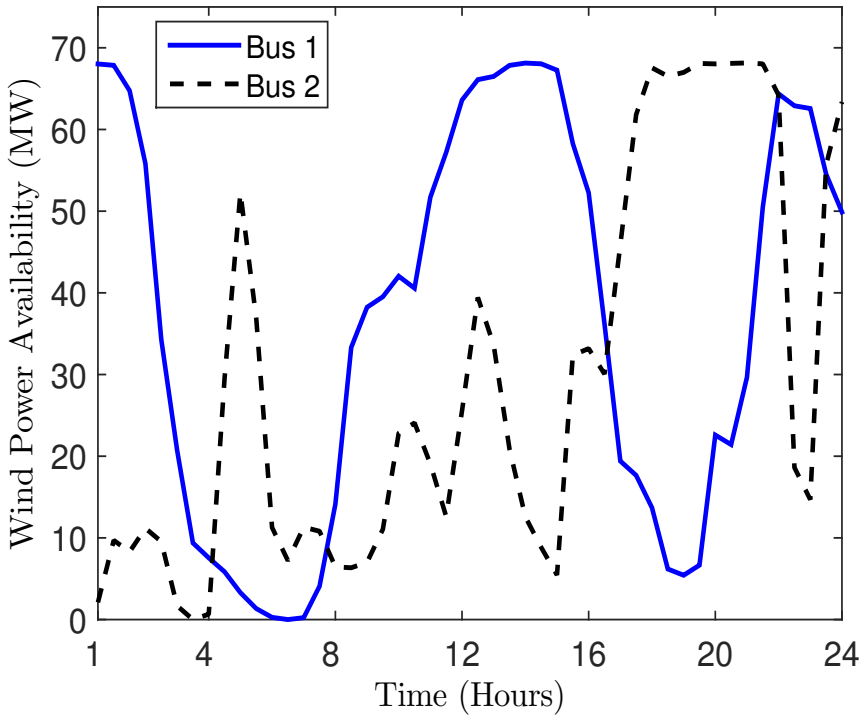

Figure 5.4: The wind power availability for 68.1 MW installed capacity based on the 2006 NREL Western Wind Resources Dataset.

discharging in (5.20) is set to \$0.1/MWh in order to enforce unimodal operations[73] and the storage operator pays the LMP for charging.

The SDR-OPF+S is implemented in Matlab [99] and the optimization problem is solved with Sedumi 1.21 [179] on a 2.2 GHz Intel Core i7 machine with 16 GB 1600 MHz DDR3. The reported results have a zero duality gap, and therefore represent a global optimum of the ACOPF+S problem in (5.16) and (5.17).

Table 5.4 compares the difference in optimal storage allocation and corresponding marginal profits at each bus for ESS units with only traditional grid services and

[73]See Theorem 5.1 in Section 5.5.

	ESS		ESS+VAr Support	
	Storage Capacity	Profits	Storage Capacity	Profits
Bus	c_n (MW/30-min)	$\pi_n^{s,*} := \pi_n^{s^P,*}$ ($)	c_n (MW/30-min)	$\pi_n^{s,*} := \pi_n^{s^P,*} + \pi_n^{s^Q,*}$ ($)
1	1.7	20.79	0	0
2	11.4	145.85	6.0	110.87
3	0	0	0	0
4	75.8	553.84	54.1	609.24
5	0	0	36.6	445.84
6-11	0	0	0	0
12	1.0	6.74	0	0
13	3.4	24.09	0	0
14	6.7	46.91	3.3	36.31
Total	100	798.37	100	1,202.39

Table 5.4: Nodal storage capacity and marginal profits for ESS without and with VAr support, with a specified roundtrip efficiency of 81%.

	Computation	ESS	ESS + VAr Support
Total System Cost ($)	$\mathbf{p}^*$ in (5.21)	205,164.00	204,697.28
I^2R Losses (MW)	$\sum_{k\in\mathcal{K},t\in\mathcal{T}} p_{k,t}^{\ell}$	151.7	145.1
Total Marginal Profit to ESS ($)	$\pi^{\mathbf{s},*}$	798.37	1,202.39

Table 5.5: A comparison of the total system cost, I^2R losses, and total marginal profit for ESS with 81% roundtrip efficiency, and either with or without VAr support. Note that the solutions reported here have a zero duality gap and therefore the SDR-OPF+S total system cost in (5.21) is equal to the ACOPF+S total system cost in (5.16).

those that also provide VAr support. Table 5.5 provides the corresponding optimal objective function value (5.16), real power losses, and total marginal profits to ESS for the two operating schemes. The net savings of $466.72 in total system costs when compensating ESS for VAr support is greater than the $404.02 increase in total marginal profits.

These results show that when ESS units provide VAr compensation, the total costs

and real power losses in the system are lower, i.e., the power system operates more efficiently and the market settlements clear at a lower operating cost. Furthermore, the added VAr from ESS units leads to higher overall system voltages; this operating state requires less current, which results in lower real power losses, as illustrated by Figures 5.5 and 5.6.

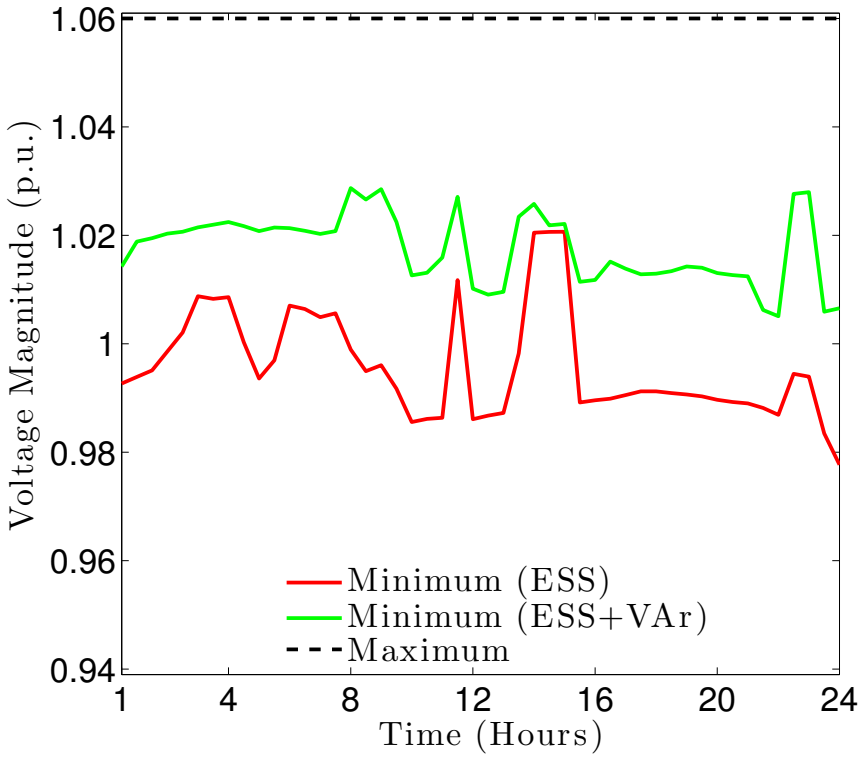

Figure 5.5: This graph illustrates the overall maximum and minimum system voltages for the network in Figure 5.2 including ESS units with and without VAr support. In both cases, the maximum allowable network voltage is 1.06 p.u.

The 50.6% increase in marginal profits to the ESS when providing VAr support is substantial. Prior to ESS integration, the only dynamic reactive power capability is provided by generating units at buses 1, 2, 3, 6, and 8. The ESS units increase the

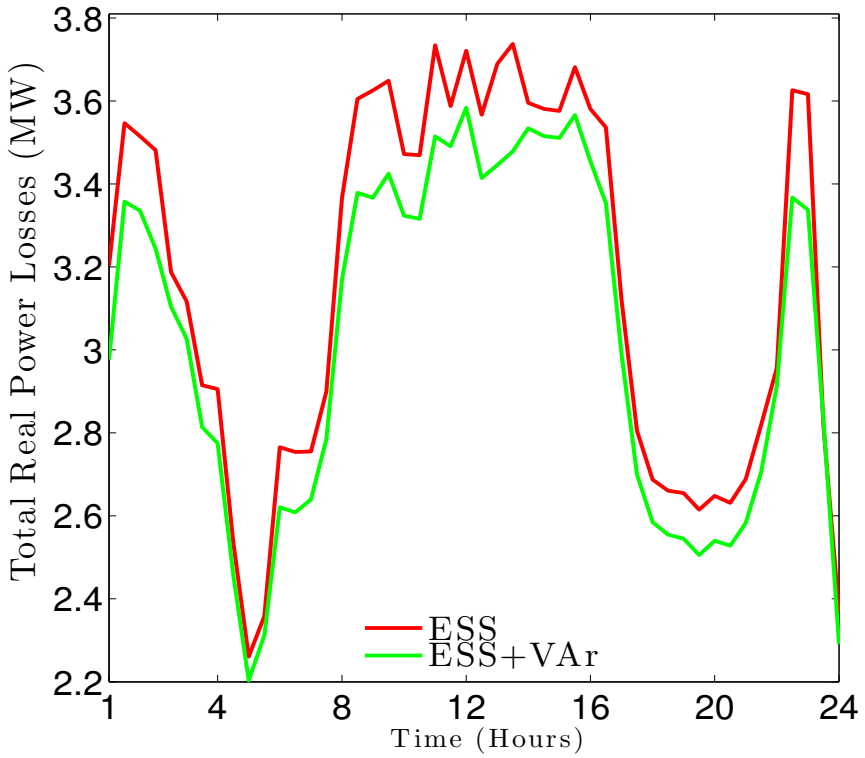

Figure 5.6: The total real power network losses (I^2R losses) corresponding to the voltage profiles in Figure 5.5.

Bus	Reactive Power Capability (MVAr)	$\max_t \lvert z_{n,t} \rvert$ Reactive Dispatch (MVAr)	Total VAr Dispatch (MVAr)
1	0	0	0
2	3.0	0.08	1.69
3	0	0	0
4	27.05	27.05	1,298.79
5	18.3	18.3	879.56
6-13	0	0	0
14	1.65	1.63	74.70
Total	50	47.06	2,254.74

Table 5.6: Reactive power capability (power rating) and maximum leading/lagging dispatch for the given operating cycle.

dynamic reactive power capability on the network by 33.8% and introduce new VAr support at buses 4, 5, and 14. Tables 5.6 and 5.7 illustrate that Q-LMP payments

	Nodal Q-LMP			ESS + VAr Support	
Bus	Minimum ($/MVAr)	Maximum ($/MVAr)	Load Weighted Mean ($/MVAr)	Total VAr Dispatch (MVAr)	Total Q-LMP Payments ($)
2	0	0	0	1.69	0
4	0.058	0.255	0.176	1,298.79	213.61
5	0.086	0.424	0.285	879.56	233.10
14	0	0.321	0.202	74.70	13.22

Table 5.7: The minimum and maximum Q-LMP prices, the load weighted mean Q-LMP and total Q-LMP payments to storage.

can be quite substantial depending on the magnitude of the Q-LMP and the amount of VAr dispatched from the ESS; whereas the reactive power capability of the ESS at bus 2 is 97.3% under-utilized, the ESS units at buses 4 and 5 are dispatching VAr support at full reactive power capability for the duration of the operating cycle. Note that the Q-LMP payments implicitly include both revenues and costs as calculated in (5.64) and (5.65), although no costs related to reactive power dispatch are incurred.

Table 5.8 reports nodal Q-LMP statistics at the buses with conventional generation, along with the total VAr dispatch and corresponding Q-LMP payment for each generator. Compared to the nodal Q-LMP statistics in Table 5.7, the marginal value of VAr support is much lower at these buses. Consequently, the Q-LMP payments to generators are significantly lower than the Q-LMP payments to ESS units that are optimally integrated to provide not only power and energy services but also VAr support.

Costs and benefits to other market participants of optimally integrating ESS units that either provide or do not provide VAr support are shown in Table 5.9. The

	Case Study: ESS (without VAr Support)				
	Nodal Q-LMP			Generator	
Bus	Minimum ($/MVAr)	Maximum ($/MVAr)	Load Weighted Mean ($/MVAr)	Total VAr Dispatch (MVAr)	Total Q-LMP Payments ($)
1	-0.012	0	-	122.64	0
2	0	0	0	304.76	0
3	-0.757	0	0	739.75	0
6	-0.008	0.207	0	656.16	47.85
8	0	0.035	-	773.33	0.85
	Case Study: ESS with VAr Support				
	Nodal Q-LMP			Generator	
Bus	Minimum ($/MVAr)	Maximum ($/MVAr)	Load Weighted Mean ($/MVAr)	Total VAr Dispatch (MVAr)	Total Q-LMP Payments ($)
1	-0.031	0	-	17.61	0
2	0	0	0	245.67	0
3	-0.764	0	-0.139	706.13	0
6	-0.165	0	-0.026	517.97	10.40
8	0	0.235	-	829.10	53.62

Table 5.8: The minimum and maximum Q-LMP prices, the load weighted average Q-LMP and total Q-LMP payments to generators.

consumer costs at bus n are computed as

$$\sum_{t\in\mathcal{T}} \left(\lambda_{n,t} P^d_{n,t} + \varphi_{n,t} Q^d_{n,t}\right), \tag{5.66}$$

and the generator marginal profits at bus n are computed as

$$\sum_{i\in\mathcal{I}(n),t\in\mathcal{T}} \left(\lambda_{n,t} p^g_{i,t} + \lambda_{n,t} p^w_{i,t} + \varphi_{n,t} q^g_{i,t} + \varphi_{n,t} q^w_{i,t} - \alpha^g_{i,t} - C^w_{i,t} p^w_{i,t}\right). \tag{5.67}$$

Based on the SDR-OPF+S dual objective function in (5.27), not all market settlements are included in the above calculations. The optimal integration of ESS with VAr support results in lower total costs to consumers and higher total marginal profits

to generators as compared to the optimal integration of ESS units that do not provide VAr support. However the effects are negligible, i.e., accounting for less than 1% of the overall benefits to consumers and marginal profits to generators. Since the total marginal profits to storage is approximately 0.9% (without VAr support) and 1.4% (with VAr support) of the overall marginal profits to producers, the large increase in marginal profits to ESS providing VAr support is inframarginal when compared to the market as a whole. Furthermore, the payments for VAr support increases marginal profits of the storage operator by 50.6%, which indicates that Q-LMP payments create substantial incentives to optimally integrate ESS units to provide services in addition to power and energy that improve operational efficiency.

	Consumer Costs		Generator Marginal Profits	
	ESS	ESS + VAr Support	ESS	ESS + VAr Support
Bus	($)	($)	($)	($)
1	-	-	52,101.34	52,191.70
2	17,600.00	17,661.68	32,932.91	33,008.10
3	154,579.53	154,558.66	1,117.54	1,110.97
4	66,983.00	66,872.91	-	-
5	9,916.90	9,926.44	-	-
6	15,022.78	14,994.88	47.85	10.40
7	-	-	-	-
8	-	-	310.45	354.33
9	38,918.46	38,943.43	-	-
10	11,836.50	11,840.61	-	-
11	5,231.05	5,227.22	-	-
12	8,123.65	8,107.98	-	-
13	16,138.23	16,111.45	-	-
14	19,492.92	19,479.95	-	-
Energy Services ($)	363,728.02	363,671.68	86,461.39	86,611.41
VAr Support ($)	114.99	53.54	48.70	64.06
Total ($)	363,843.02	363,725.22	86,510.09	86,675.47

Table 5.9: The costs to consumers and marginal profits to generators are compared for when the ESS does and does not provide VAr support.

5.8 Payments for VAr Support: Capability or Dispatch Rates?

The discussion in Section 5.7 is now extended to compare the Q-LMP payment mechanism, which pays for reactive power dispatch, to current market mechanisms, which pay for reactive power capability. The Q-LMP payment mechanism is compared to current open access transmission tariff (OATT) Schedule 2 Rates for actual system operators, more specifically ISO-NE and NYISO [180]. Both NYISO and ISO-NE pay qualified units for VAr capability, where the cost is typically allocated to customers based on a load ratio that is measured in terms of real power. The NYISO and ISO-NE VAr capability rates are $\$3,919$/MVAr-year and $\$2,190$/MVAr-year respectively [180]. Both system operators also make lost opportunity cost (LOC) payments when the qualified unit's real power output is dispatched down for the purpose of providing VAr support. LOC payments are not considered in this study since it is assumed that there is no trade-off between real and reactive power outputs from the power electronics on the ESS unit; however, such trade-offs do occur in practice for conventional generation operating along the border of its capability curve.[74]

The case study in Section 5.7 demonstrates that having ESS units which can provide VAr support is beneficial to grid operations. In current energy markets, storage operators receive LMP payments for providing real energy services and in

[74]This trade-off in ESS operations is largely dependent on the configuration of the system and energy storage technology. A growing trend for asynchronous generation is to oversize the power converters in order to increase reactive power capacity [181, 182], which may result in little to no trade-off depending upon the local reactive power needs of the system.

limited situations (e.g., pumped storage [183]) are classified as qualified units for receiving VAr payments under OATT Schedule 2; otherwise no remuneration for VAr support is provided.

Current market settlements based on nodal pricing are determined with dispatch models that include numerous simplifications of the ACOPF [6]; Table 5.10 reports additional results for the ESS+VAr support case study from Section 5.7; the results represent a global optimum to the ACOPF+S, which can be thought of as the best-case scenario. Note that a global optimum to the ACOPF+S simultaneously co-optimizes real and reactive power dispatch whereas current market settlements are suboptimal in comparison.

The results in Table 5.10 show that the introduction of a market mechanism such as Q-LMP can benefit the storage operator and therefore incentivize the storage operator to help decrease system costs. For the current market design with nodal pricing on the real power dispatch only, i.e., the LMP, the marginal profits to a storage operator without VAr support would be \$798.37, which would then decrease to \$742.46 if VAr support were also provided but Q-LMP payments are not included. However with nodal pricing also on the reactive power dispatch, i.e., Q-LMP, the overall marginal profits to the storage operator with VAr support would increase to $\$1,202.39$. This simple example illustrates that the current market design disincentivizes storage operators from providing VAr support because marginal profits decrease unless the VAr dispatch is remunerated.

Energy Services	ESS	ESS + VAr Support
Revenues ($)	5,304.55	4,798.65
Costs ($)	4,506.17	4,056.19
Profits ($)	798.37	742.46
Reactive Power Compensation		
Revenues ($)	0	459.93
Costs ($)	0	0
Profits ($)	0	459.93
Total Marginal Profits ($)	798.37	1,202.39

Table 5.10: The total revenues, costs, and marginal profits to ESS without and with VAr support; the total Q-LMP payments to the storage operator is $459.93.

Bus	Q-LMP ($/Day)	NYISO Capability Rate ($/Day)	ISO-NE Capability Rate ($/Day)
1	0	0	0
2	0.04	32.21	18.00
3	0	0	0
4	213.61	290.43	162.30
5	233.06	196.49	109.80
6-13	0	0	0
14	13.22	17.72	9.90
Total	459.93	536.85	300.00

Table 5.11: Q-LMP payments compared to the effective daily reactive power capability rates for reactive capability in NYISO and ISO-NE.

Table 5.11 compares the Q-LMP payments to the NYISO and ISO-NE capability payments. The results show that the NYISO and ISO-NE type VAr capability rates are inconsistent between the system operators. This inconsistency is also observed for the other ISOs including MISO, PJM, and CAISO [180]. The disconnect between these rates and nodal prices can lead to significant over-supply of VAr in some areas and scarcity in others. This can be thought of as a misalignment of system costs,

investment and dispatch incentives, and operational needs of the electric power grid. Through pricing the locational and temporal needs for VAr support on the system, the Q-LMP mechanism reflects the marginal value of VAr support as a paid service, is incentive compatible, and revenue adequate at a global optimum to the ACOPF+S.

5.9 Conclusions

The OPF with storage problem, ACOPF+S, is formulated in this study. The corresponding semidefinite relaxation SDR-OPF+S is then solved to determine a global optimum to the ACOPF+S. Since the ACOPF+S is a nonconvex optimization problem, the marginal values may not cover the system costs if the KKT point is not a global optimum; however by leveraging the SDR approach, properties of strong duality can be exploited to characterize market mechanisms such as the Q-LMP that are incentive compatible and support revenue adequacy.

The study assesses the potential for ESS to provide VAr support in addition to real energy and power services. Reactive power compensation is critical to efficient and reliable operations, and without a proper market mechanism to remunerate resources for this service, there is a disincentive to provide it. The results show that the Q-LMP payment provides a more rational means of compensating VAr support than the capability rate payments common in current U.S. electricity markets because the Q-LMP reflects the true marginal value for VAr support in the system. Furthermore, a Q-LMP would provide an additional revenue stream for energy storage, which can

improve the financial viability of these systems.

6 The Role of Network Losses in Optimal Storage Allocation

6.1 Prologue

The proposed studies in Chapters 3, 4, and 5 focused on solution methods to solving the OPF for the simultaneous co-optimization of real and reactive power dispatch. However in current market design, most ESS installations would not receive remuneration for reactive power compensation [180]. Furthermore, the full ACOPF is not solved in current market software but rather real power losses are incorporated.

This chapter presents an intermediate optimization problem between the DCOPF and ACOPF to optimal storage integration in order to consider power and energy services as the main profit drivers for ESS. Since the ACOPF is not currently solved in the day-ahead and real-time markets, loss factors to approximate the real power losses are incorporated into the dispatch and market settlements where marginal loss prices are a component of the marginal pricing and reflect the portion of the change in cost that is due to a change in real power losses on the network [6, 58]. The total system costs due to losses can be quite significant; in 2014, PJM accounted $1.5 billion in total costs due to marginal loss payments compared to $1.9 billion in total

congestion costs [184]. However inaccurate loss approximation can cause numerous issues including price divergence between the day-ahead and real-time markets as well as strategic bidding by market participants [185].

The real power losses can be approximated directly from the ACPF equations. The resulting real power losses approximation[75]

$$\tilde{p}^{\ell}_{k,t} = \frac{1}{2} g_k \left(\theta_{nm,t}\right)^2$$

is a quadratic equality constraint and, as a result, incorporating this expression into a DCOPF problem to obtain a DCOPF with losses formulation results in a nonconvex QCQP. A number of works have dealt with this complexity by applying a piecewise linearization to approximate the quadratic losses, which was originally proposed in [186]. However the number of variables grows as a function of the number of piecewise segments introduced to improve the loss approximation and if the dual variable to the nodal power balance of the DCOPF is negative, then the unordered piecewise segments tend to exaggerate the losses in order to lower the cost minimization objective (i.e., higher demand/losses when LMPs are negative results in decreased system costs) [187]. Others propose SLP approaches to approximate the DCOPF with losses formulation, which can converge quickly, but require iterative solves to obtain optimality and the solution technique may cycle with a poor initialization.

Extending the conference proceeding [27], this chapter proposes a DCOPF with

[75] see Section 2.6.2

loss approximation that leverages a global solution method to make this problem tractable. The following study demonstrates that a DCOPF with real power losses approximation may adequately capture the main drivers in storage dispatch and allocation for power and energy services during normal operations.[76]

6.2 Introduction and Literature Review

The DCOPF problem is a commonly applied linear approximation of the ACOPF problem that can be solved to optimality in polynomial time for large-scale networks. Consequently, there are a large number of studies that examine DCOPF-based ESS integration, e.g., [166, 173, 174, 188–190]. A major limitation of DCOPF with storage (DCOPF+S) formulations is that these studies implicitly assume that real power losses are negligible, i.e., that network power transfers are perfectly efficient. This assumption leads to inaccuracies in the actual system LMPs, which incorporate not only the marginal unit cost and the congestion costs, but also the additional dispatch costs to cover network losses. The previous study presented in Chapter 5 illustrates that LMPs[77] play a key role in ACOPF-based storage dispatch, siting and sizing decisions [26].

This work attempts to bridge the gap between ACOPF+S and DCOPF+S approaches by proposing a DCOPF+S with losses formulation, which is referred to here

[76] Emergency operations can require reactive power compensation and voltage control not readily modeled in DCOPF-based approaches, including the proposed DCOPF with losses framework.

[77] The previous study also indicates the important role of Q-LMPs, but for the purpose of analyzing power and energy services only, LMPs were proven and shown to be the key driver for the optimal integration of ESS without VAr support.

as the ℓ-DCOPF+S problem. This model has the advantage of being both more computationally tractable than the ACOPF+S model presented in Chapter 5 and more accurate than the lossless DCOPF+S formulation. It also has the advantage of explicitly isolating the role of real power losses in OPF-based ESS integration. Due to the assumptions of DCOPF-based modeling, reactive power compensation provided by ESS is not included here.[78] Related DCOPF with losses formulations have been previously studied in generalized market models, e.g., [187, 191–196], but not in the context of optimal ESS integration.

This work develops the ℓ-DCOPF+S by augmenting the standard DCOPF model with linear storage charge/discharge dynamics to incorporate the quadratic real power loss approximations derived from standard ACPF equations. Then the resulting non-convex QCQP is solved using convex relaxations that result in both SDP and SOCP formulations. The theoretical result uses arguments based on the results in [197] and [198] to prove that both of these convex relaxations equivalently provide an exact lower bound to the ℓ-DCOPF+S problem. A case study compares the performance of the ℓ-DCOPF+S formulation to that of DCOPF+S and ACOPF+S (without VAr support) formulations. The case study results demonstrate that obtaining accurate optimal storage allocation, where ACOPF+S results are the benchmark, is tightly coupled with correctly determining the LMPs.

The remainder of this chapter is organized as follows. Section 6.3 incorporates

[78] please see Chapter 5 for details on ESS with VAr support

the linear power flows and quadratic loss approximations presented in Section 2.6.2 in order to derive the ℓ-DCOPF+S problem. Section 6.4 provides the SDP and SOCP relaxations for the ℓ-DCOPF+S problem along with proofs that these relaxations are exact. Subsequently Section 6.5 compares the performance of the ℓ-DCOPF+S, DCOPF+S and ACOPF+S problems. Concluding remarks are provided in Section 6.6.

6.3 Multi-Period Lossy DCOPF with Storage Dynamics

The linear power flows and quadratic loss approximations presented in Section 2.6.2, the ACOPF+S formulation presented in Section 5.3.3 can be augmented to formulate the following multi-period ℓ-DCOPF+S problem as

$$\mathbf{p}^* := \min_{\mathbf{p^g},\mathbf{p^w},\boldsymbol{\theta},\mathbf{r^c},\mathbf{r^d},\mathbf{s},\mathbf{c}} \; f^g(\cdot) + f^w(\cdot) + f^s(\cdot) \tag{6.1}$$

subject to

$$s_{n,t} = s_{n,t-1} + \eta_n^c r_{n,t}^c - \left(\eta_n^d\right)^{-1} r_{n,t}^d \qquad \forall n \in \mathcal{N}, t \in \mathcal{T} \tag{6.2}$$

$$0 \leq r_{n,t}^c \leq R_n^c \qquad \forall n \in \mathcal{N}, t \in \mathcal{T} \tag{6.3}$$

$$0 \leq r_{n,t}^d \leq R_n^d \qquad \forall n \in \mathcal{N}, t \in \mathcal{T} \tag{6.4}$$

$$\underline{C}_n \leq s_{n,t} \leq c_n \qquad \forall n \in \mathcal{N}, t \in \mathcal{T} \tag{6.5}$$

$$\tilde{s}_{n,T} - s_{n,T} = 0 \qquad \forall n \in \mathcal{N}, t \in \mathcal{T} \tag{6.6}$$

$$\sum_{n\in\mathcal{N}} c_n \leq h \qquad \forall n \in \mathcal{N}, t \in \mathcal{T} \quad (6.7)$$

$$0 \leq p^w_{i,t} \leq C^w_{i,t} \qquad \forall i \in \mathcal{W}, t \in \mathcal{T} \quad (6.8)$$

$$\underline{P}_i \leq p^g_{i,t} \leq \overline{P}_i \qquad \forall i \in \mathcal{G}, t \in \mathcal{T} \quad (6.9)$$

$$-RR^d_i \leq p^g_{i,t} - p^g_{i,t-1} \leq RR^u_i \qquad \forall i \in \mathcal{G}, t \in \{2,\ldots,T\} \quad (6.10)$$

$$\sum_{k(n,\cdot),t} \hat{p}_{k(n,m),t} = r^d_{n,t} + \sum_{i\in\mathcal{I}(n)} \left(p^g_{i,t} + p^w_{i,t}\right) - r^c_{n,t} - P^d_{n,t} \qquad \forall n \in \mathcal{N}, t \in \mathcal{T} \quad (6.11)$$

$$\hat{p}_{k(\cdot),t} = \tilde{p}_{k(\cdot),t} + \tilde{p}^{\ell}_{k,t} \qquad \forall k(\cdot) \in \mathcal{F}, t \in \mathcal{T} \quad (6.12)$$

$$\tilde{p}_{k(n,m),t} = -b_k \theta_{nm,t} \qquad \forall k(n,m), k(m,n) \in \mathcal{F}, t \in \mathcal{T} \quad (6.13)$$

$$\tilde{p}^{\ell}_{k,t} = \frac{1}{2} g_k \left(\theta_{nm,t}\right)^2 \qquad \forall k \in \mathcal{K}, t \in \mathcal{T} \quad (6.14)$$

$$-\overline{\theta}_{nm} \leq \theta_{nm,t} \leq \overline{\theta}_{nm} \qquad \forall (n,m) \in \mathcal{A}, t \in \mathcal{T} \quad (6.15)$$

$$-\overline{P}_k \leq \hat{p}_{k(\cdot),t} \leq \overline{P}_k \qquad \forall k(\cdot) \in \mathcal{F}, t \in \mathcal{T}. \quad (6.16)$$

In the objective (6.1), the multi-period function

$$f^g(\cdot) := \sum_{t\in\mathcal{T}} \sum_{i\in\mathcal{G}} C^{g,2}_i \left(p^g_{i,t}\right)^2 + C^{g,1}_i p^g_{i,t} \quad (6.17)$$

is a strictly convex cost function with positive coefficients of the real power generation,

$$f^w(\cdot) := \sum_{t\in\mathcal{T}} \sum_{i\in\mathcal{W}} C^{w,1}_i p^w_{i,t} \quad (6.18)$$

is a linear cost function of the wind power production, and

$$f^s(\cdot) := \sum_{t\in\mathcal{T}} \sum_{n\in\mathcal{N}} C_n^{s,1} r_{n,t}^d \tag{6.19}$$

is a linear cost function of the storage discharge, which represents variable O&M costs. The cost of storage charging is not included because the storage operator implicitly pays the LMP at the bus, where the LMP at bus n is the dual variable $\lambda_{n,t}$ associated with the power balance constraint in (6.11).

Remark 6.1. *The DCOPF+S with storage problem can be recovered from the ℓ-DCOPF+S problem by setting $g_k = 0$ for $\tilde{p}_{k,t}^{\ell}$ in* (6.14)*, which corresponds to assuming zero resistances, i.e., $r_k = 0$ for all $k \in \mathcal{K}$, and therefore no network losses.*

6.4 Solution Technique

The ℓ-DCOPF+S problem defined in (6.1)$-$(6.16) is a nonconvex QCQP, which has a convex quadratic cost function (6.17) and a nonconvex quadratic equality constraint (6.14). Although the convex quadratic cost function can be equivalently reformulated as a LMI,[79] the nonconvex constraint (6.14) requires special treatment. The following proves that under certain conditions this ℓ-DCOPF+S problem can be solved to optimality through both SDR and SOCR. Furthermore, by similar arguments presented by Gayme and Topcu in [25], Slater's condition[80] is satisfied and strong duality holds

[79] see footnote 67
[80] see footnote 65

for both the SDR and SOCR problems presented below.

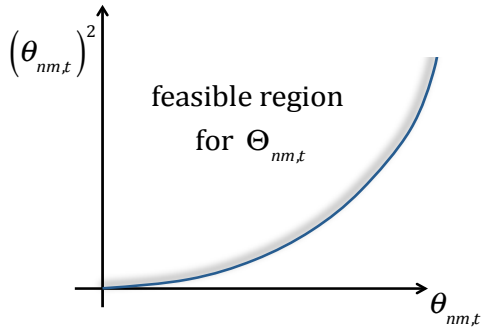

Figure 6.1: Given the angle difference $\theta_{nm,t}$ between buses n and m at time t, the slack variable $\Theta_{nm,t}$ is bounded by $(\theta_{nm,t})^2$.

First, the losses equation (6.14) is reformulated as

$$\tilde{p}^{\ell}_{k,t} = \text{tr}\left(M^{\ell}_{k}\tilde{\Theta}_{nm,t}\right), \tag{6.20}$$

where the coefficient matrix for each line $k \in \mathcal{K}$ is defined as

$$M^{\ell}_{k} := \begin{bmatrix} 0 & 0 \\ 0 & \frac{1}{2}g_k \end{bmatrix}, \tag{6.21}$$

and $\Theta_{nm,t} \in \mathbb{R}^{+}$ is a slack variable with the following lower bound:

$$(\theta_{nm,t})^2 \leq \Theta_{nm,t}, \tag{6.22}$$

as illustrated in Figure 6.1. The condition in (6.22) is equivalent to the Schur com-

plement[81] of $\Theta_{nm,t}$, i.e.,

$$\tilde{\Theta}_{nm,t} := \begin{bmatrix} 1 & \theta_{nm,t} \\ \theta_{nm,t} & \Theta_{nm,t} \end{bmatrix} \tag{6.23}$$

for all $(n,m) \in \mathcal{A}, t \in \mathcal{T}$; the corresponding variable set is referred to as $\tilde{\mathbf{\Theta}} := \{\tilde{\Theta}_{nm,t}\}_{|\mathcal{A}|\times|\mathcal{T}|}$. The following SDR and SOCR formulations are novel approaches that employ the losses calculation in $(6.20) - (6.23)$.

6.4.1 Semidefinite Relaxation

The SDR of (6.20) is then obtained by enforcing the following condition

$$\tilde{\Theta}_{nm,t} \succeq 0 \tag{6.24}$$

for all $(n,m) \in \mathcal{A}, t \in \mathcal{T}$. This SDR relaxation is exact when

$$\Theta_{nm,t} = (\theta_{nm,t})^2, \tag{6.25}$$

which implies that $\text{rank}\{\tilde{\Theta}_{nm,t}\} = 1$.

The SDR of the nonconvex QCQP in $(6.1) - (6.16)$ is then given by the following SDP:

$$\min_{\mathbf{p^g},\mathbf{p^w},\tilde{\mathbf{\Theta}},\mathbf{r^c},\mathbf{r^d},\mathbf{s},\mathbf{c}} \sum_{t\in\mathcal{T}} \sum_{i\in\mathcal{G}} \alpha^g_{i,t} + f^w(\cdot) + f^s(\cdot) \tag{6.26}$$

[81] see footnote 68

subject to

$$(6.1) - (6.13), (6.15), (6.16), (6.20), (6.24) \tag{6.27}$$

$$\begin{bmatrix} C_i^{g,1} p_{i,t}^g - \alpha_{i,t}^g & \sqrt{C_i^{g,2}} p_{i,t}^g \\ \sqrt{C_i^{g,2}} p_{i,t}^g & -1 \end{bmatrix} \preceq 0 \qquad i \in \mathcal{G}, t \in \mathcal{T}. \tag{6.28}$$

The reformulation introduces the slack variable $\alpha_{i,t}^g$ in order to represent the quadratic cost function in (6.17) as an equivalent LMI in (6.28).

The relaxed problem (6.26)−(6.28) provides the optimal solution to the ℓ-DCOPF+S in (6.1) − (6.16) when the condition in (6.25) holds, i.e., the SDP provides an exact lower bound for the original QCQP.

6.4.2 Second Order Cone Relaxation

The SOCR is obtained by first reformulating the condition in (6.22) as

$$||\theta_{nm,t}||_2^2 \leq \Theta_{nm,t} \tag{6.29}$$

using a squared l_2-norm.[82] Then the following transformation

$$4||\theta_{nm,t}||_2^2 \leq 4\Theta_{nm,t}, \tag{6.30}$$

[82]The l_2-norm is defined as $||x||_2 \coloneqq \left(\sum_{i=1}^n |x_i|^2\right)^{1/2}$.

$$4\theta_{nm,t}^2 \leq (1+\Theta_{nm,t})^2 - (1-\Theta_{nm,t})^2\,, \tag{6.31}$$

$$(1-\Theta_{nm,t})^2 + 4\theta_{nm,t}^2 \leq (1+\Theta_{nm,t})^2\,, \tag{6.32}$$

enables condition (6.22) to be represented as the second-order cone constraint[83]

$$\left\| \begin{pmatrix} 1-\Theta_{nm,t} \\ 2\theta_{nm,t} \end{pmatrix} \right\|_2 \leq 1+\Theta_{nm,t} \tag{6.33}$$

for all $(n,m) \in \mathcal{A}, t \in \mathcal{T}$; note that (6.33) is equivalent to the positive semidefinite constraint in (6.24). Furthermore, this lower bound is tight, i.e., the SOCR is exact, when (6.25) holds and therefore (6.33) is an equality.

The corresponding SOCR of the ℓ-DCOPF+S problem $(6.1)-(6.16)$ is then given by the following SOCP:

$$\min_{\mathbf{p^g},\mathbf{p^w},\tilde{\mathbf{\Theta}},\mathbf{r^c},\mathbf{r^d},\mathbf{s},\mathbf{c}} \sum_{t\in\mathcal{T}} \sum_{i\in\mathcal{G}} \alpha_{i,t}^g + f^w(\cdot) + f^s(\cdot) \tag{6.34}$$

subject to

$$(6.1)-(6.13), (6.15), (6.16), (6.20), (6.28), (6.33). \tag{6.35}$$

[83] A constraint of the form $u^T u \leq xy$ where $x \geq 0$, $y \geq 0$, $w \in \mathbb{R}^n, x, y \in \mathbb{R}$ is equivalent to the second-order cone constraint [199]

$$\left\| \begin{pmatrix} x-y \\ 2w \end{pmatrix} \right\|_2 \leq x+y.$$

Given the proposed solution techniques for the ℓ-DCOPF+S problem, the optimal solution of the SOCR in (6.34) and (6.35) provides a lower bound on the SDR in (6.26) and (6.27). Furthermore, the SOCR is exact when (6.33) is an equality.

6.4.3 Exactness of the Convex Relaxations

The following analysis proves that the SDR and SOCR in Sections 6.4.1 and 6.4.2 are exact. The proposed proof for Theorem 6.1 extends [197] and [198] to show that the optimal solution of the SDP in (6.26) – (6.28) always provides a global optimum for the ℓ-DCOPF+S problem (6.1) – (6.16). Then Corollary 6.2 shows that the optimal solution of the SOCP in (6.34) and (6.35) also provides a tight lower bound for the solution of the nonconvex QCQP in (6.1) – (6.16), *a priori* to solving the problem.

Theorem 6.1. *The optimal solution of the SDP in* (6.26) – (6.28) *provides a tight lower bound, i.e., a global optimum, for the nonconvex QCQP in* (6.1) – (6.16).

Proof. In order to prove the theorem one need only prove that the losses based on the optimal value of $\tilde{\boldsymbol{\Theta}}$ are equal to the losses $\tilde{p}^{\ell}_{k,t} = \frac{1}{2} g_k \left(\theta_{nm,t}\right)^2$ in (6.14) at the optimal value of $\boldsymbol{\theta}$ for the QCQP in (6.1) – (6.16), i.e., that $\text{rank}\{\tilde{\boldsymbol{\Theta}}\} = 1$. This condition results in the same optimal values for the power flows $-b_k \theta_{nm,t}$ in (6.13), the power balance in (6.11), and the cost function in (6.1).

Given $\tilde{\boldsymbol{\Theta}} := \{\tilde{\Theta}_{nm,t}\}_{|\mathcal{A}|\times|\mathcal{T}|}$ and (6.24), the condition in (6.22) implies

$$\frac{1}{2} g_k \left(\theta_{nm,t}\right)^2 \leq \frac{1}{2} g_k \Theta_{nm,t} \tag{6.36}$$

for all $k \in \mathcal{K}, t \in \mathcal{T}$ where $(\theta_{nm,t})^2 \in \mathbb{R}^+$.

Let $\hat{\theta}_{nm,t} = \sqrt{\Theta_{nm,t}}$ where $\hat{\theta}_{nm,t} \in \mathbb{R}^+$. Then the matrix $\begin{bmatrix} 1 & \hat{\theta}_{nm,t} \end{bmatrix}^T \begin{bmatrix} 1 & \hat{\theta}_{nm,t} \end{bmatrix}$ has the same diagonal elements as $\tilde{\Theta}_{nm,t}$, but the off-diagonal elements are $\sqrt{\Theta_{nm,t}}$ instead of $\theta_{nm,t}$. From the definition of M_k^ℓ in (6.21) all of its off-diagonal elements are zero and $\left[M_k^\ell\right]_{2,2} > 0$. Therefore

$$\tilde{p}_{k,t}^\ell = \text{tr}\left(M_k^\ell \tilde{\Theta}_{nm,t}\right) = \begin{bmatrix} 1 & \hat{\theta}_{nm,t} \end{bmatrix} M_k^\ell \begin{bmatrix} 1 & \hat{\theta}_{nm,t} \end{bmatrix}^T,$$

where

$$\text{tr}\left(M_k^\ell \tilde{\Theta}_{nm,t}\right) = \sum_{u=1}^{2} \sum_{v=1}^{2} \left[M_k^\ell\right]_{u,v} \left[\tilde{\Theta}_{nm,t}\right]_{u,v}.$$

This proves that for every optimal solution to the SDP there exists a $\theta_{nm,t}$ such that $\theta_{nm,t} = \sqrt{\Theta_{nm,t}}$ is a feasible solution to the nonconvex QCQP. Therefore, the loss approximation in (6.20) is equivalent to that in (6.14), and as such the power flows, which are linear in $\theta_{nm,t}$, and the resulting objective function in the QCQP are equal to those of the SDP. Since the SDP is a lower bound to the nonconvex QCQP, $\sqrt{\Theta_{nm,t}}$ is also an optimal solution to the nonconvex QCQP, and the relaxation is exact. □

Corollary 6.2. *Under the conditions of Theorem 6.1 the optimal solution of the SOCP in* (6.34) *and* (6.35) *provides an exact lower bound for a global optimum of the* ℓ*-DCOPF+S problem in* (6.1) − (6.16)*.*

Proof. Let $\tilde{\mathbf{\Theta}}$ be the optimal solution of the SOCP in (6.34) and (6.35). The constraint

(6.33) is equivalent to condition (6.22). Thus without loss of generality, the same proof as above can be applied to demonstrate that the SOCP in (6.34) and (6.35) is an exact relaxation of the nonconvex QCQP in (6.1) − (6.16), which is the original ℓ-DCOPF+S problem. □

6.4.4 Other Properties of the Convex Relaxations

The properties related to unimodal storage dynamics, as presented in Theorem 5.1 and Corollary 5.2, extend to both the SDP and SOCP presented here. Without loss of generality, the power balance $p_{n,t} = \text{tr}\{\Phi_n W_t\}$ in Theorem 5.1 can be replaced with the power balance $p_{n,t} = \sum_{k(n,\cdot),t} \hat{p}_{k(n,m),t}$ where $\hat{p}_{k(n,m),t} = -b_k\theta_{nm,t} + \text{tr}\left(M_k^\ell \tilde{\Theta}_{nm,t}\right)$; consequently, the results hold for both the SDP in (6.26) − (6.28) and the SOCP in (6.34) and (6.35).

6.5 Case Studies

This section reports on two case studies of a 14-bus system; one with 15% wind penetration[84] and no transmission constraints and a second one that includes binding transmission constraints, i.e., congestion. In the first case study with no congestion, optimal storage integration is expected to have the highest reduction on the economic value of losses. Whereas in the second case study, congestion relief is also a

[84]Similar to the case studies in Chapter 5, the overall wind power capacity (MW) is determined as $\omega \Big/ (1-\omega) \sum_{i\in\mathcal{G}} \overline{P}_i$ where $\omega \in (0,1]$ denotes the wind penetration as a portion of the overall generation capacity.

consideration.

The storage allocation and dispatch strategies for the DCOPF+S, ℓ-DCOPF+S, and ACOPF+S problems are compared. The SDR-OPF+S[85] is solved and provides a global optimum to the ACOPF+S, and the SOCR of the ℓ-DCOPF+S[86] is solved to determine a global optimum of the ℓ-DCOPF+S. Lastly, the DCOPF+S can be formulated using Remark 6.1. In order to maintain consistency in comparison to the ESS power and energy services modeled in the DCOPF+S and ℓ-DCOPF approaches, the following assumptions are applied to the SDR-OPF+S:

1. Capacity limits are specified on the real power flow (MW) instead of apparent power flow (MVA) for all flows $k(\cdot) \in \mathcal{F}$ and all time periods $t \in \mathcal{T}$ as

$$-\overline{P}_k \leq \text{tr}\left\{\Phi^{\ell}_{k(\cdot)} W_t\right\} \leq \overline{P}_k,$$

2. The ESS unit does not provide VAr support, i.e., $\underline{Z}_n = \overline{Z}_n = 0$, and

3. The individual loads maintain a 0.98 power factor.

The optimization problems are implemented in Matlab [99] and solved with Sedumi 1.21 [179].

Theorem 6.1 holds for all of the results shown, i.e., both the SDR and SOCR for the ℓ-DCOPF+S are exact. Furthermore, the SDR-OPF+S solutions have zero

[85] see Section 5.4.1
[86] see Section 6.4.2

duality gap. Simultaneous charging and discharging does not occur for any of the results reported in this study. The respective run times for the ℓ-DCOPF+S (as an SOCP) and DCOPF formulations are approximately 20 and 30 times faster than that of the ACOPF+S when solving on a 2.2 GHz Intel Core i7 with 16 GB 1600 MHz DDR3. For ease of reference, the case study results are designated by the problem formulation instead of the solution technique, i.e., DCOPF+S, ℓ-DCOPF+S, and ACOPF+S.

In order to evaluate the case study results, the marginal profits to ESS units is calculated as

$$\begin{aligned} \pi_n^{s,*} &:= \pi_n^{s^P,*}, \\ &:= \sum_{t\in\mathcal{T}} \lambda_{n,t}^* \left[r_{n,t}^{d,*} - r_{n,t}^{c,*} \right] - C_n^{s,1} r_{n,t}^{d,*} \end{aligned} \tag{6.37}$$

for each $n \in \mathcal{N}$; this performance metric is derived directly from Theorem 5.3 for profit maximizing storage allocation, as presented in Chapter 5. The dual variable $\lambda_{n,t}^*$ denotes the market-clearing energy price signal, i.e., the LMP, at a global optimum, and the primal variables $r_{n,t}^{d*}$ and $r_{n,t}^{c*}$ respectively denote the optimal charge and discharge rates of the ESS. The $\pi_n^{s,*}$ is based on the market-clearing outcome of the optimal solution for each time period and is a function of the revenues and costs to the storage operator at bus n over the operating cycle. Isolating the terms specific to the monetization capability of the storage operator, $\pi_n^{s,*}$ quantifies the economic value of the storage at bus $n \in \mathcal{N}$ in terms of the aggregate marginal profits over the

operating cycle.

The case study results demonstrate that these storage profits directly relate to the amount of storage allocated at each bus. In particular, higher values of $\pi_n^{s,*}$ are often associated with a larger storage allocation at bus n and the differences in values of $\pi_n^{s,*}$ amongst buses indicate the differential preference for storage allocation at one bus versus another. When $\pi_n^{s,*} = 0$ there is no storage placed at that bus. The following section describes all of the data and parameters used in the case studies.

6.5.1 Case Study Parameters and Data

The case studies are performed using the topology of the 14-bus IEEE benchmark system [177], originally illustrated in Figure 5.2 with the corresponding dataset summarized in Section 5.7 (excluding the MVA line capacity constraints).

6.5.2 Case I: 15% Wind and No Transmission Constraints

The test grid in Figure 5.2 is simulated for the first case study; in this simulation there are no transmission constraints as well as a 15% wind penetration, which is distributed evenly between wind farms at buses 1 and 2. The optimal system costs are \$159,524.05 in the DCOPF+S, \$172,044.39 in the ℓ-DCOPF+S, and \$170,368.64 in the ACOPF+S results. Table 6.1 summarizes the resulting storage allocation and $\pi_n^{s,*}$ based on the DCOPF+S, ℓ-DCOPF+S, and ACOPF+S storage integration models. These results show that failing to account for the real power losses can have

	Approximations				Full	
	DCOPF+S		ℓ-DCOPF+S		OPF+S	
Bus	c_n	$\pi_n^{s,*}$	c_n	$\pi_n^{s,*}$	c_n	$\pi_n^{s,*}$
1	7.1	19.73	0.03	0.11	0	0
2	7.1	19.73	1.9	12.42	1	6.45
3	7.1	19.73	37	156.62	37.1	150.96
4	7.1	19.73	10.7	47.82	12.1	52.92
5	7.1	19.73	0.1	0.67	0	0
6	7.1	19.73	0.2	0.78	0	0
7	7.1	19.73	1.5	6.52	0.2	1.10
8	7.1	19.73	1.5	6.44	0.2	1.01
9	7.1	19.73	1.1	4.56	1.1	5.31
10	7.1	19.73	3.6	15.05	4.6	18.24
11	7.1	19.73	0.4	1.58	0.1	0.35
12	7.1	19.73	3.4	13.82	4.0	15.55
13	7.1	19.73	13.0	53.03	13.6	53.25
14	7.1	19.73	25.5	103.99	26.2	102.96
Total	100	276.22	100	423.40	100	408.10

Table 6.1: The per bus ESS capacity c_n (in MW/30-min) and marginal profits $\pi_n^{s,*}$ (in \$) for the *baseline* scenario (15% wind and no transmission constraints).

a significant impact on the accuracy of the approximation model. More specifically, the DCOPF+S strategy equally distributes the ESS units throughout the network, whereas both the ℓ-DCOPF+S and ACOPF+S solutions place the majority of the ESS units at buses 3 and 14. Unlike the ℓ-DCOPF+S and ACOPF+S, the linear constraint set of the DCOPF+S does not capture the nonlinear relationship between the marginal storage capacity and the marginal profits, i.e., contrary to the linear DCOPF where $\pi_n^{s,*}/c_n$ is equivalent for all $n \in \mathcal{N}$. Figure 6.2 plots a sensitivity analysis to demonstrate the affect of decreasing line resistances r (i.e., decreasing real power losses) on the storage operator profits per bus; the results at $1r$ resistance correspond to the ℓ-DCOPF+S baseline reported in Table 6.1 and the results at

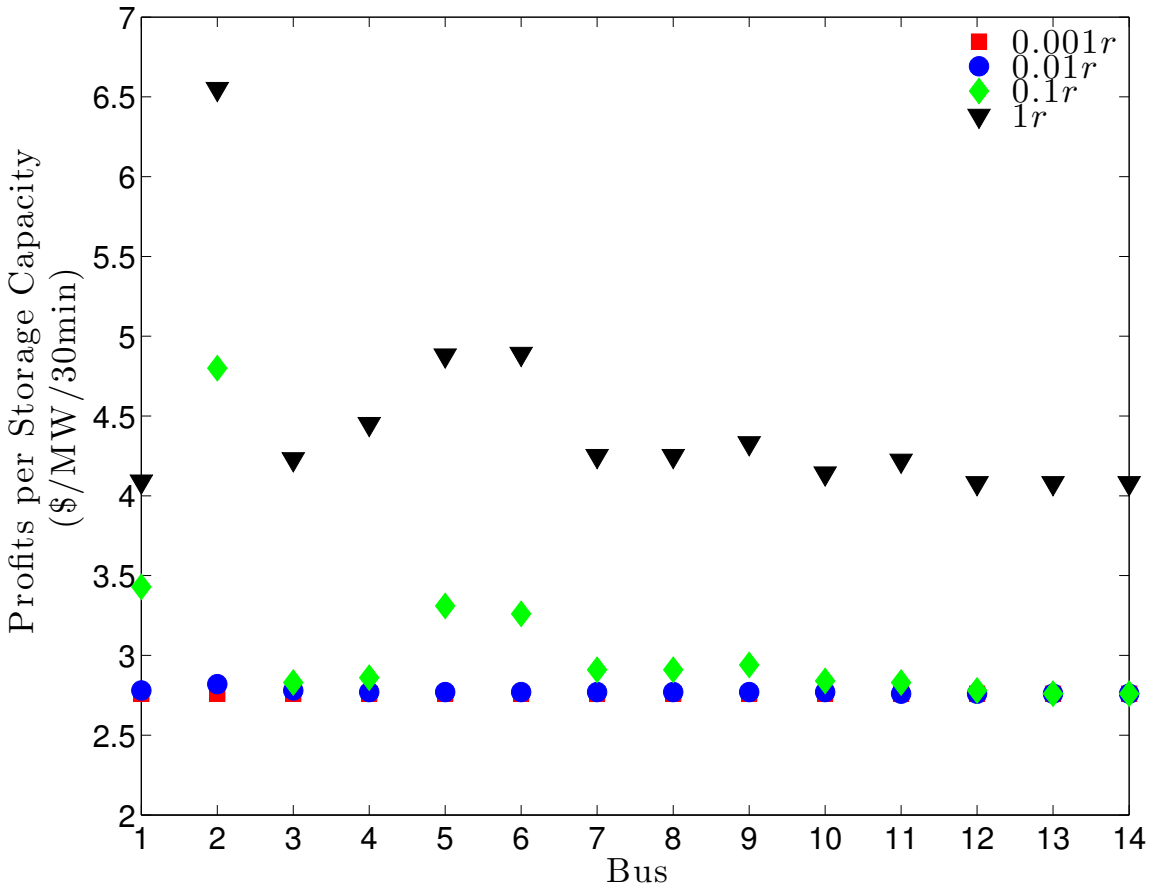

Figure 6.2: The profits per storage capacity at each bus is plotted for various multipliers on the line resistance r on all lines in the ℓ-DCOPF+S. Note that the marginal profits for the $0.001r$ results in negligible real power flow losses in the ℓ-DCOPF+S and therefore are similar to that of the DCOPF+S.

$0.001r$ resistance resemble the DCOPF+S results reported in Table 6.1 because the losses are negligible. Furthermore, Figure 6.2 illustrates that the marginal profits are highest at bus 2 for the baseline case in the ℓ-DCOPF+S. However the ℓ-DCOPF+S does not result in the exact same outcome as the ACOPF+S, which has additional nonlinear constraints on the nodal voltage limits as well as a coupling between the real and reactive flows on the network. Figures 6.3 and 6.4 demonstrate that although

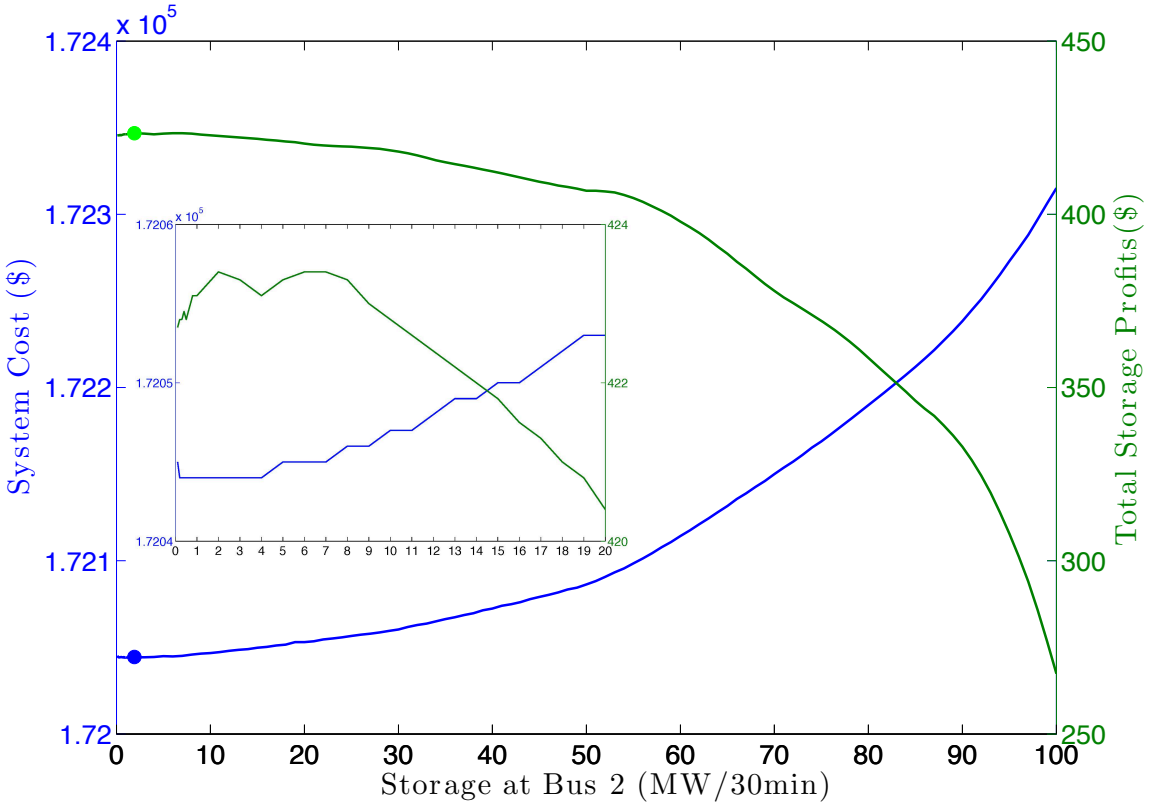

Figure 6.3: For the ℓ-DCOPF+S, the system cost plotted on the left axis and the total storage profits on the right axis for different storage allocations at bus 2 between 0.1 to 100 MW/30-min; the marker denotes the optimal solution reported where 1.9 MW/30-min of storage capacity are allocated at bus 2. Note that the inlaid graph illustrates that the highest profits for the storage operator are obtained at 1.9 MW/30-min at bus 2, which corresponds to the lowest system costs. Furthermore, there appears to be near optimal solutions, i.e. equivalent costs for allocating approximately 1 to 4 MW/30-min of storage capacity at bus 2 for the system cost rounded to the first decimal place.

there are nearly optimal solutions to the lowest system costs, the highest total storage profit occurs at the optimal solution reported here. This numerical result supports the theoretical findings as presented in equation (6.37) and originally proved in Theorem 5.3 for profit maximizing storage allocation.

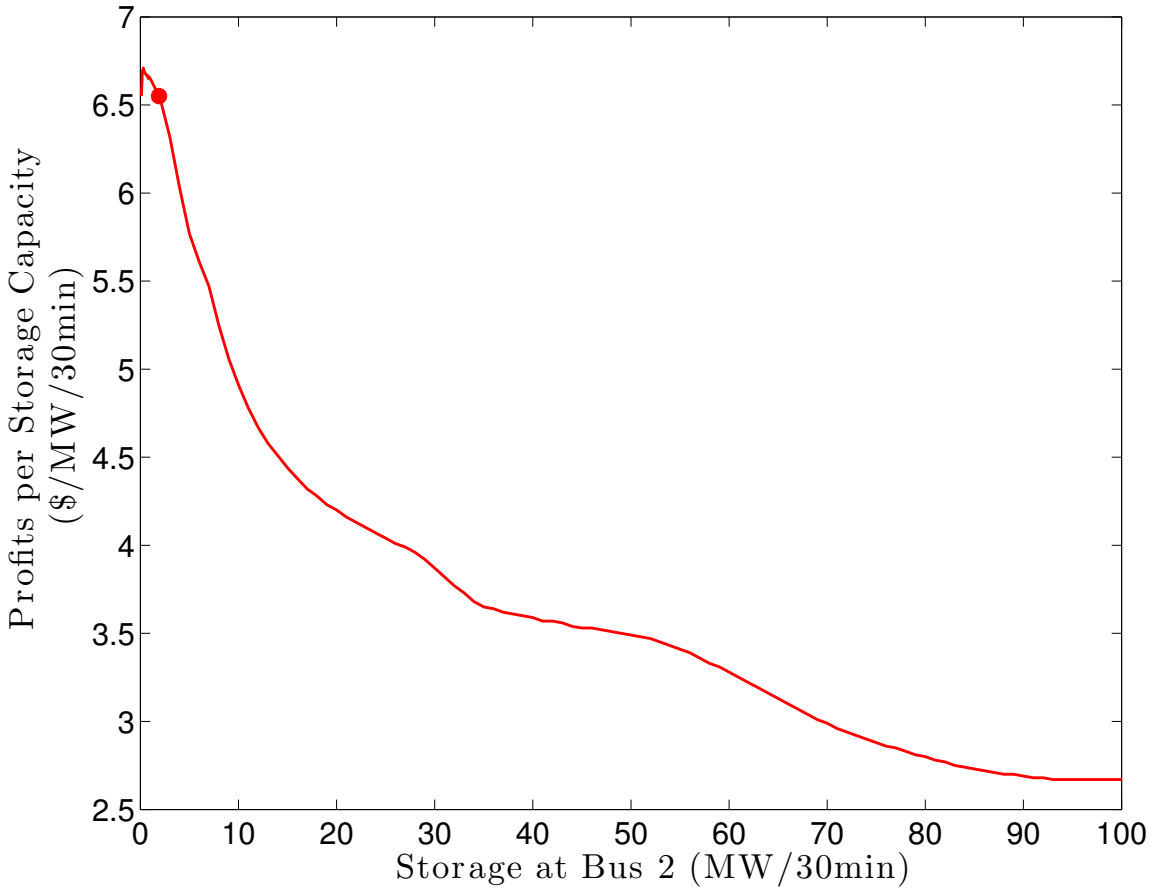

Figure 6.4: For the ℓ-DCOPF+S, the profits per storage capacity ($\pi_n^{s,*}/c_n$) at bus 2. Although $\pi_n^{s,*}/c_n$ is higher when the storage capacity at bus 2 is closer to zero, the overall profits, as illustrated in the inlay of Figure 6.3, are highest at the optimal solution (as denoted by the marker) where 1.9 MW/30-min of storage capacity is allocated at bus 2.

Furthermore, the results of the DCOPF+S greatly underestimate the value of storage when the cost drivers of the LMP are the marginal unit cost and network losses, where congestion costs are zero; since the DCOPF+S model does not include the network losses into its LMP calculation, it fails to account for the additional power dispatch requirements.

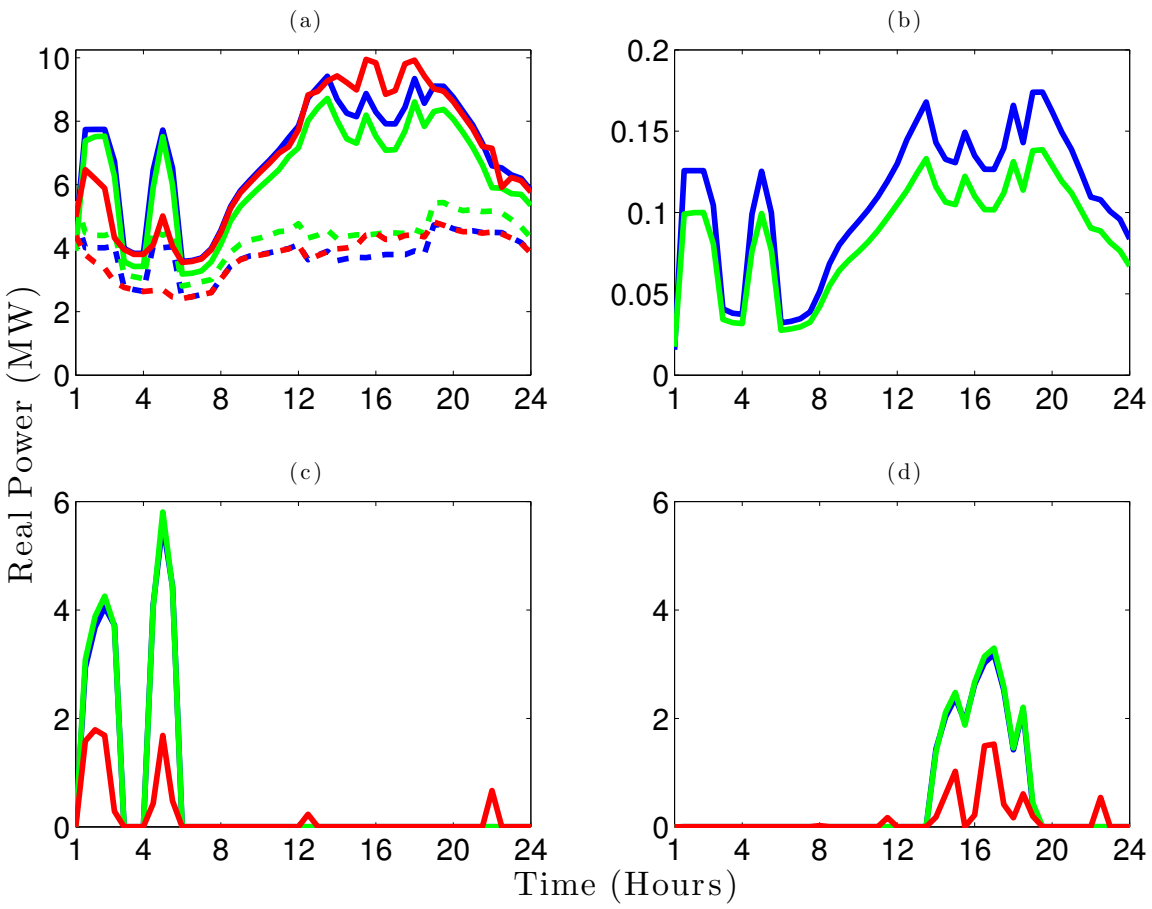

Figure 6.5: In all panels, the DCOPF+S, ℓ-DCOPF+S and ACOPF+S results are respectively shown in red, blue and green lines. (a) The real power flows (including losses) to bus 14, where the solid line denotes flow from bus 9 to 14 and the dashed line denotes flow from bus 13 to 14. (b) The total losses aggregated across lines 17 and 20. The DCOPF+S model is not plotted because there are no losses. (c) ESS charging and (d) ESS discharging at bus 14.

For example, Figure 6.5 shows the real power transfers, total real power losses, and storage charging and discharging observed at bus 14.[87] The upper left panel illustrates that the real power transfers obtained by the ℓ-DCOPF+S (blue lines) and ACOPF+S

[87]The parameters for line 17 on bus pair (9,14) are $g_{17} = 1.4238$ and $b_{17} = -3.0290$, and for line 20 on bus pair (13,14) are $g_{20} = 1.1370$ and $b_{20} = -2.3152$, respectively.

(green lines) models are similar in form but not exact in magnitude. However, the real power transfers obtained by the DCOPF+S (red lines) model are overall less accurate than the ℓ-DCOPF+S. The upper right panel of Figure 6.5 indicates that the ℓ-DCOPF+S (blue) slightly overestimates the total real power losses as compared to the ACOPF+S (green) on all of the lines connected to bus 14; the average losses are 1.05% on line 17 and 0.78% on line 20 in the ℓ-DCOPF+S results and the average losses are 0.82% on line 17 and 0.74% on line 20 in the ACOPF+S results. The lower panels plot the real power charge and discharge dynamics of the ESS units at bus 14.

	Approximations				Full	
	DCOPF+S		ℓ-DCOPF+S		OPF+S	
Bus	c_n	$\pi_n^{s,*}$	c_n	$\pi_n^{s,*}$	c_n	$\pi_n^{s,*}$
1	34.4	218.53	45.1	246.25	45.1	245.03
2	20.9	177.96	21.6	137.92	21.6	122.48
3	19.7	75.29	9	10.72	1.9	5.11
4	6.3	33.2	5.2	25.70	8.1	29.22
5	0	0	0	0	0	0
6	0	0	1.0	4.81	1.4	5.79
7	5.2	28.76	4.1	16.17	6	22.72
8	5.2	28.76	4.1	16.17	2.5	9.47
9	4.3	25.09	0	0	0	0
10	3	19.87	0.1	0.34	0.1	0.17
11	0	0	0.1	0.40	0.1	0.29
12	0	0	0.7	2.82	0.8	2.88
13	0	0	1.9	7.24	1.9	6.88
14	0.9	6.09	7	19.45	10.5	27.74
Total	100	613.55	100	487.99	100	477.78

Table 6.2: The per bus ESS capacity c_n (in MW/30-min) and profit $\pi_n^{s,*}$ (in \$) for Case II: a transmission constrained system with 15%-wind penetration.

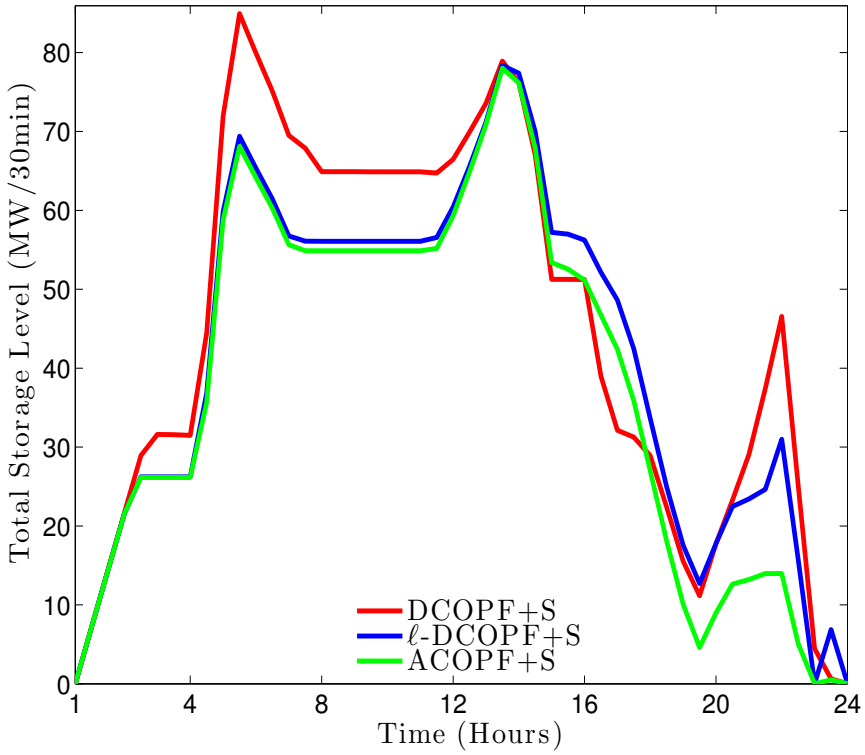

Figure 6.6: The aggregate energy storage level for all ESS installations across the network. In aggregate the ESS units cycle between charging and discharging in order to meet the demand, which peaks in hours 17 and 22.

6.5.3 Case II: 15% Wind and Binding Transmission Constraints

The second case study uses the same conditions presented as in Case I but also includes the following transmission line capacity constraints: $\overline{P}_k = 50$ MW for the lines between bus pairs $(1,2),(1,5),(2,3)$, and $(2,4)$; $\overline{P}_k = 25$ MW for the lines between bus pairs $(6,13)$ and $(9,14)$; and $\overline{P}_k = 7$ MW for the line between bus pairs $(12,13)$. The optimal system costs are \$193,350.78 for the DCOPF+S, \$201,453.52 for the ℓ-DCOPF+S, and \$201,108.43 for the ACOPF+S.

Table 6.2 shows the profits, $\pi_n^{s,*}$ and the ESS units allocated at each bus from sim-

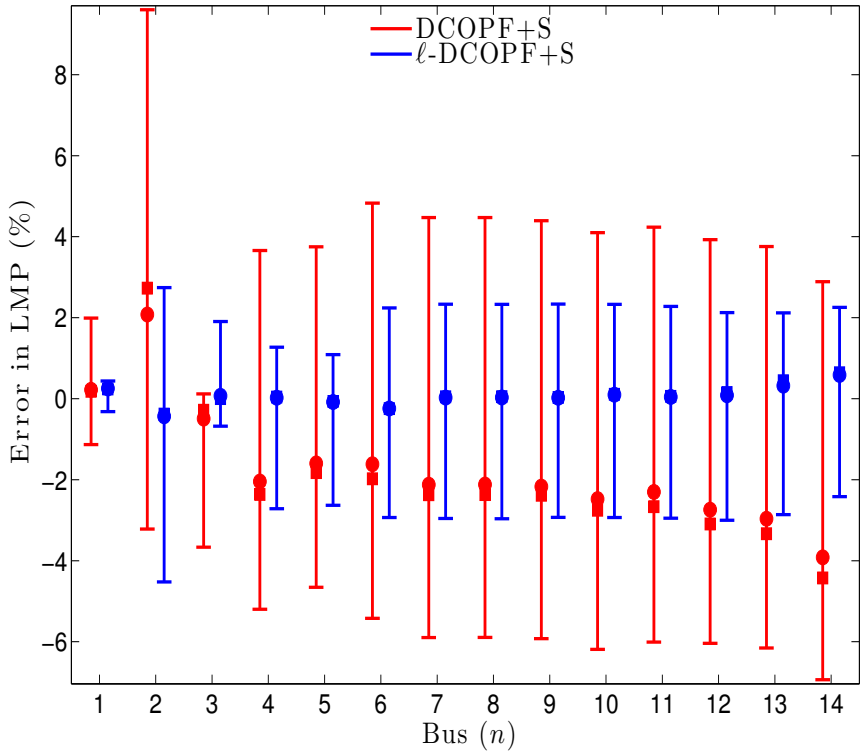

Figure 6.7: The LMP error statistics at each bus, where ACOPF+S is the baseline. The whisker plot shows the minimum and maximum of the LMP range at each node, along with the median (square) and mean (circle).

ulations of this system using the three different formulations. In general, the majority of the storage capacity is optimally integrated at buses 1, 2, and 3, i.e., 75% in the DCOPF+S solution, 75.7% in the ℓ-DCOPF+S solution, and 68.6% in the ACOPF+S solution. Again, when compared to the ACOPF+S solution the ℓ-DCOPF+S provides more accurate ESS allocation and profit estimates than the DCOPF+S. In particular, the DCOPF+S solution overestimates the marginal profits of storage by 28.4% relative to the ACOPF+S, whereas the ℓ-DCOPF+S only overestimates this quantity by 2.1%. Figure 6.6 demonstrates that the DCOPF+S solution also overestimates the

aggregate energy arbitrage potential of the system, which accounts for the increased profits reported in Table 6.2. The DCOPF+S model appears to significantly overestimate the value of energy storage when there are line limits; the DCOPF+S assumes that there is more line capacity available for real power transfers because network losses are not modeled (i.e., there is a perceived higher transfer efficiency than the actual transfer capabilities). This overestimation leads to suboptimal storage siting and dispatch strategies. Furthermore, the LMP error for bus $n \in \mathcal{N}$ at time period

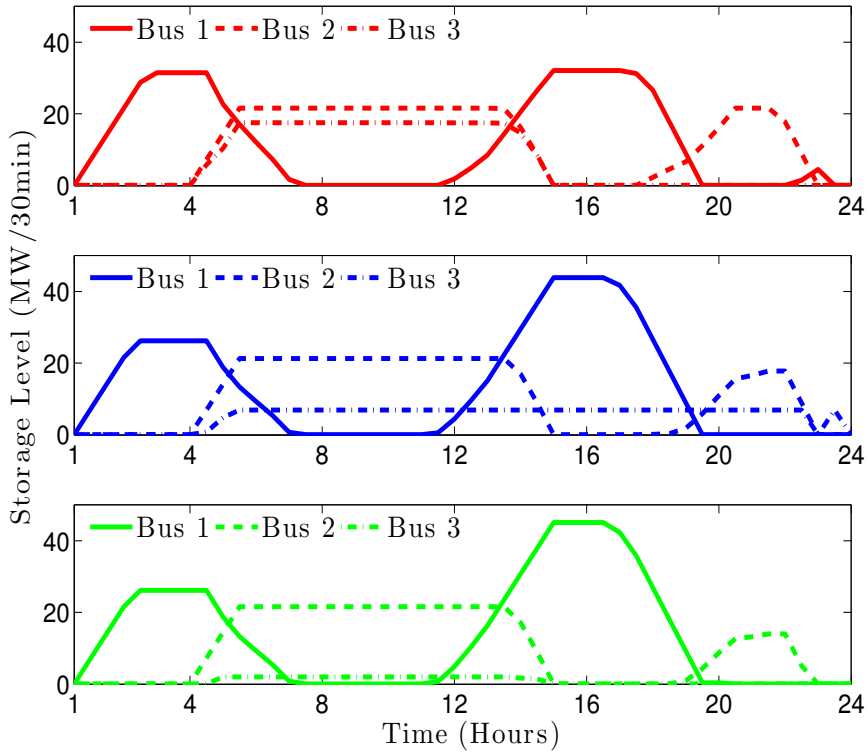

Figure 6.8: The storage level at buses 1, 2, and 3 for the DCOPF+S (red), ℓ-DCOPF+S (blue), and ACOPF+S (green).

$t \in \mathcal{T}$ for the two approximate models is calculated as

$$\left(\lambda_{n,t}^{*,ref} - \lambda_{n,t}^{*,ac}\right) / \lambda_{n,t}^{*,ac}, \tag{6.38}$$

where $\lambda_{n,t}^{*,ref}$ refers to the dual variable $\lambda_{n,t}^{*}$ from either the DCOPF+S or ℓ-DCOPF+S solution, respectively, and $\lambda_{n,t}^{*,ac}$ refers to the ACOPF+S solution. Figure 6.7 illustrates that the LMP error is higher for the DCOPF+S solution because real power losses are not accounted for in the physical constraints.

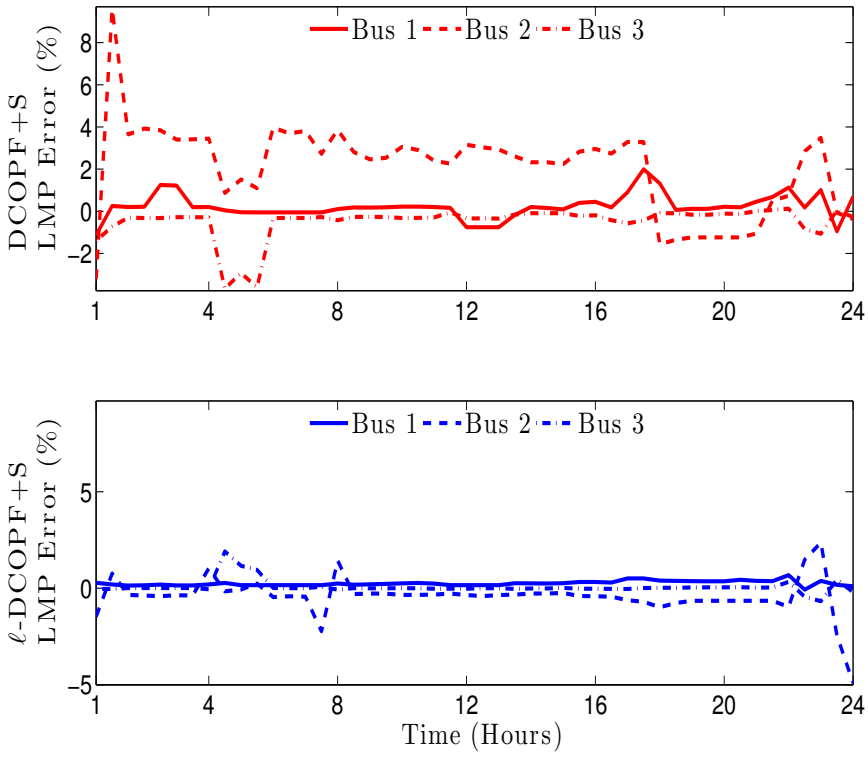

Figure 6.9: The error in LMP estimates, as calculated in (6.38), at buses 1, 2, and 3 where the ACOPF+S solution is the baseline.

Furthermore, the inaccuracies in optimal storage integration do not simply corre-

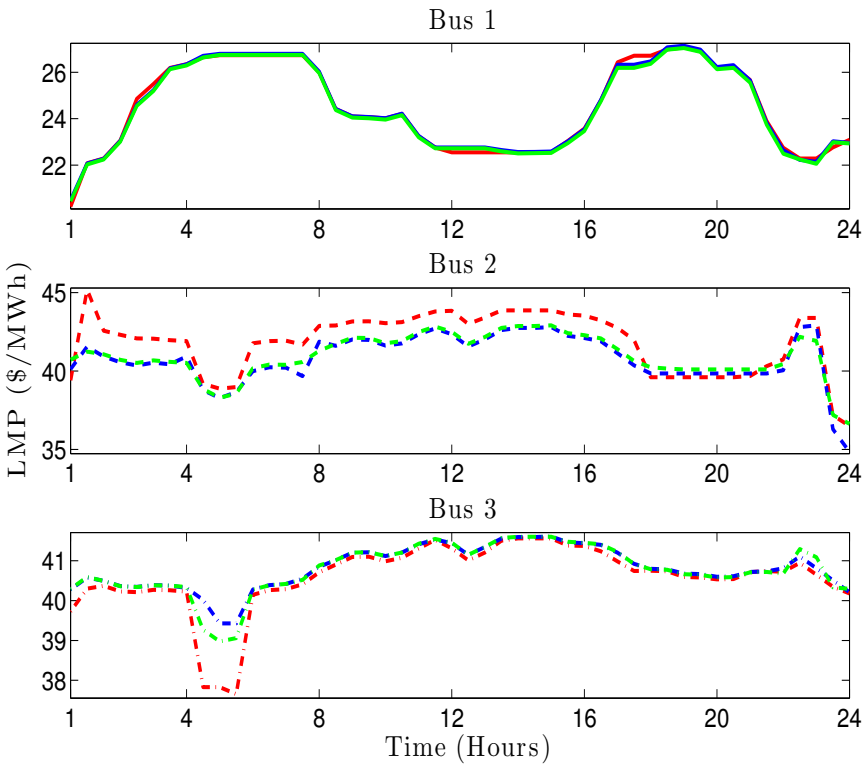

Figure 6.10: The LMP at buses 1, 2, and 3 (top to bottom panel) for the DCOPF+S (red), ℓ-DCOPF+S (blue), and ACOPF+S (green).

spond to the magnitude of LMP errors. Rather this outcome is amplified by when and where such LMP errors occur, and whether these LMP errors result in an over- or underestimation. Figures 6.8 and 6.9 illustrate the storage level and LMP errors specifically in the subnetwork with high storage integration, i.e., the subnetwork of buses 1, 2, and 3, for the three solutions. Figure 6.8 demonstrates similar trends in the storage levels at these three buses except for the ESS unit at bus 3 in the DCOPF+S solution. Figure 6.9 demonstrates that for the DCOPF+S solution the LMP values are highly underestimated during the hours that the ESS at bus 3 is charging, i.e., it is cheaper to charge in the DCOPF+S model than in the other mod-

els during the off-peak hours 4 to 6. Although the LMP errors at bus 2 are more persistent than the LMP errors at bus 3 in the DCOPF+S model, as shown in Figure 6.9, the DCOPF+S continually overestimates the LMPs at bus 2 during critical hours for both charging and discharging, as shown in Figure 6.10; this persistent overestimation does not lead to advantageous increases in the value of energy arbitrage at bus 2. However the underestimation of LMPs at bus 3 that is mainly isolated to hours 4 to 6, as shown in Figure 6.10, creates an advantageous deviation for energy arbitrage in the DCOPF+S model because of the cheaper prices paid to charge the ESS unit at bus 3. This energy arbitrage potential is artificial because it is an artifact of the lossless nature of the DCOPF+S model. Moreover, the outcome in the DCOPF+S is unrealistic because the real power losses must be accounted for through an increase in dispatch and adjustment in market settlements.

6.6 Conclusion

This study proposes a novel multi-period ℓ-DCOPF+S model to investigate the role of real power losses in OPF-based ESS integration. The problem can be solved using either the SDP or SOCP reformulation to model the quadratic real power loss approximations derived from the standard ACOPF problem. Although the SOCP is solved in this study, the theoretical results demonstrate that both of these convex relaxations provide an exact lower bound to the ℓ-DCOPF+S problem. This analysis also proves conditions that guarantee unimodal storage operations for a linear storage

model with round trip efficiencies included.

Case studies using the ℓ-DCOPF+S model indicate that it more accurately approximates the ACOPF+S results than a DCOPF+S model. In particular, the DCOPF+S model can significantly overestimate the value of energy storage when there are line limits because this approach assumes more line capacity available for real power transfers since network losses are not modeled (i.e., there is a perceived higher transfer efficiency than the actual transfer capabilities), which leads to sub-optimal storage siting and dispatch strategies. Furthermore inaccuracies in optimal storage integration can result from advantageous deviations in the LMP errors. The improved predictions of the ℓ-DCOPF+S formulation are therefore directly related to the fact that approximating the correct OPF-based results requires accurate prediction of the actual LMPs.

7 Conclusions

This chapter summarizes the work presented in this dissertation including a summary of the main contributions, limitations of the current work, and future extensions.

7.1 Main Contributions

The alternating current optimal power flow (ACOPF) problem, also referred to as the optimal power flow (OPF) problem, is at the heart of improvements in electricity market design. The simultaneous co-optimization of real and reactive power dispatch improves operating efficiency and incorporates reactive power compensation in order to provide system voltage control that enables more efficient delivery and utilization of real power. Unfortunately, solving this problem within the required time limits for the day-ahead, intra-day, and real-time markets is difficult because the ACOPF formulation is a nonconvex, nonlinear optimization problem, which is known to be NP-hard [2,3]. Therefore current security-constrained economic dispatch (SCED) and security-constrained unit commitment (SCUC) methods applied in practice oversimplify the physical problem and require operator intervention to address issues that are unrepresented in current market software.

Operator intervention to address reliability issues unnecessarily alters settlement prices by introducing uplift payments and produces suboptimal solutions [13, 15]. A report to Congress prepared by the U.S. Department of Energy (DOE) states: "the technical quality of current economic dispatch tools–software, data, algorithms, and assumptions–deserves scrutiny. Any enhancements to these tools will improve the reliability and affordability of the nation's electricity supplies" [20]. Reports by the Federal Energy Regulatory Commission (FERC) concluded that since the cost of upgrading existing independent system operator (ISO) market software is less than $10 million dollars [6] and small increases in efficiency of dispatch can be measured in billions of dollars per year, the potential benefit-to-cost ratio of better market software is at least 100 fold [21]. This dissertation work is motivated by this premise and the main contributions are briefly summarized as follows.

1. *The IV-ACOPF Formulation:* The IV-ACOPF formulation has a different mathematical representation from the canonical ACOPF formulations but is provably equivalent. The canonical ACOPF formulations compute the nonlinear and nonconvex apparent power flows, whereas the IV-ACOPF computes linear current flows based on the current injections method and then balances the nodal power injections and withdrawals through nonconvex constraints that relate the bilinear terms within each node. This work was originally published in [22].

2. *The Successive Linear Programming (SLP) IV-ACOPF Algorithm*: The SLP

IV-ACOPF algorithm is proposed to solve the IV-ACOPF formulation. This algorithm can be solved with commercial linear programming (LP) solvers, which are the industry standard for ISO market software. Current ISO market software performs an iterative algorithm but only checks for AC feasibility whereas this approach simultaneously co-optimizes real and reactive power dispatch subject to the operational and physical constraints of the AC network. The SLP algorithm can be readily extended and integrated into more complex decision processes that are more representative of actual practices, especially unit commitment (UC). This work demonstrates an acceptable quality of convergence to a best-known solution and linear scaling of computational time in proportion to network size. Moreover, the time complexity of the SLP algorithm outperforms that of the nonlinear programming (NLP) commercial solvers for the full range of test networks. As a result, the SLP algorithm is expected to outperform the NLP solvers tested, i.e., IPOPT and KNITRO, on larger scale networks. Furthermore, the SLP algorithm could be applied in parallel with both Gurobi and CPLEX from various starting points, which may further improve the reported linear time complexity. This work was originally published in [22].

3. *The Outer Approximation (OA) Algorithm for the UC with ACOPF Problem:* The UC with ACOPF constraints in this problem are solved to simultaneously co-optimize real and reactive power commitment and dispatch, whereas prior

research solves the unit commitment with alternating current (AC) feasibility.[88] The OA algorithm extends the SLP IV-ACOPF algorithm and leverages commercial MILP solvers that are currently used in the ISO market software. This work is the first study known to analyze the economic and operational impact of more accurate ACOPF constraint modeling on the UC problem when compared to copperplate and direct current optimal power flow (DCOPF) constraint modeling approaches. The results indicate considerable divergence between the market settlements and the stability and reliability requirements when overly approximated network models are assumed. The computational speeds for both the ACOPF and the ACOPF for residual unit commitment (RUC) approaches are promising: the ACOPF approach is 5–15 times slower than the DCOPF approach and incorporating the RUC to the DCOPF approach is 1.5–5 times slower than the DCOPF alone. This work was originally published in [23].

4. *Energy Storage for Transmission System VAr Support: Trade-offs Between Grid Benefits and Storage Operator Profit:* This is the first known formulation to model energy storage system (ESS) integration when distributed energy storage is used to provide VAr support in addition to traditional grid-scale storage services. The ACOPF with storage model is formulated and then the semidefinite relaxation (SDR) proposed in [24] is applied; the SDR is a convex problem for which theoretical properties can be derived under strong duality [25]. The-

[88] excluding the solution technique by Bai and Wei [127] which also considers the ACOPF constraints but in a SDP problem with a 0-1 heuristic rounding strategy

oretical results prove that optimal storage integration in a purely competitive market maximizes the storage operator's marginal profit, which is dual to minimizing system costs. The storage operator's marginal profit is demonstrated to be a function of the services provided and the locational marginal prices in AC networks. The analysis demonstrates that energy storage can make substantially higher profits by providing not only power and energy services but also reactive power compensation. This study also compares payments based on the nodal prices for reactive power to the remuneration approaches in current market practice. The results demonstrate that there may be disincentive for storage operators to provide this service if it is not adequately paid for in the market; furthermore, most storage technologies would not qualify for reactive capability rates as specified by current tariffs. The results in this study highlight a tight yet understated relation between current market design and the financial viability of large-scale storage integration in AC power systems. This work is an extension of the conference proceedings [26].

5. *Exact Convex Relaxations of an OPF Approximation with Losses:* A DCOPF with losses formulation is proposed in order to analyze how real power losses improve the DCOPF approach for optimal storage integration in AC networks when storage is remunerated for power and energy services but not for reactive power compensation, as is the case for most ESS installations in current market design. This work incorporates quadratic loss approximations derived from the

AC power flows (ACPF); the resulting formulation of the DCOPF with losses and storage model is a nonconvex quadratically constrained quadratic program (QCQP). Both a SDR and a second-order cone relaxation (SOCR) are proposed to reformulate the original QCQP as a convex problem. The main theoretical results prove that both of these relaxations provide an exact lower bound to the original QCQP. The work demonstrates that costs due to real power losses are a key component of the locational marginal price (LMP) and therefore are critical in determining optimal ESS dynamics and allocation. This work can be extended to model losses exactly for a variety of other applications. This work is an extension of the conference proceedings [27].

7.2 Publications

The following peer-reviewed journal and conference publications are directly related to this dissertation:

- A. Castillo, C. Laird, C. A. Silva-Monroy, J.-P. Watson, and R. P. O'Neill, "The unit commitment problem with AC optimal power flow constraints," *IEEE Transactions on Power Systems*, DOI: 10.1109/TPWRS.2015.2511010, 2016. (Chapter 4)

- A. Castillo, P. Lipka, J.-P. Watson, S. Oren, and R. P. O'Neill, "A successive linear programming approach to solving the IV-ACOPF," *IEEE Transactions on Power Systems*, DOI: 10.1109/TPWRS.2015.2487042, 2015. (Chapter 3)

- A. Castillo and D. F. Gayme, "Grid-scale energy storage applications in renewable energy integration: A survey," *Energy Conversion and Management*, vol. 87, pp. 885 – 894, 2014. (Chapters 5 and 6)

- A. Castillo, X. Jiang, and D. Gayme, "Lossy DCOPF for optimizing congested grids with renewable energy and storage," in *Proceedings of the 2014 American Control Conference (ACC)*, Portland, OR, June 2014, pp. 4342 – 4347. (Chapter 6)

- A. Castillo and D. F. Gayme, "Profit maximizing storage allocation in power grids," in *Proceedings of the* 52^{nd} *IEEE Conference on Decision and Control (CDC)*, Firenze, Italy, Dec. 2013, pp. 429 – 435. (Chapter 5)

7.3 Future Research

The contributions of this dissertation address some of the key challenges in ACOPF research. Certain limitations in the above contributions as well as future directions of work can be explored through the following extensions:

- *A Successive Linear Programming Approach to Solving the IV-ACOPF*: In terms of algorithm development, investigating alternative merit functions[89] or incorporating a filter method[90] can avoid the pitfalls of the current penalty function approach in order to enforce more robust performance from any ini-

[89] see footnote 40
[90] see footnote 41

tialization. Incorporating such global convergence[91] properties could further improve both the computational performance and the convergence quality of this algorithm.

- *The Unit Commitment Problem with AC Optimal Power Flow Constraints*: Since the proposed OA method spends most of the computational time in the single iteration of the master problem, further improvements to the MILP and leveraging decomposition techniques for distributed, parallel optimization could lead to significant gains. For example, Feizollahi et al. [109] apply alternating direction method of multipliers[92] (ADMM) to the unit commitment problem whereas Sun et al. [201] apply ADMM to the ACOPF problem to solve meshed networks. Furthermore, a future study could compare the fidelity and computational performance of this approach to current market practices. However this would require access to the data and market software used by the system operators.

- *Energy Storage for Transmission System VAr Support: Trade-offs Between Grid Benefits and Storage Operator Profit*: The proposed framework can be extended to incorporate other valuable ESS services (e.g., regulation)[93] as well as further investigate market design for reactive power compensation. Another extension

[91] see footnote 32

[92] A decomposition-coordination procedure that blends the benefits of dual decomposition and augmented Lagrangian methods for constrained optimization in which the solutions to small local subproblems are coordinated to find a solution to a large global problem [200].

[93] see footnote 15

would be to perform a stochastic study that builds upon the fundamental results in this study in order to determine the expected value of ESS services under uncertainty over several realizations of demand and wind profiles. Given that incorporating storage has the effect of linking different time periods together, the dimensionality of the problem can make a stochastic approach more challenging. A third extension would be to investigate optimal ESS integration on the distribution level because the direct current power flow (DCPF) assumptions do not apply to low voltage networks and the reactive power compensation and voltage control in addition to the traditional storage services become increasingly important with significant penetrations of controllable loads and distributed energy resources.

- *The Role of Network Losses in Optimal Storage Allocation*: The proposed formulation can be extended to include both investment and operations decisions of the storage operator. Also, the current framework assumes a perfectly competitive market but a future extension might include strategic behavior of storage operators.[94] This framework could provide insight into optimal control and coordinated scheduling of geographically dispersed ESS units that constitute the same investment portfolio.

- *Market Implications of Optimal Power Flow with Controllable Network Elements*: Currently in review [202], this work incorporates into the IV-ACOPF

[94] ongoing research with Roderick Go, Sonja Wogrin, and Dennice F. Gayme

formulation models of variable tap transformers, phase shifters, line switching, and unified power flow controllers; this formulation is then solved with the SLP algorithm. This study indicates a substantial economic and operational value of such devices in the real-time markets especially when stability and reliability constraints become prohibitive. Furthermore, the study indicates that optimal placement of such devices is as important as optimal control. However, appropriate incentive structures are not in place and further extensions include proposing such market mechanisms.

- *Running a More Complete Market with the SLP IV-ACOPF*: Currently in review [203], in this work the SLP algorithm determines the market settlements and corresponding services when simultaneously co-optimizing real and reactive power dispatch. A preliminary result is that current market payments based on the DCOPF approach may not cover the marginal value of reactive power compensation or may misrepresent the value of voltage control as congestion rent. Furthermore, this work demonstrates how to adequately distribute the market settlements in such a way that the prices support the cost minimization solution as determined by the SLP algorithm.

Bibliography

[1] G. Morales-España, J. M. Latorre, and A. Ramos, "Tight and compact MILP formulation for the thermal unit commitment problem," *IEEE Trans. on Power Syst.*, vol. 28, no. 4, pp. 4897–4908, 2013.

[2] A. Verma, "Power grid security analysis: An optimization approach," Ph.D. dissertation, Columbia University, 2009.

[3] K. Lehmann, A. Grastien, and P. V. Hentenryck, "AC-feasibility on tree networks is NP-hard," *IEEE Trans. on Power Syst.*, vol. PP, no. 99, pp. 1–4, 2015.

[4] J. Carpentier, "Contribution a l'etude du dispatching economique," *Bull. Soc. Francaise Elect*, vol. 3, pp. 431–447, 1962.

[5] B. Stott and O. Alsaç. (2012) Optimal power flow: Basic requirements for real-life problems and their solutions. [Online]. Available: http://www.ieee.hr/_download/repository/Stott-Alsac-OPF-White-Paper.pdf

[6] R. P. O'Neill, T. Dautel, and E. Krall, "Recent ISO software enhancements and

future software and modeling plans," Federal Energy Regulatory Commission, Tech. Rep., 2011.

[7] F. Schweppes, M. Caramanis, R. Tabors, and R. E. Bohn, *Spot Pricing of Electricity*. Kluwer, 1988.

[8] A. J. Wood, B. F. Wollenberg, and G. B. Sheblé, *Power Generation, Operation and Control*. John Wiley & Sons, 2013.

[9] The Joint Board on Economic Dispatch for the Northeast Region, "Study and recommendations regarding security constrained economic dispatch (SCED) in the Northeast," Federal Energy Regulatory Commission Docket No. AD05-13-000, Tech. Rep., 2006.

[10] [Online]. Available: http://www.iso-ne.com/markets-operations/markets/da-rt-energy-markets

[11] A. Mazer, *Electric Power Planning for Regulated and Deregulated Markets*. John Wiley & Sons, 2007.

[12] *Reliability Responsibilities and Authorities TOP-001-1*, North American Electric Reliability Corporation, 2007.

[13] E. Nicholson, "Operator-initiated commitments in RTO and ISO markets," Federal Energy Regulatory Commission, Tech. Rep., 2014.

[14] [Online]. Available: http://www.iso-ne.com/participate/support/glossary-acronyms

[15] W. Sauer, "Uplift in RTO and ISO markets," Federal Energy Regulatory Commission, Tech. Rep., 2014.

[16] M. Ilic, S. Cvijic, J. H. Lang, and J. Tong, "Operating beyond today's PV curves: Challenges and potential benefits," in *Proc. of the IEEE PES General Meeting*, 2015.

[17] *CAISO eTariff, § 34.11.*

[18] *NYISO Manual 12 Transmission and Dispatching Operations, § 5.7.4.*

[19] *Intra-PJM Tariff, OATT, attach. K, § 3.2.3.*

[20] United States Department of Energy, "The value of economic dispatch," A Report to Congress Pursuant to Section 1234 of the Energy Policy Act of 2005, Tech. Rep., 2005.

[21] M. B. Cain, R. P. O'Neill, and A. Castillo, "Optimal power flow papers: Paper 1. History of optimal power flow and formulations," Federal Energy Regulatory Commission, Tech. Rep., 2013.

[22] A. Castillo, P. Lipka, J.-P. Watson, S. Oren, and R. P. O'Neill, "A successive linear programming approach to solving the IV-ACOPF," *IEEE Trans. on Power Syst.*, DOI: 10.1109/TPWRS.2015.2487042, 2015.

[23] A. Castillo, C. Laird, C. A. Silva-Monroy, J.-P. Watson, and R. P. O'Neill, "The unit commitment problem with AC optimal power flow constraints," *IEEE Trans. on Power Syst.*, DOI: 10.1109/TPWRS.2015.2511010, 2016.

[24] J. Lavaei and S. H. Low, "Zero duality gap in optimal power flow problem," *IEEE Trans. on Power Syst.*, vol. 27, no. 1, pp. 92–107, 2012.

[25] D. F. Gayme and U. Topcu, "Optimal power flow with large-scale storage integration," *IEEE Trans. on Power Syst.*, vol. 28, no. 2, pp. 709–717, 2013.

[26] A. Castillo and D. F. Gayme, "Profit maximizing storage allocation in power grids," in *Proc. of the 52nd IEEE Conf. on Decision and Control*, Firenze, Italy, Dec. 2013, pp. 429 – 435.

[27] A. Castillo, X. Jiang, and D. F. Gayme, "Lossy DCOPF for optimizing congested grids with renewable energy and storage," in *Proc. of the 2014 American Control Conf.*, Portland, OR, June 2014, pp. 4342 – 4347.

[28] G. Andersson, "Modelling and analysis of electric power systems," Eidgenössische Technische Hochschule Zürich, Tech. Rep., 2008.

[29] D. Bienstock, *Electrical Transmission System Cascades and Vulnerability: An Operations Research Viewpoint*. Society for Industrial and Applied Mathematics, 2016.

[30] A. Gómez-Expósito, A. J. Conejo, and C. Canizares, *Electric Energy Systems: Analysis and Operation*. CRC Press, 2008.

[31] J. D. Glover, M. S. Sarma, and T. J. Overbye, *Power System Analysis and Design*. Thomson Learning, 2008.

[32] D. P. Kothari and I. J. Nagrath, *Modern Power Systems Analysis*. Tata McGraw Hill, 2003.

[33] H. H. Happ, "Optimal power dispatch–a comprehensive survey," *IEEE Trans. on Power Apparatus and Syst.*, vol. PAS-96, no. 3, pp. 841–844, 1977.

[34] L. Kirchmayer, *Economic Operation of Power Systems*. Wiley and Sons, 1958.

[35] A. Sasson and F. Jaimes, "Digital methods applied to power flow studies," *IEEE Trans. on Power Apparatus and Syst.*, vol. PAS-86, no. 7, pp. 860–867, 1967.

[36] J. Ward and H. Hale, "Digital computer solution of power flow problems," *IEEE Trans. on Power Apparatus and Syst.*, vol. 75, no. 3, pp. 398–404, 1956.

[37] J. Peschon, D. Piercy, W. Tinney, O. Tveit, and M. Cuénod, "Optimum control of reactive power flow," *IEEE Trans. on Power Apparatus and Syst.*, vol. PAS-87, no. 1, pp. 40–48, 1968.

[38] B. Stott, "Review of load-flow calculation methods," *Proceedings of the IEEE*, vol. 62, no. 7, pp. 916–929, 1974.

[39] C. A. Floudas, *Nonlinear and Mixed-Integer Optimization: Fundamentals and Applications*. Oxford University Press, 1995.

[40] R. Squires, "Economic dispatch of generation directly from power system voltages and admittances," *IEEE Trans. on Power Apparatus and Syst.*, vol. PAS-79, no. 3, pp. 1235–1244, 1960.

[41] J. Nocedal and S. Wright, *Numerical Optimization*. Spring Science and Business Media, 2006.

[42] I. A. Hiskens and R. J. Davy, "Exploring the power flow solution space boundary," *IEEE Trans. on Power Syst.*, vol. 16, no. 3, pp. 389–395s, 2001.

[43] J. Carpentier, "Optimal power flows," *International Journal of Electrical Power and Energy Systems*, vol. 1, no. 1, pp. 3–15, 1979.

[44] M. Huneault and F. D. Galiana, "A survey of the optimal power flow literature," *IEEE Trans. Power Syst.*, vol. 6, no. 2, pp. 762–770, 1991.

[45] A. Castillo and R. P. O'Neill, "Survey of approaches to solving the ACOPF," Federal Energy Regulatory Commission, Tech. Rep., 2013.

[46] S. H. Low, "Convex relaxation of optimal power flow, part I: Formulations and equivalence," *IEEE Trans. Control Netw. Syst.*, vol. 1, no. 1, pp. 15–27, 2014.

[47] ——, "Convex relaxation of optimal power flow, part II: Exactness," *IEEE Trans. Control Netw. Syst.*, vol. 1, no. 2, pp. 177–189, 2014.

[48] J. Momoh, M. El-Hawary, and R. Adapa, "A review of selected optimal power flow literature to 1993. part I: Nonlinear and quadratic programming approachs," *IEEE Trans. Power Syst.*, vol. 14, no. 1, pp. 96–104, 1999.

[49] ——, "A review of selected optimal power flow literature to 1993. part II: Newton, linear programming, and interior point methods," *IEEE Trans. Power Syst.*, vol. 14, no. 1, pp. 105–111, 1999.

[50] S. Frank, I. Steponavice, and S. Rebennack, "Optimal power flow: A bibliographic survey I," *Energy Syst.*, vol. 3, pp. 221–258, 2012.

[51] ——, "Optimal power flow: A bibliographic survey II," *Energy Syst.*, vol. 3, pp. 259–289, 2012.

[52] X. Bai, H.Wei, K. Fujisawa, and Y.Wang, "Semidefinite programming for optimal power flow problems," *International Journal of Electrical Power and Energy Syst.*, vol. 30, no. 6-7, pp. 383–392, 2008.

[53] X.-F. Wang, Y. Song, and M. Irving, *Modern Power Systems Analysis.* Spring Science and Business Media, 2010.

[54] A. von Meier, *Electric Power Systems.* John Wiley & Sons, 2006.

[55] J. Arrillaga and C. P. Arnold, *Computer Analysis of Power Systems.* John Wiley & Sons, 1990.

[56] R. D. Zimmerman, C. E. Murillo-Sánchez, and R. J. Thomas, "MATPOWER: Steady-state operations, planning and analysis tools for power systems research and education," *IEEE Trans. on Power Syst.*, vol. 26, no. 1, pp. 12–19, 2011.

[57] L. L. Grigsby, *Power System Stability and Control*. CRC Press, 2012.

[58] E. Litvinov, T. Zheng, G. Rosenwald, and P. Shamsollahi, "Marginal loss modeling in LMP calculation," *IEEE Trans. on Power Syst.*, vol. 19, no. 2, pp. 880–888, 2004.

[59] W. Rosehart and J. Aguado, "Alternative optimal power flow formulations," in *14th Power Systems Computation Conference (PSCC)*, 2002.

[60] H. Dommel, W. Tinney, and W. Powell, "Further developments in Newton's method for power system applications," in *IEEE Winter Power Meeting*, vol. CP 161-PWR, no. 70, 1970.

[61] C. Coffrin, D. Gordon, and P. Scott, "The NICTA energy system test case archive," Optimisation Research Group, NICTA, Tech. Rep., 2015.

[62] P. Kundur, *Power System Stability and Control*. McGraw-Hill Professional, 1994.

[63] S. Leyffer and A. Mahajan, "Nonlinear constrained optimization: Methods and software," Argonne National Laboratory, Tech. Rep., 2010.

[64] C. M. Chin and R. Fletcher, "On the global convergence of an SLP-filter algorithm that takes EQP steps," *Mathematical Programming*, vol. A, no. 96, pp. 161–177, 2003.

[65] M. S. Bazaraa, H. D. Sherali, and C. M. Shetty, *Nonlinear Programming: Theory and Algorithms*. John Wiley & Sons, 2013.

[66] Gurobi Optimization, Inc., "Gurobi documentation: Release 5.6," 2014.

[67] IBM Corp., "CPLEX documentation: Release 12.4," 2014.

[68] K. Purchala, L. Meeus, D. V. Dommelen, and R. Belmans, "Usefulness of DC power flow for active power flow analysis," in *IEEE Power & Energy Society General Meeting*, 2005.

[69] Nathaniel J. Davis, Sr., "Order conditionally accepting tariff revisions and requiring compliance filing for docket nos. ER12-678-000 and ER12-679-000," Federal Energy Regulatory Commission, Tech. Rep., 2012.

[70] H. Liu, L. Tesfatsion, and A. Chowdhury, "Locational marginal pricing basics for restructured wholesale power markets," in *IEEE Power & Energy Society General Meeting*, 2009.

[71] W. F. Tinney and C. Hart, "Power flow solution by Newton's method," *IEEE Trans. Power Syst.*, vol. PAS-93, pp. 859–869, 1974.

[72] O. Alsaç and B. Stott, "Decoupled algorithms in optimal load flow calculation," in *IEEE Power Engineering Society 1975 Summer Meeting*, 1975.

[73] D. S. Kirschen and H. P. V. Meeteren, "MW/voltage control in a linear programming based optimal power flow," *IEEE Transactions on Power Systems*, vol. 3, no. 2, 1988.

[74] O. Alsaç, J. Bright, M. Prais, and B. Stott, "Further developments in LP-based optimal power flow," *IEEE Trans. on Power Syst.*, vol. 5, no. 3, 1990.

[75] J. Franco, M. J. Rider, M. Lavorato, and R. Romero, "A set of linear equations to calculate the steady-state operation of an electrical distribution system," in *2011 IEEE PES Conference on Innovative Smart Grid Technologies (ISGT Latin America)*, 2011, pp. 1–5.

[76] A. Mohapatra, P. Bijwe, and B. Panigrahi, "Efficient sequential non-linear optimal power flow approach using incremental variables," *IET Generation, Trans. & Distr.*, vol. 7, no. 12, pp. 1473–1480, 2013.

[77] C. Coffrin and P. V. Hentenryck, "A linear-programming approximation of AC power flows," University of Melbourne, Tech. Rep. arXiv:1206.3614v3, 2013.

[78] S. Boyd and L. Vandenberghe, *Convex Optimization*. Cambridge University Press, 2004.

[79] S. Bose, D. F. Gayme, S. H. Low, and M. K. Chandy, "Optimal power flow over

tree networks," in *Proc. of the 49th Annual Allerton Conf. on Communication, Control and Computing*, 2011.

[80] S. Sojoudi and J. Lavaei, "On the exactness of semidefinite relaxation for nonlinear optimization over graphs: Part II," in *IEEE 52nd Annual Conference on Decision and Control (CDC)*, 2013, pp. 1051–1057.

[81] D. Das, D. P. Kothari, and A. Kalam, "Simple and efficient method for load flow solution of radial distribution networks," *Elect. Power Energy Syst.*, vol. 17, no. 5, pp. 335–346, 1995.

[82] D. K. Molzahn and I. A. Hiskens, "Sparsity-exploiting moment-based relaxations of the optimal power flow problem," *IEEE Trans. on Power Syst.*, vol. 30, no. 6, pp. 3168–3180, 2015.

[83] C. Josz, J. Maeght, P. Panciatici, and J. C. Gilbert, "Application of the moment-SOS approach to global optimization of the OPF problem," *IEEE Trans. on Power Syst.*, vol. 30, no. 1, pp. 463–470, 2015.

[84] B. C. Lesieutre, D. K. Molzahn, A. R. Borden, and C. L. DeMarco, "Examining the limits of the application of semidefinite programming to power flow problems," in *Proc. of the 49th Annual Allerton Conf. on Communication, Control and Computing*, 2011.

[85] R. Jabr, "Radial distribution load flow using conic programming," *IEEE Trans. on Power Syst.*, vol. 21, no. 3, pp. 1458–1459, Aug. 2006.

[86] R. Madani, S. Sojoudi, and J. Lavaei, "Convex relaxation for optimal power flow problem: Mesh networks." in *Asilomar Conference on Signals, Systems and Computers (ACSSC)*, 2013, pp. 1375–1382.

[87] B. Kocuk, S. Dey, and X. Sun, "Inexactness of SDP relaxation and valid inequalities for optimal power flow," School of Industrial and Systems Engineering, Georgia Institute of Technology, Tech. Rep., 2014.

[88] B. Kocuk, S. S. Dey, and A. Sun, "Strong SOCP relaxations for the optimal power flow problem," Georgia Institute of Technology, Tech. Rep., 2015.

[89] C. Coffrin, H. L. Hijazi, and P. V. Hentenryck, "The QC relaxation: Theoretical and computational results on optimal power flow," NICTA, Tech. Rep., 2015.

[90] R. E. Griffith and R. A. Stewart, "A nonlinear programming technique for the optimization of continuous processing systems," *Management Science*, vol. 7, pp. 379–392, 1961.

[91] R. Fletcher, S. Leyffer, and P. Toint, "On the global convergence of an SLP-filter algorithm," Department of Mathematics, University of Dundee, UK, Numerical Analysis Report NA/183, 1998.

[92] A. Castillo and R. P. O'Neill, "Computational performance of solution techniques applied to the ACOPF," Federal Energy Regulatory Commission, Tech. Rep., 2013.

[93] R. H. Byrd, J. Nocedal, and R. A. Waltz, "KNITRO: An integrated package for nonlinear optimization," *Large-Scale Nonlinear Optimization*, pp. 35–59, 2005.

[94] A. Wächter and L. T. Biegler, "On the implementation of a primal-dual interior point filter line search algorithm for large-scale nonlinear programming," *Math. Program.*, vol. 106, no. 1, pp. 25–57, 2006.

[95] W. E. Hart, C. Laird, J.-P. Watson, and D. L. Woodruff, *Pyomo–Optimization Modeling in Python*. Springer Publishing Company, 2012.

[96] P. Lipka, R. O'Neill, and S. Oren, "Developing line current magnitude constraints for IEEE test problems," Federal Energy Regulatory Commission, Tech. Rep., 2013.

[97] F. Palacios-Gomez, L. Lasdon, and M. Engquist, "Nonlinear optimization by successive linear programming," *Management Science*, vol. 28, no. 10, pp. 1106–1120, 1982.

[98] S. Murphy, J. Baranowski, and R. Nice, "Metering accuracy and state estimator performance," PJM, Tech. Rep., 2015.

[99] MATLAB, *version 8.3.0.532 (R2014a)*. The MathWorks Inc., 2014.

[100] M. A. Duran and I. Grossmann, "An outer-approximation algorithm for a class of mixed-integer nonlinear programs," *Mathematical Programming*, vol. 36, pp. 307–339, 1986.

[101] L. L. Garver, "Power generation scheduling by integer programming–Development and theory," *Trans. Amer. Inst. Elect. Eng. Part III: Power App. Syst.*, vol. 81, no. 3, pp. 730–734, 1962.

[102] D. Rajan and S. Takriti, "Minimum up/down polytopes of the unit commitment problem with start-up costs," IBM, Research Report RC23628, 2005.

[103] M. Carrión and J. Arroyo, "A computationally efficient mixed-integer linear formulation for the thermal unit commitment problem," *IEEE Trans. on Power Syst.*, vol. 2, no. 1, pp. 69–77, 2011.

[104] J. Ostrowski, M. F. Anjos, and A. Vannelli, "Tight mixed integer linear programming formulations for the unit commitment problem," *IEEE Trans. on Power Syst.*, vol. 27, no. 1, pp. 39–46, 2012.

[105] S. Atakan, G. Lulli, and S. Sen, "An improved MIP formulation for the unit commitment problem," Optimization Online, Tech. Rep., 2015.

[106] R. A. Jabr, "Tight polyhedral approximation for mixed-integer linear programming unit commitment formulations," *IET Generation, Transmission and Distribution*, vol. 6, no. 11, pp. 1104–1111, 2012.

[107] J. M. Morales, A. J. Conejo, and J. Pérez-Ruiz, "Economic valuation of reserves in power systems with high penetration of wind power," *IEEE Trans. on Power Syst.*, vol. 24, no. 2, pp. 900–910, 2009.

[108] L. Wu and M. Shahidehpour, "Accelerating benders decomposition for network-constrained unit commitment problems," *Energy Syst.*, vol. 1, no. 3, pp. 339–376, 2010.

[109] M. J. Feizollahi, M. Costley, S. Ahmed, and S. Grijalva, "Large-scale decentralized unit commitment," *Electrical Power and Energy Syst.*, vol. 73, pp. 97–106, 2015.

[110] N. Padhy, "Unit commitment–A bibliographical survey," *IEEE Trans. on Power Syst.*, vol. 19, no. 2, pp. 1196–1205, 2004.

[111] A. Bhardwaj, K. Kamboj, V. Shukla, B. Singh, and P. Khurana, "Unit commitment in electrical power system–A literature review," in *IEEE PEOCO*, Melaka, Malaysia, 2012, pp. 275 – 280.

[112] C. Tseng, "On power system generation unit commitment problems." Ph.D. dissertation, Department of Industry Engineering and Operations Research, University of California at Berkeley, 1996.

[113] M. R. Bussieck and A. Pruessner, "Mixed-integer nonlinear programming," GAMS Development Corporation, Tech. Rep., 2003.

[114] C. Murillo-Sanchez and R. J. Thomas, "Thermal unit commitment with nonlinear power flow constraints," in *IEEE Power & Energy Society Winter Meeting*, 1999, pp. 484–489.

[115] H. Ma and M. Shahidehpour, "Unit commitment with transmission security and voltage constraints," *IEEE Trans. Power Syst.*, vol. 14, no. 2, pp. 757–764, 1999.

[116] Y. Fu, M. Shahidehpour, and Z. Li, "Security-constrained unit commitment with AC constraints," *IEEE Trans. on Power Syst.*, vol. 20, no. 3, pp. 1538–1550, 2005.

[117] ——, "AC contingency dispatch based on security-constrained unit commitment," *IEEE Trans. on Power Syst.*, vol. 21, no. 2, pp. 897–908, 2006.

[118] W. S. Sifuentes and A. Vargas, "Hydrothermal scheduling using benders decomposition: Accelerating techniques," *IEEE Trans. on Power Syst.*, vol. 22, no. 3, pp. 1351–1359, 2007.

[119] C. E. Murillo-Sánchez, R. D. Zimmerman, C. L. Anderson, and R. J. Thomas, "Secure planning and operations of systems with stochastic sources, energy storage, and active demand," *IEEE Trans. on Smart Grid*, vol. 4, no. 4, pp. 2220–2229, 2013.

[120] A. Nasri, S. J. Kazempour, A. J. Conejo, and M. Ghandhari, "Network-

constrained AC unit commitment under uncertainty: A benders' decomposition approach," *IEEE Trans. on Power Syst.*, vol. 31, no. 1, pp. 412–422, 2016.

[121] D. Han, J. Jian, and L. Yang, "Outer approximation and outer-inner approximation approaches for unit commitment problem," *IEEE Trans. on Power Syst.*, vol. 29, no. 2, pp. 505–513, 2014.

[122] J. P. Ruiz, J. Wang, C. Liu, and G. Sun, "Outer-approximation method for security constrained unit commitment," *IET Generation, Transmission & Distribution*, vol. 7, no. 11, pp. 1210–1218, 2013.

[123] R. Fletcher and S. Leyffer, "Solving mixed integer nonlinear programs by outer approximation," *Mathematical Programming*, vol. 66, pp. 327–349, 1994.

[124] A. M. Geoffrion, "Generalized benders decomposition," *Journal of Opitmization Theory and Applications*, vol. 10, pp. 237–260, 1972.

[125] I. E. Grossmann, "Review of nonlinear mixed-integer and disjunctive programming techniques," *Optimization and Engineering*, vol. 3, pp. 227–252, 2002.

[126] P. Bonami, L. T. Biegler, A. R. Conn, G. Cornuéjols, I. E. Grossmann, C. D. Laird, J. Lee, A. Lodi, F. Margot, N. Sawaya, and A. Wächter, "An algorithmic framework for convex mixed integer nonlinear programs," *Discrete Optimization*, vol. 5, pp. 186–204, 2008.

[127] A. Bai and H. Wei, "Semi-definite programming-based method for security-constrained unit commitment with operational and optimal power flow constraints," *IET Generation, Transmission & Distribution*, vol. 3, no. 2, pp. 182–197, 2009.

[128] Y. Bai, H. Zhong, Q. Xia, C. Kang, and L. Xie, "A decomposition method for network-constrained unit commitment with AC power flow constraints," *Energy*, vol. 88, pp. 595–603, 2015.

[129] J. Malone and J. Surgeon. Reactive power and financial compensation.

[130] J. Kueck, B. Kirby, T. Rizy, F. Li, and N. Fall, "Reactive power from distributed energy," *The Electricity Journal*, vol. 19, no. 10, pp. 27–38, 2006.

[131] P.M. Subcommittee, "The IEEE reliability test system," *IEEE Trans. on Power Apparatus and Syst.*, vol. PAS-98, no. 6, pp. 2047–2054, 1979.

[132] A. Castillo. [Online]. Available: https://github.com/anyacastillo/ucacopf/tree/master#ucacopf

[133] IBM Corp., "IBM ILOG CPLEX optimization studio 12.6.2," 2015.

[134] A. Wächter and L. T. Biegler, "Line search filter methods for nonlinear programming: Motivation and global convergence," *SIAM Journal on Optimization*, vol. 16, no. 1, pp. 1–31, 2005.

[135] T. E. Dy Liacco, "The adaptive reliability control system," *Power Apparatus and Syst., IEEE Trans. on*, vol. PAS-86, no. 5, pp. 517–531, May 1967.

[136] O. Alsaç and B. Stott, "Fast decoupled load flow," *IEEE Trans. on Power Apparatus and Syst.*, vol. PAS-93, no. 3, pp. 859–869, 1974.

[137] W. A. Bukhsh, A. Grothey, K. I. M. McKinnon, and P. A. Trodden, "Local solutions of the optimal power flow problem," *IEEE Trans. on Power Syst.*, vol. 28, no. 4, pp. 4780–4788, 2013.

[138] Ziena Optimization LLC, "Knitro documentation: Release 8.1," 2012.

[139] J. F. Sturm, "Using Sedumi 1.02, a MATLAB toolbox for optimization over symmetric cones," *Optimization Methods and Software*, vol. 11-12, pp. 625–653, 1999.

[140] D. Akinyele and R. Rayudu, "Review of energy storage technologies for sustainable power networks," *Sustainable Energy Technologies and Assessments*, vol. 8, pp. 74 – 91, 2014.

[141] A. A. Akhil, G. Huff, A. B. Currier, B. C. Kaun, D. M. Rastler, S. B. Chen, A. L. Cotter, D. T. Bradshaw, and W. D. Gauntlett, "DOE/EPRI 2013 electricity storage handbook in collaboration with NRECA," Sandia National Laboratories, Tech. Rep. SAND2013-5131, 2013.

[142] A. Castillo and D. F. Gayme, "Grid-scale energy storage applications in renewable energy integration: A survey," *Energy Conversion and Management*, vol. 87, pp. 885 – 894, 2014.

[143] J. Eyer and G. Corey, "Energy storage for the electricity grid: Benefits and market potential assessment guide," Sandia National Laboratories, Tech. Rep., 2010.

[144] T. Kousksou, P. Bruel, A. Jamil, T. E. Rhafiki, and Y. Zeraouli, "Energy storage: Applications and challenges," *Solar Energy Materials and Solar Cells*, vol. 120, Part A, pp. 59 – 80, 2014.

[145] S. Tripathy, "Improved load-frequency control with capacitive energy storage," *Energy Conversion and Management*, vol. 38, no. 6, pp. 551 – 562, 1997.

[146] L. Zhang, "Study of FACTS/ESS applications in bulk power system," Ph.D. dissertation, Virginia Polytechnic Institute and State University, 2006.

[147] N. Jenkins, R. Allan, P. Crossley, D. Kirschen, and G. Strbac, "Technical impacts of embedded generation on the distribution system," in *Embedded Generation*. London, UK: The Institution of Electrical Engineers, 2000, pp. 11–12.

[148] M. Bragard, N. Soltau, S. Thomas, and R. W. D. Doncker, "The balance of renewable sources and user demands in grids: Power electronics for modular

battery energy storage systems," *IEEE Trans. on Power Electronics*, vol. 25, no. 12, pp. 3049–3056, 2010.

[149] S. C. Smith, P. K. Sen, B. Kroposki, and K. Malmedal, "Renewable energy and energy storage systems in rural electrical power systems: Issues, challenges and application guidelines," in *Proc. of the IEEE Rural Electric Power Conf. (REPC)*, 2010, pp. B4–1–B4–7.

[150] V. Scaini, "Grid support stability for reliable, renewable power," Eaton Corporation, Tech. Rep. WP083002EN, 2012.

[151] Y. M. Atwa and E. F. El-Saadany, "Optimal allocation of ESS in distribution systems with a high penetration of wind energy," *IEEE Trans. on Power Syst.*, vol. 25, no. 4, pp. 1815–1822, 2013.

[152] A. Gabash and P. Li, "Active-reactive optimal power flow in distribution networks with embedded generation and battery storage," *IEEE Trans. on Power Syst.*, vol. 27, no. 4, pp. 2026–2035, 2012.

[153] Z. Hu and W. T. Jewell, "Optimal power flow analysis of energy storage for congestion relief, emissions reduction, and cost savings," in *2011 IEEE/PES Systems Conf. and Exposition*, Phoenix, AZ, Mar. 2011.

[154] S. Bose, D. F. Gayme, U. Topcu, and K. M. Chandy, "Optimal placement of

energy storage in the grid," in *Proc. of the 51st IEEE Conf. on Decision and Control*, Maui, HI, Dec. 2012, pp. 5605–5612.

[155] J. Warrington, P. Goulart, S. Mariéthoz, and M. Morari, "A market mechanism for solving multi-period optimal power flow exactly on AC networks with mixed participants," in *Proc. of the American Control Conf.*, Montreal, QC, 2012, pp. 3101 – 3107.

[156] A. Gopalakrishnan, A. U. Raghunathan, D. Nikovski, and L. T. Biegler, "Global optimization of multi-period optimal power flow," in *Proc. of the American Control Conf.*, Washington, DC, 2013, pp. 1157 – 1164.

[157] M. Abbaspour, M. Satkin, B. Mohammadi-Ivatloo, F. H. Lotfi, and Y. Noorollahi, "Optimal operation scheduling of wind power integrated with compressed air energy storage (caes)," *Renewable Energy*, vol. 51, pp. 53–59, 2013.

[158] Z. Tan, L. Ju, J. Li, J. Li, and H. Zhang, "A two-stage scheduling optimization model and solution algorithm for wind power and energy storage system considering uncertainty and demand response," *Electrical Power and Energy Syst.*, vol. 63, pp. 1057–1069, 2014.

[159] S. Rebennack, J. Kallrath, and P. M. Pardalos, "Optimal storage design for a multi-product plant: A non-convex MINLP formulation," *Computers and Chemical Engineering*, vol. 35, pp. 255–271, 2011.

[160] W. Hogan, "Markets in reeal electric networks require reactive prices," *The Energy Journal*, vol. 14, no. 3, pp. 171–200, 1993.

[161] E. Kahn and R. Baldick, "Reactive power is a cheap constraint," *The Energy Journal*, vol. 15, no. 4, pp. 191–201, 1994.

[162] J. B. Gil, T. G. S. Román, J. J. A. Ríos, and P. S. Martín, "Reactive power pricing: A conceptual framework for remuneration and charging procedures," *IEEE Trans. on Power Syst.*, vol. 15, no. 2, 2000.

[163] S. Hao and A. Papalexopoulos, "Reactive power pricing and management," *IEEE Trans. on Power Syst.*, vol. 12, no. 1, pp. 95–104, 1997.

[164] R. P. O'Neill, E. B. Fisher, B. F. Hobbs, and R. Baldick, "Towards a complete real-time electricity market design," *Journal of Regulatory Economics*, vol. 34, pp. 220–250, 2008.

[165] C. J. Day, B. F. Hobbs, and J.-S. Pang, "Oligopolistic competition in power networks: A conjectured supply function approach," *IEEE Trans. on Power Syst.*, vol. 17, no. 3, pp. 597–607, 2002.

[166] S. Wogrin and D. F. Gayme, "Optimizing storage siting, sizing and technology portfolios in transmission-constrained networks," *IEEE Trans. on Power Syst.*, vol. 30, no. 6, pp. 3304–3313, 2014.

[167] G. C. Calafiore and L. El Ghaoui, *Optimization Models*. Cambridge University Press, 2014.

[168] S. Boyd, L. El Ghaoui, E. Feron, and V. Balakrishnan, *Linear Matrix Inequalities in System and Control Theory*. Society for Industrial and Applied Mathematics, 1994.

[169] S. Sojoudi and J. Lavaei, "Physics of power networks makes hard optimization problems easy to solve," in *Proc. of the IEEE PES General Meeting*, 2012.

[170] R. Madani, G. Fazelnia, S. Sojoudi, and J. Lavaei, "Finding low-rank solutions of sparse linear matrix inequalities using convex optimization," UC Berkeley IEOR, Tech. Rep., 2014.

[171] U.S. Energy Information Administration. (2012) Negative wholesale electricity prices occur in RTOs. [Online]. Available: http://www.eia.gov/todayinenergy/detail.cfm?id=6730

[172] U. Topcu, D. F. Gayme, S. H. Low, and P. Khargonekar, "Towards smart, flexible and efficient power systems: Vision and research challenges," in *Proc. of the American Control Conf.*, Washington, DC, June 2013, pp. 5237–5244.

[173] K. M. Chandy, S. Low, U. Topcu, and H. Xu, "A simple optimal power flow model with energy storage," in *Proc. of the 49th IEEE Conf. on Decision and Control*, 2010, pp. 1051–1057.

[174] M. Ghofrani, A. Arabali, M. Etezadi-Amoli, and M. S. Fadali, "A framework for optimal placement of energy storage units within a power system with high wind penetration," *IEEE Trans. on Sustainable Energy*, vol. 4, no. 2, pp. 434–442, 2013.

[175] R. A. Jabr, A. H. Coonick, and B. J. Cory, "A primal-dual interior point method for optimal power flow dispatching," *IEEE Trans. on Power Syst.*, vol. 17, no. 3, pp. 654–662, 2002.

[176] M. R. Irving and M. J. H. Sterling, "Economic dispatch of active power by quadratic programming using a sparse linear complementary algorithm," *Electrical Power and Energy Systems*, vol. 7, pp. 2–6, 1985.

[177] U. of Washington, "Power systems test case archive," 1993. [Online]. Available: http://www.ee.washington.edu/research/pstca

[178] National Renewable Energy Laboratory. (2006) Western wind resources dataset. [Online]. Available: http://wind.nrel.gov/Web_nrel/

[179] J. F. Sturm, "Using Sedumi 1.02, a MATLAB toolbox for optimization over symmetric cones," *Optimization Methods and Software*, vol. 11-12, pp. 625–653, 1999.

[180] Commission Staff Report, "Payment for reactive power," Federal Energy Regulatory Commission, Tech. Rep. AD14-7, 2014.

[181] B. Wu, Y. Lang, N. Zargari, and S. Kouro, *Power Conversion and Control of Wind Energy Systems*. John Wiley & Sons, 2011.

[182] I. Boldea, *Variable Speed Generators*. CRC Press, 2015.

[183] I. N. England. Open access transmission tariff (OATT) - schedule 2 volt ampere reactive (VAR). [Online]. Available: http://www.iso-ne.com/markets-operations/settlements/understand-bill/item-descriptions/oatt-schedule2-var

[184] L. Monitoring Analytics, "2014 state of the market report for PJM: Section 11 congestion and marginal losses," PJM, Tech. Rep., 2015.

[185] C. Corporation, "Current form of marginal loss pricing is inequitable, sends the wrong market signals and may lead to inefficient outcomes," ISO-NE, Tech. Rep., 2003.

[186] A. Philpott, "Experiments with load flow pricing models," in *Proceedings of CRNEC Policy Conference*, 1999.

[187] B. F. Hobbs, G. Drayton, E. B. Fisher, and W. Lise, "Improved transmission representations in oligopolistic market models: Quadratic losses, phase shifters, and DC lines," *IEEE Trans. on Power Syst.*, vol. 23, no. 3, pp. 1018–1029, 2008.

[188] A. E. Sjödin, D. F. Gayme, and U. Topcu, "Risk-mitigated optimal power flow

for wind powered grids," in *Proc. of the American Ctrl. Conf.*, Montreal, QC, June 2012, pp. 4431 – 4437.

[189] K. Dvijotham, S. Backhaus, and M. Chertkov, "Operations-based planning for placement and sizing of energy storage in a grid with a high penetration of renewables," Los Alamos National Lab, Tech. Rep., 2011.

[190] C. Thrampoulidis, S. Bose, and B. Hassibi, "On the distribution of energy storage in electricity grids," in *Proc. the 52nd IEEE Conf. on Decision and Control*, 2013, pp. 7590–7596.

[191] A. J. Conejo and J. A. Aguado, "Multi-area coordinated decentralized DC optimal power flow," *IEEE Trans. on Power Syst.*, vol. 13, no. 4, pp. 1272–1278, 1998.

[192] A. L. Motto, F. D. Galiana, A. J. Conejo, and J. M. Arroyo, "Network-constrained multiperiod auction for a pool-based electricity market," *IEEE Trans. on Power Syst.*, vol. 17, no. 3, pp. 646–653, 2002.

[193] R. A. Jabr, "Modeling network losses using quadratic cones," *IEEE Trans. on Power Syst.*, vol. 20, no. 1, pp. 505–506, 2005.

[194] F. Li and R. Bo, "DCOPF-based LMP simulation: Algorithm, comparison with ACOPF, and sensitivity," *IEEE Trans. on Power Syst.*, vol. 22, no. 4, pp. 1475–1485, 2007.

[195] M. W. Mustafa and M. H. Sulaiman, "Transmission loss allocation in deregulated power system via superposition and proportional tree methods," in *2nd IEEE Int'l Conf. on Power and Energy*, 2008, pp. 988–993.

[196] C. Coffrin, P. V. Hentenryck, and R. Bent, "Approximating line losses and apparent power in AC power flow linearizations," in *Proc. of the IEEE PES General Meeting*, 2012, pp. 1–8.

[197] S. Zhang, "Quadratic maximization and semidefinite relaxation," *Math. Program.*, vol. Ser. A, no. 87, pp. 453–465, 2000.

[198] S. Kim and M. Kojima, "Exact solutions of some nonconvex quadratic optimization problems via SDP and SOCP relaxations," *Computational Optimization and App.*, vol. 26, no. 2, pp. 143–154, 2003.

[199] F. Alizadeh and D. Goldfarb, "Second-order cone programming," *Mathematical Programming*, vol. 95, no. 1, pp. 3–51, 2003.

[200] S. Boyd, N. Parikh, E. Chu, B. Peleato, and J. Eckstein, "Distributed optimization and statistical learning via the alternating direction method of multipliers," *Foundations and Trends in Machine Learning*, vol. 3, no. 1, pp. 1–122, 2010.

[201] A. X. Sun, D. T. Phan, and S. Ghosh, "Fully decentralized AC optimal power flow algorithms," in *2013 IEEE Power and Energy Society General Meeting*, 2013, pp. 1–5.

[202] A. Castillo, C. A. Silva-Monroy, J.-P. Watson, and R. O'Neill, "Market implications of optimal power flow with controllable network elements," *Submitted to IEEE Trans. on Power Syst.*, 2016.

[203] P. Lipka, S. Oren, R. O'Neill, and A. Castillo, "Running a more complete market with the SLP IV-ACOPF," *Submitted to IEEE Trans. on Power Syst.*, 2016.

Vita

Anya Castillo holds a B.S. degree in Electrical and Computer Engineering with a Minor in Computer Science (2005) from Carnegie Mellon University, Pittsburgh, PA, and a M.S. degree in Technology and Public Policy (2009) from the Engineering System Division of the Massachusetts Institute of Technology, Cambridge, MA. In 2016 she received a Ph.D. from the Department of Geography and Environmental Engineering at the Johns Hopkins University, Baltimore, MD. From 2010-2016, she has been an Operations Research Analyst in the Office of Energy Policy and Innovation at the Federal Energy Regulatory Commission, Washington, DC. After graduation, she will join Sandia National Laboratories, Albuquerque, NM, as a Senior Engineer.